VOLUME 77 DECEMBER 6, 1973 NUMBER 25

JPCHAx

THE JOURNAL OF PHYSICAL CHEMISTRY

PUBLISHED BIWEEKLY BY THE AMERICAN CHEMICAL SOCIETY

For the Spectroscopist—

Data • Techniques • Formulas

1. CHARACTERISTIC RAMAN FREQUENCIES OF ORGANIC COMPOUNDS

By Francis R. Dollish, *Carnegie-Mellon University*, William G. Fateley, *Kansas State University*, and Freeman F. Bentley, *Department of the Air Force*

This book will be an invaluable source of data for interpreting spectra, making empirical assignments, and solving chemical and structural problems. It presents a compendium of characteristic Raman frequencies for the identification of organic compounds, cites over 1400 references to the Raman spectra of specific organic compounds, and includes an appendix of great importance in determining the molecular structure of molecules.

1973 448 pages (approx.) $22.50 (tent.)

2. VIBRATIONAL SPECTROSCOPY OF TRAPPED SPECIES: Infrared and Raman Studies of Matrix-Isolated Molecules, Radicals and Ions

Edited by H. E. Hallam, *University College of Swansea*

This is the first monograph to survey the widespread use of the matrix isolation technique in infrared and Raman spectroscopy. Each chapter is written by a specialist in the field and is an up-to-date account of a particular technique. Chapters cover free radicals and intermediates, vaporizing molecules, impurity centers in ionic and covalent crystals, clathrates, and stable molecules, including analytical applications of pseudomatrix isolation. A detailed account is also given of the apparatus required for cryogenic spectroscopy and the desirable properties of matrix materials.

1973 436 pages (approx.) $29.50 (tent.)

3. ORGANIC ELECTRONIC SPECTRAL DATA

Edited by John P. Phillips, *University of Louisville*, Henry Feuer, *Purdue University*, and B. S. Thyagarjan, *University of Idaho*

This is the 9th volume to abstract and publish in formula order various ultraviolet-visible spectra of organic compounds. Most of the compound names have been made to conform with the Chemical Abstracts system of nomenclature. The organic electronic spectral data was chosen on the basis that the compound be pure enough for satisfactory elemental analysis and for a definite empirical formula; solvent and phase be given; and sufficient data to calculate molar absorptivities be available.

1973 976 pages (approx.) $40.00 (tent.)

4. SURFACE AND COLLOID SCIENCE Electrokinetic Phenomena — Volume 7

Edited by Egon Matijevic, *Clarkson College of Technology*

Written to assist people in industry in solving problems in surface and colloid science, this volume describes theories, systems, and processes while indicating solved and unresearched problems. It treats electrokinetic phenomena in a rigorous way, giving a historic development and a digest of the newest results.

1973 368 pages (approx.) In Press

5. STRUCTURES OF THE ELEMENTS

By Jerry Donohue, *University of Pennsylvania*

This book describes the structures of all the elements in the solid state, and emphasizes pictorial representations, with numerical data for each structure. It includes lattice constants, positional parameters, interatomic distances and, where appropriate, bond and torsion angles. In many cases, the complete structural history of each element and its allotropes is given in detail. Figures in this reference volume were prepared by a talented artist-draftsman, and complicated structures are shown in more than one view for better clarity.

1973 528 pages (approx.) In Press

6. ORGANIC MOLECULAR PHOTOPHYSICS — Volume 1

Edited by John B. Birks, *University of Manchester*

The first of two volumes on organic molecular photophysics, this book gives an in-depth treatment of the spectroscopy of the π-electronic states of aromatic hydrocarbons; the fluorescence of aromatic molecular vapors; organic dye lasers; diffusion-controlled rate processes; and other topics.

1973 600 pages $37.50

WILEY-INTERSCIENCE
a division of John Wiley & Sons, Inc.
605 Third Avenue, New York, N.Y. 10016
In Canada: 22 Worcester Road, Rexdale, Ontario

093-A4307-WI

WILEY-INTERSCIENCE, Dept. 788, 605 Third Avenue, New York, N.Y. 10016

Sirs: Please send me the book(s) whose numbers I have circled: **1 2 3 4 5 6**

☐ My check (money order) for $ _____ is enclosed.

☐ Please bill me. (Restricted to the continental United States.)

Name _____

Firm _____

Address _____

City _____

State _____ Zip _____

Please add state and local tax where applicable. Prices subject to change without notice. 093-A4307-WI

THE JOURNAL OF

PHYSICAL CHEMISTRY

AMERICAN CHEMICAL SOCIETY, *1155 Sixteenth St., N.W., Washington, D. C. 20036*

Books and Journals Division

JOHN K CRUM *Director*
RUTH REYNARD *Assistant to the Director*

CHARLES R. BERTSCH *Head, Editorial Processing Department*
D. H. MICHAEL BOWEN *Head, Journals Department*
BACIL GUILEY *Head, Graphics and Production Department*
SELDON W. TERRANT *Head, Research and Development Department*

 Published biweekly by the American Chemical Society at 20th and Northampton Sts., Easton, Pa. 18042. Second-class postage paid at Washington, D. C., and at additional mailing offices.

All manuscripts should be sent to *The Journal of Physical Chemistry*, Department of Chemistry, University of Minnesota, Minneapolis, Minn. 55455.

Additions and Corrections are published once yearly in the final issue. See Volume 76, Number 26 for the proper form.

Extensive or unusual alterations in an article after it has been set in type are made at the author's expense, and it is understood that by requesting such alterations the author agrees to defray the cost thereof.

The American Chemical Society and the Editor of *The Journal of Physical Chemistry* assume no responsibility for the statements and opinions advanced by contributors.

Correspondence regarding accepted copy, proofs, and reprints should be directed to Editorial Processing Department, American Chemical Society, 20th and Northampton Sts., Easton, Pa. 18042. Head: CHARLES R. BERTSCH. Assistant Editor: EDWARD A. BORGER. Editorial Assistant: JOSEPH E. YURVATI.

Advertising Office: Centcom, Ltd., 142 East Avenue, Norwalk, Conn. 06851.

Business and Subscription Information

Send all new and renewal subscriptions *with payment* to: Office of the Controller, 1155 16th Street, N.W., Washington, D. C. 20036. Subscriptions should be renewed promptly to avoid a break in your series. All correspondence and telephone calls regarding changes of address, claims for missing issues, subscription service, the status of records, and accounts should be directed to Manager, Membership and Subscription Services, American Chemical Society, P.O. Box 3337, Columbus, Ohio 43210. Telephone (614) 421-7230.

On changes of address, include both old and new addresses with ZIP code numbers, accompanied by mailing label from a recent issue. Allow four weeks for change to become effective.

Claims for missing numbers will not be allowed (1) if loss was due to failure of notice of change in address to be received before the date specified, (2) if received more than sixty days from date of issue plus time normally required for postal delivery of journal and claim, or (3) if the reason for the claim is "issue missing from files."

Subscription rates (1973): members of the American Chemical Society, $20.00 for 1 year; to nonmembers, $60.00 for 1 year. Those interested in becoming members should write to the Admissions Department, American Chemical Society, 1155 Sixteenth St., N.W., Washington, D. C. 20036. Postage to Canada and countries in the Pan-American Union, $5.00; all other countries, $6.00. Single copies for current year: $3.00. Rates for back issues from Volume 56 to date are available from the Special Issues Sales Department, 1155 Sixteenth St., N.W., Washington, D. C. 20036.

Subscriptions to this and the other ACS periodical publications are available on microfilm. Supplementary material not printed in this journal is now available in microfiche form on a current subscription basis. For information on microfilm or microfiche subscriptions, write Special Issues Sales Department at the address above.

Notice to Authors printed in this issue

From the borders of organic chemistry . . . To the borders of theoretical physics:

Inorganic Chemistry brings you a broad range of authoritative information presenting both experimental and theoretical studies in all phases of inorganic chemistry.

Each month, this rapidly growing journal brings you the data you need on synthesis and properties of new compounds, quantitative studies regarding structure, and thermodynamics of inorganic reactions.

When you've seen the 50 or more papers offered in each issue, you'll also want to look through the Notes and Correspondence sections for their concise exchange of scientific views and ideas.

To order INORGANIC CHEMISTRY today, just complete and return the form below.

. . another ACS service

Inorganic Chemistry

Inorganic Chemistry
American Chemical Society
1155 Sixteenth Street, N.W.
Washington, D.C. 20036

Yes, I would like to receive INORGANIC CHEMISTRY at the one-year rate checked below:

	U.S.	Canada	Latin America	Other Nations
ACS Member Personal-Use One-Year Rate	☐ $18.00	☐ $22.00	☐ $22.00	☐ $23.00
Nonmember	☐ $54.00	☐ $58.00	☐ $58.00	☐ $59.00

Bill me ☐ Bill company ☐ Payment enclosed ☐

Name

Street Home ☐ Business ☐

City State Zip

P-73

THE JOURNAL OF

PHYSICAL CHEMISTRY

Volume 77, Number 25 December 6, 1973

JPCHAx 77(25) 2931–3036 (1973)
ISSN 0022-3654

COMMUNICATIONS TO THE EDITOR

■Supplementary material for this paper is available separately, in photocopy or microfiche form. Ordering information is given in the paper.

* In papers with more than one author, the asterisk indicates the name of the author to whom inquiries about the paper should be addressed.

AUTHOR INDEX

NOTICE TO AUTHORS

I. General Considerations

The Journal of Physical Chemistry is devoted to reporting both experimental and theoretical research dealing with fundamental aspects of physical chemistry. Space limitations necessitate giving preference to research articles dealing with previously unanswered basic questions in physical chemistry. Acceptable topics are those of general interest to physical chemists, especially work involving new concepts, techniques, and interpretations. Research that may lead to reexaminations of generally accepted views is, of course, welcome.

Authors reporting data should include an interpretation of the data and its relevance to the theories of the properties of matter. However, the discussion should be concise and to the point and excessive speculation is to be discouraged. Papers reporting redeterminations of existing data will be acceptable only if there is reasonable justification for repetition: for example, if the more recent or more accurate data lead to new questions or to a reexamination of well known theories. Manuscripts that are essentially applications of chemical data or reviews of the literature are, in general, not suitable for publication in *The Journal of Physical Chemistry*. Detailed comparisons of methods of data analysis will be considered only if the paper also contains original data, or if such comparison leads to a genesis of new ideas.

Authors should include an introductory statement outlining the scientific rationale for the research. The statement should clearly specify the questions for which answers are sought and the connection of the present work with previous work in the field. All manuscripts are subject to critical review. It is to be understood that the final decision relating to a manuscript's suitability rests solely with the editors.

Symposium papers are sometimes published as a group, but only after special arrangement with the editor.

Authors' attention is called to the "Handbook for Authors," available from the Special Issues Sales Department, American Chemical Society, 1155 Sixteenth St., N.W., Washington, D. C. 20036, in which pertinent material is to be found.

II. Types of Manuscripts

The Journal of Physical Chemistry publishes two types of manuscripts: *Articles* and *Communications*.

A. Articles should cover their subjects with thoroughness, clarity, and completeness. However, authors should also strive to make their *Articles* as concise as possible, avoiding unnecessary historical background. Abstracts to *Articles* should be brief—300 words is a maximum—and should serve to summarize the significant data and conclusions. The abstract should convey the essence of the *Article* to the reader.

B. Communications are of two types, *Letters* and *Comments*. Both types are restricted to three-quarters of a page (750 words or the equivalent) including tables, figures, and text, and both types of *Communications* are subject to critical review, but special efforts will be made to expedite publication.

Letters should report preliminary results whose immediate availability to the scientific community is deemed important, and whose topic is timely enough to justify the double publication that usually results from the publication of a *Letter*.

Comments include significant remarks on the work of others. The editors will generally permit the authors of the work being discussed to reply.

The category of *Notes* has been discontinued since the handling of such manuscripts was precisely the same as that of *Articles* save for the requirement of an Abstract, and since even a short *Article* will need an Abstract ultimately, it seems as well to ask the author to provide this. Short *Articles* will of course continue to be welcome contributions.

III. Introduction

All manuscripts submitted should contain brief introductory remarks describing the purpose of the work and giving sufficient background material to allow the reader to appreciate the state-of-knowledge at the time when the work was done. The introductory remarks in an *Article* should constitute the first section of the paper and should be labeled accordingly. In *Communications*, the introductory material should not be in such a separate section. To judge the appropriateness of the manuscript for *The Journal of Physical Chemistry*, the editors will place considerable weight on the author's intentions as stated in the Introduction.

IV. Functions of Reviewers

The editors request the scientific advice of reviewers who are active in the area of research covered by the manuscript. The reviewers act only in an advisory capacity and the final decision concerning a manuscript is the responsibility of the editors. The reviewers are asked to comment not only on the scientific content, but also on the manuscript's suitability for *The Journal of Physical Chemistry*. With respect to *Communications*, the reviewers are asked to comment specifically on the urgency of publication. Authors are encouraged to suggest, when submitting a manuscript, names of scientists who could give a disinterested and informed and helpful evaluation of the work. All reviews are anonymous and the reviewing process is most effective if reviewers do not reveal their identities to the authors. An exception arises in connection with a manuscript submitted for publication in the form of a comment on the work of another author. Under such circumstances the first author will, in general, be allowed to review the communication and to write a rebuttal, if he so chooses. The rebuttal and the original communication may be published together in the same issue of the journal. Revised manuscripts are generally sent back to the original reviewers, who are asked to comment on the revisions. If only minor revisions are involved, the editors examine the revised manuscript in light of the recommendations of the reviewers without seeking further opinions. For the convenience of reviewers, authors are advised to indicate clearly, either in the manu-

script or in a covering letter, the specific revisions that have been made.

V. Submission of Manuscripts

All manuscripts must be submitted in triplicate to expedite handling. Manuscripts must be typewritten, double-spaced copy, on 8½ × 11 in. paper. Legal sized paper is not acceptable. Authors should be certain that copies of the manuscript are clearly reproduced and readable. **Authors submitting figures must include the original drawings or photographs thereof, plus three xerographic copies for review purposes. These reproductions of the figures should be on 8½ × 11 in. paper.** Graphs must be in black ink on white or blue paper. Figures and tables should be held to a minimum consistent with adequate presentation of information. All original data which the author deems pertinent must be submitted along with the manuscript. For example, a paper reporting a crystal structure should include structure factor tables for use by the reviewers.

All references and explanatory notes, formerly set up as footnotes on individual pages, are now grouped at the end of the article in a section called "References and Notes." They should be numbered consecutively in the order in which they are first mentioned in the text, and the complete list of notes and literature citations should appear at the end of the manuscript. Nomenclature should conform to that used in *Chemical Abstracts* and mathematical characters should be underlined for italics, Greek letters should be annotated, and subscripts and superscripts clearly marked.

Papers should not depend for their usefulness on unpublished material, and excessive reference to material in press is discouraged. References not readily available (*e.g.*, private technical reports, preprints, or articles in press) that are necessary for a complete review of the paper must be included with the manuscript for use by the reviewers.

VI. Revised Manuscripts

A manuscript sent back to an author for revision should be returned to the editor within 6 months; otherwise it will be considered withdrawn and treated as a new manuscript when and if it is returned. Revised manuscripts returned to the editor must be submitted in triplicate and all changes should be made by typewriter. **Unless the changes are very minor, all pages affected by revision must be retyped.** If revisions are so extensive that a new typescript of the manuscript is necessary, it is requested that a copy of the original manuscript be submitted along with the revised one.

VII. Supplementary Material

From time to time manuscripts involve extensive tables, graphs, spectra, mathematical material, or other "supplementary material" which, though of value to the specialized reader who needs all the data or all the detail, does not help and often hinders the effective presentation of the work being reported. The American Chemical Society has instituted a policy of including such supplementary material in the *microfilm* editions of its journals, which are available in many scholarly libraries; in addition, interested readers will be able to obtain the microfilm material directly at nominal cost. Authors are encouraged to make use of this resource, in the interests of shorter articles (which mean more rapid publication) and clearer, more readable presentation.

Supplementary material for inclusion in the microfilm edition should accompany a manuscript at the time of its original submission to an editor. It should be clipped together and attached at the end of the manuscript, along with a slip of paper clearly indicating that the material is "supplementary material for the microfilm edition." A paragraph should appear at the end of the paper indicating the nature of the supplementary material and the means by which the interested reader might be able to obtain copies of the data without use of the microfilm edition itself. The following is an example.

Supplementary Material Available. A listing of structure factor amplitudes will appear following these pages in the microfilm edition of this volume of the journal. Photocopies of the supplementary material from this paper only or microfiche (105 × 148 mm, 20× reduction, negatives) containing all of the supplementary material for the papers in this issue may be obtained from the Journals Department, American Chemical Society, 1155 16th St., N.W., Washington, D. C. 20036. Remit check or money order for $0.00 for photocopy or $2.00 for microfiche, referring to code number JPC-00-0000.

The amount of money to be indicated in the blanks will be filled in by the Editorial Office at Easton, Pa., after the acceptance of an article.

VIII. Proofs and Reprints

Galley proofs, original manuscript, cut copy, and reprint order form are sent by the printer directly to the author who submitted the manuscript. The attention of the authors is directed to the instructions which accompany the proof, especially the requirement that all corrections, revisions, and additions be entered on the proof and not on the manuscript. Proofs should be checked against the manuscript (in particular all tables, equations, and formulas, since this is not done by the editor) and returned as soon as possible. No paper is released for printing until the author's proof has been received. Alterations in an article after it has been set in type are made at the author's expense, and it is understood that by entering such alterations on proofs the author agrees to defray the cost thereof. The filled-out reprint form must be returned with the proof, and if a price quotation is required by the author's organization a request for it should accompany the proof. Since reprinting is generally done from the journal press forms, all orders must be filed before press time. None can be accepted later, unless a previous request has been made to hold the type. Reprint shipments are made a month or more after publication, and bills are issued by the printer subsequent to shipment. Neither the editors nor the Washington office keeps any supply of reprints. Therefore, only the authors can be expected to meet requests for single copies of papers.

A page charge is assessed to cover in part the cost of publication. Although payment is expected, it is not a condition for publication. Articles are accepted or rejected only on the basis of merit, and the editor's decision to publish the paper is made before the charge is assessed. The charge per journal page is $50.

THE JOURNAL OF
PHYSICAL CHEMISTRY

VOLUME 77, NUMBER 25 DECEMBER 6, 1973

Crossed Beams Chemistry. Reactions of Barium, Strontium, and Calcium

Ronald R. Herm,* Shen-Maw Lin, and Charles A. Mims

Inorganic Materials Research Division, Lawrence Berkeley Laboratory and Department of Chemistry, University of California, Berkeley, California 94720 *(Received August 13, 1973)*

Publication costs assisted by the Lawrence Berkeley Laboratory

This paper constitutes the final report from our laboratory on crossed beams exploratory studies of the chemistry of gaseous alkaline earth atoms (M). Measured product laboratory angular distributions and derived center-of-mass (CM) recoil distributions are presented for Ba + SF_6, Ba and Sr + PCl_3, Sr and Ca + NO_2, Ba and Sr + $(CH_3)_2CHNO_2$, and Ca + CCl_3NO_2; in addition, qualitative results are presented for Ba, Sr, and Ca + $SnCl_4$ and Ba + SO_2. All derived CM product angular distributions are asymmetric, favoring scattering into the forward hemisphere (*i.e.*, $0° \leq \theta \leq 90°$, where $\theta = 0°$ is defined by the initial M velocity), except for Ba + SF_6, where the CM distribution is approximately symmetric about $\theta = 90°$. This suggests that the Ba + SF_6 reaction proceeds *via* formation of an $BaSF_6$ complex with a lifetime (τ_c) greater than its rotational period (τ_r), whereas the PCl_3, NO_2, $(CH_3)_2CHNO_2$, and CCl_3NO_2 reactions proceed *via* direct mechanisms with $\tau_c < \tau_r$. For SF_6, PCl_3, and NO_2, the qualitative behavior of the alkaline earth reaction parallels that previously reported for the analogous alkali (A) reaction. However, no evidence of an $MSnCl_3$ product from M + $SnCl_4$ is observed here, whereas $ASnCl_3$ is thought to be an important product of K, Rb, or Cs + $SnCl_4$. Also, MO is apparently the product of Ba or Sr + $(CH_3)_2CHNO_2$ in contrast to the $CsNO_2$ product formation reported for Cs + CH_3NO_2.

Earlier papers in this series reported results of crossed beams studies of reactions of alkaline earth atoms with HI,[1a] halogen molecules,[1b,c] and some halides of methane.[1d] The present paper reports on the remainder of our exploratory studies of gaseous alkaline earth atom chemistry; results are presented for reaction of Ba, Sr, and/or Ca with some inorganic halides (SF_6, PCl_3, and $SnCl_4$) as well as some oxygen-containing compounds (NO_2, SO_2, $(CH_3)_2CHNO_2$, and CCl_3NO_2). Here again, reactive cross section are characterized only semiquantitatively, the primary intention being to compare the chemical behavior of alkaline earth atoms (M) with that previously reported for alkali atoms (A).

Apparatus and Data Analysis Procedure

The apparatus is described elsewhere.[1,2] Table I gives conditions of the two beams which intersect at a right angle, resulting in a 1–5% attenuation of the M beam (beam 1) and negligible attenuation of the cross beam (beam 2). Scattered species are ionized by ~150-eV electrons and mass analyzed in a detector unit which rotates about the beam collision zone, in the plane defined by the two intersecting beams, so as to measure the laboratory (lab) product angular distribution. Table II lists the reactive systems which were examined and provides estimates (based on the approximate apparatus sensitivity) of their total reactive cross sections, Q_R.

The data analysis procedure consists[1b-d,2] in assuming that the dependence of the center-of-mass (CM) reactive cross section on CM scattering angle, θ, and product relative translational recoil energy, E', is factorable, *i.e.*

$$\sigma(\theta, E') = T(\theta)P(E') \quad (1)$$

By convention, 0° scattering angle in either the lab or CM coordinate system corresponds to a reactive event wherein the product alkaline earth halide or oxide is scattered in the direction defined by the initial M velocity. Having assumed a form of $\sigma(\theta,E')$ given by eq 1, the corresponding lab product angular distribution is computed numerically by averaging over the beam speed distributions and integrating over the unmeasured lab product recoil speed distribution. This calculated lab product angular distribution is compared with experimental measurements so that, by trial and error, a $T(\theta)$–$P(E')$ combination which pro-

TABLE I: Experimental Beam Conditions[a]

Collision partners	Alkaline earth atom beam: Source temp	Speed distribution[b,c]: α_1	a_1	Cross beam: Source conditions: Temp	Pressure	Speed distribution[b,d]: α_2	a_2	Relative collision energy, E^e
Ba + SF_6	1060	3.2	1.1	340	2.2	2.0	1.4	2.5
Ba + PCl_3	1040	3.2	1.1	360	3.5	2.2	2.0	2.9
Sr + PCl_3	990	3.8	1.3	350	3.2	2.2	1.8	2.6
Ba + SO_2	950	3.3	0.0	360	4.0	3.1	2.0	1.9
Sr + NO_2	950	3.8	1.3	350	2.2	3.6	2.0	2.1
Ca + NO_2	1050	5.9	2.0	360	4.0	3.6	2.3	2.5
Ba + $(CH_3)_2CHNO_2$	1020	3.1	1.1	390	2.6	2.7	1.8	2.4
Sr + $(CH_3)_2CHNO_2$	960	3.7	1.3	350	2.8	2.5	1.8	2.3
Ca + CCl_3NO_2	1020	5.8	1.9	320	3.8	1.8	1.7	2.8

[a] Temperatures are given in °K, pressures in Torr, speeds in 100 m/sec, and energies in kcal/mol. [b] These are parameters of the functional representation of the beam number density speed distribution employed in ref 1b-d. [c] Parameters for Ba from measurements reported in ref 2b; parameters for Sr and Ca from an extrapolation discussed in ref 2b. [d] Parameters for PCl_3, NO_2, and $(CH_3)_2CHNO_2$ from measurements reported in ref 2b; parameters for SF_6, SO_2, and CCl_3NO_2 from an extrapolation reported in ref 2b. [e] E is a characteristic translation energy of reactant approach, calculated for the most probable (number density distribution) beam speeds. If no relaxation took place during beam formation, the cross beams also possess thermal rotational and vibrational energies.

TABLE II: Summary of Reactions Studied[a]

	Alkaline earth atom (M): Ba	Sr	Ca	Mg	Mass peak detected
SF_6	R	I(SF_4^+)	NR	NR	MF^+
PCl_3	R	R	F	NS	MCl^+
$SnCl_4$	R	R	R	NR	MCl^+
SO_2	R	NR	NR	NS	MO^+
NO_2	NS	R	R	I(Ar^+)	MO^+
$(CH_3)_2CHNO_2$	R	R	NR	NS	MO^+
CCl_3NO_2	NS	NS	R	NS	MCl^+
CCl_3NO_2	NS	NS	F	NS	MO^+

[a] NS denotes that this reactive system was not studied; I (X^+), it proved impossible to draw any conclusion about this reaction because of interference from the X^+ mass peak; NR, no product signal was observed, $Q_R < \sim 1$ Å;[2] F, a product signal was observed which was too weak to permit measurement of a reliable angular distribution, ~ 1 Å$^2 < Q_R < \sim 5$ Å;[2] R, a product angular distribution was measured, $Q_R > \sim 5$ Å.[2]

vides a good fit to the data is obtained. In general, the data are of limited information content and can be fit by more than one $T(\theta)$-$P(E')$ combination so that the quantitative forms of $T(\theta)$ and $P(E')$ are not uniquely determined.[1b-d,2] Nevertheless, it does unequivocally determine the qualitative form of the product angular distribution (*e.g.*, whether $T(\theta)$ is symmetric or sharply peaked forward or backward). Moreover, it is emphasized in earlier papers of this series[1b-d] that the data also characterize the CM distributions quantitatively to lowest order because Q_F, the fraction of the products scattered into the forward CM hemisphere (*i.e.*, $0° \leq \theta \leq 90°$), and $\bar{E}'$, the most probable relative product recoil energy, are approximate invariants of the data analysis.

Results and Discussion

Reactions with Halides. In reactions with polyhalides, the experiments are unable to distinguish between alkaline earth monohalide (MX) and dihalide (MX_2) products because both species yield exclusively MX^+ upon electron bombardment ionization. Signal strengths were too weak to distinguish between these two channels by means of appearance potential measurements. Interference from reactant mass peaks also precluded the observation of mass peaks corresponding to the other product. The measured lab product angular distributions may be fit to CM distributions by assuming either product channel. Since the CM → lab transformation is dependent only on the CM recoil velocity, $\bar{u}_3$, of the species detected, the derived CM $T(\theta)$ is not dependent on the assumed product identity. This is not true for $P(E')$, however, because E' is given by

$$E' = \gamma u_3^2 \qquad (2)$$
$$\gamma = (m_3 + m_4)m_3/2m_4$$

where m_3 and m_4 are the masses of the two recoiling products. In a previous study[1d] of M + CH_2I_2, γ was quite different for the MI + CH_2I *vs.* the MI_2 + CH_2 product channels so that it was possible to draw inferences from the data regarding the likely product identity. For the reactions studied here, however, values of γ for formation of MX *vs.* MX_2 are comparable. In general, E' values derived assuming an MX_2 product are shown in parentheses, E' values derived for an MX product are shown without parentheses.

Ba + SF_6. Figure 1 shows that the measured lab angular distribution of the BaF^+ mass peak signal from the Ba + SF_6 reaction is broad and of comparable intensities on both sides of the calculated[1a] lab angular distribution (assuming an energy independent collision cross section) of center-of-mass velocity vectors, **C**. This lab distribution is well fit by CM product angular distributions, given in Figure 1 and Table III, which are broad and almost symmetric about $\theta = 90°$, typical[3] of the behavior expected if the lifetime of the complex (τ_c) is at least as long as its rotational period (τ_r). Indeed, product velocity analysis measurements[4] on the K, Rb, and Cs + SF_6 reactions show symmetric CM product angular distributions, indicating that the reactions proceed *via* a long-lived complex with τ_c greater than several rotational periods.[5] The Q_F entries in Table III indicate that, even for the $T(\theta)$ curves shown in Figure 1, the product scattering is almost evenly divided between the forward and backward CM hemispheres. Moreover, uncertainties in the data analysis suggest that the results presented here on Ba + SF_6 are consistent with a long-lived complex mechanism. For example, auxiliary calculations with a slightly altered SF_6 beam speed distribution (1.0 rather than the "best estimate" of 1.4 for the a_2 parameter of Table I) can fit the

TABLE III: M + X-R → MX + R Derived CM Reaction Cross Sections[a]

Reaction		Angular distribution[b] H_1	C_1	Q_F	Speed distribution[c] u_1	n_1	m_1	n_2	m_2	Energetics $\bar{E}'$[d]	$\langle E \rangle$[e]	ΔD_0[f]
Ba + F-SF_5	A	20°	0.40[g]	0.51	3.0	2	1	2	2	1 0	3.4 (4.5)	62 (124)
	B	250°	0.00	0.53	2.3	4	2	2	4	1 6	2.1 (2.8)	62 (124)
Ba + Cl-PCl_2		20°	0.10	0.64	3.2	2	1	2	2	1 4	4.8 (8.7)	~25 (~60)
Sr + Cl-PCl_2		20°	0.30	0.55	4.0	2	1	2	2	1 3	3.9 (7.7)	~20 (~55)
Sr + O-NO		10°	0.12	0.54	4.5	2	1.5	2	2	4 4	~6	20
Ca + O-NO		10°	0.09	0.55	6.0	2	2	2	2	3 5	~5	11
Ba + O-ONC_3H_7		30°	0.15	0.68	4.5	2	1	2	2	2 9	~15	~35
Sr + O-ONC_3H_7		10°	0.15	0.56	4.3	2	1	2	2	1 4	~5	~0
Ca + Cl-CCl_2NO_2		15°	0.20	0.57	7.0	2	1	2	2	1 8	8.5	~35

[a] Energies are given in kcal/mol and speeds in 100 m/sec. [b] These are parameters of the $T(\theta)$ function employed in ref 1d; $\theta_1 = \theta_2 = 0°$ for all reactions except that $\theta_1 = 5°$ for Sr + $C_3H_7NO_2$ and Ca + CCl_3NO_2. [c] These are parameters of the distribution function employed in ref 1d for the recoil speed of the detected product. [d] $\bar{E}'$, the most probable recoil energy, is obtained from: $dP(E')/dE'|_{E'=\bar{E}'} = 0$. [e] $\langle \bar{E}' \rangle$ is the average product recoil energy. Energies given in parentheses refer to formation of an alkaline earth dihalide product. [f] $\Delta D_0 = D_0(MX) - D_0(R-X)$; D_0 taken from, for MF and MCl, D. L. Hildebrand, *J. Chem. Phys.*, **48**, 3657 (1968); **52**, 5751 (1970); for MO, ref 31; for SF_5, D. L. Hildebrand, *J. Phys. Chem.*, 77, 897 (1973); for NO_2, ref 21; for CCl_3NO_2, assumed same as CCl_4, ref 1d; for other bonds, estimates from ref 32. [g] Gaussian part of $T(\theta)$ reflected through 90° and multiplied by 0.75.

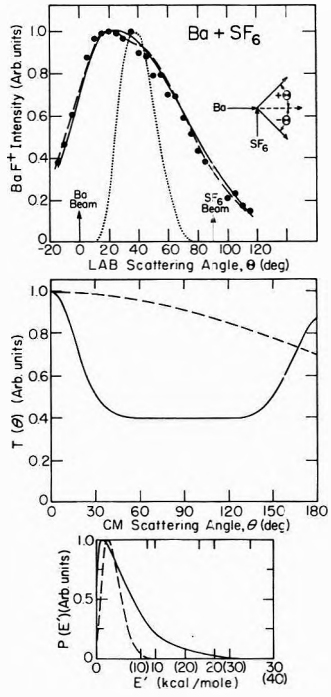

Figure 1. Data points in upper panel show measured lab angular distribution of BaF^+ signal from Ba + SF_6. Lower panels show derived CM $T(\theta)$ and $P(E')$ distributions which are also given in Table III as A (solid curve) and B (dashed curve). On the $P(E')$ plot, abscissa numbers in parentheses refer to BaF_2 + SF_4 products, numbers without parentheses refer to BaF + SF_5 products. The convention followed is that the solid $T(\theta)$ must be used in combination with the solid $P(E')$ to produce the corresponding solid curve fit to the data shown in the upper panel. Also shown in the upper panel is a calculated angular distribution of **C** (dotted curve).

data by reflecting the 0°-90° $T(\theta)$ functions shown in Figure 1 through $\theta = 90°$. The uncertainties in the form of $T(\theta)$ shown in Figure 1 prevent an analysis[3a,4] of the product angular distribution in terms of the statistical break up of an intermediate complex so as to extract information on its moments of inertia.

Product energy distributions produced by break up of a long-lived complex might be expected to partition the available energy statistically. Indeed, both $P(E')$ from K, Rb, and Cs + SF_6[4] as well as the vibrational distribution in the product CsF[6] are consistent with a transition state formulation of this energy randomization.[7] For comparison with the results reported here, this theory[7] would predict that the average product recoil energy is given by

$$\langle E' \rangle = (E + W + \Delta D_0)/(n + 2) \qquad (3)$$

where centrifugal barriers in the exit channel, which would only increase somewhat the $\langle E' \rangle$ estimate, have been neglected. Here, E, the reactant translational energy, is estimated in Table I, W, the SF_6 internal energy, has a thermal average value of 3.4 kcal/mol, and n should be 14.5[4,8] for break up of a "loose" $BaSF_6$ complex. The exoergicities, ΔD_0, are listed in Table III for two possible product channels

$$Ba + SF_6 \longrightarrow BaF + SF_5 \qquad (I)$$

or

$$Ba + SF_6 \longrightarrow BaF_2 + SF_4 \qquad (II)$$

Equation 3 provides $\langle E' \rangle$ estimates of 4.1 and 7.9 kcal/mol for channels I and II, respectively, and the experimental values are in reasonable agreement with this prediction[9] if the data are analyzed assuming channel I (see Table III). Although channel II would be favored over I on a purely statistical basis, its larger exoergicity might lead to shorter interaction times and a nonstatistical energy randomization.[10] Thus, the low resolution measurements reported here provide no basis for inferring the likely product identity because either reaction might proceed *via* initial formation of a one-electron transfer $Ba^+SF_6^-$ intermediate which, in analogy to the K, Rb, and Cs reactions, would statistically distribute the energy associated with reaction I.

Ba and Sr + PCl_3. Measured lab angular distributions of MCl^+ signal from the Ba and Sr + PCl_3 reactions are shown in Figure 2. In contrast to the BaF^+ from Ba + SF_6, the $BaCl^+$ from Ba + PCl_3 is mainly confined to smaller lab angles than the calculated **C** distribution, indicating that scattering into the forward CM hemisphere is favored. Figure 2 also shows CM product angular distributions derived for reasonable assumed forms of $P(E')$ which are specified in Table III. Auxiliary calculations reported in ref 2b which managed to fit the measurements using other assumed forms of $P(E')$ (including an unrealistic δ function referred to as the SRE analysis in ref 1b-1d) further indicate that (1) $T(\theta)$ need not peak at 0° for either reaction, but the qualitative behavior of a more sharply forward peaked $T(\theta)$ for the Ba reaction which is

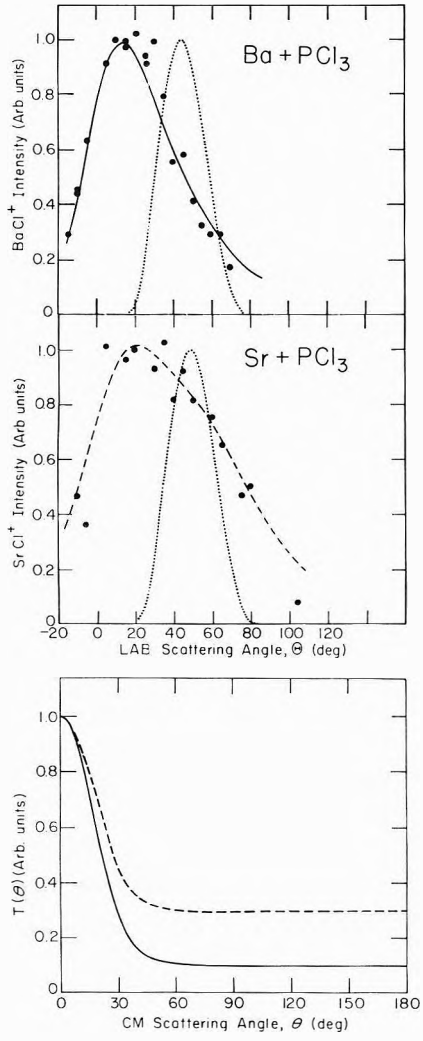

Figure 2. Data points in the upper panel show measured lab angular distribution of $BaCl^+$ signal from Ba + PCl_3 as well as the fit to the data provided by the CM $T(\theta)$ shown in the lower panel together with the $P(E')$ specified in Table III. Dotted curve shows the calculated angular distribution of **C**. Middle panel shows lab results on the Sr + PCl_3 reaction; conventions are as in the upper panel. Lower panel shows a comparison of derived CM product angular distributions for Ba (solid curve) and Sr (dashed curve) + PCl_3.

exhibited in Figure 2 appears valid; (2) Q_F is in the range of 0.64–0.72 and 0.55–0.60 for the Ba and Sr reactions, respectively; and (3) $\langle E' \rangle$ for the Ba and Sr reactions are in the range of 3–5 and 2–4 kcal/mol if MX + PCl_2 is formed, 5–9 and 4–8 if MX_2 + PCl is formed.

Thus, in contrast to the Ba + SF_6 reaction, the Ba and Sr + PCl_3 reactions proceed *via* a direct mechanism ($\tau_c < \tau_r$) wherein the products recoil preferentially into the forward CM hemisphere with only a modest fraction (~20%) of the reaction energy appearing as product recoil. Moreover, the observed $SrCl^+$ signal was appreciably weaker than the $BaCl^+$ signal. This observation as well as the observations on the Ca and Mg reactions shown in Table II indicate a particularly clear trend of decreasing Q_R in the M + PCl_3 family as M becomes less easily ionizable. In this regard, the MCl (or MCl_2) product CM angular distributions in Figure 2 follow the expected trend for direct reaction mechanisms of increasing forward scattering with increasing impact parameters leading to reaction. Product velocity analysis measurements are not available on the A + PCl_3 reactions. Primitive product angular distribution measurements indicate that Li,[11] K,[12] and Rb[13] + PCl_3 exhibit the same qualitative behavior as that found here, with reaction proceeding *via* a direct mechanism, although sideways rather than forward product scattering seems to be favored in the Li reaction.

Ba, Sr, and Ca + $SnCl_4$. Lab angular distributions of MCl^+ (corresponding to MCl and/or MCl_2) from the Ba, Sr, and Ca + $SnCl_4$ reactions were measured in ref 2b to peak sharply near $\theta = 0°$. In subsequent experiments[2b] measuring the $SnCl_4$ speed distribution, however, it was discovered that the $SnCl_4$ beam profile was unaccountedly broadened, rendering an analysis of the measured lab product angular distributions useless because of possible severe distortion by an unknown viewing factor (ref 2b and 11 discuss this possible mechanism of distortion). Nevertheless, the measured MCl^+ signals were quite strong, indicating large cross sections for reactions of Ba, Sr, and Ca with $SnCl_4$ (but not Mg; see Table II).

There is indirect evidence[4,12,14] that the K, Rb, and Cs + $SnCl_4$ reactions yield a heavier alkali product in addition to ACl, presumably the ionically bound alkali chlorostannite, $A^+SnCl_3^-$. If a similar product formed in the alkaline earth reactions, evidence of it should appear in the product mass spectrum because ionization of an ionically bound $M^+SnCl_3^-$ might be expected to involve removal of a nonbonding electron[1b] from M^+ with little rearrangement of the molecular geometry. Despite careful mass scans at various angles for the Ba, Sr, and Ca + $SnCl_4$ reactions, however, no evidence of an $MSnCl_n^+$ mass peak, for n = 0, 1, 2, 3, or 4, was observed. It is possible that any $MSnCl_3$ formed might decompose before reaching the detector. This is probably not a consideration in the alkali reactions[15] because decomposition into MCl (or ACl) + $SnCl_2$ would be endoergic even allowing for excitation of the initial chlorostannite product. In contrast, however, decomposition of any alkaline earth chlorostannite into MCl_2 + SnCl might take place because M + $SnCl_4$ → MCl_2 + SnCl + Cl is exoergic[16] by 5-10 kcal/mol. However, if $MSnCl_3$ formed in yields comparable to $ASnCl_3$, the absence of observable $MSnCl_n^+$ mass peaks would require that most of it (> ~95%) decompose before reaching the detector. Since this seems unlikely in view of the energetics, these observations suggest that, in contrast to A + $SnCl_4$, $MSnCl_3$ is not a significant product of the M + $SnCl_4$ reactions.

Reactions with Oxides. Reactions producing alkaline earth monohalide products are especially suited to crossed beams studies[1b] because electron bombardment ionization of MX is expected to produce MX^+ almost exclusively. However, the situation is less favorable for ionization of MO because a bonding, as opposed to nonbonding, electron is lost. If the fragmentation ratio, M^+/MO^+, were strongly dependent on the internal excitation of MO, it could hamper the interpretation of the experiments reported here where only the MO^+ product ion signal is analyzed. In the usual case (expected here), the M^+/MO^+ ratio should increase with increasing MO internal excitation, so that the product recoil energy distribution derived from the measured MO^+ lab angular distribution would be distorted, indicating too low a probability for low recoil energy (and high product internal excitation) reactive events. For example, this fragmentation ratio is very strongly dependent on internal excitation for ionization of alkali halides,[17] because of the weak ion-induced dipole bond in AX^+, so that it would be impractical to measure product AX scattering with the apparatus employed here.

However, this fragmentation ratio should be far less sensitive to internal excitation for ionization of MO because the MO^+ molecules should have appreciable bond dissociation energies (data in ref 18 suggest $D_0(BaO^+) \approx$ 70 kcal/mol). Mass spectral data are not available for the M^+/MO^+ fragmentation ratio of thermal CaO or SrO because the solid oxides vaporize with appreciable decomposition; data for BaO indicate[18] a Ba^+/BaO^+ ratio less than one. Furthermore, data on the Sr + NO_2 scattering reported in ref 2b indicate that, for lab scattering angles greater than ~25°, (1) the Sr^+ and SrO^+ lab angular distributions are of roughly the same shape; and (2) the SrO^+ intensity exceeds that of Sr^+ (by ~1.4). Feature 1 suggests that the Sr^+ signal arises largely from ionization of product SrO. Since the apparatus sensitivity for parent and daughter ions is approximately the same,[2b] feature 2 then indicates that the Sr^+/SrO^+ fragmentation ratio is less than one and is independent of lab scattering angle.[19] Thus, these arguments indicate that the CM product distributions, which are derived in this section by fitting measured lab MO^+ product angular distributions, cannot be significantly in error, although they could overestimate, somewhat, the fraction of the reaction energy which appears as product recoil.

Ba + SO_2. A strong BaO^+ signal was observed for scattering of Ba from SO_2. However, owing to the limited pumping capacity for SO_2 in the collision chamber, the background pressure was rather high (~6×10^{-6} Torr) during this experiment. Since the Ba beam path is rather long, this could have produced significant pressure broadening of the Ba beam, thereby introducing a possible viewing factor distortion of the measured lab product angular distribution.[20] Nevertheless, the strong BaO^+ signal observed indicates a large reactive cross section so that $D_0(BaO) \geq D_0(OS-O) = 129$ kcal/mol,[21] in agreement with the lower bound of 131.5 kcal/mol for $D_0(BaO)$ determined from a crossed-beam chemiluminescence study[22] of the Ba + NO_2 reaction.

Sr and Ca + NO_2. The fact that most of the wide angle scattering of Sr from NO_2 is due to reactive events indicates qualitatively that the cross section for this reaction is large, in agreement with the large Q_R value measured in ref 22. The lab product distributions from Sr and Ca + NO_2 shown in Figure 3 can be fit to a rather wide range of $T(\theta)$-$P(E')$ combinations. Figure 3 illustrates the range of $T(\theta)$ which can be fit to the Sr or Ca + NO_2 data for reasonable breadths in $P(E')$; less reasonable breadths (*e.g.*, a δ function) leads to broader $T(\theta)$ estimates. Nevertheless, the data, and further data analysis reported in ref 2b, clearly establish important qualitative reaction features. The Sr and Ca + NO_2 reactions show quite similar features; this is illustrated by the examples of CM distributions given in Table III. The average product recoil energy, $\langle E' \rangle$, is not well determined because of uncertainties in ΔD_0 as well as the insensitivity of the data at higher E' values; however, the dominate E' value, E', is relatively well characterized (~3–7 kcal/mol). Most importantly, $T(\theta)$ must definitely peak forward (although not necessarily precisely at 0°) with $Q_F > 0.50$ and asymmetry about $\theta = 90°$ so that the reactions proceed *via* a direct mechanism.

All of these features are in agreement with a previous crossed beams study of the Ba + NO_2 reaction.[23,24] These are also the same qualitative features reported for the Li + NO_2 reaction.[25] As pointed out in ref 25, the potential hypersurfaces for these reactions are expected to exhibit

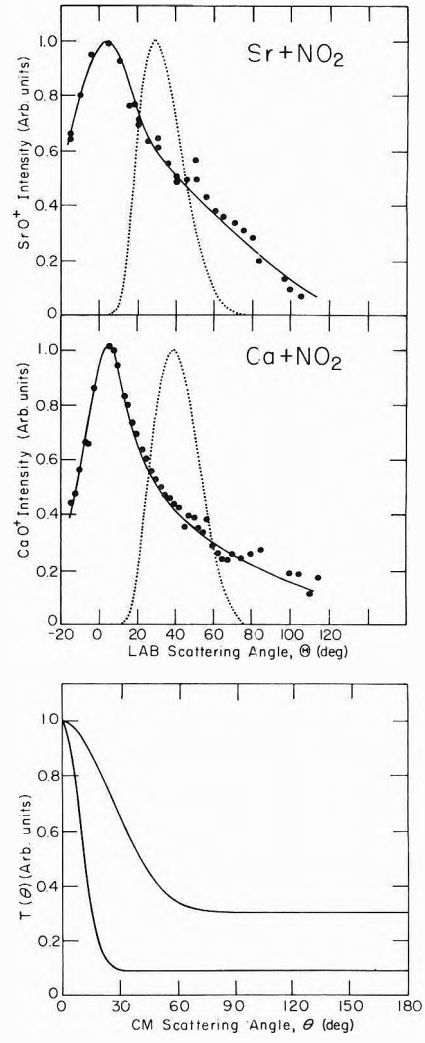

Figure 3. Two upper panels show lab product angular distributions from Sr and Ca + NO_2; solid curves through data points show fits provided by CM distributions given in Table III; dotted curves show calculated angular distributions of **C**. Lower panel shows range of "likely" CM product angular distribution for these reactions.

an inner well corresponding to formation of the MNO_2 intermediate,[26] a feature which *a priori* might have been expected to lead to a long-lived complex rather than direct reaction mechanism. The large reaction cross sections and forward product scattering which are observed suggest a reaction mechanism wherein the incoming M transfers an electron to the NO_2, and the NO_2^- which is formed immediately breaks up in the force field provided by the M^+ to form the MO + NO products.

Ba and Sr + $(CH_3)_2CHNO_2$. The K + CH_3NO_2 reaction proceeds with a large reactive cross section to give a practically isotropic product angular distribution;[27] electric deflection experiments on Cs + CH_3NO_2 have established that the products are $CsNO_2$ + CH_3.[28] Similar results have been reported for Li + CH_3NO_2,[25,29] although the product angular distribution, while still very broad, appears to favor forward scattering. Thus, it seemed of special interest to examine the reaction of Ba with a nitroalkane, as this reaction should provide an opportunity for the alkaline earth to directly assert its potential divalency, forming BaO rather than the $BaNO_2$ which would presumably form if Ba reacts *via* the mechanism characteristic of the analogous Cs reaction.

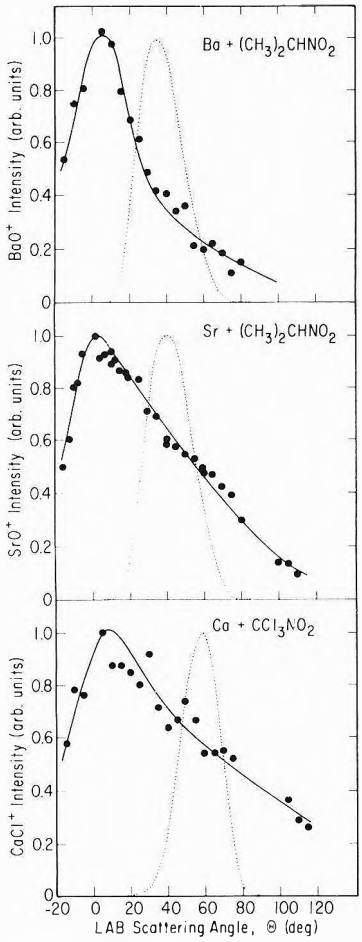

Figure 4. Measured lab angular distributions from Ba and Sr + $(CH_3)_2CHNO_2$ and Ca + CCl_3NO_2; conventions as in Figure 3.

Figure 4 shows the data measured for the reactions of Ba and Sr with 2-nitropropane.[30] For both reactions, MO^+ is the only alkaline earth containing product ion observed, although the signal-to-noise was such that MNO_2^+ (or MNO^+) should have been observed had it been present at as little as 5% of the MO^+ signal. Since MNO_2 would presumably involve a single ionic bond, its ionization should proceed *via* the removal of a nonbonding electron on the alkaline earth, suggesting that it would not be expected to fragment exclusively into MO^+. Thus, we feel that the most reasonable interpretation of the observed MO^+ product signal is that MO, rather than MNO_2, is formed *via* a direct reaction mechanism different from that characteristic of the alkali reactions.

Further support for this conclusion is provided by the shapes of the measured product angular distributions. Table III lists particular examples of CM distributions which will fit the data. Qualitatively, the product CM angular distributions resemble those shown for the NO_2 reaction in Figure 3, and other remarks regarding the CM distributions from the NO_2 reactions are generally applicable here. The data do support the general conclusion, however, that the BaO product is more sharply forward scattered (*i.e.*, larger Q_F value) than the SrO product. As for the NO_2 reactions, $\bar{E}'$ is a more reliable indication of the energy partitioning than is $\langle E' \rangle$. This is especially true for the Sr reaction because of uncertainties in ΔD_0. Indeed, the rather large cross section indicated by the data for this reaction would suggest that either D_0(SrO) in ref 31 is too low or that the $\Delta H_f°$(R-NO) − $\Delta H_f°$(R-NO_2) estimate from ref 32 is too high. At any rate, the outstanding qualitative feature of these reactions is their close similarity (especially for Ba) to the behavior of the M + NO_2 reactions. This suggests that they proceed *via* the same direct, electron-transfer intermediate mechanism.[33]

Ca + CCl_3NO_2. Table II indicates that, although a weak CaO^+ signal was seen as well, the predominate product signal observed for scattering of Ca from CCl_3NO_2 was $CaCl^+$. The measured lab $CaCl^+$ angular distribution is shown in Figure 4, and Table III provides an example of a CM distribution which adequately fits the data. In general, the CM distributions which will fit this data are similar to those found for the M + NO_2 and $(CH_3)_2CHNO_2$ reactions, so that this reaction presumably proceeds *via* a direct, electron-transfer intermediate mechanism. Comments presented on the likely shape of the true CM distributions for the NO_2 and R-NO_2 reactions are generally applicable to this reaction as well. Calculations reported in ref 2a indicate that the CM product angular distribution for Ca + CCl_3NO_2 does appear to be somewhat more sharply peaked in the forward direction than is that for Ca + CCl_4,[1d] suggesting that CCl_3NO_2 is a better electron acceptor than CCl_4. Although the nature of the molecular orbital in CCl_3NO_2 which accepts the donated electron is not known, the observation that CaCl (or $CaCl_2$) is the predominate product is not surprising since the $CCl_3NO_2^-$ intermediate would be expected to correlate asymptotically with Cl^- and CCl_2NO_2 by virtue of the large electron affinity of Cl. A similar effect is observed in the M + ICl reactions where MCl is the dominate product despite the fact that the donated electron initially enters a molecular orbital which is located primarily on the I side of the ICl molecule.[1b]

Conclusions

It seems natural to conclude these exploratory studies with some general comments on the contrasting gas-phase, single-encounter chemistry of alkaline earth and alkali atoms. One obvious possible cause of different behavior is the potential divalency of the alkaline earths. In this regard, it is gratifying that the M and Li + NO_2 reactions are quite similar, as these are the reactions for which the potential hypersurfaces are expected to be most similar. Results for the homonuclear diatomic halogens[1c] and methyl iodide[1d] also indicate that A and M atoms exhibit quite similar chemical behaviors when steric effects are likely to inhibit the potential attractive interactions between products which are expected for M, but not A, reactions. For some other reactions, on the other hand, A and M atoms show different chemical behaviors. There is some evidence for this contrasting behavior in the ICl reactions,[1b] and it is quite apparent in the CH_2I_2[1d] and R-NO_2 reactions.

Another possible cause for differences is the paired *vs.* unpaired valence structure of the reactant atoms. This would probably not be expected to be important for reactions proceeding *via* an electron-transfer intermediate which formed at large reactant separations. However, it suggests that the activation energies determined for the Ba, Sr, and Ca + HI reactions[1a] are surprising small, since the A + HI reactions would probably not proceed *via* a long-range electron transfer. At any rate, this effect or the relatively rapid rise in ionization potential (and consequent trend toward the "nonmetallic" regime) in the Ba → Mg sequence does give rise to contrasting reactivity

trends in the two families of reactions. Thus, although total reaction cross sections have not been determined, data reported here and in ref 1 indicate that Ba is as reactive as an alkali metal whereas Mg is observed to react only with halogen molecules, and Sr and Ca exhibit intermediate reactivities.[34] This behavior may be contrasted to the alkali metals, where reaction cross sections show only a modest decrease in the Cs → Li sequence.[35,36] It is interesting to note that vapor codeposition of Mg atoms and organics has recently been used in synthesis.[37] The contrasting reactivities of the alkaline earths might prove of importance in this regard if this proves to be a useful synthetic technique.

References and Notes

(1) (a) C. A. Mims, S. -M. Lin, and R. R. Herm, *J. Chem. Phys.*, **57,** 3099 (1972); (b) **58,** 1983 (1973); (c) S. -M. Lin, C. A. Mims, and R. R. Herm, *ibid.*, **58,** 327 (1973); (d) *J. Phys. Chem.*, **77,** 569 (1973).

(2) (a) S. -M. Lin, Ph.D. Thesis, University of California, Berkeley, 1972; (b) C. A. Mims, Ph.D. Thesis, University of California, Berkeley, 1973.

(3) (a) W. B. Miller, S. A. Safron, and D. R. Herschbach, *Discuss. Faraday Soc.*, **44,** 108 (1967); (b) G. A. Fisk, J. D. MacDonald, and D. R. Herschbach, *ibid.*, **44,** 228 (1967).

(4) S. J. Riley and D. R. Herschbach, *J. Chem. Phys.*, **58,** 27 (1973).

(5) Since Q_R is not measured here, τ_r cannot be estimated. Reference 4 cites τ_r estimates of $\sim 3\text{–}7 \times 10^{-12}$ sec for the analogous K–Cs + SF_6 reactions.

(6) S. Freund, G. A. Fisk, D. R. Herschbach, and W. Klemperer, *J. Chem. Phys.*, **54,** 2510 (1971); H. G. Bennewitz, R. Haertern, and G. Muller, *Chem. Phys. Lett.*, **12,** 335 (1971).

(7) S. A. Safron, N. D. Weinstein, D. R. Herschbach, and J. C. Tully, *Chem. Phys. Lett.*, **12,** 564 (1972).

(8) Actually, n should be 14 for break up into nonlinear $BaF_2 + SF_4$.

(9) R. P. Mariella, D. R. Herschbach, and W. Klemperer, *J. Chem. Phys.*, **58,** 3785 (1973), have observed less vibrational excitation of product LiF from Li + SF_6 than is expected on a statistical basis, indicating that these metal atom reactions with SF_6 need not always proceed *via* a complete energy randomization. Equation 3 might be expected to apply to the Ba + SF_6 reaction, however, because of the form of the measured product angular distribution.

(10) A similar argument is advanced in rationalizing the contrasting energy partitionings for different product channels of the Ba + Cl_2 reaction by M. Menzinger and D. J. Wren, *Chem. Phys. Lett.*, **18,** 431 (1973). It should also be noted that the exoergicity of channel II is sufficient to produce dissociation of the SF_4 product, an effect which might cause the measured $\langle E' \rangle$ value to be less than that predicted by eq 3 (see ref 9).

(11) D. D. Parrish and R. R. Herm, *J. Chem. Phys.*, **51,** 5467 (1969).

(12) J. C. Whitehead, D. R. Hardin, and R. Grice, *Mol. Phys.*, **23,** 787 (1972).

(13) K. R. Wilson and D. R. Herschbach, *J. Chem. Phys.*, **49,** 2676 (1968). As a cautionary note, however, it might be observed that this same paper incorrectly concluded that forward product scattering was favored in the Cs + $SnCl_4$ reaction due to poor kinematics and the approximate, early form of the data analysis procedure employed.

(14) The product velocity analysis measurements reported in ref 4 provide especially strong indirect evidence.

(15) Conclusions of the alkali experiments (ref 4 and 12) would probably be insensitive to any subsequent $ASnCl_3$ dissociation.

(16) Bond strengths in the tin chlorides are discussed in G. A. Oldershaw and K. Robinson, *J. Chem. Soc. A*, 2963 (1971).

(17) H. J. Loesch and D. R. Herschbach, *J. Chem. Phys.*, **57,** 2038 (1972).

(18) M. G. Inghram, W. A. Chupka, and R. F. Porter, *J. Chem. Phys.*, **23,** 2159 (1955).

(19) A crossed beams study of Ba + O_2 reached a somewhat similar conclusion regarding the Ba^+ and BaO^+ scattered signals: C. Batalli-Cosmovici and K.-W. Michel, *Chem. Phys. Lett.*, **11,** 245 (1971).

(20) Actually, estimates reported in ref 2b suggest that this pressure broadening should produce only negligible viewing factor distortion. If this is true, the data reported in ref 2b indicate that Ba + SO_2 → BaO + SO proceeds *via* a direct mechanism with a sharply forward peaked product CM angular distribution ($Q_F \approx 0.7\text{–}0.8$) and $\langle E' \rangle \approx 3\text{–}4$ kcal/mol.

(21) G. Herzberg, "Molecular Spectra and Molecular Structure III," Van Nostrand-Reinhold, New York, N. Y., 1966, recommends $D_0(OS\text{–}O) = 129$ kcal/mol but cautions that there are indications that it may be lower.

(22) C. D. Jonah, R. N. Zare, and Ch. Ottinger, *J. Chem. Phys.*, **56,** 263 (1972).

(23) J. A. Haberman, K. G. Anlauf, R. B. Bernstein, and F. J. Van Itallie, *Chem. Phys. Lett.*, **16,** 442 (1972).

(24) Our plans to study the Ba + NO_2 reaction as well so as to directly reproduce data reported by another laboratory were thwarted by an abrupt and (essentially) irreversible loss of apparatus sensitivity which brought these experiments to a premature end. However, ref 1c reports good agreement between our data on Ba + Cl_2 and that reported in ref 23.

(25) D. D. Parrish and R. R. Herm, *J. Chem. Phys.*, **54,** 2518 (1971).

(26) This is certainly true for Ca and Sr + NO_2. It is almost certainly true for Ba + NO_2 as well because an estimate of $D_0(Ba\text{–}NO_2)$, based on an empirical correlation between bond energy and length for ionic bonding (ref 27), suggests that $BaNO_2$ → BaO + NO is endoergic.

(27) R. R. Herm and D. R. Herschbach, *J. Chem. Phys.*, **52,** 5783 (1970).

(28) C. Maltz and D. R. Herschbach, *Discuss. Faraday Soc.*, **44,** 176 (1967).

(29) Actually, the identity of the product (LiO *vs.* $LiNO_2$) is not definitely established for this reaction.

(30) Nitropropane, rather than nitromethane, was chosen for study here in order that the detected product not be unduly heavier than the undetected product.

(31) L. Brewer and G. M. Rosenblatt, *Advan. High Temp. Chem.*, **2,** 1 (1969).

(32) S. W. Benson, "Thermochemical Kinetics," Wiley, New York, N. Y., 1968.

(33) Although negative ions of nitroalkanes are apparently unknown in the gas phase, $CH_3NO_2^-$ has been observed as an intermediate in the reaction of CH_3NO_2 with the hydrated electron; see A. Henglein, *Angew. Chem., Int. Ed. Engl.*, **5,** 256 (1966).

(34) Part, but not all, of this decreasing reactivity might simply be due to decreasing reaction exoergicities.

(35) Alkali metal studies are reviewed in J. L. Kinsey, "MTP International Review of Science," Vol. 9, J. C. Polanyi, Ed., Butterworths, London, 1972, Chapter 6.

(36) Exceptions to this statement arise when the reactions are practically thermoneutral (e.g., NO_2 or HCl).

(37) P. S. Skell and J. E. Girard, *J. Amer. Chem. Soc.*, **94,** 5518 (1972).

Isomerization of 1-Hexyl Radicals in the Gas Phase

K. W. Watkins

Department of Chemistry, Colorado State University, Fort Collins, Colorado 80521 *(Received June 21, 1973)*

1-Hexyl radicals were generated by the photolysis of azoethane in the presence of ethylene and high partial pressures (1060–2050 Torr) of sulfur hexafluoride. The thermal isomerization of 1-hexyl to 2-hexyl was studied in the temperature range 25–105°. The rate constant was found to be $\log k_{13}\ (\mathrm{sec}^{-1}) = 9.41 - (11.2 \times 10^3/2.3RT)$, where $R = 1.98$ cal mol^{-1} deg^{-1}. At 25° in the absence of SF_6, isomerization of vibrationally excited 1-hexyl radicals was observed. The average energy of the radicals when first formed was estimated to be 36 kcal mol^{-1}. The average rate constant for isomerization of 1-hexyl radicals with this energy was estimated from the experiments to be 5×10^7 sec^{-1}.

Introduction

There is almost a complete lack of quantitative kinetic data on alkyl radical isomerization *via* H-atom migration in thermal systems. The only isomerizations for which attempts have been made to measure Arrhenius parameters are 1-pentyl → 2-pentyl[1] and 1-hexyl → 2-hexyl.[2] Abnormally low A factors ($\sim 10^{7-8}$ sec^{-1}) and activation energies were reported in both cases. For several years it was recognized that these rate parameters were considerably in error, and higher values were supported.[3] Recently, a correction was made to the original *n*-pentyl isomerization data treatment which resulted in a much improved agreement between the estimated and experimental A factors.[4] The rate constant now appears to be $\sim 10^{11} \exp(-20 \times 10^3/RT)$ sec^{-1}.

The object of the present study was to reexamine the original system in which the rate parameters for 1-hexyl were determined[2] in order to locate the cause of the low A factor and if possible determine more reliable Arrhenius parameters.

In this system 1-hexyl radicals were generated from the photolysis of azoethane in the presence of ethylene. Some ethyl radicals added to ethylene to yield 1-butyl radicals, a fraction of which added to ethylene thus generating the 1-hexyl radical. The possible fates of 1-hexyl radicals were isomerization to 2-hexyl, addition to ethylene, and disproportionation and combination with ethyl radicals. The fate of 2-hexyl radicals was the same as that of 1-hexyl except that the rate of the reverse isomerization was negligible in the temperature range concerned.[2]

A number of improvements in technique have been implimented. In our early work[2] only hydrocarbons up to C_8 were analyzed by gas chromatography. The analysis has been extended to include C_{10} hydrocarbons. Also 3-methylheptane (the principal 2-hexyl product) can now be completely resolved from *n*-octane while earlier there was considerable overlap. In addition, the temperature range over which the isomerization was studied was changed from 80–130 to 25–105°. This results in a wider range of temperature, and the lower temperatures employed result in significantly less loss of 2-hexyl radicals by unwanted side reactions. Finally, since our early work the importance of the pressure dependence on excited radical isomerization has become better understood.[3] Thus high pressures of SF_6 (1060–2050 Torr) were added to ensure thermalization of essentially all 1-hexyl radicals.

Experimental Section

Azoethane was prepared by the oxidation of diethylhydrazine (Schuchardt) with HgO, and stored in the vapor phase in a blackened bulb. Gc analysis showed the purity of azoethane to be better than 98%. Ethylene (99.98%) was Phillips research grade. SF_6 was added as a moderator gas to each run. All gas handling was done with a conventional vacuum system with greaseless, Teflon plug, stopcocks. Pyrex reactors with volumes of 9.79 and 62.3 cm^3 were used. Unfiltered light (the lamp was placed in a Vycor lamp well) from a Hanovia 550-W medium pressure, mercury arc lamp was used for irradiation. The fraction of azoethane consumed in a run was typically ~0.20. The fraction of ethylene consumed was always less than 0.01.

After irradiation the entire reactant–product mixture was analyzed by vapor-phase gas chromatography using a 2-m alumina column (60–80 mesh). Temperature programming from 25 to 180° was required for the analysis up to C_8. An additional 20 min at 210° was required for *n*-decane to be eluted.

Products were detected by a flame ionization detector and the peak areas measured by a digital integrator. Authentic samples were used to calibrate peak areas as measured by the integrator in terms of moles of products.

Results and Rate Constant Calculations

The Mechanism. The hydrocarbon products, between C_2 and C_{10}, observed from the photolysis of azoethane in the presence of ethylene were ethane, *n*-butane, 1-butene, *n*-hexane, 1- and 2-hexene, 3-methylheptane, *n*-octane, 3-ethyl-5-methylheptane, 4-ethyloctane, 5-methylnonane, and *n*-decane. The rates of formation of products in five representative runs are given in Table I.

Reactions 1–16 were proposed previously to explain the observed products.[2,5]

$$C_2H_5N_2C_2H_5 + h\nu \longrightarrow 2C_2H_5 + N_2 \quad (1)$$

$$C_2H_5 + C_2H_4 \longrightarrow 1\text{-}C_4H_9 \quad (2)$$

$$2C_2H_5 \longrightarrow n\text{-}C_4H_{10} \quad (3)$$

$$2C_2H_5 \longrightarrow C_2H_4 + C_2H_6 \quad (4)$$

$$1\text{-}C_4H_9 + C_2H_5 \longrightarrow n\text{-}C_6H_{14} \quad (5)$$

$$1\text{-}C_4H_9 + C_2H_5 \longrightarrow 1\text{-}C_4H_8 + C_2H_6 \quad (6)$$

$$1\text{-}C_4H_9 + C_2H_5 \longrightarrow n\text{-}C_4H_{10} + C_2H_4 \quad (7)$$

TABLE I: Experimental Results for Five Typical Runs

Run[a]	Temp, K	(Azoethane)$_0$[b]	$(C_2H_4)_0$	n-C_4H_{10}[c]	1-C_4H_8	n-C_6H_{14}	1-C_6H_{12}	2-C_6H_{12}	3MHept[d]	n-C_8H_{18}	3E5MH[d]	5MN[d]	n-$C_{10}H_{22}$
	373	0.80	4.40	187	3.23	53.7	0.25	0.80	4.87	5.58	0.447	0.834	0.204
20	359	0.82	4.45	234	2.72	46.3	0.12	0.41	2.42	3.85	0.167	0.340	0.134
4	336	0.89	4.37	252	1.39	24.5	0.070	0.000	0.373	1.30	0.000		
6	312	0.89	4.23	271	0.606	11.3	0.008	0.000	0.0330	0.327			
11	297	1.58	8.57	151	0.48	8.6	0.013	0.000	0.0176	0.325			

[a] SF_6 partial pressure in runs 21, 20, 4, 6, and 11 were 1.4, 1.5, 2.0, 2.1, and 0.0 atm, respectively. [b] Reagent concentrations in mol cm^{-3} × 10^6. [c] Products are expressed in terms of mol cm^{-3} sec^{-1} × 10^{12}. [d] 3MHept = 3-methylheptane, 3E5MH = 3-ethyl-5-methylheptane, 5MN = 5-methylnonane.

$$1\text{-}C_4H_9 + C_2H_4 \longrightarrow 1\text{-}C_6H_{13} \quad (8)$$

$$2(1\text{-}C_4H_9) \longrightarrow n\text{-}C_8H_{18} \quad (9)$$

$$2(1\text{-}C_4H_9) \longrightarrow 1\text{-}C_4H_8 + n\text{-}C_4H_{10} \quad (9a)$$

$$1\text{-}C_6H_{13} + C_2H_5 \longrightarrow n\text{-}C_8H_{18} \quad (10)$$

$$1\text{-}C_6H_{13} + C_2H_5 \longrightarrow 1\text{-}C_6H_{12} + C_2H_6 \quad (11)$$

$$1\text{-}C_6H_{13} + C_2H_5 \longrightarrow n\text{-}C_6H_{14} + C_2H_4 \quad (12)$$

$$1\text{-}C_6H_{13} \longrightarrow 2\text{-}C_6H_{13} \quad (13)$$

$$2\text{-}C_6H_{13} + C_2H_5 \longrightarrow C_8H_{18}\ (3\text{-methylheptane}) \quad (14)$$

$$2\text{-}C_6H_{13} + C_2H_5 \longrightarrow 1\text{- and } 2\text{-}C_6H_{12} + C_2H_6 \quad (15)$$

$$2\text{-}C_6H_{13} + C_2H_5 \longrightarrow n\text{-}C_6H_{14} + C_2H_4 \quad (16)$$

The C_{10} products found here were assumed to result from reactions 17–26.

$$2\text{-}C_6H_{13} + C_2H_4 \longrightarrow C_8H_{17}\ (3\text{-methylheptyl}) \quad (17)$$

$$C_8H_{17} + C_2H_5 \longrightarrow C_{10}H_{22}\ (5\text{-methylnonane}) \quad (18)$$

$$2\text{-}C_6H_{13} + 1\text{-}C_4H_9 \longrightarrow C_{10}H_{22}\ (5\text{-methylnonane}) \quad (19)$$

$$C_8H_{17}\ (3\text{-methylheptyl}) \longrightarrow C_8H_{17}\ (5\text{-methyl-3-heptyl}) \quad (20)$$

$$C_8H_{17}\ (5\text{-methyl-3-heptyl}) + C_2H_5 \longrightarrow C_{10}H_{22}\ (3E5MH) \quad (21)$$

$$1\text{-}C_6H_{13} + C_2H_4 \longrightarrow 1\text{-}C_8H_{17} \quad (22)$$

$$1\text{-}C_3H_{17} + C_2H_5 \longrightarrow n\text{-}C_{10}H_{22} \quad (23)$$

$$1\text{-}C_6H_{13} + 1\text{-}C_4H_9 \longrightarrow n\text{-}C_{10}H_{22} \quad (24)$$

$$1\text{-}C_8H_{17} \longrightarrow 4\text{-}C_8H_{17} \quad (25)$$

$$4\text{-}C_8H_{17} + C_2H_5 \longrightarrow C_{10}H_{22}\ (4\text{-ethyloctane}) \quad (26)$$

No evidence for two reactions of particular interest was ever found. The 1,4 H-atom migration yielding a 3-hexyl radical, and the decomposition of 2-hexyl into propene and propyl radical were ruled out by the absence of 3-ethylhexane (which was separable from 3-methylheptane) and propene from the products.

Rate Constant for Thermal Isomerization of 1-Hexyl Radicals. The rate constant for 1-hexyl isomerization to 2-hexyl (reaction 13) was measured relative to that for 1-hexyl combination with ethyl (reaction 10).

$$\frac{R(2\text{-hexyl products})}{R(n\text{-octane})_{10}} = \frac{k_{13}}{k_{10}[C_2H_5]} \quad (i)$$

where R(2-hexyl products) = 1.4R(3-MHept) + R(3-ethyl-5-methylheptane) + R(5-methylnonane) and is the rate of formation of 2-hexyl products in moles cm^{-3} sec^{-1}. The factor 1.4 accounts for 2-hexyl radicals that react with ethyl radicals by disproportionation rather than combination. This factor was estimated previously.[2] The rates of formation of C_{10} products were not corrected for disproportionation because their contribution to R(2-hexyl products) was less than 0.2R(3-MHept). The concentration of ethyl radicals was estimated from the rate of formation of n-butane.

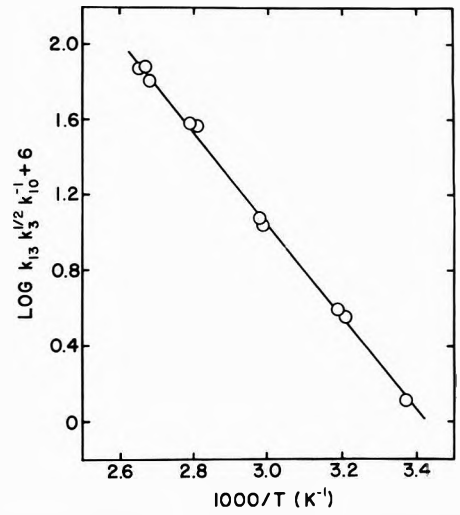

Figure 1. Arrhenius plot of the rate constant ratio $k_{13}k_3^{1/2}/k_{10}$.

$$[C_2H_5] = R^{1/2}(C_4H_{10})/k_3^{1/2}$$

The butane was corrected in the higher temperature runs for a small contribution (~2%) from reaction 7. R(n-octane)$_{10}$ was calculated by subtracting from the total R(n-octane) the octane resulting from reaction 9, *i.e.*, R(n-octane)$_{10}$ = R(n-octane) − R(n-octane)$_9$. R(n-octane)$_9$ was calculated as described previously.[2] The fraction R(n-octane)$_{10}$/R(n-octane) varied in the range from 0.32 at 378 K to 0.62 at 297 K.

Thus, the rate constant for 1-hexyl isomerization was calculated from the expression

$$\frac{k_{13}k_3^{1/2}}{k_{10}} = \frac{R(2\text{-hexyl products})}{R(\text{octane})_{10}} R^{1/2}(C_4H_{10}) \quad (ii)$$

The values of $k_{13}k_3^{1/2}/k_{10}$ obtained from expression ii are given in Table II, and in Arrhenius form in Figure 1. A least-squares treatment gave $\log(k_{13}k_3^{1/2}/k_{10}) = (2.44 \pm 0.04) - (11.2 \pm 0.1) \times 10^3/2.3RT$ where the uncertainties are the standard deviations, and R is 1.98 cal mol^{-1} deg^{-1}. Therefore, $E_{13} + \frac{1}{2}E_3 - E_{10} = 11.2$ kcal mol^{-1}, and since the activation energies for alkyl radical combi-

TABLE II: Relative Rate Constants

Temp, K	$(k_{13}k_3^{1/2}/k_{10}) \times 10^6$	Temp, K	$(k_{13}k_3^{1/2}/k_{10}) \times 10^6$
(a) Temperature Dependence			
378	74	336	12
374	77	334	11
373	64	313	3.9
359	38	312	3.6
356	37	297	1.3

Pressure, Torr	$(k_{13}k_3^{1/2}/k_{10}) \times 10^6$	k_a (sec^{-1})
(b) Pressure Dependence at 296 K		
188	1.3	
131	1.6	4×10^7
77	1.7	4×10^7
62	2.1	9×10^7
29	2.3	6×10^7

nation are essentially zero, then E_{13} = 11.2 kcal mol^{-1}. Taking log A_3 (cm^3 mol^{-1} sec^{-1}) = 13.34[6] and assuming $A_{10} = 2A_3$ leads to log A_{13} (sec^{-1}) = 9.41. The rate constant is log k_{13} (sec^{-1}) = $9.41 - (11.2 \times 10^3)/2.3RT$.

Pressure Dependence at 296 K. Previously, we pointed out that 1-hexyl radicals when first formed are vibrationally excited.[2] The average energy is 36 kcal mol^{-1} at 296 K. Since isomerization by 1,5 H-atom migration has an activation energy of only 11.2 kcal mol^{-1}, isomerization of the chemically activated radicals could occur and thus compete with thermal isomerization. Since the chemically activated radicals are stabilized by collision, high pressures (1–3 atm) of SF_6 were present in all the thermal runs. To ascertain the effects of pressure on the thermal rate constant several runs were carried out at 296 K in the absence of SF_6. From the data in Table IIb one can see that at pressures below about 200 Torr the apparent thermal rate constant increases as the pressure decreases. Since $k_{13}k_3^{1/2}/k_{10}$ should be pressure independent (assuming k_{13} is in the high-pressure region), the increase is assumed to be due to the isomerization of chemically activated 1-hexyl radicals which are not stabilized by collision below 200 Torr. The isomerization of chemically activated alkyl radicals has been reported previously.[3] For runs carried out at low pressure, the following reactions must be considered

$$1\text{-}C_4H_9 + C_2H_4 \longrightarrow 1\text{-}C_6H_{13}^* \qquad (8')$$

$$1\text{-}C_6H_{13}^* + M \xrightarrow{\omega} 1\text{-}C_6H_{13} + M\ (S) \qquad (8'')$$

$$1\text{-}C_6H_{13}^* \xrightarrow{k_a} 2\text{-}C_6H_{13}^*\ (I) \qquad (27)$$

$$2\text{-}C_6H_{13}^* + M \longrightarrow 2\text{-}C_6H_{13} + M \qquad (28)$$

The average rate constant k_a for isomerization of chemically activated 1-hexyl radicals was estimated from the expression $k_a = \omega(I/S)$ where I is the 3-methylheptane resulting only from chemically activated isomerization which is the difference between R(3-MHept) and R(3-MHept)$_{thermal}$ where $R(3\text{-MHept})_{thermal} = (k_{13}k_3^{1/2}/1.4k_{10})R(n\text{-octane})_{10}/R^{1/2}(C_4H_{10})$. S is the sum of all the products resulting from stabilization of excited 1-hexyl radicals, and is given by $S = R(n\text{-octane})_{10} + R(3\text{-MHept})_{thermal}$, and ω is the collision frequency of 1-hexyl* with bath molecules. The values of k_a calculated in this manner appear in Table IIb. These indicate that $k_a \leq 5 \times 10^7$ sec^{-1}. This result is an upper limit because stabilization (reaction 8″) was considered to occur on every collision of chemically activated 1-hexyl radicals.

Discussion

Thermal 1-Hexyl Radical Isomerization. A comparison of the present results with the earlier ones shows that the origin of the low Arrhenius parameters in the early work[2] was the spread in the data at 80°, and that these points were generally high. In addition, the inclusion of the C_{10} products in the present work raised the high-temperature relative rate constants by 15–20% whereas the low-temperature rate constants were not significantly affected.

One additional source of systematic error will be considered here. This is H-atom abstraction by 2-hexyl radicals to give *n*-hexane. The fraction of 2-hexyl undergoing this reaction could not be measured because *n*-hexane has several sources, principally reaction 5. The fraction of 2-hexyl radicals abstracting H atoms will depend on the temperature and the ethyl radical concentration. Two runs at 105° were carried out using filtered light which caused the C_2H_5 concentration to drop. In these runs the C_{10} products increased markedly, but the value of $k_{13}k_3^{1/2}/k_{10}$ was low presumably due to the loss of 2-hexyl radicals *via* H-atom abstraction. The importance of H-atom abstraction was roughly estimated by using the rate constant for abstraction by 1-pentyl.[1b] H-atom abstraction could account for 40% of the 2-hexyl radicals in the runs at 105° using filtered radiation, but this fraction dropped to only 4% when unfiltered radiation was used. This fraction becomes insignificant as the temperature is lowered. Thus, under the conditions used here of temperatures in the range of 25–105°, and using unfiltered light, H-atom abstraction by 2-hexyl was not important.

The A factor found here corresponds to $\Delta S^* = -17.6$ cal deg^{-1} mol^{-1}. This value is reasonable since it can be accounted for in terms of the freezing of four internal rotations on forming the activated complex as explained in ref 2. This result in conjunction with the recalculated A factor for 1-pentyl isomerization[4] shows that no special explanations are needed to rationalize the A factors as was necessary in the past.[1]

Isomerization of Chemically Activated 1-Hexyl Radicals. In the results section the rate constant for isomerization of 1-hexyl radicals excited to ~36 kcal mol^{-1} by reaction 8′ was estimated to be 5×10^7 sec^{-1}. This compares with a rate constant of 3.3×10^6 sec^{-1} for isomerization of 1-pentyl radicals excited to 34 kcal mol^{-1}.[3a] In the case of 1-pentyl radicals an activated complex model was used to calculate rate constants k_E as a function of energy using the RRKM theory expression for k_E. In that case the model was assumed to be essentially correct and the threshold energy was varied until agreement was found between the observed rate constant and k_E at 34 kcal mol^{-1} as calculated by the RRKM theory. The threshold energy for 1-pentyl isomerization by 1,4 H-atom migration was estimated in this way.

In the case of 1-hexyl radicals we will use the threshold energy consistent with the activation energy found here, and an activated complex model where vibration frequencies are assigned in the same fashion as for 1-pentyl to determine whether the RRKM theory will calculate a k_E in agreement with that observed.

Vibration frequencies for the isomerization complex were deduced by a procedure explained in detail in ref 3a.

TABLE III: Frequency Assignments for the Isomerization Complex (cm^{-1})

Ring deformations (12)	CH stretch (12)	Ring CH_2 modes (16)
1100 (2)	2933 (6)	CH_2 rock 940 (4)
1037 (3)	2871 (6)	CH_2 wag 1340 (4)
842 (2)		CH_2 twist 1250 (4)
458 (2)	CH bend (2)	CH_2 scissors 1450 (4)
248 (2)	1319	
reaction coordinate	936	

Modes related to the methyl group (9)	
CH_3 deformations (3)	1462 (2), 1374
CH_3 rock (2)	1168, 950
CC stretch	1000
C–C–C bend (2)	332, 418
CH_3 torsion	194

TABLE IV: Contribution of Chemically Activated Isomerization

Run	p_{total}[a]	k_a/ω	$S \times 10^{12}$ [b]	$I \times 10^{12}$	I/R· (3MHept)
21	1140	0.0028	6.60	0.018	0.0037
20	1220	0.0026	3.97	0.010	0.0041
4	1600	0.0019	1.07	0.002	0.0028
6	1680	0.0019	0.54	0.001	0.0030
11	188	0.017	0.25	0.004	0.24

[a] Torr, see Table I for partial pressure of SF_6. [b] Units, mol cm^{-3} sec^{-1}.

Published frequencies for cyclohexane[7] were used to assign the 12 ring deformation modes. The CH_2 twists, wags, bends, and rocks were also taken from cyclohexane. The full assignment is given in Table III. This activated complex model corresponds to log $A = 10.0$ and $E_{expt} - E_0 = -1.4$ kcal mol^{-1} at 298 K, where E_0 is the threshold energy, and E_{expt} is the activation energy. The calculational procedure used for the RRKM theory was described previously.[3a]

Using the frequency assignment in Table IV and a threshold energy of 12.6 kcal mol^{-1}, the rate constant was calculated to be 5.7×10^7 sec^{-1} at 36 kcal mol^{-1}. The agreement is very good, but not as good as it appears because the frequencies used for the activated complex correspond to log $A = 10^{10.0}$ whereas if the model corresponded to log $A = 9.41$ (the experimental result), k_E would equal about 2×10^7 sec^{-1}. Still the agreement tends to give confidence about the rate constants, threshold energies, and activated complex assignments found for 1-pentyl,[3a] 1-hexyl, and 3-methyl-1-butenyl radicals.[8]

Since all 1-hexyl radicals when first formed are vibrationally excited, it is necessary to show that isomerization of chemically activated 1-hexyl radicals does not contribute to the observed rate of formation of 2-hexyl products in the runs used to calculate $k_{13}k_3^{1/2}/k_{10}$. The rate of formation of 2-hexyl radicals from the isomerization of chemically activated 1-hexyl radicals is $I = (k_a/\omega)S$ where $S = R(\text{octane})_{10} + R(3\text{MHept})$. The ratio $I/R(2\text{-hexyl products}) \simeq I/R(3\text{MHept})$ is approximately the contribution of chemically activated isomerization to total isomerization. This fraction is listed in Table IV for the five typical runs given in Table I. From the ratio $I/R(3\text{MHept})$ it is concluded that the contribution of chemically activated isomerization could not affect the calculation of $k_{13}k_3^{1/2}/k_{10}$, except in run 11.

References and Notes

(1) (a) L. Endrenyi and D. J. LeRoy, *J. Phys. Chem.*, **70**, 4081 (1966); (b) K. W. Watkins, *J. Amer. Chem. Soc.*, **93**, 6355 (1971).
(2) K. W. Watkins and L. A. Ostreko, *J. Phys. Chem.*, **73**, 2080 (1969).
(3) (a) K. W. Watkins and D. R. Lawson, *J. Phys. Chem.*, **75**, 1632 (1971), and references therein; (b) E. A. Hardwidge, C. W. Larson, and B. S. Rabinovitch, *J. Amer. Chem. Soc.*, **92**, 3278 (1970); (c) C. W. Larson, P. T. Chua, and B. S. Rabinovitch, *J. Phys. Chem.*, **76**, 2507 (1972), and references therein.
(4) K. W. Watkins, *Can. J. Chem.*, **50**, 3738 (1972).
(5) K. W. Watkins and L. A. O'Deen, *J. Phys. Chem.*, **73**, 4094 (1969).
(6) N. Basco, D. G. L. James, and R. D. Suart, *Int. J. Chem. Kinet.*, **2**, 215 (1970).
(7) H. Takahashi, T. Shimanouchi, K. Fukushima, and T. Miyazawa, *J. Mol. Spectrosc.*, **13**, 43 (1964).
(8) K. W. Watkins and L. A. O'Deen, *J. Phys. Chem.*, **75**, 2665 (1971).

The Kinetics and Mechanism of the Heterogeneous Reactions of Crystallized Gibbsite Powders with Aqueous Sodium Hydroxide Solutions

A. Packter* and H. S. Dhillon

Chemistry Department, North East London Polytechnic (formerly West Ham College of Technology), London E. 15, England
(Received March 22, 1973)

The heterogeneous reactions of dilute suspensions of a series of crystallized Gibbsite powders, initial particle size l_0 varying from 2 to 55 μ, with well-stirred sodium hydroxide solutions in large excess were studied from 35 to 65°. Reaction solids and solutions were analyzed by different physical and chemical methods after various reaction times. The reactions were four-thirds order with respect to powder weight (second order with respect to powder effective surface area) and first order with respect to the mean ionic activity of the hydroxide solution. For the reactions of GiA (l_0 = 55 μm), GiB (l_0 = 38 μm), GiC (l_0 = 20 μm), Gi1D (l_0 = 6.5 μm), and Gi1E (l_0 = 2.2 μm) with sodium hydroxide solution of unit mean ionic activity, the rate constants k_{w1} ($g^{-1/3}$ hr^{-1}) at 65° were 0.078, 0.087, 0.120, 0.200, and 0.640, respectively. The rate constants for reaction with any hydroxide solution increased about nine times for a 30-fold increase in initial overall surface area. The Gibbsite crystals consisted of aggregates of smaller cubic "crystallites;" the rate constants depended on the size of these crystallites and the initial effective surface areas of the powders. The rate constants increased exponentially with reciprocal absolute temperature by a factor of four to five for a 15° temperature rise. Energies of activation varied from 92 to 97 kJ/mol. The rate-determining step for Gibbsite dissolution appears to be the reaction between hydrated hydroxyl ions adsorbed on the crystallite surfaces and adjacent reactive $Al(OH)_3$ sites.

Introduction

Heterogeneous reactions between inorganic solids and aqueous alkali solutions are of some theoretical interest. The kinetics of dissolution of silica powders by sodium and calcium hydroxide solutions has been studied by several workers.[1-6] Greenberg[6] and Halstead[3] confirmed that the rate of reaction (at high stirring speeds at 30–80°) varied linearly with residual surface area of powder and then as (residual powder weight)$^{2/3}$ and, in dilute hydroxyl solutions, also with the hydroxyl ion activity. The reactions with high surface area powders were very rapid but the reaction with coarse silica powders (2–100 μ) in this temperature range was not very significant. Few quantitative studies[7,8] have been reported on the reactions of aluminum oxides, hydrated oxides, and hydroxides with aqueous alkali solutions; these reactions are of some practical import in extractive metallurgy[9] and cement chemistry.[10] Bielanski[7] carried out some preliminary studies on the reactions of gibbsite and its dehydration products with a sodium hydroxide solution at 100°; he did not determine any reaction order (or rate constants) and made no systematic study of the variation of reaction rates with different parameters. Schrader[8] made detailed investigations of the reactions of ground gibbsites, boehmites and aluminas with a sodium hydroxide solution at one temperature; grinding modified both particle size and the crystal structure and reactivity of these materials but this worker did not study these two effects separately. Therefore, further systematic work on these reactions would be of value.

This paper presents a detailed study of the kinetics of the reactions of a series of crystallized gibbsite powders (prepared by the Bayer process) with well-shaken sodium hydroxide solutions in large excess at 20–65°. The reactions are chemically rate controlled under these conditions. The variation of rate constants with overall powder surface area and crystal structure and with temperature (and mean ionic activity) of the reaction solution was studied in detail. Activation energies were determined. A reaction mechanism for the rate-determining step of gibbsite dissolution is discussed.

Experimental Section

Materials. Gibbsite powder (Gi), particle size ranging from 4 to 60 μ (prepared by crystallization from a sodium aluminate solution), was supplied by the Aluminum Company of America (Alcoa).

GiA, -B, -C, and -D Powders. A 2% Gi suspension was prepared in 0.001 *M* sodium hydroxide solution and sedimented in 500-ml cylinders. Fractions GiA (50–60 μm, average crystal length l_0 = 55 ± 3 μm), GiB (30–50 μm, l_0 = 38 ± 2 μm), GiC (10–30 μm, l_0 = 20 ± 1 μm), and GiD (3–10 μm, l_0 = 6.3 ± 0.3 μm) were collected, washed, and dried to constant weight at 100°.

Gi powder was ground for 10 min in a pestle and fractionated as above. Fraction Gi(10 m)D (l_0 = 6.5 ± 0.5 μm) was collected and dried.

Gi1D and -1E Powders. Gi powder was ground in a ball mill for 1 hr and the ground material was fractionated as above. Fractions Gi1D (3–10 μm, l_0 = 6.5 ± 0.5 μm) and Gi1E (1–3 μm, l_0 = 2.2 ± 0.3 μm) were collected and dried.

These powders were analyzed by different chemical and physical methods. Chemical analysis was by standard methods.[11]

X-Ray Diffraction.[12] The X-ray diffraction pattern was photographed with a Phillips 11.4-cm powder camera, using Co radiation, Fe filtered. The sample was mounted in a 0.3-mm diameter beryllium glass capillary and rotated continuously during the 6-hr exposure. The d spacings

were measured and the patterns compared with those given in the ASTM X-ray powder data file 1969.

Infrared Spectrophotometry.[13] The dried powders were reground in an agate mortar to <2 μm size and dispersed in potassium bromide disks under pressure of 15 tons over the area of the disks. The spectra were obtained on an Infra-Scan ir spectrophotometer against a pure potassium bromide reference disk of the same thickness; the time for scanning from 4000 to 650 cm^{-1} was 16 min.

Thermogravimetric analysis was by standard methods.[14a]

Differential Scanning Calorimetry. The powders (10 mg) were scanned at 16°/min in a Perkin-Elmer differential scanning calorimeter (DSC-1B) over the range 20–500°.

Optical Microscopy.[15] Small amounts of powder were dispersed in a trace of glycerol and batches of 200 crystals were studied with a Swift PN polarizing microscope at magnification ×40 to ×140. Maximum lengths (l_x) were noted and the numbers $n_{j-1,j}$ of crystals in ten equivalent length ranges $0 - l_1 \ldots l_{j-1} - l_j \ldots l_{x-1} - l_x$ were determined. The average initial crystal lengths (l_0) were estimated as

$$l_0 = \left(\sum_{j=1}^{j=x} n_{j-1,j} l_{j-1,j}^{\,3} / \sum_{j=1}^{j=x} n_{j-1,j}\right)^{1/3} \text{ cm}$$

where $l_{j-1,j} = (l_{j-1} + l_j)/2$.

Overall initial surface areas (S_0) were estimated as

$$S_0 = 6\sum_{j=1}^{j=N} n_{j-1,j} l_{j-1,j}^{\,2} / \rho \sum_{j=1}^{j=N} n_{j-1,j} l_{j-1,j}^{\,3} \text{ cm}^2 \text{ g}^{-1}$$

where ρ is the density of gibbsite.

Chemical and physical properties (other than particle size distribution) were not affected by 1 hr grindings. The chemical analysis of the powders was 0.998 $Al(OH)_3$, 0.002 Na_2O, 0.0002 Fe_2O_3, and <0.0001 SiO_2.

The X-ray diffraction pattern contained the main lines of gibbsite and no lines of bayerite or boehmite were noted; this indicates >0.98 gibbsite content. No diffuse lines from amorphous material were noted.

The ir spectra were identical with those reported for pure natural hydrargillite.[13]

The thermal gravimetric analysis (TGA) thermograms were similar to those reported for pure gibbsite ;[14a] weight losses at 300 and 1000° indicated 0.995 $Al(OH)_3$ content. The differential scanning calorimeter (DSC) thermograms showed decomposition (to boehmite) from 260 to 340° with a peak at 315–320°; $(-\Delta H)$ for this decomposition varied from 790 to 810 J/g. These thermograms were similar to Brindley's differential thermal analysis thermograms for a pure crystallized gibbsite.[14b]

Optical Microscopy. Gibbsites GiA to GilE cyrstals were roughly cubic in form; these coarser crystals were in turn made up of aggregates of smaller cubic "crystallites" of 2–10 μm length. A similar structure was reported by previous workers[16] for "Bayer" crystals grown from sodium aluminate solutions.

Sodium hydroxide solutions (0.5–10 M) were prepared from AR material in double glass-distilled CO_2-free water. Hydroxide concentrations were determined by titration against standard hydrochloric acid. Mean ionic activities at temperatures up to 70° were obtained from Åckerlof's work.[17]

EDTA solution (0.1 *M*), zinc sulfate solution (0.01 *M*), and acetic acid–ammonium acetate buffer solution (1 *M*) for Al analysis were prepared from AR materials in double distilled water. Dithizone solution (0.001 *M*) was prepared from 0.025 g of B.D.H. reagent dissolved in 100 ml of 95% ethanol.

Reaction Procedure

Gibbsite powder (initial weight W_0 = 0.8 g) was completely redispersed in large excess (100 ml) aqueous sodium hydroxide solution in a Quickfit flask by vigorous shaking at 1000 vibrations/min for 15 sec. The reaction flask was then shaken at 240 vibrations/min for the reaction proper in a Dubnoff shaker-water bath,[18] thermostated at ±1°.

Aliquots of the reaction solution (1 ml) were withdrawn for chemical analysis after different reaction times. This aliquot was diluted to 10 ml and centrifuged at 1000 rpm for 5 min to remove any traces of suspended fine powder that would react with the EDTA solution; 5-ml solutions were then withdrawn and analyzed for aluminate anion by a modified Waenninen's method.[19] 0.01 *M* EDTA solution (5 ml) and 1 *M* acetic acid–ammonium acetate buffer solution (10 ml) were added and the solution was heated to 80° for 2 min to convert all aluminate to complexed aquoaluminum cation at pH 4.5; the solution was cooled and then 95% ethanol (10 ml) and 0.001 *M* dithizone solution (2 ml) were added. The excess EDTA was back-titrated against zinc sulfate (0.01 *M*) from a microburet. Then 1 ml of the reacted EDTA solution = 0.7800 mg of $Al(OH)_3$ dissolved as aluminate.

In several runs, a series of separate flasks, each containing the same suspension, was used and successive flasks were removed from the bath after different times. The unreacted powder from each flask was washed with distilled water, filtered, and dried to constant weight W_t at 100°. The physical properties of these powders were studied by the methods described above.

Results

Physical and Chemical Changes. A series of gibbsite powders, of initial average crystal lengths l_0 = 6–55 μm, was prepared by sedimentation of a gibbsite powder crystallized from sodium aluminate solution. Two other powders, l_0 = 2–6 μm, were prepared by 1-hr ball-milling and sedimentation. The powders were dispersed as 0.8 g/100 ml suspensions in sodium hydroxide solutions of concentrations C = 0.5–10 *M* and their dissolution was studied at 35–65°. The hydroxide concentration was in large excess; this eliminated any variation of reaction rate with hydroxide concentration during a run, simplified the kinetics, and allowed separate study of the effect of initial powder surface area and hydroxyl ion activity.

The gibbsite powders first adsorbed rapidly from one to more than three monolayers of hydroxyl ion and then dissolved to form aluminate anion.[18] Solid and reaction solution were analyzed after different times of reaction. The residual solid weights (W_t) and gibbsite crystal lengths (l_t) decreased continuously during the reaction. The crystals retained their cubic form for over 80% reaction and so the dissolution was three directional.

The X-ray diffraction patterns, ir spectra, and the TGA and DSC thermograms of the solids were not modified after 80% reaction with hot sodium hydroxide solution. That is, the solid retained the composition $Al(OH)_3$ and there was no dehydration to AlOOH during prolonged contact with this solution. The aluminate concentrations $(W_{sol})_t$ in solution, as determined by the modified Waen-

ninen method, were found equivalent in all cases to the weight losses ΔW_t of the gibbsite solids.

Diffusion. The rate of diffusion of hydroxyl ions from sodium hydroxide solution of activity a (g/ml) to the surface of suspended particles of length l (cm) would generally be

$$(dW_{OH}/dt)_D = Sh\ Da/l\ g\ cm^{-2}\ sec^{-1}$$

D ($cm^2\ sec^{-1}$) is the diffusion coefficient of the hydroxyl ions, $Sh = [2 + 0.6Re^{0.5}Sc^{0.33}]$ is the dimensionless Sherwood number; in turn, $Re = (vl\rho_{sol}/\eta_{sol})$ and $Sc = (\eta_{sol}/\rho_{sol}D)$ where v is the particle velocity, and η_{sol} and ρ_{sol} are the viscosity and density of the solution. In well-stirred suspensions, Re would be determined by the stirring rate. In poorly stirred suspensions of particles of length $l < 0.0025$ cm, Re would be determined by the terminal velocity of the particles through the liquid and Sh might approach the value Sh = 2 for an infinite stagnant medium;[20,21a] the minimum rate of transfer of hydroxyl ions would then be

$$\left(\frac{dW_{OH}}{dt}\right)_{D\,min} = \frac{2Da}{l}\ g\ cm^{-2}\ sec^{-1} = \frac{120Da}{l}\ g\ cm^{-2}\ min^{-1}$$

In poorly stirred suspensions of coarser particles of length $l \geq 0.0025$ cm, the mass transfer rate approaches a lower minimum value of $(dW_{OH}/dt)_{D\,min} = 120Da/0.0025 = 0.48 \times 10^{-3}\ D\ a$ g $cm^{-2}\ min^{-1}$. The minimum $(dW_{OH}/dt)_{D\,min}$ values for diffusion of hydroxyl ions from sodium hydroxide solutions at 65° to the surfaces of the gibbsite particles studied in this work were then estimated from the above equations. For these diffusions, $l = l_0$; $D_{C,T}$ values were estimated from electrical equivalent conductivities from the relation[21a] $D_{C,T} = (\Lambda_{C,T}/\Lambda_{0.25})D_{0.25}$ ($\Lambda_{C,T}$ values were taken from the work of Mehta[21b] and Klochko[21c] and $D_{0.25}$, $\Lambda_{0.25}$ are the values for infinite dilute solutions at 25°). a values were assumed equal to the mean ionic activities $a_\pm$.[17] The results were as follows:

for GiA (and GiB)/2M NaOH solution,
$(dw_{OH}/dt)_{Dmin} = 20 \times 10^{-3}$ g $cm^{-2}\ min^{-1}$

	/4 M	37
	/6 M	63
	/8 M	74
for GiC	/2 M	24
	/4 M	46
	/6 M	73
	/8 M	88
for GilD	/1 M	40
	/2 M	73
	/4 M	132
	/6 M	210
and for GilE	/1 M	140
	/2 M	230
	/3 M	350
	/4 M	460

Low suspension permeabilities might reduce the Sherwood numbers to some extent[22] but the shaking conditions used in this work would still probably result in overall Sherwood numbers $Sh \gg 2$; the actual rates of diffusion of hydroxyl ions would then be many times the estimated minimum values.[20]

On the other hand, the experimentally measured initial rates of dissolution of gibbsites GiA to Gi1E, expressed as $(dW_{OH}/dt)_{exp}$, the rate of reaction of hydroxyl ion per cm^2 powder surface at 65° were as follows:

for GiA (and B)/2 M NaOH solution,
$(dw_{OH}/dt)_{exp} = 0.1 \times 10^{-3}$ g $cm^{-2}\ min^{-1}$

	/4 M	0.2
	/6 M	0.35
	/8 M	0.5
for GiC	/2 M	0.1
	/4 M	0.2
	/6 M	0.3
	/8 M	0.4
for Gi1D	/1 M	0.05
	/2 M	0.1
	/4 M	0.2
	/6 M	0.4
and for Gi1E	/1 M	0.05
	/2 M	0.1
	/3 M	0.2
	/4 M	0.3

These rates were not modified by increasing the shaking rate to 600 vibrations/min.

The experimental rates were several hundred times lower than the corresponding minimum rates of mass transfer of hydroxyl ions by diffusion, as estimated above. The minimum rates of diffusion at 35° were estimated in the same manner; these were about one-half the minimum diffusion rates at 65°. On the other hand, the experimental initial rates at 35° were about one-twentieth the experimental rates at 65°. These values indicated also that the energy of activation for the dissolution of gibbsite was far higher, over this temperature range, than $E_{act\,D}$ = 20–25 kJ/mol, the energy of activation for diffusion of hydroxyl ions in sodium hydroxide solutions.

These results all confirmed that the measured rates were actually the rates of slow chemical reactions at the powder crystal surfaces; the reactions were chemically rate controlled and the rates were not modified by (even slower) diffusion effects.

Reaction Kinetics

The kinetics of heterogeneous solid–liquid reactions are generally studied by measurement of residual solid weight (W_t) after different reaction times. W_t values were, in turn, conveniently determined by analysis of the reaction solution for $(W_{sol})_t$; then $W_t = (W_0 - \Delta W_t) = [W_0 - (W_{sol})_t]$.

A few per cent of high defect surface material dissolved rapidly. The rate of reaction then decreased concomitantly with decrease in powder weight and surface area. For over 80% dissolution (over the range $(W_t/W_0)^{-1/3} = 1.04$–2) the function $[(W_t/W_0)^{-1/3} - 1] = (\alpha_t^{-1/3} - 1)$ varied linearly with reaction time t. Typical results are presented in Figure 1 and other figures and are available on microfilm (see paragraph at end of paper regarding supplementary material). The gibbsite powders then reacted with hydroxide solutions (in large excess at constant concentration) according to a four-thirds order mechanism with respect to residual powder weight (and second order with respect to residual powder surface area); at any time

$$dW/dt = -k_w W_t^{4/3}\ g\ hr^{-1} \qquad (1)$$

where k_w is the rate constant with respect to powder weight (units in $g^{-1/3}\ hr^{-1}$). Integrating eq 1

TABLE I: Reactions of Gibbsite Powders with Well-Stirred Sodium Hydroxide Solutions[a]

		k_w, $g^{1/3}$ hr^{-1}					
C, M	$a_\pm$, M	GiA (S_0 = 0.04 m^2/g)	GiB (S_0 = 0.06 m^2/g)	GiC (S_0 = 0.12 m^2/g)	Gi(10 m)D (S_0 = 0.38 m^2/g)	Gi1D (S_0 = 0.37 m^2/g)	Gi1E (S_0 = 1.1 m^2/g)
0.5	0.34					0.074	0.156
1	0.68			0.070	0.122	0.148	0.307
1.5	0.97					0.206	0.644
2	1.33	0.102	0.115	0.141	0.259	0.243	0.928
2.5	1.78						1.26_4
3	2.18					0.438	1.85_6
4	3.28	0.234	0.272	0.410	0.605	0.672	3.52_5
5	4.73					1.11_6	
6	6.66			0.912		1.44_8	
8	12.5			1.72_4			
	k_{w1} at $a_\pm$ = 1 M	0.078	0.087	0.120	0.200	0.200	0.600

[a] W_0 = 0.8 g/100 ml suspension. Rate constants (k_w) at 65°.

$$dW/W_t^{4/3} = -k_w\,dt$$

therefore

$$3\left[\frac{1}{W_t^{1/3}} - \frac{1}{W_0^{1/3}}\right] = \frac{3}{W_0^{1/3}}[\alpha_t^{-1/3} - 1] = k_w t$$

where

$$\alpha_t = W_t/W_0, \text{ and } k_w = \frac{3}{W_0^{1/3}}\left[\left(\alpha_t^{-1/3} - 1\right) \text{ vs. } t \text{ plot}\right] g^{-1/3}\ hr^{-1} \quad (2)$$

Rate constants (k_w) were determined from the gradients of the ($\alpha_t^{-1/3} - 1$) *vs.* t plots, according to the above equation. Typical results for reactions of various gibbsites at 65° are collected in Table I; mean ionic activities are also included.

Hydroxide Ion Concentration. The rate of dissolution of the powders increased linearly with hydroxide concentration up to C = 3–4 M and then more rapidly. The rate constants increased linearly with the mean ionic activity (a_α) of the reaction solutions up to $a_\pm > 15$ M; see Figure 2. That is

$$k_w = k_{w_1} a_\pm \quad g^{-1/3}\,hr^{-1} \quad (3)$$

where $k_w = k_{w1}$ at $a_\pm = 1$ M. Equation 1 then becomes, more generally

$$dW/dt = -k_{w_1} W_t^{4/3} a_\pm \quad g\ hr^{-1} \quad (4)$$

k_{w1} values were estimated from the k_w *vs.* $a_\pm$ plots for the different gibbsites and are included in Table I.

Surface Area. The rate of dissolution of any fraction was not affected by grinding for up to 1 hr. The rate of reaction with any hydroxide solution increased with increase in the overall powder surface area. Gi1E powder of initial surface area S_0 = 1.1 m^2/g reacted about nine times more rapidly than GiA powder of S_0 = 0.04 m^2/g, that is, for a 30-fold increase in surface area.

Temperature. The rate of dissolution of the gibbsites by any hydroxide solution increased by a factor of 4–5 for a 15° temperature rise; rate constants varied exponentially with reciprocal temperature. Typical k_w *vs.* $1/T$ plots are presented in Figure 3.

Rate constants k_{wi} of chemically controlled heterogeneous reactions vary with temperature according to the relation

$$k_{w_1} = PZ \exp[-E_{act}/RT] \quad (5)$$

where P and Z are steric and collision factors, and E_{act} is energy of activation. It was assumed that the preexponential terms varied with temperature to a far lower order of magnitude than the exponential term. E_{act} values were then determined from the equation

$$E_{act} = k\partial \ln k_{w_1}/\partial(1/T) \quad (6)$$

The energies of activation for the reactions of GiA, GiB, GiC, Gi1D, and Gi1E were 97, 92, 93, 94, and 97 kJ/mol, respectively. There was no significant variation with the powder surface area.

Discussion

Rates of Reaction and Effective Surface Area. Rates of heterogeneous solid–liquid reactions are generally determined by the original effective surface area of the reaction solid and its residual effective surface area and the activity of the reaction ions in solution after different times. The Gibbsite crystals studied in this present work consisted of aggregates of smaller "crystallites" and the effective surface areas might be many times the overall surface areas measured by optical microscopy.

As a model for the reactions studied in this work, we considered the dissolution of W_0 grams of powder that contained N cubic crystals of average initial length l_0; these consisted of e^3N cubic "crystallites" of average initial length l_{eff0}, where $e = l_0/l_{eff0}$. Then the powder weights at times 0,t would be

$$W_0 = \rho N l_0^3 \quad g$$

$$W_t = \rho N l_t^3 \quad g$$

The effective surface areas, for three-directional dissolution, at times 0,t would be

$$A_{eff0} = 6e^3 N l_{eff0}^2 = 6eNl_0^2 = eA_0 \quad cm^2$$

$$A_{eff\,t} = eA_t \quad cm^2$$

A_0 and A_t are overall surface areas at times 0,t. Then, the initial specific overall surface area would be

$$S_0 = A_0/W_0 = 6/\rho l_0 \quad cm^2\ g^{-1} \quad (7a)$$

while the initial specific effective surface area would be

$$S_{eff0} = A_{eff0}/W_0 = 6/\rho l_{eff0} \quad cm^2\ g^{-1} \quad (7b)$$

Also

$$A_0 = (6N^{1/3}/\rho^{2/3})W_0^{2/3} = \bar{A}W_0^{2/3}$$

then

$$A_{eff0} = e\bar{A}W_0^{2/3} \quad (8a)$$

$$A_{eff_t} = e\bar{A}W_t^{2/3} \quad (8b)$$

Then, eq 4 may be expressed as

$$dW/dt = -k_{w_1}W_t^{4/3}a_\pm = (-k_{w_1}/e^2\bar{A}^2)A_{eff_t}{}^2a_\pm = -ka_1A_{eff_t}{}^2a_\pm \text{ g hr}^{-1} \quad (9)$$

where ka_1 is the rate constant with respect to powder surface area. That is

$$k_{w_1} = e^2\bar{A}^2ka_1 = (\bar{A}_{eff0}{}^2/W_0^{4/3})ka_1 \quad (10)$$

and k_{w1} values actually depend on k_{a1} and $A_{eff0}{}^2$.

Generally, the rate-determining step in three-directional reactions is the reaction between crystal surface and reacting ions in the bulk of solution; then, dW/dt varies as A_{eff_t} (or $W_t^{1/3}$) and $(a_{OH^-})_{sol}$ or $a_\pm$.[6] The results of this work suggest that the rate of dissolution of gibbsites is determined rather by a three-directional reaction between crystallite surfaces and hydroxyl ions adsorbed on these surfaces.[18,23]

We compared the rate constants for reactions of gibbsites GiA to Gi1D with those for reactions of gibbsite Gi1E. Gi1E is probably a similar material to the original seeds that were used for the crystallization of the coarser gibbsites and therefore, for this material, we assumed that the initial effective surface area $(S_{eff0})_E$ equalled the initial overall surface area $(S_0)_E$; then, according to eq 10, the initial effective surface areas of the other powders were

$$S_{eff0} = r^{1/2}(S_0)_E \text{ cm}^2 \text{ g}^{-1} \quad (11)$$

where $r = k_w/(k_w)_E$, while

$$l_{eff0} = 6/\rho S_{eff0} \text{ cm} \quad (12)$$

S_{eff0} and l_{eff0} values were then estimated from r values according to the above equations.

For GiA (l_0 = 55 μm), $r^{1/2}$ = 0.32; S_{eff0} = 0.35 m^2/g, l_{eff0} = 7 μm; GiB (38 μm), $r^{1/2}$ = 0.35; S_{eff0} = 0.38 m^2/g, l_{eff0} = 6.3 μm; GiC (20 μm), $r^{1/2}$ = 0.39; S_{eff0} = 0.42 m^2/g, l_{eff0} 5.8 μm; Gi1D (6.5 μm), $r^{1/2}$ = 0.55; S_{eff0} = 0.61 m^2/g, l_{eff0} = 4 μm. These l_{eff0} values ranged from 4 to 7 μm, compared with the measured overall values from 6.5 to 55 μm. The larger crystals must consist of aggregates of more than 500 crystallites.

Schrader[8] carried out extensive X-ray diffraction analyses on gibbsite crystals, similar to those studied in this work. These former studies showed primary subunits in gibbsite crystals of 0.04-μ equivalent diameter, far smaller than the "crystallites" shown by optical microscopy. Rate constants might then be determined by the rates of reaction of hydroxyl ions with (and hence the effective surface areas of) such subunits; the above values for rate constant ratios would then suggest l_{eff0} values for Gibbsite subunits varying from about 0.04 μm for Gi1E to about 0.13 μm for GiA.

Mechanism. Gibbsite crystals (and crystallites) are made up from a continuous hexagonal lattice structure of Al atoms coordinated through O atoms with six hydroxyl groups;[24] these crystals dissolve to form aluminate anions of similar structure.[9,25] The energy of activation for the dissolution is far lower than the energy required to break actual Al–O bonds;[26] therefore, complete $Al(OH)_3$ sections must be dissolved out from the continuous lattice to form $[Al(OH)_4(H_2O)_2]^-$ anions. The dissolution probably starts at highly reactive defect sites on the crystallite surfaces.[18,27] The reaction might then occur by the following route; (i) reactive anion defect sites are hydrated

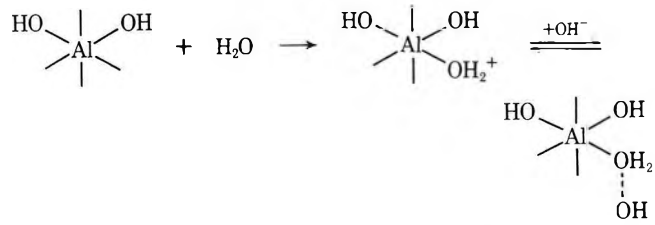

(ii) adsorbed hydroxyl ions diffuse along the crystallite surface to adjacent reactive sites; (iii) hydroxyl ions (hydrated) react slowly with these sites to form aluminate anions in the solution,

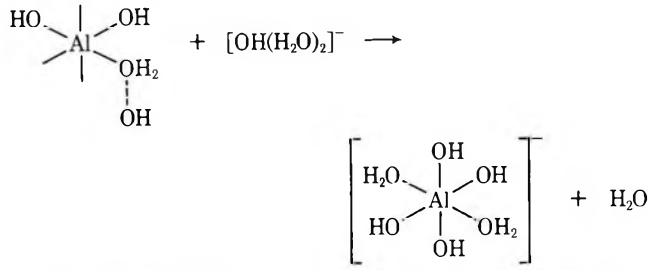

Reactive sites and aluminate anions are represented schematically in two dimensions. As these reactive sites are removed, new reactive sites are probably exposed simultaneously, until the whole surface layer of crystallite is dissolved. As each such layer is dissolved, fresh surface with reactive sites would be exposed and the reaction would proceed continuously.

Supplementary Material Available. Figures 1–3 will appear following these pages in the microfilm edition of this volume of the journal. Photocopies of the supplementary material from this paper only or microfiche (105 × 148 mm, 20× reduction, negatives) containing all of the supplementary material for the papers in this issue may be obtained from the Journals Department, American Chemical Society, 1155 16th St., N.W., Washington, D. C. 20036. Remit check or money order for $3.00 for photocopy or $2.00 for microfiche, referring to code number JPC-73-2942.

References and Notes

(1) D. W. Clelland, *J. Appl. Chem.*, **3**, 182 (1953).
(2) G. O. Assarsson, *J. Phys. Chem.*, **60**, 197, 1559 (1956).
(3) P. E. Halstead, *Nat. Bur. Stand. (U. S.), Monogr.*, **43**, 321 (1960).
(4) I. Bergman, *J. Appl. Chem.*, **11**, 369 (1961).
(5) S. A. Greenberg, *J. Phys. Chem.*, **61**, 960 (1957).
(6) S. A. Greenberg, *J. Phys. Chem.*, **65**, 12 (1961).
(7) A. Bielanski, *Rocz. Chem.*, **30**, 995 (1956).
(8) R. Schrader, *Z. Anorg. Chem.*, **350**, 120, 130, 137 (1967).
(9) T. G. Pearson, *RIC (Roy. Inst. Chem.) Monogr.*, **3** (1955).
(10) H. W. Taylor, "The Chemistry of Cement," Academic Press, London, 1964.
(11) A. I. Vogel, "Quantitative Inorganic Analysis," Longmans, Green and Co., New York, N. Y., 1962, Chapter 4, p 436; Chapter 14, p 885.
(12) H. P. Klug and A. E. Alexander, "X-Ray Diffraction Proceedures," Wiley, New York, N. Y., 1954 Chapter 7.
(13) L. D. Frederickson, *Anal. Chem.*, **26**, 1883 (1955).
(14) (a) L. Torkar, *Monatsh. Chem.*, **93**, 512 (1961); (b) G. O. Brindley, *Amer. Mineral.*, **46**, 771 (1961).
(15) J. Zussman, "Physical Methods in Determinative Mineralogy," Academic Press, London, 1969, Chapter 2.
(16) J. Scott, "Extractive Metallurgy of Aluminium," Vol. 1, Interscience, New York, N. Y., 1963, p 203.
(17) G. Åckerlof, *J. Amer. Chem. Soc.*, **59**, 1855 (1937).

(18) (a) A. Packter and H. S. Dhillon, *Z. Phys. Chem.*, **252**, 34 (1973); (b) H. S. Dhillon, Ph.D. Thesis, London University, 1971.
(19) E. Waenninen, *Anal. Chem. Acta*, **12**, 308 (1955).
(20) T. H. James, *J. Amer. Chem. Soc.*, **65**, 39 (1943).
(21) (a) P. Harriott, *Amer. Ind. Eng. Chem. J.*, **8**, 93 (1962); (b) S. M. Mehta, *Curr. Sci.*, **5**, 129 (1946); (c) M. S. Klochko, *Russ. J. Inorg. Chem.*, **4**, 964 (1959).
(22) E. J. Wilson, *Ind. Eng. Chem., Fundam.*, **5**, 9 (1966).
(23) W. T. Granquist, *Proc. Nat. Conf. Clays Clay Minerals, 6th, 1959*, 292 (1959).
(24) W. A. Deer, *et al.*, "Rock Forming Minerals," Longmans, Green and Co., New York, N. Y., 1965, pp 5 and 93.
(25) J. D. Hem, *Advan. Chem. Ser.*, **No. 73**, 98 (1968).
(26) N. V. Sidgwick, "The Chemical Elements and Their Compounds," Vol. 1, Oxford University Press, London, 1950, p 419.
(27) S. J. Gregg, *J. Chem. Soc.*, 3804 (1955).

The Role of the Excited States in the Photochemical and Photophysical Behavior of Tris(ethylenediamine)chromium(III) in Aqueous Solutions

R. Ballardini,[1a] G. Varani,[1a] H. F. Wasgestian,[1b] L. Moggi,*[1c] and V. Balzani[1c]

Istituto Chimico dell'Università, Centro di Studio sulla Fotochimica e Reattività degli Stati Eccitati dei Composti di Coordinazione del CNR, Ferrara, Italy, Institut für physikalische Chemie der Universität, Frankfurt Main, Germany, and Istituto Chimico "G. Ciamician" dell'Università, Bologna, Italy *(Received June 8, 1973)*

The quenching of the $Cr(en)_3^{3+}$ photolysis by some transition metal ions has been investigated in aqueous solution at 15°. It has been shown that, as happens for the phosphorescence quenching, $MnCl_2$ does not exhibit any quenching effect, whereas $CoCl_2$ and $FeCl_2$ do quench the photoreaction. It is also shown that the photoreaction is less quenched than the phosphorescence under the same experimental conditions. Specifically, 40% of the photoreaction directly originates from the lowest quartet excited state ($^4T_{2g}$) prior to intersystem crossing to the lowest doublet (^2E_g), whereas the remaining 60% is due to molecules which pass through ^2E_g and thus can be quenched. A quantitative analysis based on all the data which are available concerning the photochemical and photophysical behavior of $Cr(en)_3^{3+}$ shows that, most probably, the quenchable part of the photoreaction also comes from $^4T_{2g}$, after back intersystem crossing from ^2E_g. Values of about 0.6 and 1 are obtained for the forward and back intersystem crossing efficiencies. The actual values for all the rate constants of the steps that depopulate the ^2E_g state are discussed.

Introduction

The photochemistry[2,3] and luminescence[3,4] investigations in the field of coordination compounds have proceeded almost independently so far, although it is obvious that their results are complementary for the understanding of the excited-state behavior. The main reason for this unsatisfactory situation lies in the fact that most coordination compounds do not exhibit appreciable luminescence under the experimental conditions (fluid solutions near room temperature) in which photochemistry is usually observed. Cr(III) complexes, however, constitute a noticeable exception in this regard.[5] As a matter of fact, the possibility of comparing phosphorescence and photolysis quenching[6-10] or sensitization[11,12] has recently led to important progress in the understanding of the excited state behavior of Cr(III) complexes.

$Cr(en)_3^{3+}$ is one of the most thoroughly investigated Cr(III) complexes. The quantum yield of its aquation reaction is constant, regardless of whether the excitation is carried out in the quartet[13] or doublet[14] bands. It has also been shown that this complex is able to exhibit luminescence under the same experimental conditions in which its photochemistry can be studied.[11,15] Moreover, the apparent activation energies of the photoreaction,[14,15] phosphorescent intensity,[5,15] and phosphorescence lifetime[14,15] have recently been obtained. An attempt to use the sensitization technique for elucidating the photochemical role of the lowest doublet and the lowest excited quartet states did not give satisfactory results.[11] The sensitization approach seems to be a very difficult one indeed, because of (i) the lack of selectivity of the spin selection rules for intermolecular electronic energy transfer when the acceptor is a Cr(III) complex, and (ii) the difficulty of obtaining a selective population of the lowest doublet or the lowest excited quartet simply on energy grounds.[12] The quenching approach, on the contrary, has been proved to be much more successful.[6-10]

We have recently shown[16] that the phosphorescence intensity and lifetime of $Cr(en)_3^{3+}$ can be quenched by $CoCl_2$ and $FeCl_2$ (but not by $MnCl_2$) in aqueous solutions at room temperature. Here we will report the results of an investigation on the quenching of the $Cr(en)_3^{3+}$ photoreaction under the same experimental conditions. We will also discuss all of the available results on the photochemical and photophysical behavior of this complex as an attempt to elucidate the role played by the various excited states.

Experimental Section

Materials. Tris(ethylenediamine)chromium(III) chloride dihydrate, $[Cr(en)_3]Cl_3 \cdot 2H_2O$, was prepared following the procedure indicated in the literature.[17] $FeCl_2 \cdot 3H_2O$,

$CoCl_2 \cdot 6H_2O$, $MnCl_2 \cdot 4H_2O$, and all the other chemicals used were of reagent grade.

Apparatus. The equipment used for irradiation with 365-nm light was that previously described.[18] Radiations of 464 nm were isolated from an incandescent lamp by means of a Schott and Genossen interference double filter (T_{max}, 30%; half width, 17 nm). For more details concerning this equipment, again see ref 18. The reaction cells were standard spectrophotometric cells (thickness, 1 cm; capacity, 3 ml) housed in a thermostated cell holder. All experiments were carried out at 15°. The intensity of the incident light, which was of the order of 10^{-7} $Nh\nu$/min, was measured by means of a ferric oxalate actinometer.[19] Spectrophotometric measurements were performed with an Optica CF4 NI spectrophotometer. pH measurements were carried out by means of a Knick KpH 34 pH meter.

Procedure. A weighed amount of the complex was dissolved in the selected medium so as to obtain a 5×10^{-2} M solution. This operation was carried out in red light. The medium used was a slightly acidified aqueous solution (pH ~2.5) which contained the desired concentration of the quencher. The maximum quencher concentration was 3.5 M for $CoCl_2$ and 2.0 M for $FeCl_2$ and $MnCl_2$. In some experiments, the Cl^- concentration was adjusted to the desired value by adding KCl ($MgCl_2$ was not used since it was found to interfere in the pH measurements). Excitation was carried out at 365 or 464 nm, depending on whether $CoCl_2$ and $MnCl_2$ or $FeCl_2$ were used (note that the quantum yield of $Cr(en)_3^{3+}$ photoaquation is independent of the wavelength of irradiation[13]). These experimental conditions were practically the same as those used for some of the luminescence experiments.[16] The choice of a higher $Cr(en)_3^{3+}$ concentration (5×10^{-2} M instead of 2.5×10^{-2} M) was dictated by the need of minimizing secondary photochemical reactions (see below). Under the experimental conditions used, all the incident light was absorbed by the solution and the fraction of light absorbed by the quencher was ≤16% for $CoCl_2$, ≤4% for $FeCl_2$, and ≤3% for $MnCl_2$. During irradiation, the solution was stirred by bubbling a stream of purified N_2. It is well known that in acid solution the photoreaction of $Cr(en)_3^{3+}$ consists in the rupture of one Cr–N bond, followed by the protonation of the detached ethylenediamine end, and the coordination of a water molecule to Cr (see reaction 1).[13] The thermal aquation reactions of $Cr(en)_3^{3+}$ and of its primary photoproduct are known to be negligible under the experimental conditions used.[11,13] The occurrence of the photoreaction was followed by measuring the pH variations during the irradiation with a glass-reference combined microelectrode. Because of the sensitivity of this method, only a small amount (3–5%) of the complex needed to be decomposed, so that the occurrence of secondary photochemical processes was negligible. The measured pH variations were converted into variations of H^+ concentration, (*i.e.*, into variations of $Cr(en)_3^{3+}$ concentration, see eq 1) by means of calibration plots obtained by titrating a portion of the solution under investigation with 0.1 N KOH.

Results

According to previous investigations,[11,13] the irradiation of $Cr(en)_3^{3+}$ in the region between 250 and 442 nm causes the occurrence of reaction 1, with a quantum yield independent of the irradiation wavelength. Specifically, under the experimental conditions used in this work, the quantum yield was found to be 0.40 ± 0.05 at 442 nm.[11] The presence of oxygen did not affect the quantum yield.[11] In each one of our experiments, linear plots of H^+ consumption *vs.* $Nh\nu$ absorbed by the complex were obtained and the quantum yield for reaction 1 was then calculated as described in the procedure. We have found that the quantum yields at 365 and 464 nm were equal to that previously obtained at 442 nm, within experimental error.

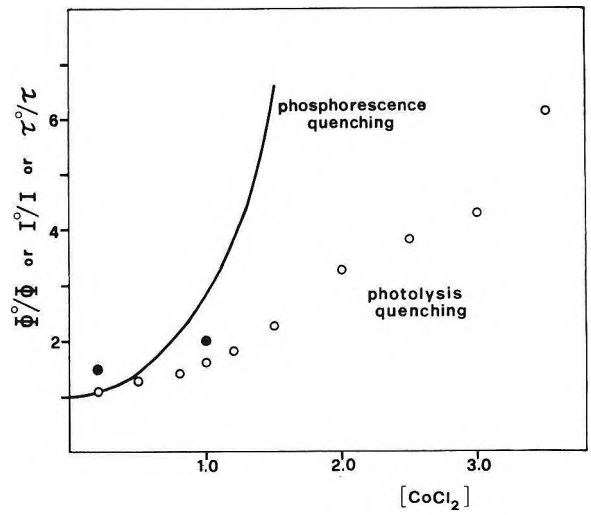

Figure 1. Quenching of the $Cr(en)_3^{3+}$ photoreaction by $CoCl_2$. The solid circles refer to solutions whose $[Cl^-]_{tot}$ was adjusted to 4.0 by adding KCl. The solid curve represents the quenching of the phosphorescence intensity or lifetime (from ref 16).

$$Cr(en)_3^{3+} + H_3O^+ \xrightarrow{h\nu} Cr(en)_2(enH)(H_2O)^{4+} \quad (1)$$

When the photoreaction was carried out in the presence of KCl (up to 4 M) or $MnCl_2$ (up to 2 M), the quantum yield did not exhibit any appreciable change. The photoreaction, however, was quenched by $CoCl_2$ and $FeCl_2$. The Stern–Volmer plot for $CoCl_2$ is shown in Figure 1, where the corresponding plot for the phosphorescence quenching[16] is also reported for comparison purposes. A few experiments were carried out in solutions where the Cl^- concentration had been adjusted to 4.0 M by adding KCl. The results of such experiments (Figure 1) showed that the addition of Cl^- enhanced the quenching effect. The quenching by $FeCl_2$ showed behavior very similar to that found for $CoCl_2$.

Discussion

The results obtained in the present paper show that (i) KCl and $MnCl_2$ do not quench the $Cr(en)_3^{3+}$ photolysis, whereas $CoCl_2$ and $FeCl_2$ exhibit a quenching effect; (ii) the Stern–Volmer plot for the quenching of $CoCl_2$ shows a positive curvature; and (iii) the quenching effect of $CoCl_2$ increases with increasing Cl^- concentration. From a *qualitative* point of view, these results are the same as those previously obtained,[16] under the same experimental conditions,[20] for the quenching of the $Cr(en)_3^{3+}$ phosphorescence. Therefore, by analogy with the phosphorescence quenching, the photolysis quenching seems to involve electronic energy transfer to Co(II) (or Fe(II)) species, whose nature (and then, quenching ability) changes with increasing $CoCl_2$ or Cl^- concentration.[16]

It should be noted, however, that a *quantitative* comparison (see Figure 1) between the phosphorescence and photolysis quenching shows that the photolysis is *less* quenched than the phosphorescence. This means that part

of the photoreaction must originate from excited molecules that do not pass through the equilibrated doublet state ^2E_g, which is the one responsible for the phosphorescence emission. This is exactly the same conclusion which Chen and Porter[6] arrived at in the case of $Cr(NH_3)_2(NCS)_4^-$. Following Chen and Porter's interpretation, the unquenchable part of the photoreaction directly originates from the lowest excited quartet state, $^4T_{2g}$, whereas two paths can be considered for the quenchable part: reaction in the doublet state, or thermal repopulation of the quartet state *via* back intersystem crossing from the doublet, followed by reaction in the quartet.

In order to discuss this problem, we will make reference to the scheme shown in Figure 2, where all the significant deactivation steps of the $^4T_{2g}$ and ^2E_g states have been taken into consideration. As shown in the previous paper,[16] several Co(II) species, each one having a different quenching ability, are present under the experimental conditions used. Therefore, the actual values of the overall bimolecular quenching constants, k_q and k_q' in Figure 2, depend on the relative abundances α_i of the Co(II) species

$$k_q = \Sigma_i \alpha_i k_{qi}; \quad k_q' = \Sigma_i \alpha_i k_{qi}'$$

This, however, does not affect our discussion since we will only compare the photolysis and emission quenching under the same experimental conditions.

The comparison of the intensity and lifetime quenching of the phosphorescence emission has shown[16] that only the ^2E_g state is quenched for $[CoCl_2] \leq 1.5$. Under such conditions, a steady-state treatment based on the scheme of Figure 2 gives (for the meanings of the symbols used, see footnote 21)

$$\Phi = \frac{k_r K_E + k_i k_r' + k_r k_q' C_q}{K_T K_E - k_i k_i' + K_T k_q' C_q} \tag{2}$$

$$\Phi(\text{phosph}) = \frac{k_i k_e'}{K_T K_E - k_i k_i' + K_T k_q' C_q} \tag{3}$$

and, assuming a steady state for $^4T_{2g}$ (after the exciting flash has decayed)[22,23]

$$\tau = \frac{K_T}{K_T K_E - k_i k_i' + K_T k_q' C_q} \tag{4}$$

The corresponding equations for Φ^0, Φ^0(phosph), and τ^0 can be easily obtained by equating C_q to zero in eq 2, 3, and 4, respectively. The following equations can thus be written

$$\frac{\Phi^0}{\Phi} = \left\{1 + \frac{K_T k_q'}{K_T K_E - k_i k_i'} C_q\right\}\left\{1 + \frac{k_r k_q'}{K_E k_r + k_i k_r'} C_q\right\}^{-1} \tag{5}$$

$$\frac{\Phi^0(\text{phosph})}{\Phi(\text{phosph})} = \frac{I^0}{I} = \frac{\tau^0}{\tau} = 1 + \frac{K_T k_q'}{K_T K_E - k_i k_i'} C_q \tag{6}$$

As previously mentioned, the experimental fact $I^0/I > \Phi^0/\Phi$ implies that $k_r \neq 0$.

Generally speaking, the steady-state quantum yields Φ^0 and Φ may receive contributions from three distinct paths.

(1) Direct reaction from $^4T_{2g}$ prior to intersystem crossing to the doublet; the quantum yield for this path is given by

$$\varphi_1^0 = \frac{k_r}{K_T} \tag{7}$$

It is obviously unaffected by the quenching of the ^2E_g state.

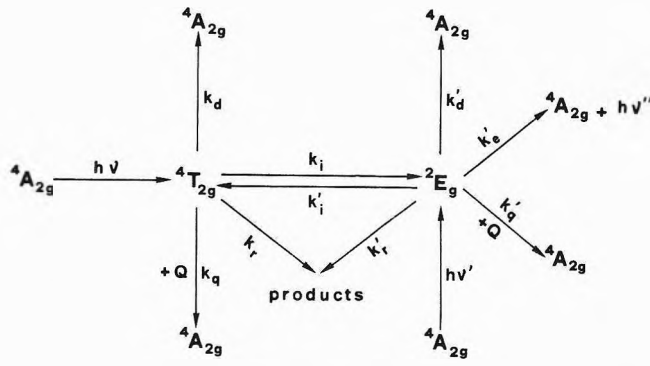

Figure 2. Schematic representation of the steps involved in the photochemical and photophysical behavior of $Cr(en)_3^{3+}$.

(2) Reaction from $^4T_{2g}$ by molecules which have passed (once or several times) through ^2E_g; the quantum yield of this path is given by

$$\varphi_2^0 = \frac{k_r}{K_T} \frac{k_i k_i'}{K_T K_E - k_i k_i'} \tag{8}$$

or

$$\varphi_2 = \frac{k_r}{K_T} \frac{k_i k_i'}{K_T K_E - k_i k_i' + K_T k_q' C_q} = \varphi_2^0 \frac{I}{I^0} \tag{9}$$

in the absence or in the presence of the quencher, respectively.

(3) Direct reaction from ^2E_g, with quantum yield

$$\varphi_3^0 = \frac{k_i k_r'}{K_T K_E - k_i k_i'} \tag{10}$$

or

$$\varphi_3 = \frac{k_i k_r'}{K_T K_E - k_i k_i' + K_T k_q' C_q} = \varphi_3^0 \frac{I}{I^0} \tag{11}$$

in the absence or in the presence of the quencher, respectively.

Therefore, the experimental quantum yields in the absence and in the presence of the quencher are given by

$$\Phi^0 = \varphi_1^0 + \varphi_2^0 + \varphi_3^0 \tag{12}$$

$$\Phi = \varphi_1^0 + \varphi_2 + \varphi_3 = \varphi_1^0 + (\varphi_2^0 + \varphi_3^0)\frac{I}{I^0} \tag{13}$$

Combining eq 12 and 13, one obtains

$$\frac{\Phi}{\Phi^0} = \frac{\varphi_1^0}{\Phi^0} + \left(\frac{\varphi_2^0}{\Phi^0} + \frac{\varphi_3^0}{\Phi^0}\right)\frac{I}{I^0} \tag{14}$$

According to this last equation, a plot of Φ/Φ^0 against I/I^0 (or τ/τ^0) should be linear. As is shown in Figure 3, our experimental results do agree with this expectation. From the intercept and slope of this linear plot, the following values may be obtained

$$\varphi_1^0 = 0.15 \tag{15}$$

$$\varphi_2^0 + \varphi_3^0 = 0.25 \tag{16}$$

Therefore, we can conclude that about 40% of the photoreaction directly comes from the quartet state prior to intersystem crossing to the doublet, whereas the remaining 60% is due to molecules which pass through the doublet. It is very interesting to note that, as shown in Figure 1, more than 80% of the reaction can be quenched for very high $CoCl_2$ concentrations.[24] This probably means that,

TABLE I: Summary of the Experimental Results Concerning the Photochemical and Photophysical Behavior of $Cr(en)_3^{3+}$ in Acid Aqueous Solutions[a]

	Quantum yield or lifetime (temp, °C)	Apparent activation energy (temp, °C)	Ref
Φ^0	0.40 (15°)		11
	0.37 (10°)	~5 kcal/mol (5–15°)[b]	13,14
	0.34 (5°)		13
φ_1^0	0.15 (15°)	...	This work
$\varphi_2^0 + \varphi_3^0$	0.25 (15°)	...	This work
$\Phi^0(^2E_g)$	0.40 (15°)		14
	0.38 (10°)	~5 kcal/mol (5–15°)	14
	0.30 (5°)		14
Φ^0(phosph)	$<1 \times 10^{-3}$ (20°)[c]	10.5 kcal/mol (5–70°)[b]	5
τ^0	1.33 μsec (~20°)	8.2 kcal/mol (0–20°)[b]	16,14
$\tau_r = 1/k_e'$	7 msec[d]	...	This work

[a] For the meanings of the symbols used, see footnote 21. [b] In a mixed solvent, the following values have recently been obtained for the apparent activation energies of Φ^0, Φ^0(phosph), and τ^0: 3.7, 12.7, and 10.8 kcal/mol.[15] [c] Unpublished experimental result from our laboratory. The value calculated by means of eq 3 and 4 is 1.2×10^{-4}. [d] Radiative lifetime calculated according to $\tau_r = 3.9 \times 10^8/\bar{\nu}^2 \int \epsilon d\nu$ with $\nu = 14.9$ kK. The doublet absorption was separated from the tail of the quartet absorption. The integral was graphically determined.

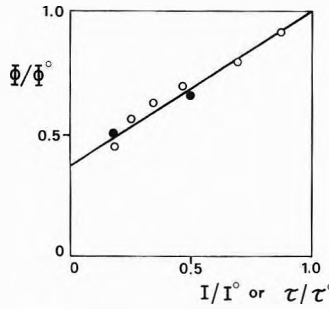

Figure 3. Plot of Φ/Φ^0 against I/I^0 (or τ/τ^0) under the same experimental conditions. Open circles refer to the data obtained for $C_q \leq 1.5$ without added Cl^-. Solid circles refer to the data obtained for $C_q = 0.2$ or 1.0, and $[Cl^-]_{tot} = 4.0$.

under such extreme conditions, the quartet state also begins to be quenched.

The comparison between our results and other ones recently reported in the literature (see Table I) permits us to obtain some more specific information on the behavior of the $^4T_{2g}$ and ^2E_g excited states. According to Chen and Porter,[14] the quantum yield of the photoreaction upon irradiation in the ^2E_g band is the same, within experimental error, as that obtained when the irradiation is performed in the $^4T_{2g}$ band. Note that the same is true for two other complexes (*i.e.*, $Cr(NH_3)_6^{3+}$ and $Cr(urea)_6^{3+}$) for which a similar investigation has been carried out.[2] On the basis of our scheme (Figure 2), the quantum yield of the photoreaction upon ^2E_g excitation is given by

$$\Phi^0(^2E_g) = \frac{k_r k_i' + k_r' K_T}{K_T K_E - k_i k_i'} \quad (17)$$

From eq 8, 10, 16, and 17, taking into account that $\Phi^0(^2E_g)$ is 0.40 (at 15°), the $^4T_{2g} \rightarrow {}^2E_g$ intersystem crossing efficiency, k_i/K_T, results to be about 0.63 (at 15°). Moreover, since $k_r/K_T = 0.15$ (eq 15), k_d/K_T is equal to 0.22. Thus, the efficiency of each step which depopulates $^4T_{2g}$ is known.

We will now try to discuss the relative importance of the various steps which depopulate ^2E_g. In particular, our aim is to establish whether or not the doublet state is directly responsible for part of the observed photoreaction. As one can see from Table I, the photoreaction quantum yields obtained upon $^4T_{2g}$ or ^2E_g irradiation are equal within experimental error and, moreover, they exhibit the same temperature dependence. This means that, if both path 2 and path 3 were operative, k_r/k_d should be equal to k_r'/k_d' and, moreover, these two ratios should exhibit the same temperature dependence. This would undoubtedly be a very unlikely coincidence. Therefore, we will only consider the two limiting cases which are obtained on the assumption that the quenchable part of the photoreaction derives entirely either from path 2 or from path 3.

(A) If the quenchable part of the photoreaction originates entirely from path 3, k_i' must be equal to zero (otherwise, since $k_r \neq 0$, φ_2^0 would also be different from zero). In this limiting case, the following equations can thus be written

$$\Phi^0 = \frac{k_r K_E + k_r' k_i}{K_T K_E} = \frac{k_r}{K_T} + \frac{k_i}{K_T}\frac{k_r'}{K_E} \quad (18)$$

$$\Phi^0(^2E_g) = \frac{k_r'}{K_E} \quad (19)$$

$$\Phi^0(\text{phosph}) = \frac{k_i k_e'}{K_T K_E} \quad (20)$$

$$\tau^0 = \frac{1}{K_E} \quad (21)$$

Taking into account the experimental data (Table I), the following values for the various rate constants may be obtained (at 15°): $K_E = 0.59 \times 10^6$ sec^{-1}, with an activation energy of 8.2 kcal/mol; $k_i' \sim 0$; $k_e' \sim 0$; $k_r' = 0.24 \times 10^6$ sec^{-1}, with an activation energy of about 6 kcal/mol; $k_d' = 0.35 \times 10^6$ sec^{-1}, with an activation energy of about 13 kcal/mol. Such a very large value for the activation energy of k_d' seems unlikely, especially if one considers that, at the same time, k_i' should be zero although the energy gap between ^2E_g and $^4T_{2g}$ is presumably lower than 13 kcal/mol.[11] An even more disturbing feature is that the quantum yields obtained by excitation in the quartet or doublet bands, which in this hypothesis are given by very different expressions (eq 18 and 19), are equal and exhibit the same temperature dependence (see Table I). Therefore, this limiting case is rather unsatisfactory.

(B) If the quenchable part of the photoreaction is assumed to derive entirely from path 2, k_r' is obviously equal to zero. Moreover, in order to account for the constancy of the quantum yield upon irradiation in the $^4T_{2g}$

and ^2E_g bands, the $^2E_g \rightarrow {}^4T_{2g}$ intersystem crossing must have almost unitary efficiency (*i.e.*, $K_E \sim k_i'$). The following equations can thus be written.

$$\Phi^0 = \frac{k_r}{k_r + k_d} \quad (22)$$

$$\Phi^0(^2E_g) = \frac{k_r}{k_r + k_d} \quad (23)$$

$$\Phi^0(\text{phosph}) = \frac{k_i}{k_r + k_d} \frac{k_e'}{K_E} \quad (24)$$

$$\tau^0 = \frac{K_T}{k_r + k_d} \frac{1}{K_E} \quad (25)$$

From eq 7, 22, and 25, it follows that $\varphi_1{}^0\tau^0 = \Phi^0/K_E$. From this last equation and from the experimental results of Table I, a value of 1.6×10^6 sec^{-1} can be obtained for K_E. Therefore, the rate constants of the various steps which depopulate ^2E_g are as follows (at 15°): $K_E = 1.6 \times 10^6$ sec^{-1}, with an activation energy of about 8 kcal/mol; $k_i' \sim K_E \sim 1.6 \times 10^6$ sec^{-1}, with the same activation energy as K_E; k_e', k_r', and $k_d' \ll k_i'$. This condition is obviously only valid for high temperatures. On cooling, the strongly temperature dependent k_i' becomes less important. Then the deactivation proceeds mainly *via* emission and direct radiationless transitions, which are only moderately temperature dependent. As one can see, in this case there are no disturbing features. For example, the value of about 8 kcal/mol for the activation energy of the back intersystem crossing (*i.e.*, for the $^4T_{2g}$–^2E_g energy gap) is a reasonable one. Moreover, the fact that the quantum yields obtained by $^4T_{2g}$ or ^2E_g excitation are equal and exhibit the same temperature dependence (Table I) is not surprising since they are actually given by the same expression (see eq 22 and 23). Finally, the conclusion that depopulation *via* $^4T_{2g}$ is the dominant thermal relaxation process of ^2E_g at elevated temperatures is in agreement with the results previously obtained from luminescence studies of other Cr(III) complexes.[22,23]

Summing up, it seems probable that the photoreaction of $Cr(en)_3^{3+}$ completely originates from $^4T_{2g}$ molecules and that the $^4T_{2g} \rightarrow {}^2E_g$ and $^2E_g \rightarrow {}^4T_{2g}$ intersystem crossing steps have efficiencies of ~0.6 and ~1, respectively (at 15°). These results are very similar to those obtained by Chen and Porter[6] for $Cr(NH_3)_2(NCS)_4^-$ and, to some extent, to those more recently obtained by Langford, *et al.*,[7,8] for $Cr(phen)_3^{3+}$ and $Cr(NH_3)_6^{3+}$. It is also very interesting to recall that in the case of $Cr(CN)_6^{3-}$, where the back intersystem crossing is precluded even at room temperature because of the vary large $^4T_{2g}$–^2E_g energy gap, quenching[9] and sensitization[12] studies have clearly shown that *all* the photoreaction occurs from $^4T_{2g}$. Therefore, all the results so far obtained on the Cr(III) photochemistry suggest that only the quartet excited states are responsible for the photoreactivity, and that the doublet states are substitution inert. However, when back intersystem crossing to the excited quartets occurs, these doublet states function as "parking places" for excited molecules which can in this case undergo the reaction by a "delayed" process.

Acknowledgments. The authors express their appreciation to Professor V. Carassiti for his interest in this study. This work was partly supported by the Deutsche Forschungsgemeinschaft and by the Consiglio Nazionale delle Ricerche.

References and Notes

(1) (a) Ferrara University; (b) Frankfurt University; (c) Bologna University.
(2) V. Balzani and V. Carassiti, "Photochemistry of Coordination Compounds," Academic Press, London, 1970.
(3) P. D. Fleischauer, A. W. Adamson, and G. Sartori, *Progr. Inorg. Chem.*, **17**, 1 (1972).
(4) P. D. Fleischauer and P. Fleischauer, *Chem. Rev.*, **70**, 199 (1970).
(5) N. A. P. Kane-Maguire and C. H. Langford, *Chem. Commun.*, 895 (1971).
(6) S. N. Chen and G. B. Porter, *Chem. Phys. Lett.*, **6**, 41 (1970).
(7) N. A. P. Kane-Maguire and C. H. Langford, *J. Amer. Chem. Soc.*, **94**, 2125 (1972).
(8) C. H. Langford and L. Tipping, *Can. J. Chem.*, **50**, 887 (1972).
(9) H. F. Wasgestian, *J. Phys. Chem.*, **76**, 1947 (1972).
(10) G. B. Porter, S. N. Chen, H. L. Schläfer, and H. Gausmann, *Theoret. Chim. Acta*, **20**, 81 (1971).
(11) V. Balzani, R. Ballardini, M. T. Gandolfi, and L. Moggi, *J. Amer. Chem. Soc.*, **93**, 339 (1971).
(12) N. Sabbatini and V. Balzani, *J. Amer. Chem. Soc.*, **94**, 7587 (1972); N. Sabbatini, M. A. Scandola, and V. Carassiti, *J. Phys. Chem.*, **77**, 1307 (1973).
(13) W. Geis and H. L. Schläfer, *Z. Phys. Chem. (Frankfurt am Main)*, **65**, 107 (1969).
(14) S. N. Chen and G. B. Porter, Abstracts of the X Informal Conference on Photochemistry, Stillwater, Okla., May 1972, p 155.
(15) W. Geis, H. F. Wasgestian, and H. Kelm, *Ber. Bunsenges. Phys. Chem.*, **76**, 1093 (1972).
(16) H. F. Wasgestian, R. Ballardini, G. Varani, L. Moggi, and V. Balzani, *J. Phys. Chem.*, in press.
(17) M. Linhard and M. Weigel, *Z. Anorg. Allg. Chem.*, **271**, 115 (1953).
(18) V. Balzani, R. Ballardini, N. Sabbatini, and L. Moggi, *Inorg. Chem.*, **7**, 1398 (1968).
(19) C. G. Hatchard and C. A. Parker, *Proc. Roy. Soc., Ser. A*, **235**, 518 (1956).
(20) The different $Cr(en)_3^{3+}$ concentrations (see procedure) and the slight difference in temperature (15° for the photochemical experiments and 20° for the luminescence ones) do not affect a quantitative comparison between the photochemistry and luminescence data. For example, the I^0/I ratio changes only of about 2% in going from 20 to 15°.
(21) The meanings of the symbols used are as follows: Φ^0, quantum yield of the photoreaction upon irradiation in the quartet bands; $\varphi_1{}^0$, unquenchable part of Φ^0 upon complete quenching of ^2E_g; $\varphi_2{}^0$ and $\varphi_3{}^0$, quenchable parts of Φ^0 upon complete quenching of ^2E_g (the subscripts 2 and 3 refer to the two different paths that the quenchable part can originate from); $\Phi^0(^2E_g)$, quantum yield of the photoreaction upon irradiation in the ^2E_g band; $\Phi^0(\text{phosph})$ and I^0, quantum yield and intensity of the phosphorescence emission upon irradiation in the quartet bands; τ^0, lifetime of the phosphorescence emission; $K_T = k_i + k_r + k_d$; $K_E = k_i' + k_r' + k_d' + k_e'$; C_Q, overall quencher concentration. When used without the superscript zero, Φ, φ, I, and τ refer to quantities obtained in the presence of quenchers. Lower case k's are the rate constants for the steps represented in Figure 2.
(22) F. Diomedi Camassei and L. S. Forster, *J. Chem. Phys.*, **50**, 2603 (1969).
(23) W. J. Mitchell and M. K. DeArmond, *J. Lumin.*, **4**, 137 (1971).
(24) Note that it was impossible to study the phosphorescence quenching under such extreme experimental conditions because the phosphorescence was almost completely quenched for much lower $CoCl_2$ concentrations[16] (see Figure 1).

Positive Hole Migration in Pulse-Irradiated Water and Heavy Water

Hajime Ogura and William H. Hamill*

Department of Chemistry and the Radiation Laboratory,[1] University of Notre Dame, Notre Dame, Indiana 46556
(Received June 25, 1973)

Publication costs assisted by the U. S. Atomic Energy Commission

The formation of Cl_2^- at high concentrations of NaCl in pulse-irradiated neutral aqueous solutions is attributed to electronic migration of the positive hole to Cl^- (forming Cl_2^-) and the lifetime of H_2O^+ is limited by formation of H_3O^+. The probability P of forming Cl_2^- will be expressed by $P = \nu_1([Cl^-]/55)/\{[Cl^-]/55) + \nu_2\}$ where ν_1 is the frequency of hole migration and ν_2 is the frequency of H transfer from H_2O to H_2O^+. It has been found that $(\nu_1/\nu_2)_{D_2O} = 1.2(\nu_1/\nu_2)_{H_2O} = 25$ in concentrated aqueous solutions of NaCl and 26 in 1 M $NaC_2H_3O_2$. In dilute solutions of H^+ and Cl^- the specific rate of Cl_2^- formation is 1.17 greater in H_2O than in D_2O. The ratio (ν_1/ν_2) at 100°/(ν_1/ν_2) at 25° $\cong$ 1.1 in H_2O and in D_2O after correcting for thermal expansion. It is proposed that neither ν_1 nor ν_2 involves thermal activation and that H transfers to H_2O^+ at a frequency 2×10^{14} sec^{-1}.

Introduction

Anbar and Thomas[2] observed Cl_2^- in concentrated pulse-irradiated neutral solutions of NaCl. They considered both reactions 1a and b as possible mechanisms (as well as variations of 1b) and preferred the spur reaction, 1b. They found $k = 1.66 \times 10^{10}$ M^{-2} sec^{-1} for dilute H^+ and Cl^-.

$$H_2O^+ + Cl^- \longrightarrow H_2O + Cl \quad (1a)$$

$$H_3O^+ + OH + Cl^- \longrightarrow 2H_2O + Cl \quad (1b)$$

Hunt[3] and his group, using Cerenkov reabsorption spectroscopy, observed Cl_2^- in concentrated neutral solutions of NaCl at very early times. There was no evidence of growth which would be expected for a spur reaction.

Recent work in Czapski's laboratory[4] showed that neither 0.5 M Na_2SO_4 nor 0.4 M Na_2HPO_4 affected the yield of Cl_2^- in 2 M NaCl. A similar result was found by Fisher[5] in this laboratory for addition of 1 M Na_2SO_4 to 1 M NaCl. These results are consistent with the assumption that reaction 1b in the acidic spur is responsible for any appreciable part of the yield of Cl_2^- in neutral solutions of Cl^-.

If formation of Cl_2^- at netural pH proceeds by mechanism 2a,b then doubling the yield of OH by addition of N_2O[5] should double the yield of Cl_2^-. In fact, there was no increase in the optical absorption at 350 nm. Since $[Cl_2^-]/[HOCl^-]$ remains constant under these conditions by mechanism 2a,b it follows that $HOCl^-$ is either not present at significant concentration or that it does not absorb appreciably at 350 nm.

$$Cl^- + OH \rightleftharpoons HOCl^- \quad (2a)$$

$$HOCl^- + Cl^- \rightleftharpoons Cl_2^- + OH^- \quad (2b)$$

Electron transfer from an anion to H_2O^+ presumably entails suppression of OH formed by reaction 3, where the H atom transferred was hydrogen bonded prior to ionization. The validity of mechanism 1a can therefore be tested by the effects of high concentrations of easily oxidized anions on G(OH), the 100-eV yield. Neither acetate nor oxalate ions react rapidly with OH, while both strongly suppress G(OH).[5]

$$H_2O^+ - - - H - OH \longrightarrow H_3O^+ + OH \quad (3)$$

The competition between reactions 1a and 3 has been described empirically[5] by

$$P = \frac{G(Cl_2^-)}{G^0} = \frac{\sigma_1[Cl^-]}{\sigma_1[Cl^-] + \sigma_2} \quad (4)$$

where the probability P of electron transfer from Cl^- to H_2O^+ is obtained from the observed yield $G(Cl_2^-)$ and G^0 the available yield of precursor H_2O^+. From the data of Anbar and Thomas,[2] $G^0 = 3.8$ and $\sigma_1/\sigma_2 = 0.38$.

A simple physicochemical model is now proposed to account for anion (A^-) oxidation and OH suppression. It is assumed that the positive hole migrates electronically from H_2O^+ to H_2O. The rate at which it transfers to A^-, instead of a molecule of H_2O, is given by $\nu_1[A^-]/55$ where ν_1 is the frequency of hole transfer and $[A^-]$ is expressed as molarity. The competing first-order process is reaction 3 which occurs at frequency ν_2. We have, then, formula 5 for solutions of Cl^-. The upper and lower bounds of ν_1 correspond to charge migration in a conduction band and to hopping. The upper and lower bounds of ν_2 correspond to the H–OH vibrational frequency and to thermally activated passage of H over a barrier.

$$P = \frac{G(Cl_2^-)}{G^0} = \frac{\nu_1[Cl^-]/55}{\nu_1[Cl^-]/55 + \nu_2} \quad (5)$$

The model suggests two experimental tests. One is the isotope effect on ν_1/ν_2 in H_2O and in D_2O. The other is the temperature coefficient of ν_1/ν_2 in H_2O and in D_2O. The results of these experiments are reported here. For these solutions, pH ~4 in the absence of added HCl.

Experimental Section

Irradiations were performed with an Arco LP-7 linear accelerator of ~8-MeV electrons using 5-nsec pulses at ~4-A beam current. Other experimental details have been described.[5] The dose delivered was measured in terms of OD(e_{aq}^-) at 600 nm for N_2-purged water and all other measurements have been normalized on this basis. The yield of Cl_2^- was measured in terms of the OD at 350

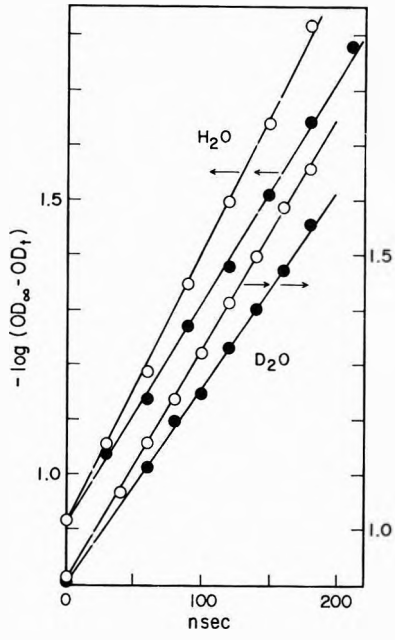

Figure 1. The optical density for reaction of 0.05 *M* NaCl (O) and 0.04 *M* NaCl (●) in H_2O (left scale) and D_2O (right scale), both in 10^{-2} *M* acid.

nm. All solutions of NaCl were saturated with CO_2 to suppress absorption by e_{aq}^-.

Triply distilled H_2O was used, but Mallinkrodt 99.8% D_2O was used as received. For measurements of Cl_2^- in concentrated solutions of NaCl, and in the presence of $\gtrsim$10 m*M* e^- scavengers, the highest purity is quite unnecessary. The NaCl was reagent grade quality.

Experimental Results

A simple demonstration of an isotope effect is provided by the effect of concentrated acetate ion on the yield of hydroxyl radical (measured as I_2^-) in H_2O and D_2O. Solutions contained 0 or 1.0 *M* $NaC_2H_3O_2$ and 0.1 *M* KI with 0.05 *M* CH_3I to remove e_{aq}^-. The OD of I_2^-, measured at 390 nm, was constant from 30 to 100 nsec. In H_2O, solutions with and without acetate had OD's of 0.241 and 0.298 at 30 nsec, and in D_2O the OD's were 0.245 and 0.333, respectively. By analogy with eq 4, $(\nu_2/\nu_1)_{H_2O} = 1.54\ (\nu_2/\nu_1)_{D_2O}$ for 1 *M* $NaC_2H_3O_2$ where $1.54 = (\Delta OD/OD)_{D_2O}/(\Delta OD/OD)_{H_2O}$ and the OD's were measured at 390 nm. No correction has been applied to the ΔOD's since the ratio of rate constants for reaction of OH with $C_2H_3O_2^-$ and I^- is 9.2×10^{-3} [5] and the corrections cancel in the ratio within the experimental error. Since $(\sigma_2/\sigma_1)_{H_2O} = 3.2$ for solutions of acetate ion,[5] $(\sigma_2/\sigma_1)_{D_2O} = 2.1$ or, by eq 4, $(\nu_2/\nu_1)_{D_2O} = 0.038$.

The kinetic isotope effect for reactions 1b and 1c was

$$D_3O^+ + OD + Cl^- \longrightarrow 2D_2O + Cl \qquad (1c)$$

measured because of its possible bearing on the mechanism of Cl^- oxidation in the spur. In solutions containing 0.05 *M* or 0.04 *M* NaCl, 0.01 *M* HCl, and saturated with CO_2 the specific velocity constants were $k_{H_2O} = 1.85 \times 10^{10}$ or $1.91 \times 10^{10}\ M^{-2}\ sec^{-1}$ and $k_{D_2O} = 1.60 \times 10^{10}$ or $1.62 \times 10^{10}\ M^{-2}\ sec^{-1}$, based on the results in Figure 1. The average ratio k_{H_2O}/k_{D_2O} is 1.17.

To test for an isotope effect in the formation of Cl_2^- at pH ~4, concentrations of chloride ion in the range 0.5–5 *M* were used in four series of measurements. All solutions were saturated with CO_2 to remove weak absorption of

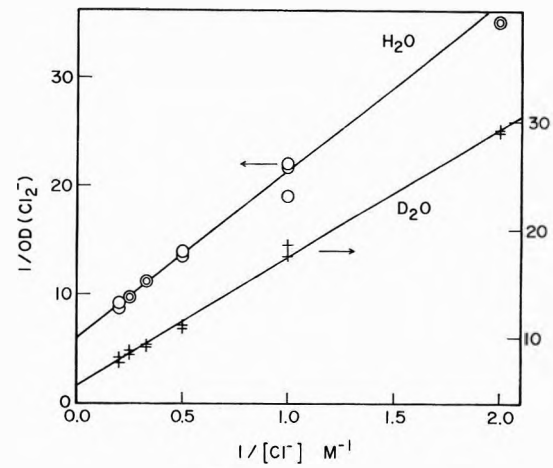

Figure 2. The OD of Cl_2^- at 350 nm and 30 nsec for concentrated solutions of NaCl, saturated with CO_2.

e_{aq}^- at 350 nm. The results, which were normalized to a common dose using $OD(e_{aq}^-)$ at 600 nm, appear in Figure 2. The intercepts and ratios of (slope)/(intercept) are 6.0 and 2.60 for H_2O and 5.5 and 2.18 for D_2O. In terms of eq 5, $(\nu_2/\nu_1)_{H_2O}/(\nu_2/\nu_1)_{D_2O}$ is 1.20. By eq 4, $\nu_2/\nu_1 = 0.048$ for H_2O and 0.040 for D_2O in solutions of NaCl. For solutions of $NaC_2H_3O_2$ the ratio ν_2/ν_1 was 0.058 for H_2O and 0.039 for D_2O.

Yields of Cl_2^- in H_2O and D_2O at ~100° were also measured for 0.5–5 *M* NaCl but they did not obey eq 4, decreasing too rapidly as $[Cl^-]$ decreased. Using only the results for 4 and 5 *M* NaCl, $OD(Cl_2^-)$ at 100°/$OD(Cl_2^-)$ at 25° was 0.80 in D_2O and 0.78 in H_2O. Since the specific volume of water is 4% greater at the higher temperature, the observed $OD(Cl_2^-)$ should be corrected accordingly. The electron density entails a similar correction, and the effect on $[Cl^-]$ involves an additional ~2.5%. The corrected temperature coefficients are therefore ~0.90 for both H_2O and D_2O. In terms of an Arrhenius dependence, $E_{act} \cong 0.014$ eV.

Discussion

The yield ratios $(Cl_2^-)_{H_2O}/(Cl_2^-)_{D_2O}$ for dilute solutions of Cl^- at pH 2 and for concentrated solutions of Cl^- at pH ~4 were ~1.2 and ~0.8, respectively. These isotope effects cannot be reconciled with reactions 1b and 1c in spurs as the exclusive mechanism to form Cl_2^- in concentrated neutral solutions.

The decreased yield of OH or OD at ~10 nsec in concentrated solutions of acetate ion includes a small but corrigible contribution from the conventional scavenging of OH by $C_2H_3O_2^-$. The major mechanism can be accounted for by electron transfer to H_2O^+. If this terminal step is preceded by several hole transfers between H_2O^+ and H_2O, as assumed, then the overall efficiency should be relatively insensitive to the choice of anion, provided that it is easily oxidized. Values of ν_2/ν_1 in H_2O for Cl^-, $C_2H_3O_2^-$, and $C_2O_4^{2-}$ are 0.048, 0.058, and 0.096,[5,6] respectively.

The failure of the results at 100° to conform to eq 5, particularly in the more dilute solutions, can be attributed to heterolysis of Cl to form H^+ and Cl^-. Such an effect was observed previously for several H-containing solutes[5] and the corresponding reaction may occur with water at 100°. It should be less important the higher the concentration of Cl^-.

The temperature dependence of the yield of Cl_2^- indicates that the activation energies E_1 and E_2 for ν_1 and ν_2 are the same, and possibly zero, both in H_2O and in D_2O. Since there is an isotope effect in ν_1/ν_2, zero point energies must also be equal for E_1 and E_2 if they are not zero. If $E_1 = E_2 = \hbar\omega = 0.5$ eV, a quantum of vibrational stretching, then the rate constant for reaction 2 is $\nu_2 \sim 10^6\ sec^{-1}$ and therefore disallowed.

If $E_1 = E_2 \neq 0$ and both involve translational energy alone it can be estimated that $\nu_1 = A_1 \exp(-E_1/kT)$ with $A_1 \cong 10^{13}\ sec^{-1}$ and $\nu_1 < 10^{13}\ sec^{-1}$. Since $\nu_1 = 21\nu_2$ for H_2O, $\nu_2 < 5 \times 10^{11}\ sec^{-1}$. This is less than H^+-transfer frequency between nearest neighbor acid and base, *e.g.*, by Raman line broadening.[7] These considerations indicate that $E_1 = E_2 = 0$ and, if so, then H-atom transfer by reaction 2 occurs on the first nearest approach. The average time required is half the vibrational period, or the rate is twice the O–H vibrational stretching frequency. That is, $\nu_2 = 2.2 \times 10^{14}\ sec^{-1}$ in H_2O and $1.6 \times 10^{14}\ sec^{-1}$ in D_2O. Since ν_1/ν_2 is 21 in H_2O and 25 in D_2O, $\nu_1 = 4.6 \times 10^{15}\ sec^{-1}$ in H_2O and $4.0 \times 10^{15}\ sec^{-1}$ in D_2O. The ratios ν_1/ν_2, in terms of the model, are the numbers of molecules visited (some twice) by a migrating hole. These values approximate those calculated previously.[8]

The isotope effect on ν_1 suggests interaction of the migrating hole with molecular vibrations. If the hole migrates from oxygen to oxygen along H bridges, the frequency should depend upon the phase angle and, to some extent, upon the vibrational frequency.

Acknowledgment. The authors are indebted to Professor Gideon Czapski for helpful comments.

References and Notes

(1) The Radiation Laboratory of the University of Notre Dame is operated under contract with the U. S. Atomic Energy Commission. This is AEC Document No. COO-38-904.
(2) M. Anbar and J. K. Thomas, *J. Phys. Chem.*, **68**, 3829 (1964).
(3) J. W. Hunt, private communication.
(4) E. Peled, D. Meisel, and G. Czapski, *J. Phys. Chem.*, **76**, 3677 (1972).
(5) M. M. Fisher and W. H. Hamill, *J. Phys. Chem.*, **77**, 171 (1973).
(6) In ref 5 the ratio of (slope)/(intercept) for solutions of $C_2O_4^{2-}$ should have been combined with $\sigma_{I^-}/\sigma_d = 0.6$ for iodide ion from the work of P. L. T. Bevan and W. H. Hamill, *Trans. Faraday Soc.*, **66**, 2533 (1970).
(7) M. M. Krevoy and C. A. Mead, *Discuss. Faraday Soc.*, **39**, 166 (1965).
(8) S. Kalarickal, Ph.D. Dissertation, University of Notre Dame, 1956.

Radicals Formed by the Reaction of Electrons with Amino Acids and Peptides in a Neutral Aqueous Glass[1]

M. D. Sevilla* and V. L. Brooks

Department of Chemistry, Oakland University, Rochester, Michigan 48063 *(Received July 5, 1973)*

Publication costs assisted by the U.S. Atomic Energy Commission and Oakland University

The reactions of electrons with a number of amino acids, *N*-acetylamino acids, *N*-acetylpeptides, and peptides in a neutral aqueous glass (12 *M* LiCl-D_2O) have been investigated by electron spin resonance spectroscopy. Electron attachment to the amino acids, glycine and alanine, at 77°K results in immediate deamination. For amino acids with more reactive side groups, *e.g.*, glutamic acid, anion radicals are found with the electron localized on the side group. For all peptides we find immediate N-terminal deamination upon electron attachment at 77°K. Where glycine is at the N terminal, upon warming to the softening point of the glass, deamination is followed by abstraction from an α-carbon position. Stable anions are found for *N*-acetylamino acids and *N*-acetylpeptides after electron attachment. These anions undergo deamination of a secondary amine group upon warming to 165°K. Further warming results in hydrogen abstraction to form an α-carbon radical. These results are compared to those found in an alkaline glass (8 *M* NaOD). It is found that changes in protonation at nitrogen sites greatly affect stability and hyperfine splittings of radicals produced after electron attachment. McLachlan spin density calculations confirm the experimental result that deprotonation at the nitrogen in peptide α-carbon radicals can significantly alter the α-carbon proton splitting. Finally, the results found in this study are discussed in terms of other recent work utilizing pulse radiolysis, product analysis, and esr. Good agreement is found between the various techniques.

Introduction

Investigations of the radiolysis of amino acids and peptides in aqueous solution and in the solid state have shown the importance of the electron as a primary intermediate in radical production.[2-7] In our previous studies the reactions of electrons with amino acids[8] and peptides[9] were investigated in an alkaline aqueous glass (8 *M* NaOH) by use of electron spin resonance (esr) spectroscopy. The mechanisms elucidated in these investigations were in good agreement with those suggested from reaction rate studies and product analysis in aqueous solution

at room temperature,[2] as well as more recent pulse radiolytic[3] and esr studies.[4]

Comparison of the results of our previous work on amino acids with those found by esr investigations of single crystals of amino acids showed that the environment often determines the most stable "final" radical in a reaction sequence.[8] To determine the effect of such a change in environment on radical reactions initiated by electron attachment, the reactions of electrons with amino acids and peptides in a *neutral* aqueous glass (12 *M* LiCl) were investigated in this work.

The results of this study show that the stabilities of radicals produced after electron attachment often differ greatly in the neutral glass from those found in the alkaline medium. In several cases hyperfine splittings for the same radical are found to differ significantly in the two matrices. Both these effects are attributed to changes in protonation on radical nitrogen sites induced by the pH difference between the two matrices.

Experimental Section

The experimental procedure was essentially that used in our previous work in 8 *M* NaOD (92% D)[8,9] except that 12 *M* LiCl was employed to form the glass.[10,11] In this technique a solution of 12 *M* LiCl (D_2O) containing 10 m*M* $K_4Fe(CN)_6$ and *ca.* 50 m*M* solute is cooled to 77°K. The glass formed is photolyzed with 2537-Å light at 77°K for times usually less than 1 min. Photolysis of the solute is unlikely due to the presence of $K_4Fe(CN)_6$ and the low extinction coefficient at 2537 Å for these compounds. Electrons are formed by the photolysis of $K_4Fe(CN)_6$. Some of the electrons are trapped in the glass and some react with the solute. The trapped electrons are photobleached with an incandescent lamp. They become mobile and react with the solute.

Other experimental details have been described in our previous work.[8-10]

Results and Discussion

Electron Reactions with Amino Acids in 12 M LiCl (D_2O). The reactions of electrons with glycine and L-alanine at 77°K resulted in the spectra shown in Figure 1A and 1B. The hyperfine splittings of 21.5 G due to two hydrogens for glycine and 24 G due to four approximately equivalent hydrogens for alanine as well as the well-resolved anisotropic structure in these spectra show that they are clearly those of the deaminated radicals (reaction 1).[4-6,8,12] The anion radicals which are the likely intermedi-

$$ND_3^+CHRCO_2^- + e^- \longrightarrow [ND_3^+CHRCO_2^{2-}] \longrightarrow ND_3 + \cdot CHRCO_2^- \quad (1)$$

ates and which were found to be stable in 8 *M* NaOD up to 160°K are not stable at 77°K.[8] In each spectrum the outer components are due to deuterium atoms. They are found even in the absence of a solute and are most likely due to the reaction of electrons with D^+ (aq) in the aqueous matrix.[13] For glycine the proportion of deuterium atoms to the deaminated radical is greater than that for all other amino acids studied. This may be due to reaction 2 which has been

$$ND_3^+CH_2CO_2^- + e^- \longrightarrow D\cdot + ND_2CH_2CO_2^- \quad (2)$$

suggested from work in aqueous solution at room temperature.[2] Warming samples to 170°K where the glass softens resulted only in the loss of signal, presumably by radical-radical recombination, without further reaction. These results contrast to the results found in the alkaline glass

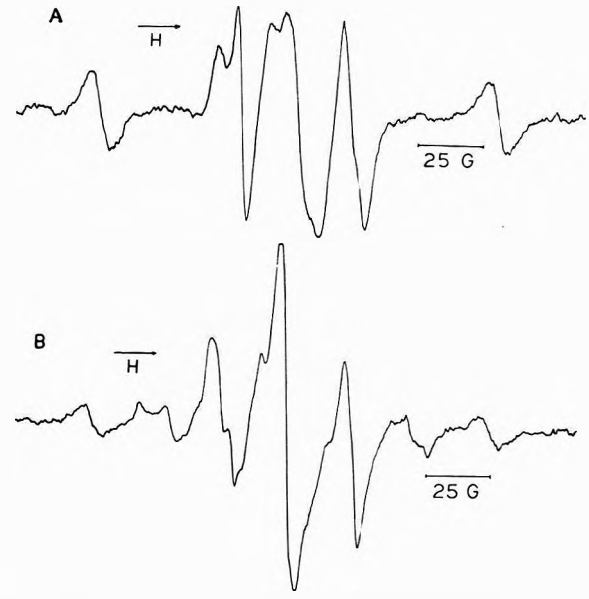

Figure 1. Electron spin resonance spectra of the deaminated radical species, $\cdot CHRCO_2^-$, produced after electron attachment to glycine (A) and L-alanine (B) at 77°K in 12 *M* LiCl. The outer components in each spectrum are due to deuterium atoms and are found in all subsequent spectra at 77°K.

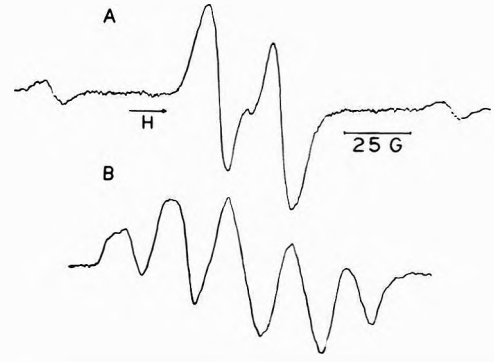

Figure 2. Esr spectra of radicals produced by the reaction of electrons with L-glutamic acid. (A) The anion radical at 77°K. The electron is likely localized on the carboxyl group of the side chain. (B) The deaminated radical, $CO_2H-CH_2CH_2\dot{C}H-CO_2^-$, at 165°K.

where it was found that the anion deaminated at *ca.* 180°K and that upon warming to the softening point of the glass the deaminated radical abstracted a hydrogen atom from the α-carbon position of the parent compound to produce a radical of the form $ND_2\dot{C}RCO_2^-$.[8] The results found at 77°K in 12 *M* LiCl suggest that the protonation of the amine group potentiates the amino acid anion for deamination.

Due to solubility problems the amino acids with larger alkyl side chains, *i.e.*, leucine, isoleucine, and valine, did not yield clear results.

For several amino acids with more reactive side groups we find reaction with the electron produces a stable anion at 77°K. The reaction of electrons with L-glutamic acid results in the spectra shown in Figure 2. At 77°K a 24.7-G doublet is found (Figure 2A) which, upon warming to 165°K, converts to a five-line spectrum with 22-G separation between the components (Figure 2B). The initial spectrum is attributed to the anion. The electron is likely localized on the side chain carboxyl group. This is indicated for several reasons. First, the side chain carboxyl

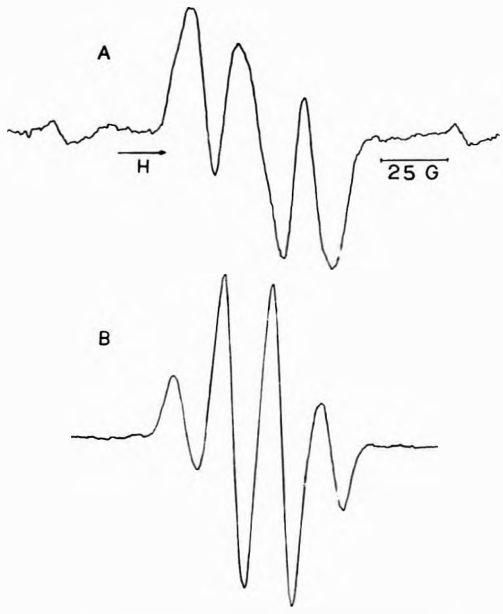

Figure 3. Esr spectra of radicals produced by the reaction of electrons with glycyl-L-alanine. (A) The N-terminal deaminated radical, $\cdot CH_2C(O)NDCH(CH_3)CO_2^-$, at 77°K. (B) The radical produced by abstraction from the C-terminal α-carbon position, $ND_3^+CH_2C(O)NDC(CH_3)CO_2^-$, at 165°K.

group is protonated to a much greater extent at neutral pH than the other group.[14] A protonated carboxyl group would stabilize an extra electron. Second, the results for glycine and alanine showed amino acid anions of the unprotonated carboxyl group are not stable at 77°K in 12 *M* LiCl. Finally, esr spectra of glutamic and aspartic acids in 8 *M* NaOH where both carboxyl groups are unprotonated show little reaction between the electron and the doubly charged amino acids. Thus the doublet splitting found for the glutamic acid anion is likely due to one of the methylene protons adjacent to the side chain carboxyl group. The other proton must therefore be in a configuration so as not to produce a resolved splitting. Orientations with $\theta_1 \approx 20°$ and $\theta_2 \approx 260°$ would result in such splittings.[15] The spectrum found on warming is interpretable in terms of the deaminated radical, $HO_2C\text{-}CH_2\text{-}CH_2\text{-}\dot{C}H\text{-}CO_2^-$, with hyperfine splittings of approximately 44 (one β proton), 22 (second β proton), and 22 G (α proton). The intensity ratio expected from this interpretation is 1:2:2:2:1 and is in good agreement with experiment. The results for glutamic acid are confirmed by those found for L-aspartic acid in 12 *M* LiCl. The esr spectra show a 24.6-G doublet at 77°K and a quintet of *ca.* 1:2:2:2:1 at 165°K with a 21-G average separation between the components.

The observed β-proton splittings for the deaminated radicals of glutamic and aspartic acid would result from β-proton orientations with $\theta_1 \approx 0°$ (44 G) and $\theta_2 \approx 120°$ (22 G). These results are similar to those found for the deaminated radical of leucine in 8 *M* NaOD.[8] From a consideration of steric factors the leucyl radical would be expected to have a similar conformation to those of the glutamic and aspartic acid radicals.

The reactions of electrons with L-aspargine in 12 *M* LiCl-D_2O also produced an initial spectrum (27.6-G doublet) consistent with a stable anion. The electron in this case is considered to be localized on the amide linkage of the side chain. The anion remained stable upon warming to 170°K. In 12 *M* LiCl-H_2O a further reaction was noted upon warming to 170°K to give a 1:2:1 triplet of 22-G separation.

Reaction of Electrons with Dipeptides in 12 M LiCl. The reaction of electrons with the dipeptides glycylglycine and glycyl-L-alanine at 77°K yielded nearly identical 21.5-G triplet spectra (see Figure 3A for glyala). This triplet is ascribed to the radical produced by deamination of the N-terminal amino group. Deamination of the secondary amino group in glygly would result in the glycine deamination spectrum which has a characteristic anisotropic structure (see Figure 1A). Whereas deamination of the secondary amine group in glyala would yield the same alanyl radical spectrum as found in Figure 1B. Warming the deaminated radicals to 165°K (softening point of glass) results in a 18.5-G doublet spectrum for glygly and a 18.7-G 1:3:3:1 quartet for glyala (see Figure 3B). These spectra are indicative of abstraction of an hydrogen atom from an α-carbon position of the parent compound. For glygly abstraction from either position would produce the observed 18.5-G doublet, however, for glyala the quartet is clear evidence for abstraction from the C-terminal α-carbon position as shown in reaction 3.

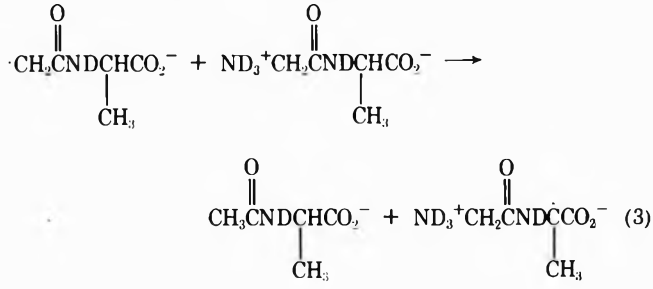

The C-terminal α-carbon radical has been found to predominate in the esr studies of irradiated single crystals of glygly[16] and has been shown to be an intermediate from the studies of the radiation chemistry of glygly in dilute aqueous solution.[17] Considering our results for glyala, abstraction from the C-terminal α carbon in glygly may be favored here as well. In our previous results in 8 *M* NaOD we found stable anions of the dipeptides at 77°K which only underwent deamination upon warming to 180°K.[9] The deaminated radicals subsequently abstracted from an α-carbon position. However, for glyala it was not as clear which of the α-carbon positions was the site of abstraction as in this present work.

Reaction of electrons with L-alanylglycine results in immediate N-terminal deamination to give an alanyl radical whose esr spectrum consists of the expected 24-G quintet. Further reaction occurred upon warming to 170°K, but only slowly. The spectrum observed at 170°K consisted of an overlap of the deaminated radical and an abstracted radical. The deaminated radical is apparently relatively stable toward abstraction in this case.

Reaction of electrons with glycyl-L-leucine results in N-terminal deamination to yield an esr spectrum of the familiar 22-G glycyl triplet. Upon warming these samples to 170°K evidence is found for abstraction from the leucyl side chain not the α-carbon position. The spectrum at 170°K consists of eight principle components separated by 24.8 G in the approximate intensity ratios expected for seven nearly equivalent protons. The only radical consistent with such a spectrum is the radical produced by abstraction from the tertiary carbon of the alkyl side group, $(CH_3)_2\dot{C}CH_2\text{-}R$.[18] The same radical was found at this point in 8 *M* NaOD, however, upon further warming it

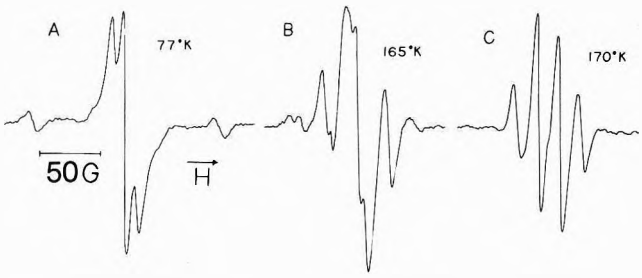

Figure 4. Esr spectra of radicals procuced by the reaction of electrons with *N*-acetyl-L-alanine. (A) The anion radical at 77°K. (B) The deaminated radical, $\cdot CH(CH_3)CO_3^-$, at 165°K. This spectrum is overlapped with that in A. (C) The radical, $CH_3CONDC(CH_3)CC_3^-$, produced by abstraction.

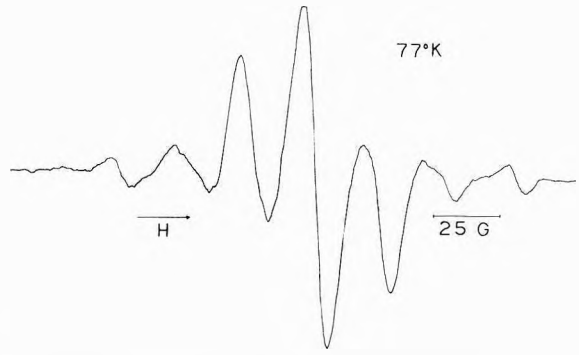

Figure 5. The esr spectrum of the N-terminal deaminated radical produced by electron attachment to L-alanylglycylglycylglycylglycine at 77°K. Warming resulted in no further radical species.

abstracted from the α-carbon position.[9] In 12 *M* LiCl we find that the leucyl radical undergoes no further reaction upon warming other than radical–radical recombination.

Reaction of Electrons with N-Acetylamino Acids and Peptides. The reaction of electrons with *N*-acetyl-L-alanine at 77°K resulted in the spectrum shown in Figure 4A. The 11.5-G triplet is associated with the anion or protonated anion radical.[19] However, it is not clear from the structure of the esr spectrum on which functional group the electron is localized. In our previous work in 8 *M* NaOD it was found that the electron localized on the peptide linkage.[9] This was concluded from an investigation of the temperature dependence of the methyl group hyperfine splitting in the anion. The anion shows no such temperature dependence in 12 *M* LiCl. Warming the sample to 160°K results in deamination of the secondary amine group to give the spectrum of the alanyl radical shown in Figure 4B. Due to the relatively high temperature of deamination there was some difficulty in complete separation of radical species and the spectrum in Figure 4B is overlapped with that of the "anion" radical. Further warming to 170°K results in the 17.9-G 1:3:3:1 quartet spectrum shown in Figure 4C. This is good evidence for abstraction from the α-carbon position (reaction 4). For

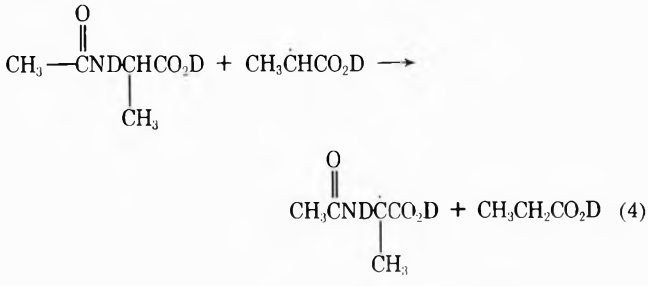

$$CH_3\text{—}\overset{\overset{O}{\|}}{C}NDCHCO_2D + CH_3\dot{C}HCO_2D \longrightarrow \underset{CH_3}{\overset{\overset{O}{\|}}{CH_3CNDC}}\dot{C}O_2D + CH_3CH_2CO_2D \quad (4)$$

N-acetylglycine an initial spectrum consisting of a 23-G doublet (77°K) is irreversibly converted upon warming to 170°K to a 17.5-G doublet. The initial doublet is associated with the anion and the 17.5-G doublet with the abstracted radical. We believe that the fact that no intermediate (*i.e.*, $\cdot CH_2CO_2^-$) was observed is accounted for by the stability of the anion which necessitated the warming of the sample to the softening point of the glass before further reaction could take place. For *N*-acetylglycylglycine the 24.2-G doublet initially observed at 77°K does show evidence for the deaminated intermediate ($\cdot CH_2C(O)\sim$) upon warming to 162°K. Further warming again results in a spectrum (18.2-G doublet) associated with the radical produced by abstraction from an α-carbon position. The reaction sequence found for the reaction of electrons with *N*-acetylamino acids and peptides in 12 *M* LiCl, *i.e.*, anion formation, deamination, and abstraction, is in good agreement with the results found in the 8 *M* NaOD glass; however, the abstraction step did not occur for *N*-acetylalanine in the alkaline medium.[9]

Reactions of Electrons with Several Oligopeptides. The reactions of electrons with two tripeptides, glycylglycylglycine and L-alanylglycylglycine, and a pentapeptide, L-alanylglycylglycylglycylglycine, were studied. At 77°K electron attachment to glyglygly produced to 21.5-G triplet without anisotropic structure. Since the results for the *N*-acetylpeptides show that secondary deamination does not occur at 77°K in 12 *M* LiCl, this triplet must then arise from N-terminal deamination. Warming the sample to 170°K resulted in a clearly resolved 18-G doublet which we associate with abstraction from one of the α-carbon positions on the parent peptide. The results found for alaglygly and alaglyglyglygly were virtually identical. In each case a 24-G quintet was found at 77°K after electron attachment (see Figure 5 for alaglyglyglygly). Upon warming to 165°K the very small deuterium atom signal was lost and the quintet became more isotropic in character with intensity ratios of 1:4:6:4:1; however, no further reaction was noted for either peptide. Since the quintet spectrum could only arise from the deamination of the alanyl residue, these results are excellent evidence for N-terminal deamination in these larger peptides as well.

Spin Density Calculations for Protonated and Deprotonated α-Carbon Radicals. The α-carbon radicals found for the dipeptides, *N*-acetylpeptides, and oligopeptides (glyglygly) give significantly larger hyperfine splittings in 12 *M* LiCl than in 8 *M* NaOD. For example, for glygly, glyala, *N*-acetylglygly, and glyglygly, 18.5, 18.7, 18.2, and 18-G hyperfine splittings are observed in 12 *M* LiCl; whereas in 8 *M* NaOH, 14, 13.5, 13.2, and 13-G splittings are observed. Esr studies of similar radicals in aqueous solution[20] and in the solid state[16,21-23] report splittings in the range 17–18 G in better agreement with our results in 12 *M* LiCl. The difference in splitting for the same radical in the two media may be explained by the deprotonation of the peptide nitrogen in 8 *M* NaOD. McLachlan spin density calculations employing usual parameters for the protonated and unprotonated structures of a glycine peptide have been performed and are reported in Table I. As can be seen the spin density at the α-carbon site is significantly reduced by the deprotonation of the peptide nitrogen. For comparison to experimental splittings a value of $Q^H(\dot{C}H) = 27$ G was employed.[24] The α-carbon hyperfine splittings are in excellent agreement with the observed experimental values for the glycine pep-

TABLE I: Theoretical Hyperfine Splittings of Peptide Radicals in Neutral and Alkaline Glasses

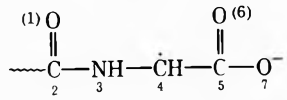

Position	McLachlan spin density[a,b]	Hyperfine splittings, G: Theoretical	Hyperfine splittings, G: Experimental (glygly)
1	0.020		
2	0.004		
3	0.134	3.5 (N)[c]	
4	0.721	19.5 (H)	18.5
5	0.009		
6	0.057		
7	0.057		

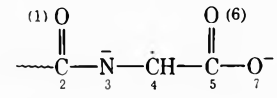

Position	McLachlan spin density	Hyperfine splittings, G: Theoretical	Hyperfine splittings, G: Experimental (glygly)
1	0.074		
2	0.061		
3	0.182	4.9 (N)	
4	0.494	13.2 (H)	14.0
5	0.075		
6	0.057		
7	0.057		

[a] HMO parameters used were $h_O = 1.5$, $h_N = 0.8$, $h_{NH} = 1.5$, $k_{C=O} = 1.6$, $k_{C-O} = 1.2$, $k_{C-\bar{N}} = 1.08$, $k_{C-NH} = 0.8$. [b] $\lambda = 1.0$. [c] $Q^N(N) = 27$.

tides. In addition, since $Q^H(CH_3)$ is approximately equal to $Q^H(CH)$,[24] the calculated results are in good agreement with those found for glyala as well.

Conclusions and Comparison to Other Work

We find that electron attachment to amino acids and peptides at 77°K in 12 *M* LiCl results in immediate deamination which occurs at the N-terminal position for the peptides. Anion radicals which were found to be stable up to 180°K in our previous work in 8 *M* NaOH are not observed.[9] We attribute this to a lowering of the activation energy for deamination by protonation of the N-terminal amine group. Since it is known that the anion of the peptide linkage protonates readily ($pK \geq 13.5$),[25] it is likely that this deamination reaction occurs before such a stabilization reaction takes place.

The mechanism of N-terminal deamination in simple peptides is in agreement with a number of other studies which include the esr of the steady-state radiolysis of aqueous solutions of peptides,[4] pulse radiolysis in aqueous solutions of a number of peptides,[3] product analysis studies after radiolysis of aqueous solutions of peptides,[2,17] and even the esr of peptides irradiated in the solid state.[16c] The agreement among the results of such a variety of techniques indicates there can be little doubt that the initial step in the reaction of electrons with simple oligopeptides is N-terminal deamination. However, there has been one report which claims C-terminal decarboxylation after electron attachment to dipeptides.[26] It is not clear that the experimental methods (photolysis of frozen aqueous solutions of 0.1 *M* peptides containing phenylalanine) used in this study produce free electrons.

Our observations that protonation of the amine group lowers the activation energy for deamination in amino acid and peptide anions is in accord with the results of Neta and Fessenden who studied electron reactions with several amino acids and glycylglycine in aqueous solution.[4] They found deamination takes place to a lesser extent at higher pH. Our observation is also in agreement with the results of a pulse radiolysis study by Simic and Hayon who find that the anion of glycylmethyl ester is observed at pH 12.6 whereas only the deaminated species is found at lower pH.[3]

For peptides with glycine at the N-terminal position we find that N-terminal deamination is followed by abstraction from the parent peptide to form an α-carbon radical (except for glycylleucine where abstraction occurred from the leucyl side chain). These results are in excellent agreement with the recent results of Garrison, *et al.*, who have studied the radiolysis of glycylglycine in dilute oxygen free solutions.[17] They find that N-terminal deamination is followed by abstraction to form C-terminal α-carbon radicals and subsequently by recombination of radicals. A similar mechanism was proposed both by these workers in the radiolysis of solid glycylglycine,[17] and by Melo in the recent esr study of irradiated glycylglycine single crystals.[16c]

Where an alanine residue is at the N-terminal position there appears to be a greater stability to the deaminated radical and a lessened tendency to abstract from the α-carbon position. The abstraction step was found to occur for such peptides in the alkaline medium.[9]

For acetylamino acids and acetylpeptides the reaction sequence (anion formation, secondary deamination, and abstraction from an α-carbon position) is found in 12 *M* LiCl as it was in 8 *M* NaOD. Rodgers, Sokol, and Garrison report that reaction of electrons with *N*-acetylalanine in high concentration leads to liberation of free alanine through a bimolecular reaction of the protonated anion.[27] The low concentrations used in our study and the rigid matrix would prevent such a reaction before the deamination step took place.

Acknowledgment. The authors wish to express their appreciation for support from the U. S. Atomic Energy Commission and the Oakland University Research Committee.

References and Notes

(1) This research was supported in part by the Division of Biomedical and Environmental Research of the U. S. Atomic Energy Commission.
(2) W. M. Garrison, *Radiat. Res. Rev.*, **3**, 285 (1972).
(3) M. Simic and E. Hayon, *Radiat. Res.*, **48**, 244 (1971).
(4) P. Neta and R. W. Fessenden, *J. Phys. Chem.*, **74**, 2263 (1970).
(5) H. C. Box, H. G. Freund, and K. T. Lilga, *J. Phys. Chem.*, **74**, 40 (1970).
(6) J. Sinclair, *J. Chem. Phys.*, **55**, 245 (1971).
(7) H. Swenson and G. C. Moulton, *Radiat. Res.*, **53**, 366 (1973).
(8) M. D. Sevilla, *J. Phys. Chem.*, **74**, 2096 (1970).
(9) M. D. Sevilla, *J. Phys. Chem.*, **74**, 3366 (1970).
(10) M. D. Sevilla, *J. Phys. Chem.*, **76**, 3577 (1972).
(11) L. Kevan in "The Chemical and Biological Action of Radiations," M. Haissinsky, Ed., Masson, Paris, 1969.
(12) V. T. Srinivasan and A. Van De Vorst, *Int. J. Radiat. Biol.*, **19**, 133 (1971).
(13) (a) J. Jortner and R. M. Noyes, *J. Phys. Chem.*, **70**, 770 (1966);

(b) R. Livingston, A. Zeldes, and E. H. Taylor, *Discuss. Faraday Soc.*, **19**, 166 (1955).
(14) "Handbook of Chemistry and Physics," 51st ed., Chemical Rubber Publishing Co., Cleveland, Ohio, 1970.
(15) See ref 8 and references therein for a complete description of the relationship between β-proton splitting and dihedral angle.
(16) (a) W. C. Lin and C. A. McDowell, *Mol. Phys.*, **4**, 333 (1961); (b) R. S. Mangaracina, *Radiat. Res.*, **32**, 27 (1967); (c) T. B. Melo, *Int. J. Radiat. Biol.*, **23**, 247 (1973).
(17) W. M. Garrison, H. A. Sokol, and W. Bennett-Corniea, *Radiat. Res.*, **53**, 376 (1973).
(18) (a) F. Patten and W. Gordy, *Radiat. Res.*, **14**, 573 (1961); (b) W. Snipes and J. Schmidt, *ibid.*, **29**, 194, (1966); (c) E. G. Liming, *ibid.*, **39**, 252 (1969).
(19) Protonation is likely under these conditions and could occur either at the peptide linkage to form $\sim$C(OH)-NH$\sim$ or carboxyl group to form C(OH)$_2$.
(20) P. Neta and R. W. Fessenden, *J. Phys. Chem.*, **75**, 738 (1971).
(21) R. C. Drew and W. Gordy, *Radiat. Res.*, **18**, 552 (1963).
(22) G. Saxebol, T. B. Melo, and T. Henrikson, *Radiat. Res.*, **51**, 31 (1972).
(23) I. Miyagawa, Y. Kurita, and W. Gordy, *J. Chem. Phys.*, **33**, 1599 (1960).
(24) J. Bolton in "Radical Ions," E. T. Kaiser, Ed., Interscience, New York, N. Y., 1968.
(25) M. Simic and E. Hayon, *J. Phys. Chem.*, **77**, 996 (1973).
(26) A. Meybeck and J. Meybeck, *Photochem. Photobiol.*, **16**, 359 (1972).
(27) M. A. J. Rodgers, H. A. Sokol, and W. M. Garrison, *J. Amer. Chem. Soc.*, **90**, 795 (1968).

Electron Spin Resonance Studies of the Effect of Ion Pairing on Some Simple Reactions Involving the Tetracyanoethylene Anion Radical

M. T. Watts, M. L. Lu, R. C. Chen, and M. P. Eastman*

Department of Chemistry, The University of Texas at El Paso, El Paso, Texas 79968 *(Received July 16, 1973)*

Publication costs assisted by The University of Texas at El Paso

The role of ion pairing in electron transfer, radical–radical dimerization, and solubility reactions involving the tetracyanoethylene anion radical ($TCNE^-$) have been investigated. Studies of the electron transfer rate between $TCNE^-$ and neutral TCNE in dimethoxyethane (DME) yield $k(15°) = 2.6 \times 10^8\ M^{-1}$ sec^{-1} and $E_a = 5.2 \pm 0.1$ kcal/mol. Similar studies in acetonitrile (MeCN) yield $k(15°) = 3.2 \times 10^9\ M^{-1}$ sec^{-1} and $E_a = 2.3 \pm 0.1$ kcal/mol. The rate in DME is considered to be that for the loose ion pair while that in MeCN is for the free ion. Complexation of the cation portion of the ion pair, which forms in DME, by the crown ethers dibenzo-18-crown-6 and perhydrodibenzo-18-crown-6 does not alter the reaction rate or the activation energy for the electron transfer process. Esr studies indicate that the dimerization of K^+TCNE^- in tetrahydrofuran and methyltetrahydrofuran is inhibited or prevented by the addition of crown ethers. The spectral parameters for the crown ether complexed K^+TCNE^- ion pair are $g_{||} = 2.00256$, $g_\perp = 2.00288$, $A_{||} = 5.56 \pm 0.1$ G, and $A_\perp = -0.32 \pm 0.03$ G. The solubility of alkali metal salts of TCNE in benzene are enhanced by crown ethers. The dissolved species are shown to exist as tight ion pairs with properties very dependent on the nature of the crown ethers. Structures for the crown ether complexed ion pair are discussed.

Introduction

A number of simple reactions involving the alkali metal salts of tetracyanoethylene (TCNE) can be conveniently studied in solution by means of esr spectroscopy. These reactions include electron transfer,[1,2] Heisenberg spin exchange,[3,4] and radical–radical dimerization.[3,5,6] Ion pairing has been considered to be an important factor in all of these reactions but details about ion pairing in solutions containing the $TCNE^-$ anion radical have been lacking.[7]

The effects of various counterions on the electron transfer rate between the $TCNE^-$ anion radical and its neutral molecule in dimethoxyethane (DME) and in tetrahydrofuran (THF) have recently been reported.[2] The rate constant at room temperature for the transfer reaction was about 10^8 sec^{-1} M^{-1} in all cases studied. In general, the results indicated that ion pairing was important in determining the nature of the electron transfer process. In these studies no account was taken of the fact that alkali metal salts of $TCNE^-$ are known to dimerize in THF.[3,5,6] It is possible that under some conditions the reaction between TCNE and a radical dimer could be a line-broadening process. In addition, it should be noted that neutral TCNE forms π complexes with DME, THF, and a variety of other solvents.[8] When π complexes form in a solvent, the electron transfer reaction should be considered to be between a free ion or radical ion pair and a solvent complexed neutral molecule.

Heisenberg spin exchange has been studied for KTCNE in DME and in THF.[3] This work has indicated that KTCNE forms ion pairs in both solvents and dimerizes in THF. Recently, the effect of crown ethers, a class of macrocyclic polyethers which complex strongly alkali metal ions, on the Heisenberg spin-exchange rate for K^+TCNE^- ion pairs in DME has been reported.[4] These studies have shown that KTCNE exists as a loose ion pair in DME and that the K^+ ion in the ion pair is complexed in a 1:1 ratio by the cyclic polyether dibenzo-18-crown-6 (DBC). The equilibrium constant at 15° for this complexation was determined to be $4 \times 10^3\ M^{-1}$.

The dimerization of alkali metal salts of TCNE in ethereal solvents has been investigated by esr and optical techniques.[3,5,6] The esr studies of Heisenberg exchange in THF solutions of KTCNE suggest that ion pairs are involved in the formation of the dimer. In general, solutions in which the ion pairs are present are characterized by a yellow color while the color of the dimer is pinkish.[6] Frozen solutions of NaTCNE and KTCNE have a color characteristic of the dimer and exhibit either no esr signal or a very weak structureless signal.[5,9]

The purposes of this paper are to investigate the role of ion pairing in electron transfer reactions involving $TCNE^-$, to discover the extent to which ion pairing is important in the dimerization of TCNE salts, and to explore new reactions involving $TCNE^-$ and its ion pairs. In these reactions the effects of crown ethers on ion pair reactivity will be investigated.

Experimental Section

The spectrometer used in these experiments and the techniques used to correct for modulation frequency broadening have been previously described.[4] Measurements of g value were carried out using a Varian V-4532 dual sample cavity. All g values were determined relative to the signal produced by KTCNE in DME (2.00279 ± 0.00002).[10] The measurements of electron transfer rates were carried out in the slow exchange limit and all experiments in which the temperature was varied were corrected to a constant concentration of neutral TCNE by means of published densities.[11,12] The viscosities for DME and MeCN were taken from the literature.[11,12] In these experiments the overlap of hyperfine lines could be neglected because $\Gamma/A_N < 0.3$.[3,13] Here Γ is the line width and A_N is the ^{14}N hyperfine splitting constant for the $TCNE^-$ radical.

In order to obtain a larger filling factor the esr experiments in which benzene and other low dielectric solvents were used were carried out in a sample tube equipped with a 3-mm i.d. Thermal American Spectrosil quartz side arm. The sample tubes used in these experiments were cleaned in several ways to determine whether ions from the wall of the sample tube were participating in ion pair formation. Such effects have previously been noted by Graceffa and Tuttle.[14]

The first cleaning technique employed involved washing the sample tube in water, soaking the tube in dichromate cleaning solution, washing with water, and soaking in an ethanolic sodium or potassium hydroxide solution. The sample tube was then carefully washed with distilled deionized water and dried. In the second technique employed the sample tubes were washed in 50:50 concentrated H_2SO_4–HNO_3 and were then washed in distilled deionized water and dried. The third technique involved soaking the sample tube in a benzene–crown ether solution, washing with acetone, and drying.

The acetonitrile (MeCN) used in these experiments was twice distilled from P_4O_{10} and stored under vacuum, while the benzene was dried and stored over sodium ribbon. The TCNE was purchased from Eastman Organic Chemicals and was purified by recrystallization from 1,2-dichloroethane followed by two sublimations. The macrocyclic polyethers, dibenzo-18-crown-6 (DBC) and perhydrodibenzo-18-crown-6 (PHBC), were purchased from Aldrich Chemical Co. The DBC was recrystallized from toluene and dried under vacuum (mp 163–164°). The PHBC was crystallized a number of times from n-hexane and dried under vacuum. No attempt was made to separate the isomers of PHBC. Samples of isomers A and B of PHBC were obtained from E. I. du Pont de Nemours and Company, Inc. The NaTCNE and KTCNE were prepared as described in the literature.[15]

It was observed that degassed solutions of TCNE in carefully dried DME and MeCN showed noticeable decomposition of the TCNE within several days of preparation. Presumably, this was due to the decomposition of the π complex formed between the solvent and the TCNE. The $TCNE^-$ radical, by itself, was stable for long periods of time in both solvents. To minimize the error due to the decomposition of neutral TCNE, line width measurements were begun immediately after adding the neutral TCNE to the radical containing solutions. This addition was accomplished by means of a break-seal. To avoid systematic errors, the order (with respect to temperature) in which the line widths were determined was randomized and the results at 15° were checked intermittently throughout the experiments. It is believed that the decomposition of TCNE is not a significant factor in these experiments.

Results and Discussion

(*a*) *Electron Transfer.* The studies on TCNE reported here were carried out in the region of slow exchange where the observed exchange rate constant k_{obsd} is given by the expression[16,17]

$$k_{obsd} = \frac{1.52 \times 10^7(\Gamma - \Gamma_0)f_m}{[TCNE]} \quad (1)$$

Here Γ and Γ_0 are the first derivative line widths in the presence and absence of transfer, and f_m is a statistical factor which compensates for the lack of observable line-broadening effects in electron transfer between radicals with the same nuclear spin configuration.

When a reaction involves a diffusion step and a reaction step, k_{obsd} is related to the rate constant for the reaction step, $k_{act.}$, and the rate constant for the diffusion step, k_{diff}, by the expression[18]

$$\frac{1}{k_{obsd}} = \frac{1}{k_{diff}} + \frac{1}{k_{act.}} \quad (2)$$

For the electron transfer reaction considered k_{diff} can be estimated from the expression[3,18]

$$k_{diff} = \frac{RT}{750\eta} \quad (3)$$

Here η represents the viscosity of the solvent.

Figure 1 shows a plot of log k_{obsd} and of log $k_{act.}$ *vs.* $1/T$ for KTCNE–TCNE in MeCN. A least-squares fit of the data for $k_{act.}$ to the Arrhenius equation yields $A = 1.8 \pm 0.4 \times 10^{11}$ M^{-1} sec^{-1} and $E_a = 2.3 \pm 0.1$ kcal/mol. The value of $k_{act.}$ at 15° is 3.2×10^9 M^{-1} sec^{-1}. The estimated error in this value is 10–15%.

Figure 2 shows a plot of $k_{act.}$ for KTCNE–TCNE in DME. Here $k_{act.} \simeq k_{obsd}$ since $k_{diff}^{-1} \ll k_{obsd}^{-1}$. The least-squares fit of the Arrhenius equation gives $A = 2.4 \pm 0.2 \times 10^{12}$ M^{-1} sec^{-1} and $E_a = 5.2 \pm 0.1$ kcal/mol. The experimental value of $k_{act.}$ at 15° in this case is 2.6×10^8 M^{-1} sec^{-1} with an estimated error of 10%.

The relationship between the structure of ion pairs in solution and the rate of electron transfer has been investigated for a variety of systems.[19-23] In general, the rates for loose ion pairs have been shown to be $10^8 \sim 10^9$ M^{-1} sec^{-1} with an activation energy of 2.9–3.6 kcal/mol, while

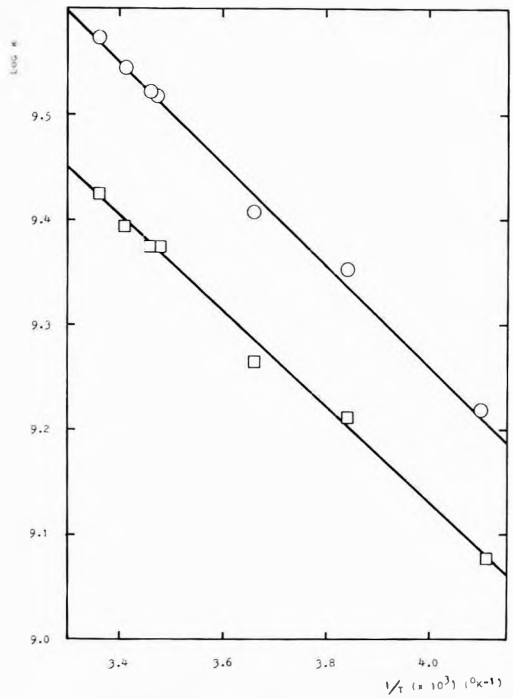

Figure 1. $k_{act.}$ (O) and k_{obsd} (□) vs. $1/T$ for 1.5×10^{-3} M TCNE and 3×10^{-4} M KTCNE in MeCN.

those for tight ion pairs are 10^6–10^7 M^{-1} sec^{-1} with an activation energy of 4–6 kcal/mol. The rate constants for free anion radicals are $\geq 10^9$ M^{-1} sec^{-1} and have an activation energy of ~2–3 kcal/mol.

A comparison of the above information with the data in Figures 1 and 2 suggests that under the experimental conditions reported here KTCNE exists primarily as free ions in the high dielectric solvent MeCN and as an ion pair in DME. This latter conclusion is supported by esr studies of Heisenberg spin exchange and by determinations of K_{diss} for anion radical salts in DME.[3,24]

The activation energy for the electron transfer process in DME is characteristic of that for a tight ion pair, while the rate for the transfer process is close to that for a loose ion pair. No alkali metal hyperfine splittings have ever been observed for alkali metal salts of TCNE in DME even though such systems yield very narrow esr line widths.[3] In a following section it is shown that under certain conditions $TCNE^-$ can form tight ion pairs with well defined alkali metal hyperfine splittings. Thus it would seem that the ion pair which forms in DME has properties more characteristic of a loose ion pair than a tight ion pair. The observation that the electron transfer rate in MeCN differs by an order of magnitude from the value in DME and is near the diffusion controlled limit suggests that π complex formation between TCNE and the solvent does not affect the rate of electron transfer significantly.

Based on the preceding, it would be predicted that crown ethers would affect the electron transfer rate in DME, where ion pairs are implicated in the electron transfer reaction, but not in MeCN, where free ions are implicated. The addition of DBC to MeCN solutions of KTCNE and TCNE produced a 10% reduction in the transfer rate and no change in the activation energy within experimental error (~10%). In these studies it was assumed that the complexation constant for DBC and K^+ in MeCN was similar to that for DBC and Na^+ in dimethylformamide.[25] Surprisingly, however, crown ether seemed to have little effect on the rate of electron transfer for

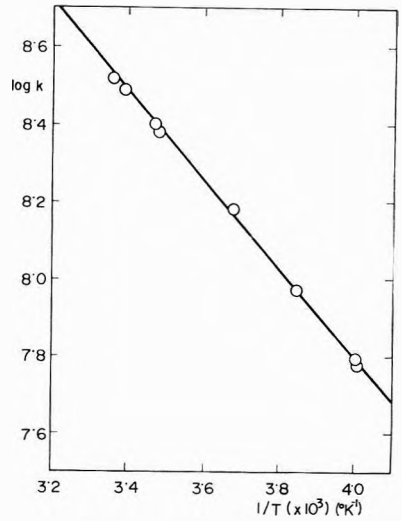

Figure 2. $k_{act.}$ vs. $1/T$ for 3×10^{-2} M TCNE and 1×10^{-4} M KTCNE in DME.

K^+TCNE^- in DME. The results of experiments in which TCNE was added by means of a break-seal to solutions of KTCNE and DBC are summarized in Table I.

In these experiments the line width of the DBC–KTCNE solutions were accurately determined as a function of temperature before the addition of the TCNE. Additional experiments were carried out in which DBC was added to solutions of KTCNE and TCNE. In these experiments the addition of DBC produced no change within experimental error in the transfer rate at 15°.

Previous studies have shown that DBC complexes the K^+TCNE^- ion pair according to the reaction DBC + K^+, $TCNE^- \rightleftarrows$ DBC,K^+,$TCNE^-$. The equilibrium constant for this reaction is about 4×10^3 M at 15°. Based on studies of ion pairing in other systems the equilibrium constant for a similar reaction involving PHDC and K^+ would be expected to be about the same or larger.[26] Thus, in the experiments involving crown ethers, summarized in Table I, essentially all of the K^+TCNE^- ion pairs are complexed by crown ethers.

The values of E_a and A in Table I for the samples containing crown ethers were determined over the temperature range of 15–37°. It was difficult to investigate reliably the transfer reaction over a wider temperature range due to the dissociation of the crown ether complex at high temperatures and the precipitation of crown ethers at lower temperatures. The errors in E_a and A, given in Table I, represent only the standard deviation in the least-squares slope and intercept as determined from studies on a single sample. The estimated error in the $k_{act.}$ values at 15° are about 10–15% except for the radical concentration of 1.5×10^{-3} M. Here the error is estimated to be somewhat larger.

Clearly, the experiments summarized in Table I indicate that complexing the cation portion of the K^+TCNE^- ion pair with crown ethers does not alter the electron transfer rate within experimental error. This result implies that the activation energy for the transfer process is not affected by the change in the cation solvation resulting from crown ether complexation. The observation that the measured rate constant does not change significantly when the radical concentration is increased by a factor of 10 implies that dissociation of the K^+TCNE^- ion pair is not significant even at 1×10^{-4}. This observa-

TABLE I: A Summary of Experimental Studies of Electron Transfer for KTCNE in DME in the Absence and Presence of Crown Ethers

KTCNE, *M*	CE,[a] *M*	$k_{act.}$ (15°), M^{-1} sec^{-1}	E_a, kcal/mol	A, M^{-1} sec^{-1}
1×10^{-4}	0	2.6×10^{8}	5.2 ± 0.1	$2.4 \pm 0.2 \times 10^{12}$
3×10^{-4}	5×10^{-3} [b]	3.4×10^{8}	5.1 ± 0.2	$2.6 \pm 0.1 \times 10^{12}$
1×10^{-4}	4×10^{-3} [c]	3.1×10^{8}	4.6 ± 0.2	$9.7 \pm 3 \times 10^{11}$
1.5×10^{-3}	4×10^{-3} [b]	2.3×10^{8}	~5	$\sim 1.5 \times 10^{12}$

[a] Crown ether concentration. [b] PHBC isomers A and B. [c] DBC.

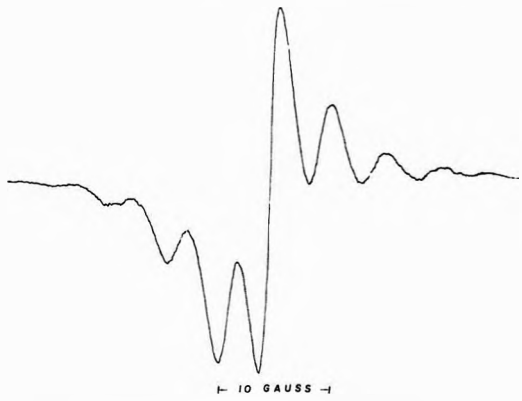

Figure 3. First derivative *x*-band esr spectrum of DBC, K^+, $TCNE^-$ in MTHF at 103°K.

tion supports the contention previously made that K_{diss} for the K^+TCNE^- ion pair is $\sim 10^{-6}$ or less.[4]

Szwarc, *et al.*, on the basis of studies of electron transfer reactions, have reported that in a sodium naphthalenide ion pair the Na^+ ion can be complexed by a molecule of tetraglyme to form what appear to be two distinct glymated sodium naphthalenide ion pairs.[22] It was suggested that the ion pair with the faster exchange rate was solvated to a greater degree than the ion pair with the slower rate and that the electron transfer from the more solvated ion pair could proceed with little or no solvent rearrangement about the Na^+ ion. The work on sodium naphthalenide indicated that complexation of the cation in a radical ion pair by a polydentate ether could alter the nature of the ion pair and the rate of the electron transfer reaction. In contrast to the studies on the naphthalene anion radical no evidence was obtained in the above studies of $TCNE^-$ for a change in the electron transfer rate upon ion pair complexation by crown ethers or for the formation of more than one type of complexed ion pair.

(*b*) *The Dimerization Reaction.* The observation that loose ion pairs were involved in the dimerization of $TCNE^-$ in THF suggested that this reaction might be prevented or inhibited by complexing the cation portion of the ion pairs with bulky crown ethers.[3] Experimental studies between 15 and 25°, similar to those previously described, showed that for a radical concentration of 10^{-3} *M* and crown ether concentrations of $\sim 2 \times 10^{-3}$ *M* most of the ion pairs in THF and MTHF were complexed by crown ethers.[4,9]

Solutions of KTCNE and DBC in MTHF when rapidly cooled to 77°K remained yellow, indicating the presence of the radical ion pair. When rapidly cooled these MTHF solutions showed no evidence of precipitation of the crown ethers. Solutions of DBC and KTCNE in THF behaved similarly except that the frozen solution had a dark reddish color differing in hue from solutions in which there was no crown ether. In both MTHF and THF precipitation of the crown ether occurred when the samples were slowly cooled.

Figure 3 shows the spectrum obtained from a MTHF solution of KTCNE and DBC. Spectra obtained from THF solutions were similar. An analysis of a spectrum obtained at 103°K was carried out using the procedure of Lefebvre and Maruani.[27] This analysis yielded the following spectral parameters: $g_{\parallel} = 2.00256 \pm 0.00008$; $g_{\perp} = 2.00288 \pm 0.00008$; $A_{\parallel} = 5.56 \pm 0.1$ G; and $A_{\perp} = -0.32 \pm 0.03$ G. Symons, *et al.*, have presented arguments for the sign of $A_{\perp}$ and $A_{\parallel}$.[28]

The above values agree with those obtained from a solution of KTCNE in C_2D_5OD at 97°K, where presumably the $TCNE^-$ exists as a free ion, and with those obtained in rare gas matrices.[29,30] The *g* values differ, however, from those obtained from solutions of NaI and TCNE in THF. It is interesting to note that although an NaI–TCNE mixture, in which NaI is in excess, at 77°K produces a signal similar to that in Figure 3 a solution of pure NaTCNE in THF when frozen yields no esr spectrum.[9]

The above results indicate that complexation of K^+TCNE^- ion pair by crown ethers either prevents the dimerization reaction or allows the solvent to trap the complexed ion pairs upon rapid freezing. Esr studies of the effect of crown ethers on the Heisenberg spin exchange rate in THF solutions of KTCNE suggest that complexation prevents the dimerization reaction and that for radical concentrations $\sim 10^{-3}$ *M* most of the radicals remain in the form of ion pairs after complexation.[4,9] A quantitative analysis of the results has not been carried out because at the low temperature where dimerization is most significant the solubility of crown ethers is severely limited.[6,31]

(c) *Solubility in Benzene and Tight Ion Pairing.* On the basis of what has been reported concerning the effects of crown ethers on the solubility of salts in benzene and on ion pairing in solutions of TCNE salts, it seemed reasonable that crown ethers might form a benzene soluble complex with NaTCNE or KTCNE.[4,31,32] It also seemed reasonable that the nature of the crown ether ion pair complex formed in benzene might differ substantially from that formed in ether type solvents.

Initial studies showed that no esr signal from dissolved radicals could be observed from mixtures of solid KTCNE or NaTCNE and benzene. The addition of DBC to such mixtures produced yellow solutions which yielded distinctive esr spectra. Figure 4 shows the signal obtained from a solution of 1×10^{-3} *M* in DBC and 1×10^{-4} *M* in NaTCNE. In general, excess polyether was necessary to dissolve both NaTCNE and KTCNE in benzene. This suggests either that more than one crown ether molecule is associated with each M^+TCNE^- ion pair or that an equilibrium for the formation of the complex can be written as DBC + S $\rightleftarrows$ complex. Here S represents either

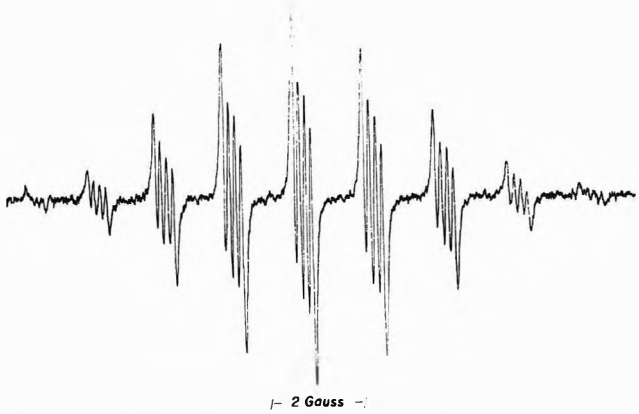

Figure 4. First derivative *x*-band esr spectrum of DBC–NaTCNE tight ion pair complex in benzene at 51°.

solid MTCNE or MTCNE which is dissolved in benzene and is in equilibrium with solid MTCNE. It should be noted that no esr signal was observed from M^+TCNE^- tight ion pairs in cyclohexane solutions of DBC and PHBC. This seems to indicate that the ion pair complex is solvated to some degree by benzene.

An analysis of spectra obtained between 9 and 106° yielded the information that the four nitrogen nuclei in the $TCNE^-$ portion of the NaTCNE and KTCNE complex are completely equivalent and that each line is split by the interaction of the unpaired electron with one alkali metal nucleous. The observed ^{14}N isotropic hyperfine splitting constant (A_N) was 1.57 ± 0.01 G over the temperature range studied. The value of A_N for K^+TCNE^- in DME is 1.575 G.[1c] The values of A_{Na}, as determined from computer simulations of the spectra, are shown in Figure 5. No dependence of A_{Na} on the DBC concentration was observed. The decrease in alkali metal splitting with decreasing temperature was accompanied by an increase in line width; thus the resolution of the spectral components decreased at lower temperatures. The value of A_K was about 15 to 20 mG at 30° and showed only a slight temperature dependence.

The absolute g value for both complexes was determined to be 2.00278 ± 0.00003. Relative g value measurements showed that g(KTCNE–DME) > g(NaTCNE–benzene) > g(KTCNE–benzene) as expected on the basis of previous detailed studies of the effect of ion pairing on g value.[33,34]

Based on experiments carried out in ether solvents it seems reasonable to assume at this point that a 1:1 DBC–NaTCNE complex forms in benzene.[4] The observations that the TCNE-nitrogens are completely equivalent and that A_M is quite small suggest a possible structure for the complex in which the oxygen atoms of the DBC and the $TCNE^-$ are in parallel planes and the alkali metal ion lies somewhere along the line joining the center of the DBC and the $TCNE^-$. This model places the M^+ ion in a nodal plane of the wave function for the unpaired electron on $TCNE^-$ [35] and allows for the possibility that the alkali metal ion is shifted slightly away from the center of the plane of oxygen atoms in the crown ether. Smid, *et al.*, has previously discussed a similar model based on nmr and optical studies of a fluorenyl crown ether complex[36] and has demonstrated that crown ethers can coordinate externally to tight pairs.[37,38]

The alkali metal hyperfine splitting in this model arises from two sources.[33] The first is the vibration of the alkali metal ion out of the nodal plane and the consequent direct transfer of unpaired spin onto the metal ion. The second is through exchange mechanisms involving the unpaired electron and closed shell electrons. The first source produces a positive contribution to the alkali metal HFSC while the second can produce a negative contribution. Knowledge of the sign of the HFSC is necessary to determine the relative contribution of the two mechanisms to the overall splitting.

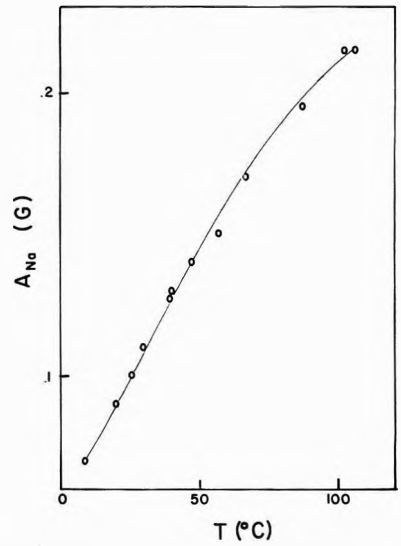

Figure 5. Metal atom hyperfine splittings for the DBC–NaTCNE tight ion pair over the temperature range 9–106°.

Esr studies of the tight ion pairs formed at 25° in benzene solutions of PHBC show that the ^{23}Na hyperfine splitting for isomer A is 0.240 G and that for isomer B is 0.340 G. These ion pairs are being investigated in detail to determine if the spectral differences between isomer A and isomer B complexes can yield information about the structure of the complex. In the optical studies of fluorenyl sodium and potassium both crown complexed contact ion pairs and crown separated ion pairs were observed.[37] No difference was noted in the spectra due to ion pairs complexed by isomers A and B of PHBC. In contrast to the work reported here, esr studies have indicated that complexation by crown ethers of the cation in an anthracenide radical ion pair prevents the formation of a contact ion pair in ether solvents.[39]

In both the MTCNE–DBC and TCNE–PHBC complexes the maximum in the optical spectrum was shifted to lower wavelengths. Solutions of KTCNE in DME have a maximum in the optical spectrum at about 430 nm, while the DBC–KTCNE complex in benzene has a maximum at about 415 nm. Similar shifts due to ion pairing in the optical spectrum of the fluorenyl anion have been extensively investigated.[40]

Acknowledgments. Helpful discussions with W. C. Herndon and R. A. Marcus are gratefully acknowledged. The spectral parameters for the crown complexed ion pairs were determined by C. Polnaszek and J. H. Freed. The A and B isomers of PHBC were provided by H. K. Frensdorff of E. I. duPont de Nemours and Company, Inc. Some of the equipment used in this work was purchased through a grant from Research Corporation. This research was supported by the Robert A. Welch Foundation of Houston, Texas.

References and Notes

(1) W. D. Philips, J. C. Rowell, and S. I. Weissman, *J. Chem. Phys.*, **33**, 626 (1960).
(2) (a) M. Ogasawara, Takaoka, and K. Hayashi, *Bull. Chem. Soc. Jap.*, **46**, 35 (1973); (b) R. Chang and J. Piehler, *ibid.*, **46**, 1296 (1973).
(3) M. P. Eastman, R. G. Kooser, M. R. Das, and J. H. Freed, *J. Chem. Phys.*, **51**, 2690 (1969).
(4) M. T. Watts, M. Lu, and M. P. Eastman, *J. Phys. Chem.*, **77**, 625 (1973).
(5) M. Itoh, *Bull. Chem. Soc. Jap.*, **45**, 1947 (1972).
(6) R. Chang, *J. Phys. Chem.*, **74**, 2029 (1970).
(7) M. C. R. Symons, *J. Phys. Chem.*, **71**, 172 (1970).
(8) (a) R. E. Merrifield and W. D. Phillips, *J. Amer. Chem. Soc.*, **80**, 2778 (1958); (b) R. Vars, L. A. Tripp, and L. W. Pickett, *J. Phys. Chem.*, **66**, 1754 (1962); (c) D. F. Iten and M. Calvin, *J. Chem. Phys.*, **42**, 3760 (1965); (d) F. E. Stewart, M. Eisner, and W. R. Carper, *ibid.*, **44**, 2866 (1966).
(9) M. L. Lu, Master's Thesis, University of Texas at El Paso, 1973.
(10) M. R. Das and J. H. Freed, unpublished results.
(11) C. Carvajal, K. J. Toile, J. Smid, and M. Szwarc, *J. Amer. Chem. Soc.*, **87**, 5548 (1965).
(12) J. Timmermans, Ed., "Physico-Chemical Constants of Pure Organic Compounds," Vol. I, Elsevier Publishing Co., Amsterdam, 1965.
(13) W. Plachy and D. Kivelson, *J. Chem. Phys.*, **47**, 3312 (1967).
(14) P. Graceffa and T. R. Tuttle, Jr., *J. Chem. Phys.*, **50**, 1908 (1969).
(15) O. W. Webster, W. Mahler, and R. E. Benson, *J. Amer. Chem. Soc.*, **84**, 3678 (1962).
(16) L. H. Piette and W. A. Anderson, *J. Chem. Phys.*, **30**, 899 (1959).
(17) R. Chang, *J. Chem. Educ.*, **47**, 563 (1970).
(18) R. A. Marcus, *J. Chem. Phys.*, **43**, 3477 (1965).
(19) N. Hirota, *J. Phys. Chem.*, **72**, 127 (1967).
(20) N. Hirota, R. Carraway, and W. Shook, *J. Amer. Chem. Soc.*, **90**, 3611 (1968).
(21) G. L. Malinoski, W. H. Bruning, and R. Griffin, *J. Amer. Chem. Soc.*, **92**, 2865 (1970).
(22) K. Hofelman, J. Jagur-Grodzinski, and M. Szwarc, *J. Amer. Chem. Soc.*, **91**, 4645 (1969).
(23) B. F. Wong and N. Hirota, *J. Amer. Chem. Soc.*, **94**, 4419 (1972).
(24) P. Chang, R. V. Slates, and M. Szwarc, *J. Phys. Chem.*, **70**, 3180 (1966).
(25) E. Shchori, J. Jagur-Grodzinski, Z. Luz, and M. Shporer, *J. Amer. Chem. Soc.*, **93**, 7133 (1971).
(26) H. K. Frensdorff, *J. Amer. Chem. Soc.*, **93**, 600 (1971).
(27) R. Lefebvre and J. Maruani, *J. Chem. Phys.*, **42**, 1480 (1965).
(28) J. A. Brivati, J. M. Gross, M. C. R. Symons, and D. J. A. Tinling, *J. Chem. Soc.*, 6504 (1965).
(29) C. F. Polasznek, Ph.D. Thesis, Cornell University, Ithaca, N. Y., 1973.
(30) P. H. Kasi, *Accounts Chem. Res.*, **4**, 329 (1971).
(31) C. J. Pedersen, *J. Amer. Chem. Soc.*, **89**, 7017 (1967).
(32) D. J. Sam and H. E. Simmons, *J. Amer. Chem. Soc.*, **94**, 4024 (1972).
(33) J. L. Sommerdijk and Egbert De Boer in "Ions and Ion Pairs in Organic Reactions," M. Szwarc, Ed., Wiley-Interscience, New York, N. Y., 1972, p 322.
(34) W. G. Williams, R. J. Pritchett, and G. K. Fraennkel, *J. Chem. Phys.*, **52**, 5584 (1970).
(35) J. Feuer, Ph.D. Thesis, Texas Tech University, 1970.
(36) K. H. Wong, G. Konizer, and J. Smid, *J. Amer. Chem. Soc.*, **92**, 666 (1970).
(37) U. Takaki, T. E. Hogan Esch, and J. Smid, *J. Phys. Chem.*, **76**, 2152 (1972).
(38) U. Takaki, T. E. Hogen Esch, and J. Smid, *J. Amer. Chem. Soc.*, **93**, 6760 (1971).
(39) J. L. Dye, M. T. Lok, F. J. Tehan, R. B. Coolen, N. Papadakis, J. M. Ceraso, and M. G. Debacker, *Ber. Bunsenges. Phys. Chem.*, **75**, 659 (1971).
(40) J. Smid in "Ions and Ion Pairs in Organic Reactions," M. Szwarc, Ed., Wiley-Interscience, New York, N. Y., 1972, p 85.

Study of Iron–Nitrosyl Complexes Formed in Zeolites

J. W. Jermyn, T. J. Johnson, E. F. Vansant, and J. H. Lunsford*

Department of Chemistry, Texas A & M University, College Station, Texas 77843 *(Received June 19, 1973)*

Publication costs assisted by The Robert A. Welch Foundation

Nitric oxide reacted with ferrous ions in iron-exchanged zeolites yielding high-spin ($S = 3/2$) and low-spin ($S = 1/2$) $[Fe(I)NO]^{2+}$ complexes. The high-spin complex, which was formed upon adsorption of nitric oxide at low pressures, is characterized by an epr spectrum with $g_\perp = 4.07$ and $g_\parallel = 2.003$ and an infrared band at 1890 cm^{-1}. The low-spin complex was formed in a Y-type zeolite upon adsorption of nitric oxide followed by evacuation of the sample at 25°. It is characterized by an epr spectrum with $g_{xx} = 2.015$, $g_{yy} = 2.055$, and $g_{zz} = 2.089$ and an infrared band at 1778 cm^{-1}. No ^{14}N or ^{57}Fe hyperfine structure was observed. Both complexes were thermally stable at 25°; however, at elevated temperatures the low-spin complex was more stable. About 20% of the ferrous ions were involved in complex formation, regardless of the exchange level. The high-spin complex was favored in the Y-type zeolite, whereas the reverse was true in a mordenite sample. The epr spectrum of a weakly held form of nitric oxide was attributed to a $NO–Na^+$ complex involving residual sodium ions. A slightly more stable NO species with an infrared band at 1822 cm^{-1}, but no comparable epr spectrum, was also observed.

Introduction

The importance of transition metal complexes in the dissociation and reduction of NO has resulted in a series of experiments on nitrosyl complexes formed in zeolites. Nitric oxide forms a weakly bonded complex with Cu(I) in a Cu(I)Y zeolite.[1] The unpaired electron is about 20% localized on the copper with equivalent $3d_{z^2}$ and 4s character. The analogous $[Ag(I)NO]^+$ complex has been observed recently in a Ag(I)Y zeolite.[2] In addition, a much more stable silver complex is formed at higher NO pressures. This has been attributed to $[Ag(I)_2NO]^{2+}$ where the NO is located in the sodalite unit between two silver ions.

Although a number of iron-nitrosyl compounds are known, there has been essentially no effort to characterize

them in zeolites. Boudart and coworkers[3] observed only a small alteration in the Mössbauer spectrum of Fe(II) upon adsorption of nitric oxide, which suggested weak interactions. In the present work infrared and electron paramagnetic resonance (epr) evidence indicates the formation of rather stable iron-nitrosyl complexes with a fraction of the iron which is present in the zeolite. Two more weakly bound forms of nitric oxide were also detected. As expected, the more stable complexes result in an alteration in the oxidation state and spin state of the ferrous ions. Both mordenite and Y-type zeolites have been studied in order to determine differences in the formation of complexes within these two crystalline aluminosilicates.

Experimental Section

Two NaY samples and one Na mordenite sample were exchanged according to the procedure described by Delgass, *et al.*[4] The ferrous ion concentration and the repetition of exchange were varied in a manner which produced 2×10^{19}, 3×10^{20}, and 7×10^{19} exchangeable Fe^{2+} ions per gram of zeolite on a hydrated basis for the three samples which are designated as FeY(1), FeY(2), and FeM, respectively. The value for FeY(2) corresponds to 48% exchange of the original sodium ions with ferrous ions. Two additional mordenite samples were prepared starting with Fe_2O_3. One batch of Fe_2O_3 enriched to 68% iron-57 was obtained from the Oak Ridge National Laboratory and the other was not enriched. In parallel steps the Fe_2O_3 was dissolved in concentrated HCl and the solution was evaporated four times almost to dryness. The pH was adjusted to 2 with NaOH and 2.0 g of Na mordenite was added to the respective 100-ml solutions. The exchange which was carried out for 16 hr resulted in 6×10^{18} exchangeable Fe^{3+} ions per gram of zeolite.

The zeolite samples were degassed briefly at room temperature and then in 100° increments to 400°. A small amount of Fe^{3+}, as indicated by the epr spectrum, was then reduced by heating the sample in H_2 at 400°. In some cases the samples were oxidized in O_2 before the reduction step in order to remove a trace amount of carbonaceous material which was present on the zeolite.

The NO gas contained small amounts of N_2O and NO_2 which were present as impurities. These were removed by repeatedly distilling off a fraction of the NO and collecting it at −196° until the blue color due to N_2O_3 was no longer observed in the frozen material.

The epr and infrared cells have been described previously.[5,6] The infrared cell, however, was modified by the addition of a platinum tray which was located above the zeolite sample. The tray contained a relatively large amount of NaY zeolite which acted to remove gaseous impurities. When the device was employed, the color of the sample remained off-white throughout the experiment, whereas without the additional zeolite the sample plate took on a dark color.

Infrared spectra were obtained at room temperature with a Beckman IR-12 spectrophotometer which was operated in both the absorption and transmission modes. The programming of the slit widths was such that a maximum resolution of 3 cm^{-1} was maintained. The self-supporting zeolite plates had a density of 10 mg/cm^2 and a maximum transmission of approximately 60%.

A Varian E6S spectrometer was used to obtain the epr spectra which were recorded with the sample at either 25 or −196°. The g values and spin concentrations were calculated relative to a phosphorus-doped silicon standard. A numerical double integration procedure was used to determine the spin concentration.

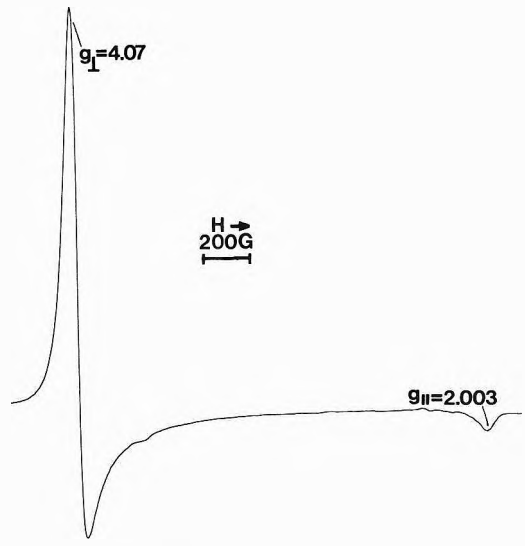

Figure 1. Epr spectrum of $S = 3/2$ $[Fe(I)NO]^+$ in a Y-type zeolite. Spectrum recorded with the sample at −196°.

Results

Epr Studies. The epr spectrum of the reduced iron-exchanged zeolites revealed only a broad background spectrum and a weak spectrum centered around $g = 2.00$, which is attributed to Mn^{2+} impurities. Mössbauer studies on similar zeolites indicate that most, if not all, of the iron was present in the ferrous state.[4]

The addition of successive amounts of nitric oxide at 25° resulted in the appearance of the spectrum (spectrum A) shown in Figure 1 and for FeY(2) Figure 2a-c. Essentially all of the nitric oxide was adsorbed on the sample up to a level of 2×10^{19} NO molecules/g of zeolite, and the spin concentration was equivalent to the number of molecules of gas adsorbed within a rather large experimental error. (An estimated error of ±30% in the spin concentration of this species resulted from an uncertainty in the baseline over the extended region of integration.) The spectrum continued to grow in intensity as more nitric oxide was added, up to a residual pressure of 50 Torr.

This spectrum, which is characterized by $g_\perp = 4.07$ and $g_\parallel = 2.003$, was observed in varying concentrations on all of the zeolites studied. No iron-57 hyperfine structure could be resolved. The maximum spin concentrations along with the iron concentrations for three different samples are listed in Table I. It is evident that the paramagnetic species constitutes 15–20% of the exchangeable iron. The spectrum could be observed at room temperature as well as at −196°, although the parallel component was difficult to detect at the higher temperature because of line broadening.

Evacuation of the sample at 25° for 1 hr resulted in a small increase in the signal intensity; however, the intensity of the spectrum was reduced by 50% upon evacuation at 50° for 1 hr (Figure 2d). The signal reappeared at a somewhat reduced intensity upon a second addition of nitric oxide.

Another prominent spectrum (spectrum B) was observed following evacuation of NO from the sample at 25 or 50°, provided the Y-type zeolite was not cooled to −196° in the presence of nitric oxide. This spectrum,

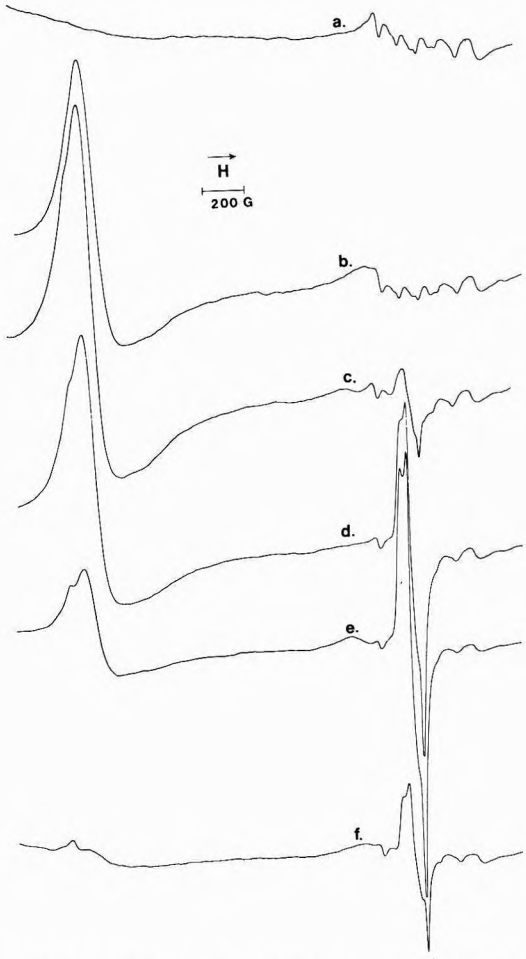

Figure 2. Epr spectra of high-spin and low-spin $[Fe(I)NO]^{2+}$ complexes in a Y-type zeolite recorded with the sample at 25°: (a) before addition of NO, amplification of 2; (b) 1 Torr of NO, amplification of 2; (c) 10 Torr of NO, evacuated 15 sec, amplification of 2; (d) sample under vacuum 1 hr at 25°, amplification of 1.2; (e) sample under vacuum 1 hr at 50°, amplification of 1.0; (f) sample under vacuum 1 hr at 100°, amplification of 1.2.

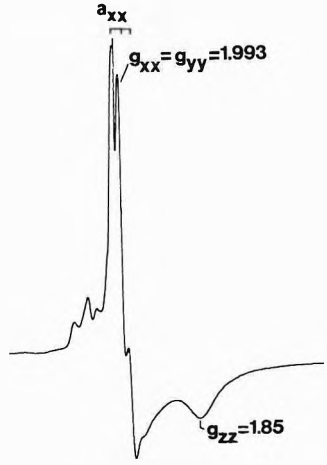

Figure 3. Epr spectrum of weakly adsorbed NO in iron-exchanged mordenite. Spectrum recorded with the sample at −196°.

which is depicted in Figure 2d,e grew in intensity for evacuation times up to 4 hr at 25° and 1 hr at 50°. Further evacuation at 100° reduced the intensity to 30% of the maximum obtained at 50°. With the mordenite samples

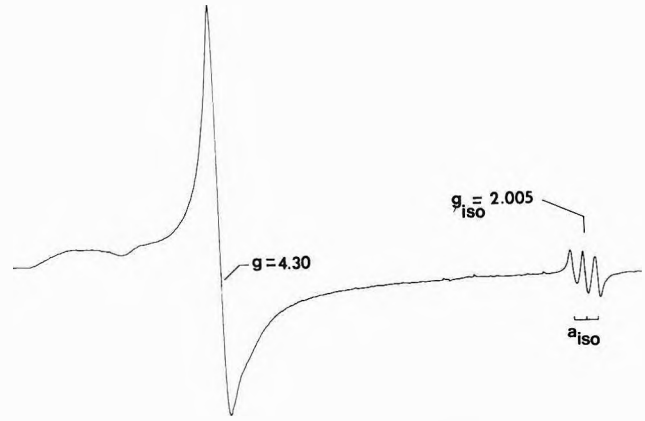

Figure 4. Epr spectrum of Fe(II)Y zeolite following adsorption of 200 Torr of NO_2. Spectrum recorded with the sample at −196°.

spectrum B was observed even without evacuation of the nitric oxide, but the removal of nitric oxide greatly increased its intensity. Cooling the sample of mordenite in the presence of nitric oxide did not prevent the formation of the complex. Spectrum B is characterized by g_{xx} = 2.015, g_{yy} = 2.055, and g_{zz} = 2.089. In the spectrum of the samples containing ^{57}Fe a slight broadening of the line width was observed, but no hyperfine structure was resolved. The splitting in each of the three principal directions must be less than 5 G. The maximum spin concentrations of the species responsible for spectrum B are listed in Table I.

The spectrum of a third paramagnetic species (spectrum C) was observed only at −196° on samples which contained a relatively large amount of nitric oxide. It is characterized by g_{xx} = g_{yy} = 1.993 and g_{zz} = 1.85. A poorly resolved triplet is assigned to a ^{14}N hyperfine splitting with a_{xx} = 32 G. Spectrum C, which is more prominent on the mordenite sample, is shown in Figure 3.

Since NO is known to dissociate on zeolites at low temperatures giving N_2O and ultimately NO_2, it was desirable to study the spectra which resulted from the adsorption of NO_2.[6] The spectrum shown in Figure 4 was observed when 200 Torr of purified NO_2 was adsorbed at 25°. The signal at g = 4.30 is due to Fe^{3+} in distorted tetrahedral symmetry.[7-9] The same spectrum of the Fe^{3+} ion was also formed by the oxidation of the zeolites in molecular oxygen at 400°. The nearly symmetric lines at g = 2.005 with a_{iso} = 56 G may be attributed to NO_2 which is librating in the zeolite cavities.[10]

At 25° molecular oxygen reacted rapidly and irreversibly with the species responsible for spectrum B. Simultaneously, the Fe^{3+} spectrum grew in intensity, but no NO_2 spectrum was observed. Spectrum A decreased about 20% in intensity. Spectrum A and the Fe^{3+} spectrum were reversibly broadened in the presence of molecular oxygen.

Infrared Studies. All of the infrared studies were carried out on the Y-type zeolites. As shown in Figure 5, the successive addition of NO resulted at first in the formation of a band at 1890 cm^{-1} followed by the formation at higher pressures (>5 Torr) of a band at 1822 cm^{-1} and a weak shoulder at 1930 cm^{-1}.

A 15-sec evacuation of the sample to remove gas-phase NO did not alter the spectrum. Extended evacuation of the sample at 25° resulted in a very significant decrease in the amplitude of the bands at 1822 and 1930 cm^{-1}. The formation of a new band at 1778 cm^{-1} was also observed. Evacuation of the sample at 50° for 1 hr resulted in a de-

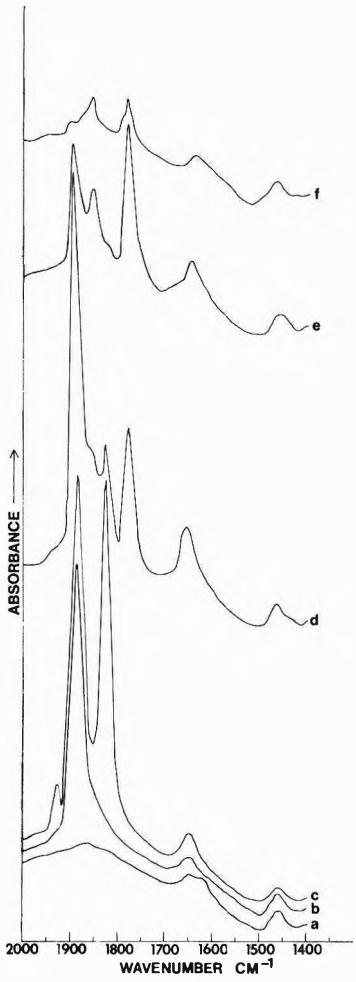

Figure 5. Infrared spectrum of an Fe(II)Y zeolite: (a) before addition of NO; (b) 1 Torr of NO; (c) 10 Torr of NO, evacuated 15 sec; (d) sample under vacuum 4 hr at 25°; (e) sample under vacuum 1 hr at 50°; (f) sample under vacuum 1 hr at 100°.

TABLE I: Spin Concentrations and Exchangeable Iron Concentrations in Zeolites

Zeolite	Spin concentration, spins/g × 10^{-19}		Iron concentration, atoms/g × 10^{-19}
	High-spin $[Fe(I)NO]^{2+}$	Low-spin $[Fe(I)NO]^{2+}$	
FeY(1)	0.3 ± 0.1	0.1 ± 0.03	2
FeY(2)	3 ± 1	2 ± 0.7	30
FeM	0.1 ± 0.03	1 ± 0.3	7

crease in the band at 1890 cm^{-1}, but the band at 1778 cm^{-1} actually increased about 20% in amplitude. The latter band was weak following evacuation at 100° for 1 hr.

Cooling the sample to −78° in the presence of 600 Torr of nitric oxide effected the disproportionation reaction as indicated by strong bands due to N_2O, NO_2, and N_2O_3. A brief evacuation of the sample resulted in the formation of covalently bonded nitrites as previously reported for a decationated Y zeolite.[6]

Discussion

Interpretation of the Data. Spectrum A is characteristic of an ion in an $S = 3/2$, $M_s = \pm 1/2$ spin state with the zero field splitting, $D \gg h\nu$. Griffith has shown that for this case $g_\perp \simeq 4.0$ and $g_\parallel = 2.00$.[11] Nitric oxide undoubtedly reacts with Fe^{2+} ions in the zeolites to form either an $[Fe(III)NO]^{2+}$ or an $[Fe(I)NO]^{2+}$ complex with three unpaired electrons. The epr spectrum alone cannot be used to distinguish between the two possibilities, although the infrared evidence strongly favors a reduction of the iron ion by nitric oxide, giving $[Fe(I)NO]^{2+}$.

TABLE II: Relative Amplitudes of the Spectra

Treatment of the sample	Normalized spectra at $g \simeq 4.0$ and at 1890 cm^{-1}		Normalized spectra at $g \simeq 2.0$ and at 1778 cm^{-1}	
	Epr spectrum	Ir spectrum	Epr spectrum	Ir spectrum
1 Torr of NO	0.6	0.7	0	0
10 Torr of NO; under vacuum 15 sec at 25°	0.8	0.9	0.09	~0
under vacuum ≥ 1 hr at 25°	1.0	1.0	0.6	0.8
under vacuum 1 hr at 50°	0.5	0.3	1.0	1.0
under vacuum 1 hr at 100°	0.03	0.03	0.3	0.2

The N-O stretching frequency has often been used as an indication of the direction of charge transfer, either from or to the nitrosyl ligand. It has been suggested that stretching frequencies in the range of 1700–2300 cm^{-1} are indicative of coordinated NO^+.[12] Stretching frequencies below 1700 cm^{-1} are often attributed to NO^-, although frequencies in the latter range may reflect the bending of the M-N-O bond.[13] As is demonstrated in Figures 2 and 5 and in Table II, the observed band at 1890 cm^{-1} correlates well with spectrum A over a wide range of experimental conditions. This infrared band clearly falls within the range expected for NO^+.

Although a number of low-spin nitrosyl complexes of Fe(I) are known, there are very few examples of Fe(I)NO complexes with $S = 3/2$, which are in the spin-free configuration. On the basis of Mössbauer spectra and magnetic susceptibility measurements Danon[14] has concluded that in pentaaquonitrosyliron(I) sulfate, $[Fe(I)(H_2O)_5NO]SO_4$, the Fe(I) is in a spin-free configuration.

Spectrum B, with three g values close to g_e, must be assigned to an iron–nitrosyl complex in an $S = 1/2$ spin state. Here too, the epr spectrum does not allow one to distinguish between the Fe(I) and Fe(III) ions. Normally, low-spin d^5 ions have one g value which is less than g_e; however, Symons and coworkers[15] have assigned a spectrum with $g_{||} = 2.0142$ and $g_\perp = 2.0716$ to $[Fe(III)(CN)_5NO]^-$.

Again, the infrared spectrum may be used to distinguish between the possible oxidation states. The band at 1778 cm^{-1} and spectrum B are obviously related to the same complex as indicated by the data in Figures 2 and 5 and in Table II. The infrared frequency suggests that the complex is $[Fe(I)NO]^{2+}$.

Apparently the $[Fe(I)NO]^{2+}$ complex in the zeolites is near the crossover point, and the simple adsorption and desorption of nitric oxide at room temperature results in the formation of the low-spin isomer. The amplitude of the spectra indicates that the high-spin species is not converted to the low-spin form, but rather new low-spin complexes are formed from Fe(II) which was previously coordinated in a different manner. Perhaps the location of the iron at two different sites in the zeolite is responsible for the two different isomers, although the influence of mo-

lecular oxygen on the spectrum suggests that both complexes are exposed to the supercage.

A model is proposed in which the high-spin complex is in distorted tetrahedral (C_{3v}) symmetry, and the low-spin complex is in distorted square planar (C_{2v}) symmetry. In the high-spin complex three of the ligands are oxide ions of the zeolite structure, whereas the fourth ligand is nitric oxide. Mingos[16] has recently discussed energy level diagrams for various nitrosyl complexes with respect to the M-N-O bond angles. It is clear from these diagrams that a slightly distorted tetrahedral complex with a linear NO bond would result in nearly degenerate $a_1(d_{z^2})$ and $e(\pi^*(NO), d_{xz}, d_{yz})$orbitals which contain three electrons. This would, of course, give rise to an $S = 3/2$ spin state. Formation of a distorted square planar (C_{2v}) symmetry with NO as one of the equitorial ligands ($MNOX_3$ where $X = O^{2-}$) results in the electronic configuration

$$b_2(d_{yz},\pi^*(NO))^2,\ b_1(d_{xz},\pi^*(NO))^2,\ a_2(d_{xy})^2,$$

$$a_1(d_{x^2} - d_{y^2})^1,\ b_1(\pi^*(NO), d_{xz}),\ b_2(\pi^*(NO), d_{yz}),\ a_1(d_{z^2})$$

Such a model for the low-spin configuration is consistent with the observation that $g_{xx} \neq g_{yy} \neq g_{zz}$. Mixing *via* spin–orbit coupling of the $a_1(d_{x^2} - d_{y^2})$ orbital with the $a_1(d_{xy})$, $b_1(d_{xz}, \pi^*(NO))$, and $b_2(d_{yz}, \pi^*(NO))$ orbitals would account for the principal g values being greater than 2.

The presence of two spin states of the same complex has been observed for several iron–nitrosyls involving a Schiff's base.[17] Here the reversible transition from a spin state of 3/2 to a spin state of 1/2 was achieved by simply lowering the temperature of the sample. This change in spin state was detected by a decrease in NO stretching frequency from 1712 to about 1630 cm^{-1}. It should be noted that in this case the iron was formally assigned the 3+ oxidation state; nevertheless, a decrease of 82 cm^{-1} in stretching frequency may be compared with a decrease of 112 cm^{-1} observed for the iron complex in the zeolite. The decrease has been attributed to less metal-to-NO π bonding in the $S = 3/2$ spin state because of fewer electrons in the appropriate orbitals.

In view of the relatively large ^{57}Fe and ^{14}N hyperfine splitting which has been detected in several Fe(I)–nitrosyl complexes[18,19] it is significant that no hyperfine splitting was observed in the present work. Values of $A_{iso}(^{57}Fe)$ down to −15 G have been observed for Fe(I)–nitrosyl complexes.[18] Less negative values have been attributed to appropriate mixing of the 4s orbital with the orbital containing the unpaired electron.[19] In the present case C_{2v} symmetry would allow mixing of the 4s and $d_{x^2-y^2}$ orbitals; hence, a value of A_{iso} near zero is certainly possible. Likewise, partial delocalization into the 2p orbitals of the oxide ion ligands would also result in a reduction in the magnitude of the hyperfine constants. The absence of any nitrogen splitting indicates that the unpaired electron resides mainly in orbitals of the metal or oxide ions, but it does not preclude back-donation from filled orbitals; *i.e.*, the $b_2(d_{yz}, \pi^*(NO))$ and $b_1(d_{xz}, \pi^*(NO))$ orbitals.

The g values and ^{14}N hyperfine splitting of spectrum C are similar to those reported previously for NO absorbed in various zeolites including BaY, NaY, and ZnY.[20-22] In all of these zeolites the spectra are characterized by $g_{xx} = g_{yy} \simeq 2.00$ and $g_{zz} < 2.00$ with $a_{xx} \simeq 30$ G. The exact value of g_{zz} depends on the crystal field gradient at the NO molecule, which in turn is a function of the charge and position of the cation. For divalent cations values of g_{zz} range from 1.89 to 1.93. Adsorption on aluminum in decationated zeolites resulted in values of g_{zz} near 1.95 and the presence of ^{27}Al hyperfine splitting.[20] For NO in NaY values of $g_{zz} = 1.86 \pm 0.01$ and 1.83 ± 0.01 have been reported. In the iron-exchanged zeolite the NO may either be weakly complexed with low-spin Fe(II) or with the remaining sodium ions. The latter case is favored since the facile reduction of Fe(II) by nitric oxide has been demonstrated and the observed value of $g_{zz} = 1.85$ is consistent with a weak NO–sodium ion complex.

It should be pointed out that the complex responsible for spectrum C is much less stable than the species which is characterized by the band at 1822 cm^{-1}. The latter may be due to a dinitrosyl–iron complex which could be a precursor of $[Fe(I)NO]^{2+}$ in the low-spin state, since the decrease in amplitude of the band at 1822 cm^{-1} roughly parallels the formation of the band at 1778 cm^{-1}.

Comparison with Other Studies. Kasai[22] has reported the reduction of nickel from the +2 to +1 oxidation state upon adsorption of nitric oxide in a Y-type zeolite. The results were not interpreted in terms of a nickel–nitrosyl complex; however, Gallezot, *et al.*,[23] have shown by X-ray diffraction techniques that nitric oxide is capable of reducing the population of Ni^{2+} ions in the hexagonal prisms, presumably by the formation of complexes. This would explain why the g values observed by Kasai differed somewhat from those of Ni^{+} formed by reduction with sodium metal. The ability of NO to effect the relocation of metal ions may also be important in the formation of the low-spin $[Fe(I)NO]^{2+}$ complex.

Although the Mössbauer studies by Boudart and coworkers[3] failed to reveal any significant change in the Fe^{2+} spectrum upon adsorption of nitric oxide, it is possible that 10% of the iron ions could have been involved in complex formation without detection. Unlike the epr spectra reported here, the Mössbauer spectrum includes all of the iron which is present in the zeolite. The Mössbauer spectrum of the high-spin $[Fe(I)NO]^{2+}$ complex in the zeolite would probably appear similar to that of the $[Fe(I)NO(H_2O)_5]^{2+}$ complex reported by Danon,[14] which had an isomer shift of +1.46 mm/sec relative to Cr and a quadrupole splitting of 1.70 mm/sec. These values indicate that the spectrum of the iron–nitrosyl complex in the zeolite may overlap considerably with the major inner and outer peaks of Fe^{2+} which have been observed;[3] thus, it is unlikely that the Mössbauer spectrum of the nitrosyl complex would have been resolved under the conditions employed.

Acknowledgments. The authors wish to acknowledge the experimental work of Mr. Duc Tran during part of this investigation. One of us (E. F. V.) greatly thanks the Belgische National Fonds Voor Wetenschappelÿk Onderzoek for a research grant as "Aspirant." This work was supported by The Robert A. Welch Foundation under Grant No. A-257.

References and Notes

(1) C. C. Chao and J. H. Lunsford, *J. Phys. Chem.*, **76**, 1546 (1972).
(2) C. C. Chao and J. H. Lunsford, submitted for publication.
(3) W. N. Delgass, R. L. Garten, and M. Boudart, *J. Phys. Chem.*, **73**, 2970 (1969).
(4) W. N. Delgass, R. L. Garten, and M. Boudart, *J. Chem. Phys.*, **50**, 4603 (1969); R. L. Garten, W. N. Delgass, and M. Boudart, *J. Catal.*, **18**, 90 (1970).
(5) J. H. Lunsford, *J. Phys. Chem.*, **72**, 2141 (1968).
(6) C. C. Chao and J. H. Lunsford, *J. Amer. Chem. Soc.*, **93**, 71 (1971).

(7) T. Castner, G. S. Newell, W. C. Holton, and C. P. Slichter, *J. Chem. Phys.*, 32 668 (1960).
(8) H. H. Wickman, M. P. Klein, and D. A. Shirley, *J. Chem. Phys.*, 42, 2113 (1965).
(9) B. D. McNichol and G. T. Pott, *J. Catal.*, **25**, 223 (1972).
(10) T. M. Pietrzak and D. E. Wood, *J. Chem. Phys.*, **53**, 2454 (1970).
(11) J. S. Griffith, *Discuss. Faraday Soc.*, **25**, 81 (1958).
(12) P. Gans, *J. Chem. Soc. A*, 943 (1967).
(13) J. A. McGinnety, *MTP Int. Rev. Sci.*, 5, 229 (1972).
(14) J. Danon, *J. Chem. Phys.*, **41**, 3378 (1964).
(15) M. B. D. Bloom, J. B. Raynor, and M. C. R. Symons, *J. Chem. Soc. A*, 2459 (1969).
(16) D. M. P. Mingos, *Inorg. Chem.*, **12**, 1209 (1973).
(17) A. Earnshaw, E. A. King, and L. F. Larkworthy, *J. Chem. Soc. A*, 2459 (1969).
(18) C. C. McDonald, W. D. Phillips, and H. F. Mower, *J. Amer. Chem. Soc.*, **87**, 3319 (1965).
(19) B. A. Goodman, J. B. Raynor, and M. C. R. Symons, *J. Chem. Soc. A*, 2572 (1969).
(20) J. H. Lunsford, *J. Phys. Chem.*, **74**, 1518 (1970).
(21) J. H. Lunsford, *J. Phys. Chem.*, **72**, 4163 (1968).
(22) P. H. Kasai and R. J. Bishop, *J. Amer. Chem. Soc.*, **94**, 5560 (1972).
(23) P. Gallezot, Y. Ben Taarit, and B. Imelik, *J. Catal.*, **26**, 481 (1972).

Dielectric Properties of Some Clathrate Hydrates of Structure II[1]

S. R. Gough, R. E. Hawkins, B. Morris,[2] and D. W. Davidson*

Division of Chemistry, National Research Council of Canada, Ottawa, Canada K1A OR9 *(Received August 14, 1973)*

Publication costs assisted by NRCC

Dielectric measurements between 1.8 and 250°K are reported for the isostructural hydrates of tetrahydrofuran, trimethylene oxide, and acetone. The characteristic shape of the high-temperature absorption arising from reorientation of water molecules is better represented by two discrete relaxation times than by a continuous distribution of the Cole–Cole or Fröhlich type. The activation volume for water reorientation, 4.4 ± 0.3 $cm^3\ mol^{-1}$ for tetrahydrofuran hydrate at 211°K, is similar to values found in other disordered ices. At low temperatures, very broad absorption by the guest molecules and failure of the guest contribution to the permittivity to increase as $1/T$ show the perturbing effect of the variable (but relatively small) electrostatic fields of the orientationally disordered water molecules. Permittivities of 3.5 to 4.0 at 4°K for the three hydrates include large contributions from rotational oscillations of guest molecules at far-infrared frequencies. The relaxation rate of H_2S in the small cages of the double hydrates exceeds 1 MHz at all temperatures down to 1.8°K.

Introduction

As indicated schematically in Figure 1, clathrate hydrates of dipolar guest molecules are characterized by two widely separated regions of dielectric absorption and dispersion, one associated with reorientation of the water molecules of the ice-like lattice, the other with the much faster reorientation of the guest molecules in the almost spherical cages. Most previous dielectric studies at frequencies below 1 MHz have been concerned with the definition of the water relaxation region and its dependence on the nature of the encaged molecules although the relatively large values of $\epsilon_{\infty 1}$ (Figure 1) obtained at temperatures between 77 and 200°K clearly included a substantial contribution from rapid reorientation of polar guest molecules. Among hydrates of structure II,[3] the water relaxation has been studied in the hydrates of tetrahydrofuran,[4] dihydrofuran,[4] propylene oxide,[4] trimethylene oxide,[4] 1,3-dioxolane,[5] cyclobutanone,[6] and acetone,[6] as well as in the hydrate of the nonpolar sulfur hexafluoride.[7]

Dielectric absorption by encaged tetrahydrofuran and acetone molecules has been observed[8] near 90°K at frequencies in the GHz region. At low temperatures the reorientation rates of guest molecules may be brought into the sub-megahertz frequency range where dielectric measurements of good accuracy may be made, as in the recently reported[6] case of cyclobutanone hydrate.

The rotational mobility of guest molecules depends both on geometric factors (the size and shape of the guest molecule with respect to the cage) and on the interaction of the dipole moment of the guest molecule with the electrostatic fields of the water molecules.[9] Only the larger of the two kinds of cages is normally occupied in structure II hydrates. This cage is formed by four hexagonal and twelve pentagonal rings of hydrogen-bonded water molecules and, as a result of the orientational disorder of the water molecules, possesses an average (statistical) tetrahedral symmetry ($\bar{4}3m$). Such symmetry is absent however in individual cages and the orientation dependence of the energy of the guest molecule differs in different cages because of the variation in the magnitude and direction of the resultant electrostatic fields and in the positions of the hydrogen atoms of the water molecules. The dielectric relaxation behavior of the guest molecules provides information not only about the reorientation rates in "average" cages but also about the distribution of electrostatic fields in different cages.

In the present study, low-frequency dielectric measurements of tetrahydrofuran, trimethylene oxide, and acetone hydrates have been extended to 4°K and below. The dispersion regions associated with reorientation of both the host and guest molecules have been defined, the shape of the water dispersion region examined, and the pressure dependence of the relaxation rate of water molecules de-

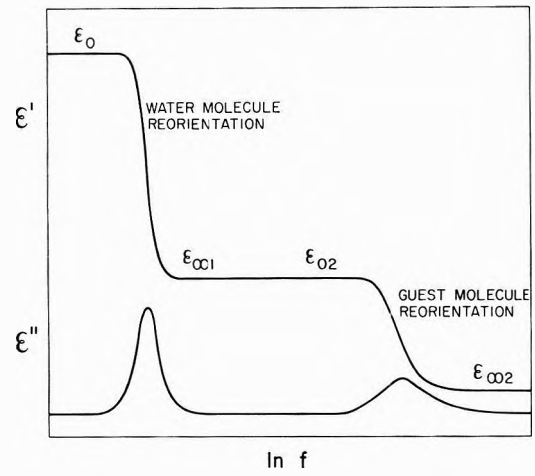

Figure 1. Schematic frequency dependence of the permittivity and absorption of a clathrate hydrate of a polar molecule.

termined. Measurements of tetrahydrofuran–hydrogen sulfide and trimethylene oxide–hydrogen sulfide double hydrates have been used to explore the reorientation of H_2S in the smaller (pentagonal dodecahedral) cages.

Experimental Methods

Hydrate samples were prepared in the dielectric cells by freezing solutions of 1:16.9 to 1:17.0 mole ratio of hydrate former (<0.1% impurity by gas chromatography) to conductivity water. Hydrate formation and sample homogeneity were promoted by thermal conditioning for periods of 4–10 days at temperatures several degrees below the hydrate decomposition temperatures, *e.g.*, at 1° for tetrahydrofuran, −18° for trimethylene oxide, and −30° for acetone hydrate, the corresponding decomposition temperatures being 4.3,[10] −9,[11] and −20°,[6] respectively. Hydrate formation was followed during conditioning by examination of the shape and amplitude of the water dispersion region.[4]

Double hydrates were prepared *in situ* by subjecting an aqueous solution of trimethylene oxide to several atmospheres pressure of H_2S at 6° for several days and by successive conversion to hydrate of thin layers of tetrahydrofuran solution at 10° under 1 atm of H_2S. Neither method gave a quantitative cell filling factor; voids within the sample were less apparent in the second. Samples were analyzed for H_2S content at the end of the measurements.

In order of increasing frequency the three-terminal dielectric bridges employed in the measurements between 1 Hz and 1 MHz were a low-frequency bridge constructed after the design of Berberian and Cole,[12] a General Radio 1615-A transformer ratio-arm capacitance bridge, a GR 716-C Schering bridge with guard circuit, and a GR 1682 1-MHz automatic capacitance bridge. The five-terminal feature of the 1 MHz bridge resulted in elimination of cable errors to the top of the cryostat; a small inductive error introduced by the 1 m of Microdot cable extending to the dielectric cell was corrected by calibration.

The dielectric cells were designed to reduce errors related to sample contraction on cooling. The "split-cylinder" cell[6,13] with parallel electrodes and an air capacitance of ~1 pF, used for the measurements of trimethylene oxide hydrate and some measurements of tetrahydrofuran hydrate, was subject to a ~2% uncertainty of cell constant at low temperatures. More accurate and reproducible results were obtained with the coaxial cell recently described,[14] which was used for measurements of acetone and tetrahydrofuran hydrates. Variation of the cell constant (~5 pF) between 2 and 273°K, ideally no more than a few tenths per cent,[14] was ignored. A second coaxial cell of the same design but with brass parts replaced by stainless steel was used for the hydrates containing H_2S. Measurements of the water dispersion region of tetrahydrofuran hydrate to pressures up to 3.0 kbars were made with the cell previously used for studies of ice (see Figure 1b of ref 15), with the same method of pressure generation and measurement.

Most measurements reported here were made in an Andonian Associates liquid helium cryostat at equilibrated temperatures.[14] Temperatures were measured by an Au(0.7 atom % Fe) *vs.* chromel P thermocouple in the case of trimethylene oxide, otherwise by calibrated Ge resistors at low and Cu–constantan thermocouples at high temperatures.

Water Dispersion Region

Static Permittivities ϵ_0. Earlier measurements[4-7] of the amplitude of the dispersion region associated with reorientation of water molecules in eight structure II hydrates suggested that $(\epsilon_0 - \epsilon_{\infty 1})$ is relatively insensitive to the nature of the guest molecule. Low values found for acetone hydrate[6] and, at low temperatures, for trimethylene oxide hydrate[4] could reasonably be associated with the incongruent formation of these two hydrates from ice and a liquid phase, a process accompanied by sample contraction and incomplete filling of the interelectrode space. Effects of this kind were less pronounced with the cells used in the present study. These gave, for example, a measured ϵ_0 of 71 for acetone hydrate at 165°K (*cf.* values of about 50 previously found[6,16]) and 79 for trimethylene oxide hydrate at 145°K (*vs.* 69[4]). For tetrahydrofuran hydrate the present results agree well with the earlier ones, *e.g.*, at 187°K $\epsilon_0 = 82$ (*vs.* 80[4]).

We conclude that the proper static permittivity of structure II hydrates may be represented by

$$\epsilon_0 - \epsilon_{\infty 1} = 14{,}900/T \qquad (1)$$

to within about 2 permittivity units, independent of the type of guest molecule, over the temperature range from about 165°K to the decomposition point.

The value of g, the Kirkwood correlation factor, for water molecules in the hydrate lattice derived by comparison of eq 1 with

$$\epsilon_0 - \epsilon_{\infty 1} = 2\pi N(n^2 + 2)^2 g\mu^2/(9kT) \qquad (2)$$

depends on the choice of n^2. With the contribution of guest molecules neglected, $n^2 = 1.59$ is obtained for the square of the optical refractive index from the corresponding value for ice (1.72) and the Lorentz–Lorenz equation,[4] and $g = 2.6$. Inclusion of the contribution of guest molecules of polarizability 7 Å^3 raises n^2 to about 1.79 and reduces g to 2.3. The insensitivity of $(\epsilon_0 - \epsilon_{\infty 1})$ to the nature of the guest molecules so far examined apparently reflects the similarity of their polarizabilities (Table I), the range from 6.2 to 7.9 Å^3 corresponding to a change of only about 2% in $(\epsilon_0 - \epsilon_{\infty 1})$.

A value of g of 2.3 indicates a smaller positive correlation between the directions of the water-molecule dipoles in the clathrate hydrate lattice than is found in ice Ih ($g = 3.4$) and the orientationally disordered high-pressure polymorphs of ice ($g = 2.6$ to 3.4[17]). It is likely that the prevalence of five-membered rings (which outnumber hexagonal rings by 9 to 1 in the clathrate lattice) reduces the

positive correlation between dipole directions possible in the generally more dendritic ices.

Distribution of Relaxation Times. The shape of the complex permittivity locus associated with reorientation of the lattice water molecules (*e.g.*, Figure 2) appears also to be characteristic of the lattice structure alone. It can be approximately described as a Cole–Cole arc[18] with relatively small values of α which change with temperature from 0.020 at −25° to 0.050 at −105° and 0.07 at −130°. However, in all the hydrates examined, consistent departure from this representation occurs in the perpendicular approach to $\epsilon_{\infty 1}$ on the high-frequency side of the plot.[6] The real nature of the approach to ϵ_0 is more difficult to establish because of the effects of ionic impurities (space-charge and electrode polarization, dc conductance) which normally occur at low frequencies, particularly in the presence of traces of liquid phase in samples containing excess hydrate former. On the other hand, preparation of hydrate from a solution containing excess water leads to overlap by a low-frequency dispersion region associated with the presence of ice Ih.[4,6] Under such circumstances the proper hydrate behavior may be best defined by measurements at pressures and temperatures where any excess water exists as ice II, an orientationally ordered form of low conductivity;[17] the complex permittivity plot then (*e.g.*, Figure 2) clearly tends to approach ϵ_0 at 90° to the ϵ' axis.

We have attempted to determine the best of three alternative representations of the shape and frequency dependence of the complex permittivity. These include the Cole–Cole equation

$$\epsilon' - \epsilon_{\infty 1} = \frac{\epsilon_0 - \epsilon_{\infty 1}}{2} \times \left[1 - \frac{\sinh \{(1-\alpha) \ln \omega\tau_0\}}{\cosh \{(1-\alpha) \ln \omega\tau_0\} + \sin (\alpha\pi/2)}\right]$$

$$\epsilon'' = \frac{\epsilon_0 - \epsilon_{\infty 1}}{2} \times \frac{\cos (\alpha\pi/2)}{\cosh \{(1-\alpha) \ln \omega\tau_0\} + \sin (\alpha\pi/2)} \quad (3)$$

and the Fröhlich equation[19]

$$\frac{\epsilon' - \epsilon_{\infty 1}}{\epsilon_0 - \epsilon_{\infty 1}} = \frac{1}{2} + \frac{2}{A}(C \cos\theta + C^3 \cos(3\theta)/3 + C^5 \cos(5\theta)/5 + \ldots)$$

$$\frac{\epsilon''}{\epsilon_0 - \epsilon_{\infty 1}} = \frac{2}{A}(C \sin\theta + C^3 \sin(3\theta)/3 + C^5 \sin(5\theta)/5 + \ldots) \quad (4)$$

whose shape is very nearly semielliptical about a major axis coinciding with the ϵ' axis when, as in the present instance, the relaxation times τ_1 and τ_2 between which the distribution function $G(\ln \tau)d \ln \tau$ has a constant value are not widely separated. In eq 4, $A = \ln(\tau_2/\tau_1)$, $C = \tanh(A/4)$, and $\theta = 2 \tan^{-1}(\omega^2\tau_1\tau_2)^{1/2}$. The third trial representation consists of a superposition of m Debye processes

$$\epsilon' - \epsilon_{\infty 1} = \sum_{i=1}^{m} \Delta\epsilon_i/(1 + \omega^2\tau_i^2)$$

$$\epsilon'' = \sum_{i=1}^{m} \Delta\epsilon_i\omega\tau_i/(1 + \omega^2\tau_i^2) \quad (5)$$

to establish whether the results are compatible with a limited number of discrete relaxation times.

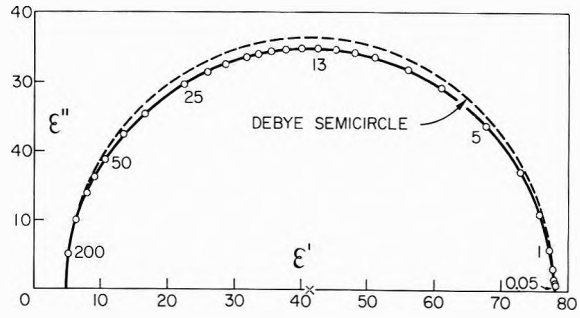

Figure 2. Complex permittivity plot of the water relaxation region of tetrahydrofuran hydrate at 211.3°K and 3.0 kbars. Frequencies are shown in kHz.

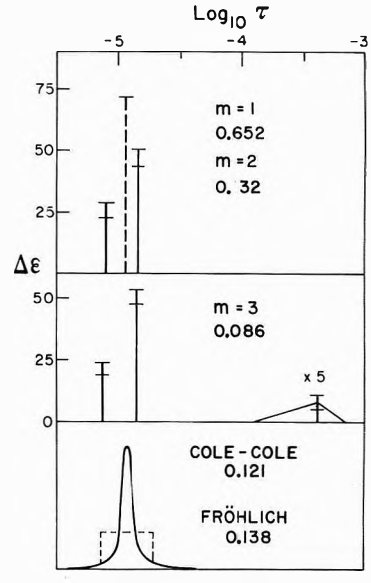

Figure 3. Representation of the water dispersion region of tetrahydrofuran hydrate (211.3°K, 3.0 kbars) by multiple relaxation times. Data at 25 frequencies between 1 and 200 kHz. Dashed line is single "best" relaxation time.

The statistical analysis used a nonlinear regression method which incorporated Marquardt's algorithm[20] for rapid convergence of the adjustable parameters to the values which gave the best fit of the 50 to 74 values of ϵ' and ϵ''. These were chosen to cover the dispersion–absorption region with reasonable completeness and uniformity (*cf.*, for example, the points between 1 and 200 kHz in Figure 2). All ϵ' and ϵ'' values were given equal weight. The adjustable parameters were $\epsilon_{\infty 1}$, $\epsilon_0 - \epsilon_{\infty 1}$, τ_0, and α in eq 3, $\epsilon_0 - \epsilon_{\infty 1}$, $(\tau_1\tau_2)^{1/2}$, and A in eq 4, and the $2m$ values of $\Delta\epsilon_i$ and τ_i in the Debye spectrum. In the last two cases an experimental value of $\epsilon_{\infty 1}$ was employed, based, in part, on extrapolation of accurately measured values at lower temperatures.

Results of the analysis of the locus of Figure 2 are shown in Figure 3 where the standard deviations (σ) are shown beside the relaxation time spectra found. (In Figures 3 and 4 horizontal line segments represent conventional standard error limits of $\Delta\epsilon_i$ and the lengths of bases of triangles those of τ_i if the latter exceed ±5%.) The "best" Fröhlich distribution (with $\tau_1/\tau_2 = 2.68$) is seen to be slightly inferior to the "best" Cole–Cole distribution (α = 0.031) undoubtedly because the high-frequency data are lightly weighted. Two Debye relaxation times which differ by a factor of 2 define the data about as well as the continuous distributions. With $m = 3$ a relatively minor,

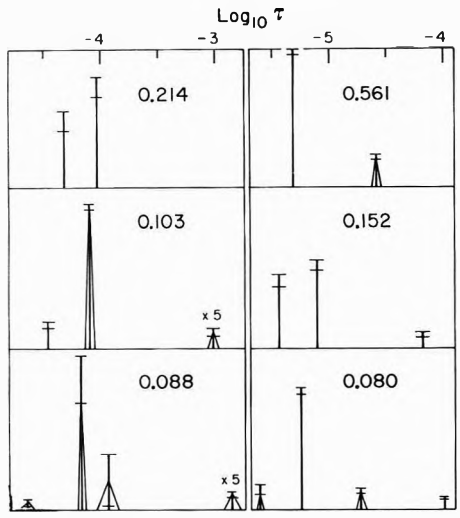

Figure 4. Multiple relaxation times of dioxolane hydrate (left) at 203.5°K and 1 bar (37 frequencies between 0.05 and 200 kHz), and tetrahydrofuran hydrate (right) at 211.3°K and 20 bars (25 frequencies between 1 and 200 kHz). Numbers are combined standard deviations of ϵ' and ϵ''.

slow, and poorly defined relaxation process is added, with no substantial change in the two major relaxation processes. (Note that the vertical scale of the third process has been magnified by a factor of 5 for clarity.) The value of σ, at 0.086, is now comparable to the experimental error. With $m = 4$ (not shown) σ was unchanged, the two major contributions were again little affected but the third process for $m = 3$ was split into a $\Delta\epsilon = 0.5$ component at $\tau = 6.6 \times 10^{-5}$ sec and a slow component whose $\Delta\epsilon$ and τ values oscillated greatly during the later stages of convergence but maintained a constant $\Delta\epsilon/\tau$ ratio equivalent in its effects to a small parallel dc conductance.

Figure 4 (left) shows the results for a dioxolane hydrate sample, the contribution of a relatively large dc conductance of 3.0×10^{-11} ohm^{-1} cm^{-1} to ϵ'' having been subtracted in advance. The best Cole–Cole fit ($\alpha = 0.037$) gave $\sigma = 0.192$. For $m = 2$ and 3 the Debye analysis gave results rather similar to Figure 3, the larger σ's reflecting the poorer fit of the lower frequency data. A satisfactory fit was achieved with $m = 4$ where, however, most of the parameters are seen to be poorly defined. No further reduction of σ occurred at $m = 5$.

The right half of Figure 4 refers to a sample of tetrahydrofuran hydrate whose experimental locus at low frequencies was seriously distorted by the presence of ice Ih. The relatively high σ for $m = 3$ and the pronounced drop at $m = 4$ suggest that the effect of the ice is not adequately represented by a single Debye contribution.

We conclude from these and nine other sets of data analyzed that the relaxation of the water molecules may be represented with fair consistency by two Debye relaxation processes, one twice as slow as the other. The possibility of further relaxation times is obscured, even for the best hydrate samples analyzed, by variable and spurious effects which can only be approximately treated in terms of frequency-independent parallel conductance and space-charge polarization of the simple Debye form. This conclusion is a consequence of the statistical analysis. Although there is no general theory of estimation of confidence regions of nonlinear parameters, useful estimates may be made in terms of linear theory. Thus, the conventional one-parameter intervals at the 95% confidence level (Student's $t = 2$) are twice as great as the standard errors shown in Figure 3, while the 95% support-plane confidence intervals (F test) range from about three times (for $m = 2$) to four times (for $m = 4$) these standard errors. Even for $m = 3$ there is a strong coupling between the $\Delta\epsilon_i$ of the two principal relaxation processes (correlation coefficient ~0.995) and between these and the corresponding τ_i's (0.98 to 0.99). In these circumstances neither the amplitude nor the times are accurately determined. It is unfortunate that the statistical significance of a resolution of the relaxation behavior of ice Ih into as many as seven Debye processes has not been discussed.[21]

TABLE I: Relaxation of Water in Structure II Hydrates

Guest molecule	α_M, Å^3	τ_0, μsec (233.2°K)	E_A, kcal mol^{-1}
SF_6	6.46	780	12.3
1,3-Dioxolane	6.72	5.4	8.7
2,5-Dihydrofuran	7.74	1.5	7.5
Tetrahydrofuran	7.93	1.0	7.4
Trimethylene oxide	6.23	0.48	7.0
Propylene oxide	6.18	2.0	8.0
Acetone	6.41	0.57	6.5
Cyclobutanone	7.57	0.49	6.5

The existence of a number of dielectric relaxation times reflects the presence in the hydrate lattice of crystallographically nonequivalent sites and orientations of the water molecules. In terms of the Bjerrum mechanism[22] of molecular reorientation in ice, the orientational defects diffuse at somewhat different rates along different hydrogen-bonding paths in the lattice. Since the lattice is a four-connected network it is not surprising that the distribution of relaxation times is relatively narrow.

An analysis of the reorientation kinetics expected from the lattice structure has been given elsewhere.[23] As many as eight discrete relaxation times are predicted for structure II hydrates. It is possible that these eight relaxation processes, some of which will make only minor contributions to the permittivity, may be approximately reduced to the two found experimentally.

Temperature Dependence of the Relaxation Rate. Relaxation times τ_0 at −40° and Arrhenius activation energies for eight structure II hydrates, as derived from the frequencies of maximum loss, are collected in Table I. These results are mainly from earlier work,[4-7] which in the case of tetrahydrofuran, trimethylene oxide, and acetone hydrates is confirmed (to within 2% of τ_0) by new measurements in the low-temperature cells. Departures at low temperatures from linearity of ln τ_0 in $1/T$ are noted as before.[6] It appears that the relaxation is normally dominated by Bjerrum defects produced by interaction of the guest molecules (possibly by occasional hydrogen bonding) with the lattice, while at low temperatures "extrinsic" Bjerrum defects, originating at impurity centers or dislocations, may predominate. The sensitivity of the relaxation rate, but not of the shape of the relaxation spectrum, to the nature of the guest molecule, suggests that the number of Bjerrum defects is much more variable from hydrate to hydrate than their rate of diffusion.

Pressure Dependence of the Relaxation Rate. Measurements of τ_0 at 500-bar intervals between 1 and 3000 bars at 211.3°K gave an activation volume of 4.4 ± 0.3 cm^3 mol^{-1} for tetrahydrofuran hydrate. This hydrate has previously been shown[10] to be stable to about 3.5 kbars at

somewhat higher temperatures. This activation volume is similar to values found for other forms of ice: 2.9[24] and 3.8[25] cm^3 mol^{-1} for Ih and 4.4–4.8 cm^3 mol^{-1} for ices III, V, and VI at 3, 5, and 8 kbars, respectively.[17]

Guest-Molecule Dispersion Region

Static Permittivities ϵ_{02}. Because of the wide frequency separation between the dispersion regions associated with water and guest molecule reorientations, the permittivity $\epsilon_{02} = \epsilon_{\infty 1}$ could be followed over a large temperature range. This permittivity is shown as a heavy line for temperatures between 200 and 20°K or below in Figures 5 and 6. At relatively high temperatures ϵ_{02} varies approximately as $1/T$ as indicated, and also very nearly as the square of the dipole moment of the guest molecule, as previously shown[6] for the eight species of guest molecule given in Table I. These observations show that the guest molecules effectively undergo isotropic reorientation at relatively high temperatures.

At lower temperatures ϵ_{02} fails to rise as $1/T$ and passes through a broad flat maximum at about 45°K in the cases of tetrahydrofuran and acetone hydrates and at 35°K in the case of trimethylene oxide hydrate. There is clearly an increasing degree of anisotropy in the reorientational process as the temperature gets lower and the energy differences between the preferred orientations of the guest molecules become increasingly large in comparison with kT. At very low temperatures dispersion of the permittivity occurs as the measuring frequencies become comparable to the reorientation rates of the guest molecules. When these become sufficiently slow (*e.g.*, in acetone hydrate below 19°K) the value of ϵ_{02} cannot be estimated from measurements at frequencies above 1 Hz. In principle, ϵ_{02} should approach $\epsilon_{\infty 2}$ as T approaches 0°K, since the orientational disorder of the water molecules ensures only one orientation of least energy on the part of the guest molecule in each cage. (See Electrostatic Fields below.)

Relaxation Times. Complex permittivity plots associated with reorientation of guest molecules are illustrated in Figure 7. These loci are very broad and, in contrast with the water loci at much higher temperatures, are only incompletely defined at a fixed temperature by measurements over the frequency range of measurement. The distributions of relaxation times are clearly very broad, particularly in the direction of small times. In all three hydrates, dispersion and absorption at low audio frequencies are still detectable at 4°K and below.

Figure 8 shows the variation with temperature of the dielectric absorption at 1 kHz. Results for cyclobutanone hydrate are taken from the earlier study.[6] Although plots of this kind illustrate the gross effect of molecular size on the reorientation rate (fastest for trimethylene oxide, the molecule with the smallest maximum dimension, and slowest for cyclobutanone, the largest) they obscure the real asymmetry of the frequency dependence of the absorption.

Frequencies of maximum absorption are plotted against $1/T$ in Figure 9 and the corresponding Arrhenius activation energies given in Table II. Because of the breadth of the loss curves, these frequencies are subject to more than the usual uncertainty. The absorption measurements[8] at frequencies up to 8.5 GHz yielded frequencies of maximum absorption of 14 GHz at 88°K for tetrahydrofuran hydrate and 37 GHz at 93°K for acetone hydrate, as estimated with the dubious assumption of Debye shape. Combination of these values with the temperatures at

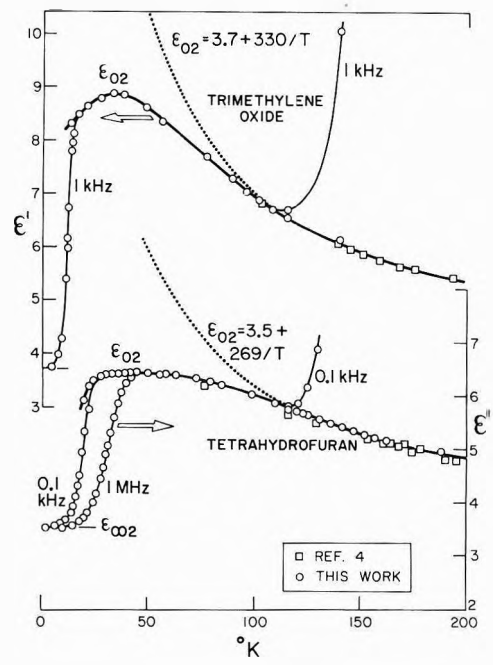

Figure 5. Temperature dependence of $\epsilon_{02} = \epsilon_{\infty 1}$ of tetrahydrofuran and trimethylene oxide hydrates. Permittivities measured at some fixed frequencies are also shown.

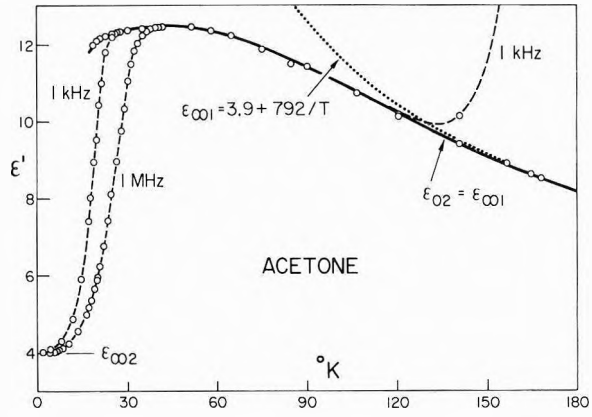

Figure 6. Temperature dependence of ϵ_{02} of acetone hydrate.

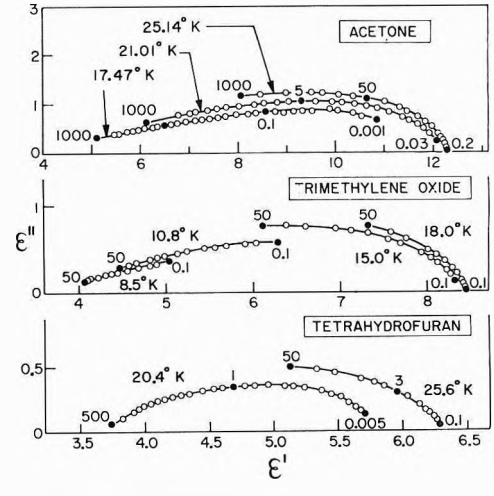

Figure 7. Complex permittivity loci due to relaxation of guest molecules at a number of temperatures. Frequencies are shown in kHz.

TABLE II: Dielectric Properties Related to Guest Molecules

Guest molecule	Value of ϵ_{02} at 168°K	100°K	50°K	20°K	Temp (°K) of max absorption at 0.1 kHz	10 kHz	1 MHz	E_A, kcal mol^{-1}
Tetrahydrofuran	5.08	6.00	6.42	5.86	19.47	24.24	32.05	0.91
Trimethylene oxide	5.63	6.93	8.57	8.63	10.71	14.06	20.28	0.41
Acetone	8.6	11.05	12.47	12.11	18.26	21.88	27.23	1.02
Cyclobutanone	9.8	11.2	11.5		28.9	35.4		1.44

TABLE III: Low-Temperature Permittivities and Estimated Frequencies of Rotational Oscillation

Guest molecule	$\epsilon_{\infty 2}$ (exptl 4°K)	$\epsilon_{\infty 2}$ (calcd) (eq 6 with α_M)	α_M*, Å^3	μ, D	I_C, amu Å^2	I_B, amu Å^2	ν_C, cm^{-1}	ν_B, cm^{-1}
SF_6	2.9 ± 0.1[a]	3.04		0				
Tetrahydrofuran	3.5 ± 0.1	3.11	16	1.63	126.1	72.5	17	22
Trimethylene oxide	3.7 ± 0.2	3.03	19	1.93	75.1	43.1	21	28
Acetone	4.0 ± 0.1	3.04	22	2.88	103.0	49.7[b]	24	35[c]
Cyclobutanone	3.6 ± 0.2	3.08	18	2.89	142.1	105.1	25	29

[a] 200°K. [b] I_A. [c] ν_A.

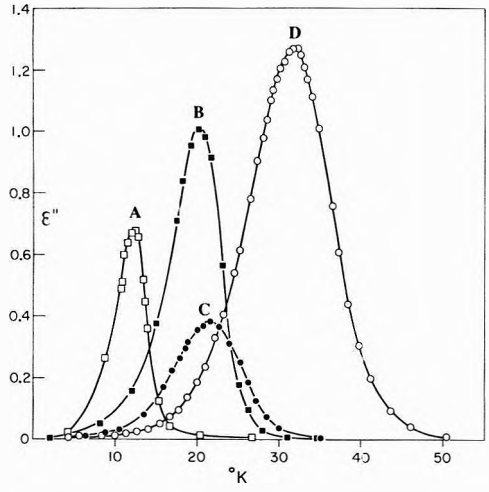

Figure 8. Dielectric absorption at 1 kHz by (A) trimethylene oxide, (B) acetone, (C) tetrahydrofuran, and (D) cyclobutanone encaged in structure II hydrates.

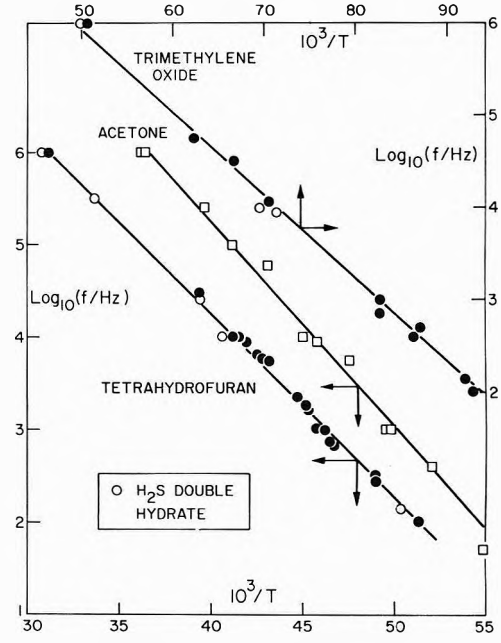

Figure 9. Arrhenius plots of the frequencies of maximum dielectric absorption by the guest molecules.

which the loss is greatest at 1 MHz (Table II) gives 0.96 and 0.81 kcal/mol for tetrahydrofuran and acetone hydrates, respectively, as average activation energies over intermediate temperatures. These values do not differ greatly from the values of 0.91 and 1.02 kcal/mol found at the lower temperatures of the present study. Since the latter values refer to temperatures where reorientation is far from isotropic and where the shape of the absorption is dependent on temperature (*cf.* Figure 7), they have no simple quantitative significance. However, the frequency of maximum loss corresponds to a relaxation time on the long-time side of the center of gravity of a broad distribution of times and the above activation energies may reflect the heights of the barriers to reorientation in cages where the perturbing electrostatic fields of the water molecules (see below) are relatively small.

Low Temperature Permittivities $\epsilon_{\infty 2}$. At the lowest temperatures the measured values of the permittivity tend toward $\epsilon_{\infty 2}$, the frequency-independent values which include no contribution from orientational relaxation. These are estimated (Table III) to an accuracy which is limited by sample inhomogeneity and uncertainty in the cell constant and not by the method of extrapolation. At somewhat higher temperatures, however, the uncertain extrapolation to infinite frequency of complex loci like those of Figure 7 prevents definition of the temperature dependence of $\epsilon_{\infty 2}$.

It is of interest to compare values of $\epsilon_{\infty 2}$ with the values expected for guest molecules of "normal" polarizability given by the Onsager cavity model

$$\frac{(\epsilon_{\infty 2} - 1)(2\epsilon_{\infty 2} + 1)}{3\epsilon_{\infty 2}} = \frac{(\epsilon^0 - 1)(2\epsilon^0 + 1)}{3\epsilon^0} + \frac{4\pi N_M}{1 - f_M\alpha_M}\alpha_M \quad (6)$$

where ϵ^0 is the low-temperature permittivity of the empty hydrate lattice, N_M is the number per cm^3 of guest mole-

cules of polarizability α_M, and $f_M = 2(\epsilon_{\infty 2} - 1)/a^3(2\epsilon_{\infty 2} + 1)$ is the reaction field factor at the center of a spherical void of radius a equal to the mean "free radius" (3.2 Å) of the almost spherical cage. We estimate $\epsilon^0 = 2.81$ by equating the first term of the right-hand side of eq 6 to $(\epsilon_\infty - 1)(2\epsilon_\infty + 1)d_r/(3\epsilon_\infty)$, where $\epsilon_\infty = 3.10$ for ice Ih and $d_r = 0.888$, the ratio of the density of the empty hydrate lattice to that of ice. Here the assumption is made that the contribution of the water molecules to ϵ^0 differs from their contribution to ϵ_∞ of ice only through their different populations.

With the "normal" polarizabilities[6] given in column 2 of Table I, eq 6 has been used to derive the values of $\epsilon_{\infty 2}$ in column 3 of Table III. Except for nonpolar SF_6, these values are much smaller than the experimental values. The differences cannot be removed by adjustment of a; this would require $a = 1.7$ Å for acetone hydrate, for example, a value unrealistically small for the clathrate in view of the effective value of 3.04 Å applicable to liquid acetone at 0°.[6] The more likely explanation lies in values of the polarizability which are two to three times as large as those normally associated with these molecules. The polarizabilities required (with $a = 3.2$ Å) for formal fit by eq 6 of the experimental values of $\epsilon_{\infty 2}$ are given as α_M^* in Table III.

Since inflated polarizability is not found for SF_6 hydrate, nor for such nonpolar guest molecules as argon,[26] nitrogen,[26] and cyclopropane[27] in clathrate hydrates of structure I, its presence seems to require a permanent dipole moment in the guest molecule. The presence at low temperatures of large amplitude, low-frequency rotational oscillations of the guest molecules about their equilibrium orientations is clearly indicated. The magnitude of these librational frequencies may be roughly estimated from the classical relationship

$$\alpha_i = \mu^2/(12\pi^2\nu_i^2 I_i) \qquad (7)$$

which may be derived,[28] for simple harmonic oscillation of frequency ν_i about an axis of moment of inertia I_i perpendicular to the dipolar axis, with polycrystalline averaging. There are two such axes of oscillation which we take to be principal axes of inertia of the guest molecule. We also assume, in the absence of information about the shape of the restraining potential functions, that the two force constants $k_i = 4\pi^2\nu_i^2 I_i$ are the same and therefore that the two oscillations make equal contributions to the polarizability. Equation 7 may then be used, with $\alpha_i = (\alpha_M^* - \alpha_M)/2$, to calculate the frequencies of oscillation given in Table III.[29] Although the individual frequencies derived in this approximate manner are of limited numerical significance, relatively intense absorption in the 20–30-cm^{-1} region of the far-infrared is anticipated. Insofar as the electrostatic fields of the cage water molecules affect the preferred orientations and the restraining potentials to a different extent in different cages, the infrared absorption ascribable to rotational oscillations is expected to be broad.

Effect of Rotational Oscillations on ϵ_{02}. The contribution to the polarizability discussed above affects the applicability of the Onsager equation for ϵ_{02} at relatively high temperatures

$$\frac{(\epsilon_{02} - 1)(2\epsilon_{02} + 1)}{3\epsilon_{02}} = \frac{(\epsilon_{\infty 2} - 1)(2\epsilon_{\infty 2} + 1)}{3\epsilon_{\infty 2}} + \frac{4\pi N_M \mu_M^2}{3kT(1 - f_M\alpha_M)^2} \qquad (8)$$

TABLE IV: Experimental and Calculated Values of ϵ_{02} at 168°K

Guest molecule	ϵ_{02} (exptl)	ϵ_{02} (calcd) (eq 6 and 8)	ϵ_{02} (calcd) (eq 8 and $\epsilon_{\infty 2}$ (exptl))
Tetrahydrofuran	5.08	4.72	5.16
Trimethylene oxide	5.63	5.14	5.83
Acetone	8.6	8.02	9.1
Cyclobutanone	9.8	8.07	9.1

Use in eq 8 of $\epsilon_{\infty 2}$ values which are derived from eq 6 with normal polarizabilities and $a = 3.2$ Å gives values of ϵ_{02} (Table IV, column 3) which are consistently too low. Substitution of the *experimental* low-temperature $\epsilon_{\infty 2}$ values into eq 8 gives values (column 4) which are much closer to those measured at 168°K. The extent of agreement may be partly fortuitous since the 4°K values of $\epsilon_{\infty 2}$ are unlikely to be valid at 168°K and the contribution of enhanced polarizability to the second term of eq 8 has been ignored. It may be noted that, because of the directional nature of the contribution of rotational oscillations to the polarizability, these oscillations contribute to the polarization of the medium by the guest dipole but not to the polarizability relating the dipole moment induced in the guest molecule to its reaction field.[6]

It is concluded that modification of the Onsager equation to include the effect of rotational oscillations appears to account at least qualitatively for the hitherto unexplained[4] high values of ϵ_{02}. Test of the extent to which the cavity of the Onsager model for liquids, with a defined by the mean molecular volume $(4/3)\pi a^3 = V/N$, may be replaced by the real cage in clathrates requires further study at higher temperatures and frequencies.

Electrostatic Fields of Water Molecules. As already discussed in some detail,[9] the resultant electrostatic field of the water molecules of the cage shows a distribution of magnitude and direction in different cages because of the sixfold orientational disorder of each of the water molecules. In the simplest model there are four equivalent preferred directions (for example, those in which the O end of the guest molecule points toward the center of a hexagonal ring of water molecules) in the absence of electrostatic perturbation. Presence of an electrostatic field removes the equivalence of the orientations and, in the general case, results in three relaxation times in each cage, a very broad distribution of relaxation times over all cages, and a decrease in contribution to the permittivity with decrease of temperature as the orientations favored by the field become increasingly occupied.

The resultant fields arising from the *dipole moments* of the cage water molecule are, for geometric reasons, relatively small. Indeed, if all the water molecules were located on the surface of a sphere and all O-O-O angles were tetrahedral, the resultant dipole field at the cage center would be zero.[9] For the actual geometry of the 16-hedral cage there is a distribution at the cage center of relatively small dipolar fields around a median value which is about 0.6 as large as the field of a single water dipole a cage radius away.[9]

In Figure 10 is plotted the ratio of the actual orientational contribution to the permittivity, $\epsilon_{02} - \epsilon_{\infty 2}$, to the contribution for *isotropic* reorientation. The latter was estimated from

$$\epsilon_{02}(\text{isotropic}) - \epsilon_{\infty 2} = A/T \qquad (9)$$

with A evaluated for each guest species from the experi-

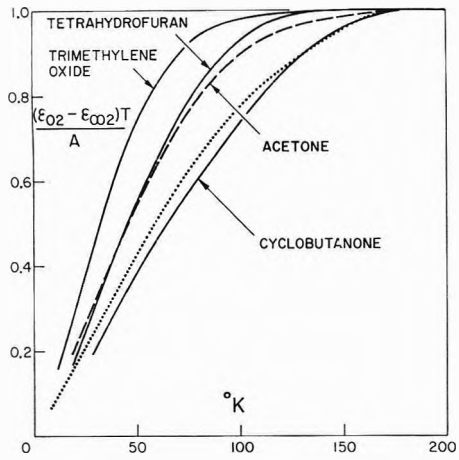

Figure 10. Ratio of experimental permittivity contribution by reorientation of guest molecule to contribution for isotropic reorientation. The dotted curve was calculated for tetrahydrofuran hydrate for the model described in the text.

mental ϵ_{02} at a relatively high temperature (168°K). If the departure of this ratio from unity is attributed to electrostatic interactions and if the positions of different guest dipoles are similar (say all at the cage centers), the ratio should, at a fixed temperature, decrease as the dipole moment of the guest molecule increases. This is not the case; the largest ratio occurs for trimethylene oxide, whose dipole moment is larger than that of tetrahydrofuran, and the ratio for cyclobutanone is substantially smaller than for acetone, although these ketones have similar dipole moments. Since, however, the magnitude and direction of the resultant electrostatic field depends on the position of the dipole in the cage, it appears that the smaller guest molecules are more able than larger molecules to adjust their positions to accommodate a variety of orientations of comparable energy and therefore to maintain a larger polarization.

The dotted curve in Figure 10 shows the polarization ratio $P(T)/P(168°K)$ calculated for a simple model of tetrahydrofuran hydrate in which the guest dipole is restricted to four positions within the cage which are displaced by 0.7 Å from the cage center along the lines to the centers of the hexagonal rings and to corresponding orientations coincident with these lines in which the negative end of the dipole is outward. At these sites the center of mass of the tetrahydrofuran molecule is close to the cage center. The populations of the four configurations are proportional to $\exp(\mu_i \cdot E_i/kT)$, where μ_i is the dipole moment vector of configuration i and E_i is the resultant field at i of the 28 water dipoles of the cage. The dipole moment of a water molecule has been taken to be 2.6 D, the value estimated by Coulson and Eisenberg[30] for the water molecule in ice. The polarization was then calculated[9] for each of 72 randomly generated configurations of the cage water molecules, and the result averaged. This simple model, which gives, for example, only 80% of the isotropic polarization at 168°K, is certainly too restrictive.

Since the experimental behavior is only consistent with small resultant electrostatic fields, it appears that the quadrupole moment tensor of the hydrate water molecule is considerably more isotropic than that of the isolated water molecule.[9]

Double Hydrates with H_2S. The results for the double hydrates of tetrahydrofuran and trimethylene oxide with H_2S show the average relaxation rate of H_2S molecules, predominantly located in the small pentagonal dodecahedral cages, to be faster than 1 MHz down to 1.8°K. This conclusion follows from (a) the lack of a distinct region of absorption and dispersion at higher temperatures which could be associated with the presence of H_2S, (b) a permittivity at the lowest temperatures (about 4.7 for $THF \cdot 0.26H_2S \cdot 17H_2O$ at 1.82°K) sufficiently high as to suggest an important contribution from persisting reorientation of H_2S molecules, and (c) a rise in dielectric absorption with decrease in temperature below 6°K (*e.g.*, at 1 MHz from 0 ± 0.001 at 6°K to 0.011 ± 0.001 at 1.82°K for $THF \cdot 0.26H_2S \cdot 17H_2O$) which increases with the frequency.

Exceptionally rapid reorientation of H_2S is consistent with its small size (maximum van der Waals diameter 4.1 Å)[31] in relation to the pentagonal dodecahedral cage (free diameter 5.0 Å), its relatively small dipole moment (0.92 D), and the smallness of the resultant electrostatic field of the 20 water dipoles of this cage. The dipolar field at the center of a *regular* dodecahedron of water molecules has been shown[9] to range from 0 to 0.68 times the field of one water dipole a cage radius away, the median value being about one quarter of the single-dipole field.

References and Notes

(1) Issued as NRCC No. 13614.
(2) Present address, Polysar Ltd., Sarnia, Canada
(3) M. von Stackelberg and H. R. Müller, *Z. Elektrochem.*, **58**, 25 (1954).
(4) R. E. Hawkins and D. W. Davidson, *J. Phys. Chem.*, **70**, 1889 (1966).
(5) A. Venkateswaran, J. Easterfield, and D. W. Davidson, *Can. J. Chem.*, **45**, 884 (1967).
(6) B. Morris and D. W. Davidson, *Can. J. Chem.*, **49**, 1243 (1971).
(7) Y. A. Majid, S. K. Garg, and D. W. Davidson, *Can. J. Chem.*, **46**, 1883 (1968).
(8) M. Davies and K. Williams, *Trans. Faraday Soc.*, **64**, 529 (1968).
(9) D. W. Davidson, *Can. J. Chem.*, **49**, 1224 (1971).
(10) S. R. Gough and D. W. Davidson, *Can. J. Chem.*, **49**, 2691 (1971).
(11) J.-C. Rosso and L. Carbonnel, *C. R. Acad. Sci. Paris*, **274**, 1108 (1972).
(12) J. G. Berberian and R. H. Cole, *Rev. Sci. Instrum.*, **40**, 811 (1969).
(13) S. K. Garg, B. Morris, and D. W. Davidson, *J. Chem. Soc., Faraday Trans. 2*, **68**, 481 (1972).
(14) S. R. Gough, *Can. J. Chem.*, **50**, 3046 (1972).
(15) S. R. Gough and D. W. Davidson, *J. Chem. Phys.*, **52**, 5442 (1970).
(16) G. J. Wilson and D. W. Davidson, *Can. J. Chem.*, **41**, 264 (1963).
(17) G. J. Wilson, R. K. Chan, D. W. Davidson, and E. Whalley, *J. Chem. Phys.*, **43**, 2384 (1965).
(18) K. S. Cole and R. H. Cole, *J. Chem. Phys.*, **9**, 341 (1941).
(19) K. Higasi, *Monogr. Ser. Res. Inst. Appl. Elec., Hokkaido Univ.*, **No. 9** (1961).
(20) D. W. Marquardt, *J. Soc. Ind. Appl. Math.*, **11**, 431 (1963).
(21) A. von Hippel, D. B. Knoll, and W. B. Westphal, *J. Chem. Phys.*, **54**, 134 (1971).
(22) N. Bjerrum, *Mat. Fys, Medd. Dansk Vid. Selsk.*, **27**, 3 (1951).
(23) D. W. Davidson in "Water: A Comprehensive Treatise," Vol. 2, F. Franks, Ed., Plenum Press, New York, N. Y., 1973.
(24) R. K. Chan, D. W. Davidson, and E. Whalley, *J. Chem. Phys.*, **43**, 2376 (1965).
(25) H. Granicher in "Physics of Ice," N. Riehl, B. Bullemer, and H. Engelhardt, Ed., Plenum Press, New York, N. Y., 1969.
(26) S. R. Gough, E. Whalley, and D. W. Davidson, *Can. J. Chem.*, **46**, 1673 (1968).
(27) Y. A. Majid, S. K. Garg, and D. W. Davidson, *Can. J. Chem.*, **47**, 4697 (1969).
(28) R. L. McIntosh, "Dielectric Behavior of Physically Adsorbed Gases," Marcel Dekker, New York, N. Y., 1966, p 145.
(29) Note that all α's are directional averages.
(30) C. A. Coulson and D. Eisenberg, *Proc. Roy. Soc., Ser. A*, **291**, 445 (1966).
(31) H_2S is the smallest polar molecule known to form a clathrate hydrate.

A Derivation of the Thermodynamics of Polymer Solutions through Use of the Free Volume Concept. B. The Heat of Mixing

Jean Dayantis

C.N.R.S., Centre de Recherches sur les Macromolécules, 67-Strasbourg, France *(Received February 12, 1973)*

Publication costs assisted by the Centre de Recherches sur les Macromolécules

Theoretical relationships for the enthalpy of mixing polymer with solvent have been derived using the free volume concept. The theory is not restricted to polymer solutions but should apply to mixtures of simple liquids as well. To calculate the effect of the "expansion" of the polymer and of the "compression" of the solvent which occurs during the mixing process, following the scheme adopted in this work, the function $W(T) = \alpha(T)\gamma(T)V_M(T)T$ has been used where α is the thermal expansion coefficient, γ the thermal pressure coefficient, V_M the molar volume, and T the absolute temperature. The theory has been developed assuming first that the mixing free volume fractions of the solvent v_1^m and of the polymer v_2^m are equal to the free volume fraction v_m of the mixture. Then, the theory has been modified in order to include the case where $v_1^m \neq v_2^m \neq v_m$. The following *n*-alkane mixtures have been investigated: C_8–C_{16}, C_6–C_{16}, C_6–C_{22}, and C_6–C_{36}. Also polyisobutylene mixtures with hexane, octane, and hexadecane have been investigated. It is found theoretically, upon assuming that $v_1^m = v_2^m = v_m$, that at room temperature C_8–C_{16}, C_6–C_{16}, and the polyisobutylene–*n*-alkane mixtures should have small and positive pair interchange energies. This is in conformity with experience. However, as the temperature is increased from 20 to 100°, this interchange energy is found to become negative for C_8–C_{16} and C_6–C_{16} mixtures, unless the hypothesis of equal free volume fractions in the pure components and in the solution is abandoned. Other mixtures than C_8–C_{16} and C_6–C_{16} mixtures could not be presently investigated at higher temperatures due to the lack of data for α and especially for γ as a function of temperature.

I. Introduction

In a preceding article[1] the entropy of mixing of polymer with solvent has been derived using the free volume concept. The present paper is concerned with the enthalpy of mixing derived on the same basis. Only nondilute solutions are considered. This article, as well as the previous one, is conceived as an attempt toward deriving the thermodynamics of solutions and especially polymer solutions independently of any cell model theory of the liquid state.[2-10] Since the cell model theory of the liquid state is only an idealized and approximate description of real liquids, the idea of deriving the thermodynamics of solutions using the free volume concept, but independently of any cell model theory, may be a useful one, and deserves at least to be carefully explored.

Thorough critical reviews of cell model theories of the liquid state have been given by Barker[11] and by Levelt and Cohen.[12] Consideration of these reviews leads to the conclusion that the assumed similarity of the liquid and the solid structure, although useful in some cases, does not generally lead to relevant values for the parameters of the liquid state (*e.g.*, the coefficient of thermal expansion α or the coefficient of isothermal compressibility κ). These deficiencies should be even more apparent when solutions are considered, as shown previously.

The free volume in a pure component is defined as the volume $\Phi(T)$ at the temperature T°K minus the volume $\Phi(0)$ at 0°K. A more relevant term for this quantity would be the "expansion volume," the term free volume being reserved for the empty volume, as pointed out by Haward in his recent review on occupied volumes.[13] The term free volume will be used instead throughout this work, since it is the one most often used. It appears that the free volume, as above defined, is the relevant physical quantity to use when adopting a free volume approach to the problem of solutions. The free volume fraction v_i of component i is taken equal to

$$v_i = [\Phi_i(T) - \Phi_i(0)]/\Phi_i(T) \qquad \begin{matrix} i = 1, \text{solvent} \\ i = 2, \text{polymer} \end{matrix} \qquad (1)$$

These definitions being recalled, the mixing process will now be assumed to be equivalent to the following scheme.[1]

(a) The solvent is compressed from the initial volume Φ_1^0 to the mixing volume

$$\Phi_1^m = \Phi_1^0(1 - v_1)/(1 - v_m) \qquad (2)$$

whereas the polymer is expanded from the initial volume Φ_1^0 to the mixing volume

$$\Phi_2^m = \Phi_2^0(1 - v_2)/(1 - v_m) \qquad (3)$$

where

$$v_m = \varphi_1 v_1 + \varphi_2 v_2 \qquad (4)$$

φ_1 and φ_2 being the volume fractions of solvent and of polymer.

(b) Compressed solvent and expanded polymer are mixed without volume change.

(c) The mixture is compressed (or expanded) to its true value so as to take into account the excess volume of mixing.

Let us recall that Scott[14] and McGlashan, *et al.*,[15] have considered various mixing processes. The process considered by these authors which approaches most the above scheme is the so called "equal volume per segment" mixing process. The reader is refered to the original papers for further comparison.

The above scheme for the mixing process, if relevant, should apply to all mixtures of nonelectrolytes, whether mixtures of simple liquids or polymer-solvent mixtures. For usual simple liquids at room temperature and atmospheric pressure, the free volume fraction varies within a rather narrow range of values. Consequently, the free volume fraction in the mixture should be close to that in the pure components and effects arising from free volume fraction differences should be generally small. Therefore in this case, as expected, the regular solution theory, using a rigid lattice as background, constitutes a quite acceptable approximation in many instances. On the other hand, an obvious fact when polymer-solvent mixtures are considered is that in the pure components the free volume fractions are quite different. A value of $\rho = v_2/v_1$ near one-half has been estimated in the preceding paper. Haward's review on occupied volumes supports this estimation.[13] Now, in the mixture, the free volume fraction v_m will have some intermediate value between v_1 and v_2. As a result of this and of thermal agitation, it is quite impossible that the mean distance $\overline{a_{11}}$ between solvent-solvent pairs in the mixture will retain the same value $\overline{a_{11}}^0$ as in the pure solvent. An equivalent argument may be considered for the polymer-polymer segment pairs, so that we generally expect that

$$\overline{a_{11}} < \overline{a_{11}}^0 \tag{5}$$

and

$$\overline{a_{22}} > \overline{a_{22}}^0 \tag{6}$$

The simplest possible assumption is that

$$\overline{a_{11}} = \overline{a_{22}} = \overline{a_{12}} \tag{7}$$

and this leads to the previous scheme for the mixing process.

More generally, when the simplest assumption, eq 7, does not hold, one should write, considering inequalities 5 and 6

$$\Phi_1^m = \Phi_1^0(1 - v_1)/(1 - v_1^m) \tag{8}$$

and

$$\Phi_2^m = \Phi_2^0(1 - v_2)/(1 - v_2^m) \tag{9}$$

where

$$\overline{a_{22}}^0 < \overline{a_{22}} < \overline{a_{12}} < \overline{a_{11}} < \overline{a_{11}}^0 \tag{10a}$$

$$v_1 > v_1^m > v^m \tag{10b}$$

and

$$v_2 < v_2^m < v_m \tag{10c}$$

In order that the scheme assumed for the mixing process be of any use, the contributions due to steps a, b, and c must be evaluated and this is done in section II.

II. Heat of Mixing

In a first approach the simplest assumption 7 will be assumed to hold and the corresponding relationships derived. In a second stage, these relationships will be corrected so as to take into account inequalities 10.

Step a. First the heat contributions arising from the compression of the solvent from the volume Φ_1^0 to the volume Φ_1^m and from the expansion of the polymer from the volume Φ_2^0 to the volume Φ_2^m will be evaluated. There are two different ways of bringing component i from the volume Φ_i^0 to the volume Φ_i^m: (1) the component may be heated (or cooled) at constant pressure until the volume reaches the required value Φ_i^m; (2) the component may be compressed (or depressed) isothermally and reversibly until the volume reaches the value Φ_i^m. Process 1 leads to an expression depending on parameters which are readily accessible experimentally and will be the only one to be considered here.

Only the work of the internal pressure contributes in step a of the mixing process to the heat of mixing. To calculate the work of the internal pressure $(\partial E/\partial V)_T$, one may multiply both sides of the so-called thermodynamic equation of state by dV

$$P_{ex}\,dV = T(\partial P/\partial T)_V\,dV - (\partial E/\partial V)_T\,dV \tag{11}$$

If the external pressure P_{ex} is sufficiently small so that the elementary work $P_{ex}\,dV$ may be neglected, then one may write

$$dQ = P_{in}\,dV = T(\partial P/\partial T)_V\,dV \tag{12}$$

As previously indicated we shall consider that the volume changes by varying the temperature, while the pressure is kept constant. Introducing the coefficient of thermal expansion eq 12 becomes, considering component i

$$dQ_i = \alpha_i(T)\gamma_i(T)V_M^i(T)T\,dT \tag{12'}$$

where α_i is the coefficient of thermal expansion, γ_i the thermal pressure coefficient, V_M^i the molar volume of component i, and T the absolute temperature. The total heat evolved during the isobaric compression and expansion processes will be equal to

$$I_1 = \int_{T_0}^{T_0+\Delta T_1} W_1(T)\,dT \tag{13a}$$

$$I_2 = \int_{T_0}^{T_0+\Delta T_2} W_2(T)\,dT \tag{13b}$$

where

$$W_i(T) = \alpha_i(T)\gamma_i(T)V_M^i(T)\,dT \quad i = 1,2 \tag{14}$$

$$\Delta T_1 = \frac{1}{\overline{\alpha_1}}\frac{\Phi_1^m - \Phi_1^0}{\Phi_1^0} = -\frac{1}{\overline{\alpha_1}}\frac{v_1 - v_2}{1 - \varphi_1 v_1 - \varphi_2 v_2}\varphi_2 = -\frac{1}{\overline{\alpha_1}}\frac{v_1 - v_2}{1 - v_m}\varphi_2 \tag{15}$$

$$\Delta T_2 = \frac{1}{\overline{\alpha_2}}\frac{\Phi_2^m - \Phi_2^0}{\Phi_2^0} = +\frac{1}{\overline{\alpha_2}}\frac{v_1 - v_2}{1 - \varphi_1 v_1 - \varphi_2 v_2}\varphi_1 = -\frac{1}{\overline{\alpha_2}}\frac{v_1 - v_2}{1 - v_m}\varphi_1 \tag{16}$$

$$v_m = \varphi_1 v_1 + \varphi_2 v_2 \tag{17}$$

$\overline{\alpha_1}$ and $\overline{\alpha_2}$ are mean values of $\alpha_1(T)$ and $\alpha_2(T)$ in the temperature ranges T_0, $T_0 + \Delta T_1$ and T_0, $T_0 + \Delta T_2$. If now we mix n_1 moles of solvent with n_2 moles of polymer, the temperature being T_0 and the pressure sufficiently low, the heat exchange with the surroundings due to the work of the internal pressures of the solvent and of the polymer will be equal to

$$\Delta Q_{\text{internal press}} = n_1 I_1 + n_2 I_2 = n_1\int_{T_0}^{T_0+\Delta T_1} W_1(T)\,dT + n_2\int_{T_0}^{T_0+\Delta T_2} W_2(T)\,dT \tag{18}$$

This quantity is readily determined if the three coefficients α, γ, and V_M, all of them being readily accessible experimentally, are known as a function of temperature.

Step b. This is the usual interchange energy contribution, the only one taken into account in Flory's old theory of solutions. Let us write

$$Q_{\text{interch energy}} = RT\zeta n_1\varphi_2 \tag{19}$$

where

$$\zeta = z\overline{\Delta w_{12}}/kT \tag{20}$$

$$\overline{\Delta w_{12}} = \tfrac{1}{2}(\overline{w_{11}} + \overline{w_{22}}) - \overline{w_{12}} \tag{21}$$

$2\overline{\Delta w_{12}}$ is the mean energy change when replacing one solvent-solvent and one polymer-polymer pair by two polymer-solvent pairs, z being the number of nearest neighbors. ζ is therefore the original Flory χ. Letting

$$kT\zeta = z\overline{\Delta w_{12}} = I_3 \tag{22}$$

one obtains

$$Q_{\text{interch energy}} = n_1\zeta_2 I_3 \tag{23}$$

Step c. The heat contribution arising from the isothermal compression (or expansion) of the mixture from the volume with no excess volume to the real volume will be set equal to

$$\Delta Q_{\text{excess volume}} = (n_1 + n_2)I_4 = (n_1 + n_2)\int_{T_0}^{T_0+\Delta T_3} W_{12}\, dT \tag{24}$$

$$W_{12}(T) = \alpha_{12}(T)\gamma_{12}(T)V_M{}^{12}T \tag{25}$$

$$\Delta T_3 = \frac{1}{\overline{\alpha_{12}}}\frac{\Phi^{\Xi}}{\Phi_1{}^0 + \Phi_2{}^0} \tag{26}$$

$$\alpha_{12} = \alpha_1\varphi_1 + \alpha_2\varphi_2 \tag{27a}$$

$$\gamma_{12} = \gamma_1\varphi_1 + \gamma_2\varphi_2 \tag{27b}$$

$$V_M{}^{12} = xV_M{}^1 + (1 - x)V_M{}^2 \tag{27c}$$

It is thus assumed that by taking arithmetic mean values for α_{12}, γ_{12}, and $V_M{}^{12}$ only a negligible error in introduced. The excess volume of mixing Φ^E will be considered presently to be an additional parameter which will have to be experimentally determined. However, Φ^E will be determined within the framework of the present theory in a future article.

Summing up contributions a, b, and c, one obtains for the enthalpy of mixing at low pressure n_1 moles of solvent and n_2 moles of polymer

$$\Delta H = \Delta Q_{\text{internal press}} + \Delta Q_{\text{interch energy}} + \Delta Q_{\text{excess vol}} = n_1I_1 + n_2I_2 + n_1\varphi_2I_3 + (n_1 + n_2)I_4 \tag{28}$$

The experimental determination of ΔH requires thus the knowledge of α, γ, and V_M as a function of temperature for both components, of $I_3 = z\Delta w_{12}$, and, also, of the molar excess volume $\Phi_M{}^E = \Phi^E/(n_1 + n_2)$ as a function of φ_2.

III. Partial Molar Heats of Mixing.

a. Partial Molar Heat of Mixing of the Solvent. By definition

$$\overline{\Delta h_1} = [\partial\Delta H/\partial n_1]_{T,P,n_2} \tag{29}$$

From eq 28 one immediately obtains

$$\overline{\Delta h_1} = \underbrace{I_1 + n_1(\partial I_1/\partial n_1)}_{\overline{\Delta h_1{}^1}} + \underbrace{n_2(\partial I_2/\partial n_1)}_{\overline{\Delta h_1{}^2}} + \underbrace{\varphi_2{}^2 I_3}_{\overline{\Delta h_1{}^3}} + \underbrace{I_4 + (n_1 + n_2)(\partial I_4/\partial n_1)}_{\overline{\Delta h_1{}^4}} \tag{30}$$

Using the two eq 13 and eq 24 for I_1, I_2, and I_4 the above expression is found equal to

$$\overline{\Delta h_1} = \int_{T_0}^{T_0+\Delta T_1} W_1(T)\, dT + n_1W_1(T_0 + \Delta T_1)(\partial(\Delta T_1)/\partial n_1) + n_2W_2(T_0 + \Delta T_2)(\partial(\Delta T_2)/\partial n_1) + \varphi_2{}^2 I_3 + \int_{T_0}^{T_0+\Delta T_3} W_{12}(T)\, dT + (n_1 + n_2)W_{12}(T_0 + \Delta T_3)(\partial(\Delta T_3)/\partial n_1) \tag{30'}$$

ΔT_1, ΔT_2, and ΔT_3 are given by eq 15, 16, and 26, respectively. $\partial(\Delta T_1)/\partial n_1$ and $\partial(\Delta T_2)/\partial n_1$ are easily derived from eq 15 and 16 and one obtains

$$\frac{\partial(\Delta T_1)}{\partial n_1} = \frac{1}{n_1}\frac{\varphi_1\varphi_2}{\overline{\alpha_1}}\frac{(v_1 - v_2)(1 - v_1)}{(1 - v_m)^2} \tag{31}$$

$$\frac{\partial(\Delta T_2)}{\partial n_1} = \frac{1}{n_1}\frac{\varphi_1\varphi_2}{\overline{\alpha_2}}\frac{(v_1 - v_2)(1 - v_2)}{(1 - v_m)^2} \tag{32}$$

In order to obtain an expression for $\partial(\Delta T_3)/\partial n_1$ some hypothesis has to be made regarding the variation of Φ^E with the volume fraction φ_i of one of the components. It will be assumed that a fair description of the excess volume is generally given by the equation

$$\Phi^E/(n_1 + n_2) = A\varphi_2(1 - \varphi_2) \tag{33}$$

where A is an experimental constant. Then, from

$$\frac{\partial}{\partial n_1}\left\{\frac{\Phi^E}{\Phi}\right\} = \frac{1}{\Phi}\frac{\partial\Phi^E}{\partial n_1} - \frac{\Phi^E}{\Phi^2}\frac{\partial\Phi}{\partial n_1}$$

using eq 33 and the fact that by hypothesis, step b

$$\Phi = n_1V_M{}^1 + n_2V_M{}^2$$

one obtains, $V_M{}'^2$ being the molar volume of 1 mol of segments

$$\left[\frac{\partial\Delta T_3}{\partial n_1}\right]_{T,P,n_2} = \frac{A}{\overline{\alpha_{12}}}\frac{(n_1 + n_2)(1 - \varphi_2)\varphi_2}{n_1V_M{}^1 + n_2V_M{}^2} \times \left[\frac{1}{n_1}(3\varphi_2 - 1) - \frac{1}{n_1 + n_2}\frac{V_M{}^1}{xV_M{}'^2}\varphi_2\right] \tag{34}$$

$\overline{\Delta h_1}$ is thus entirely determined using the same parameters as those necessary to determine ΔH.

b. Partial Molar Heat of Mixing of the Polymer. Since

$$\overline{\Delta h_2} = [\partial\Delta H/\partial n_2]_{T,P,n_1} \tag{35}$$

one obtains, from eq 28

$$\overline{\Delta h_2} = \underbrace{(\partial I_1/\partial n_2)}_{\overline{\Delta h_2{}^1}} + \underbrace{I_2 + n_2(\partial I_2/\partial n_2)}_{\overline{\Delta h_2{}^2}} + \underbrace{\varphi_1{}^2 I_3}_{\overline{\Delta h_2{}^3}} + \underbrace{I_4 + n_2(\partial I_4/\partial n_2)}_{\overline{\Delta h_2{}^4}} \tag{36}$$

The explicit form of this equation may be evaluated as for the partial molar enthalpy of the solvent using eq 13 and 24.

IV. Flory–Huggins Interaction Parameter χ.

As pointed out by Guggenheim[16] many years ago, the Flory–Huggins interaction parameter χ should be written

as the sum of an entropic and of an enthalpic contribution

$$\chi = \chi_S + \chi_H \tag{37}$$

Using the free volume concept, the entropic part χ_S of χ has already being derived in the previous paper, yielding

$$\chi_S = -\frac{\overline{\Delta S_1^E}}{R\varphi_2^2} = -\frac{1}{\varphi_2^2} \times \left\{\ln\left[1 - \varphi_2(1-\rho)\right] + \frac{1-\rho}{1-\varphi_2(1-\rho)}\varphi_1\varphi_2 + \frac{c'(1-\rho)}{1-\varphi_2(1-\rho)}\varphi_2^2\right\} \tag{38}$$

where it is recalled that ρ is the ratio v_2/v_1 and $c' = w(c/3)(V_M^1/V_M'^2)$, c being the Prigogine parameter for the external degrees of freedom of the polymer segments and w a constant lying being ½ and ⅓.

On the other hand, the enthalpic part χ_H is given by

$$\chi_H = \overline{\Delta h_1}/RT\varphi_2^2 \tag{39}$$

or

$$\chi_H = \frac{1}{RT\varphi_2^2}[\overline{\Delta h_1^1} + \overline{\Delta h_1^2} + \overline{\Delta h_1^3} + \overline{\Delta h_1^4}] \tag{40}$$

where the values of the $\overline{\Delta h_1^i}$ are indicated in eq 30 and 30′. The total χ thus appears as the sum of χ_S and χ_H given by eq 38 and 40, respectively. The explicit expression is too cumbersome to be written on a single line. Nevertheless, the only physical parameters required for the actual calculations are as before α, γ, and V_M as a function of T for each species plus the c' parameter. (v_1, v_2, and ρ are deduced from the molar volumes if the molar vlume at 0°K is known.)

The Flory–Huggins χ parameter appears therefore as a recipient where several items of various kinds have been enclosed. The present analysis shows that χ is the sum of two entropic and of four enthalpic contributions. Let us recall that the χ parameter in Flory's early work was just that included in the term $\overline{\Delta h_1^3}/RT\varphi_2^2$.

Extrapolation of χ to Zero Polymer Concentration. A necessary prerequisite for eq 38 and 40 to be meaningful in that they should extrapolate to some constant value when φ_2 tends to zero.[17] In other words, the term in φ_2 should vanish when expanding in powers of φ_2. This is indeed found to be the case, as shown in the microfilm edition of this paper (see footnote 21).[18]

V. Modifications Arising from Unequal Free Volume Fractions of Mixing

All the previous results have been derived on the basis of the validity of eq 7. Hypothesis 7 (*i.e.*, the two eq 7) is the simplest possible one and one must start with it. However, it is not the most reasonable. In physical terms, exact validity of this hypothesis would mean that the kinetic energy per molecule or segment is several orders of magnitude greater than the expansion energy per molecule or segment. Simple qualitative calculations show however that the kinetic energy, although greater than, is generally of the same order of magnitude as the expansion energy. Therefore eq 7 will often be an inadequate approximation and the heat of mixing and all subsequent quantities will have to be recalculated according to inequalities 10. Thus, the two integrals (13a) and (13b) will be replaced by

$$I_1' = \int_{T_0}^{T_0+\Delta T_1'} W_1(T)\,dT \tag{13a′}$$

and

$$I_2' = \int_{T_0}^{T_0+\Delta T_2'} W_2(T)\,dT \tag{13b′}$$

where

$$\Delta T_1' = \frac{1}{\overline{\alpha_1}}\frac{\Phi_1'^m - \Phi_1^0}{\Phi_1^0} = \frac{1}{\overline{\alpha_1}}\frac{v_1^m - v_1}{1 - v_1^m} \tag{15′}$$

$$\Delta T_2' = \frac{1}{\overline{\alpha_2}}\frac{\Phi_2'^m - \Phi_2^0}{\Phi_2^0} = \frac{1}{\overline{\alpha_2}}\frac{v_1^m - v_2}{1 - v_2^m} \tag{16′}$$

In eq 15′ and 16′ inequalities 10 for v_1^m and v_2^m have to be fulfilled.

It is convenient to introduce two constants K_1 and K_2 such that

$$I_1' = \int_{T_0}^{T_0+\Delta T_1'} W_1(T)\,dT = K_1\int_{T_0}^{T_0+\Delta T_1} W_1(T)\,dT = K_1 I_1 \tag{13a′}$$

$$I_2' = \int_{T_0}^{T_0+\Delta T_2'} W_2(T)\,dT = K_2\int_{T_0}^{T_0+\Delta T_2} W_2(T)\,dT = K_2 I_2 \tag{13b′}$$

This permits writing the enthalpy of mixing as

$$\Delta H = n_1K_1I_1 + n_2K_2I_2 + n_1\varphi_2I_3 + (n_1 + n_2)I_4 \tag{28′}$$

If it is assumed, as a first step, that K_1 and K_2 are nearly independent of composition (*i.e.*, $dK_1/dn_1 = dK_1/dn_2 = dK_2/dn_1 = dK_2/dn_2 \simeq 0$), then the equations obtained in paragraphs III and IV for the partial enthalpies of mixing and for χ_H will be very simply modified by multiplying the relevant terms by K_1 and K_2.

VI. Applications

The previous results have been applied (A) to mixtures of *n*-alkanes and (B) to solutions of polyisobutylene (PIB) in *n*-alkanes. Since the pair interchange energy is not known exactly and further depends on the volume, the excess enthalpy H^E cannot be directly determined using eq 28. Therefore we shall reverse the argument and calculate the quantity $Z = H^E - S - I_4$ where H^E is the experimental heat of mixing data, and S and I_4 are the contributions due to steps a and c of the mixing process. In particular if the value calculated for S is relevant, one should find for Z a value which depends on the temperature but remains positive, as should the pair interchange energy.

A. Mixtures of n-Alkanes. The following mixtures of *n*-alkanes have been investigated: C_8–C_{16}, C_6–C_{16}, C_6–C_{22}, and C_6–C_{36}. For these mixtures reliable α, γ, and V_M data are available.[6] However, excess enthalpies H^E and excess volumes V^E as a function of temperature are only available for the two first mixtures, so that a comprehensive analysis of the two last mixtures is impeded by the lack of sufficient data.

The volume at 0°K, which is needed to calculate v_1, v_2, and v_m in eq 15 and 16 has been calculated using the empirical relationship established by Doolittle.[19]

The procedure used to calculate the integrals I_1 and I_2 (eq 13) was the following. First, an approximate estimation of the boundary values ΔT_1 and ΔT_2, as given by eq 15 and 16, was made using the values $\alpha_1(T_0)$ and $\alpha_2(T_0)$ at the mixing temperature for the coefficient of thermal expansion, instead of the mean values $\overline{\alpha_1}$ and $\overline{\alpha_2}$. Next, improved values $\Delta T_1'$ and $\Delta T_2'$ were calculated, using in

TABLE I

	t^0	t^1	t^2	t^3	t^4
C_6	1.6053	-6.2060×10^{-3}	6.2389×10^{-5}	-3.3765×10^{-7}	8.0658×10^{-10}
C_8	1.7853	-3.9552×10^{-3}	-1.0321×10^{-5}	2.1456×10^{-7}	-8.3747×10^{-10}
C_{16}	3.0374	-1.3350×10^{-2}	5.5363×10^{-5}	-1.1106×10^{-7}	4.4749×10^{-12}
C_{22}	3.8624	-1.3269×10^{-2}	2.2994×10^{-5}	4.7385×10^{-9}	-3.9847×10^{-11}
C_{36}	6.3970	-2.7142×10^{-2}	5.7134×10^{-5}	-4.1826×10^{-8}	-7.5212×10^{-10}
PIB	75.031	-2.5837×10^{-1}	3.5694×10^{-4}	4.0139×10^{-7}	1.9757×10^{-10}

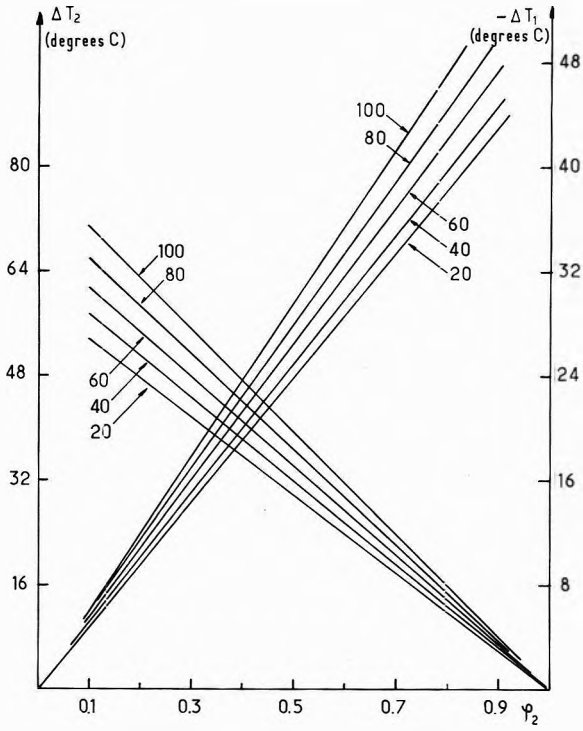

Figure 1. ΔT_1 and ΔT_2 values *vs.* volume fraction of C_{16} for C_8–C_{16} mixtures. The mixing temperatures are indicated on the curves. Curves with increasing slopes refer to ΔT_1.

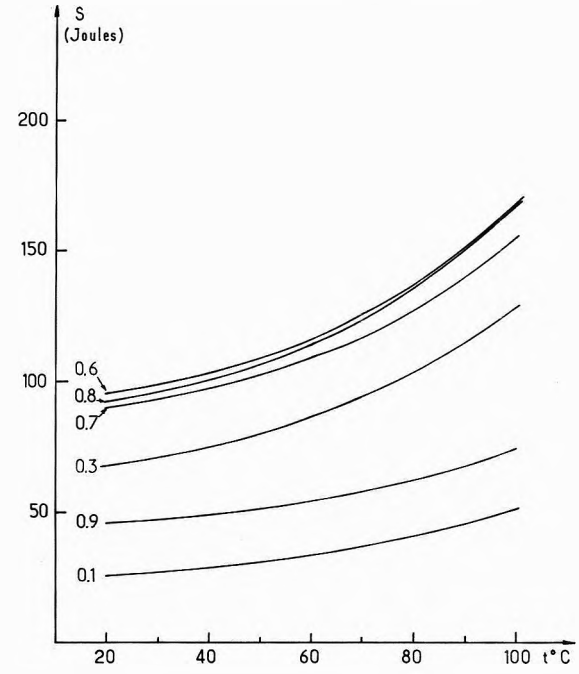

Figure 2. Sum $S = xI_1 + (1 - x)I_2$ for C_8–C_{16} mixtures at various volume fractions of C_{16} as a function of temperature.

eq 15 and 16 the values $\alpha_1(T_0 + \Delta T_1/2)$ and $\alpha_2(T_0 + \Delta T_2/2)$. Finally, $\overline{\alpha_1}$ and $\overline{\alpha_2}$ were approximated by the values $\alpha_1(T_0 + \Delta T_1'/2)$ and $\alpha_2(T_0 + \Delta T_2'/2)$. This approximation has proven to be sufficient in all cases excepting C_6–C_{36} mixtures, where the magnitude of the limit ΔT_1 for hexane made necessary a correction resulting from the curvature of the α *vs.* T curve. In all cases the α value used is estimated to approach the true value $\tilde{\alpha}$ to better than 0.5%. Once the limits of integration were determined, the polynomials $W(T) = \alpha(T)\gamma(T)V_M(T)T$ were calculated, using the polynomials for α, γ, and V_M measured by Orwoll and Flory[16] (in preference to polynomials of other authors reported in the same work). The expansion polynomials for $W(T)/T$ are tabulated in Table I, t being the temperature in degrees centigrade.

Finally, the compression integrals I_4 at various temperatures were calculated, using experimental values for the excess volumes and eq 25 to 27. All the above calculations were performed on a Univac 1108 computer. The results for each of the above mixtures will now be briefly discussed.

C_8–C_{16} Mixtures. This mixture approaches a mixture of simple liquids. In Figure 1 the ΔT_1 and ΔT_2 values are plotted and in Figure 2 the sum $S = xI_1 + (1 - x)I_2$ where x represents the molar fraction of the first component is

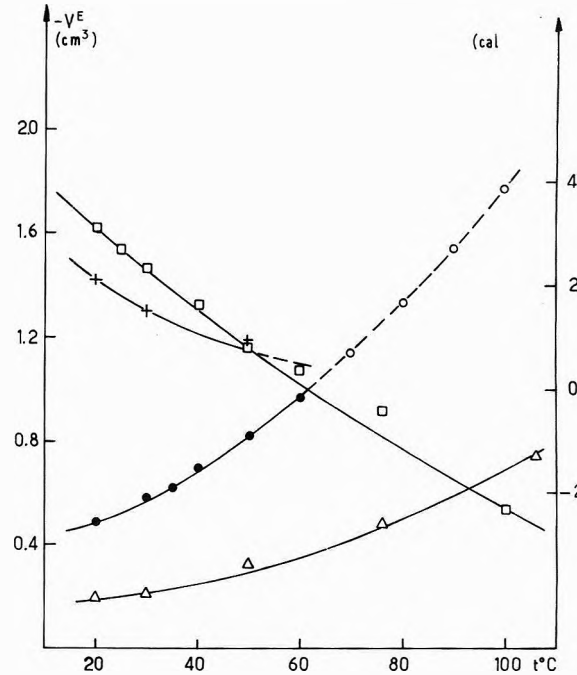

Figure 3. Excess volumes V^E and excess enthalpies H^E for C_8–C_{16} and C_6–C_{16} mixtures: △, V^E for C_8–C_{16}; ○, V^E for C_6–C_{16} mixtures; +, H^E for C_8–C_{16}; and □, H^E for C_6–C_{16} mixtures. From data reported by Orwoll and Flory.[6]

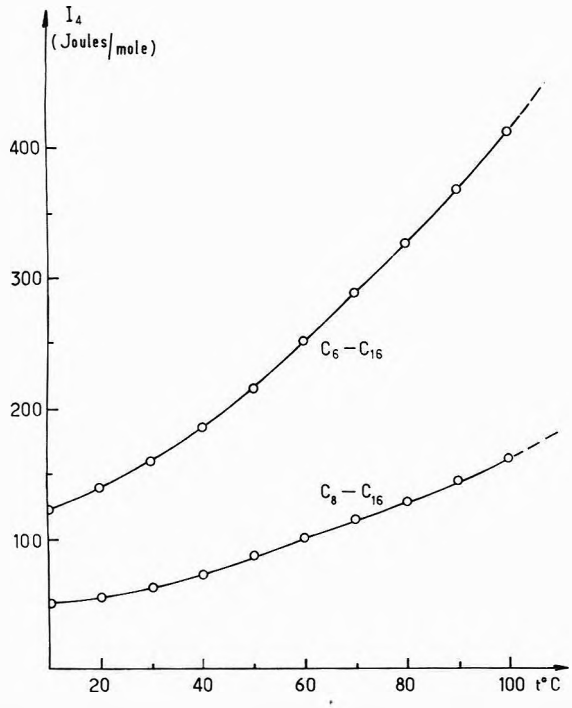

Figure 4. Compression integrals I_4 for C_8–C_{16} and C_6–C_{16} mixtures *vs.* temperature.

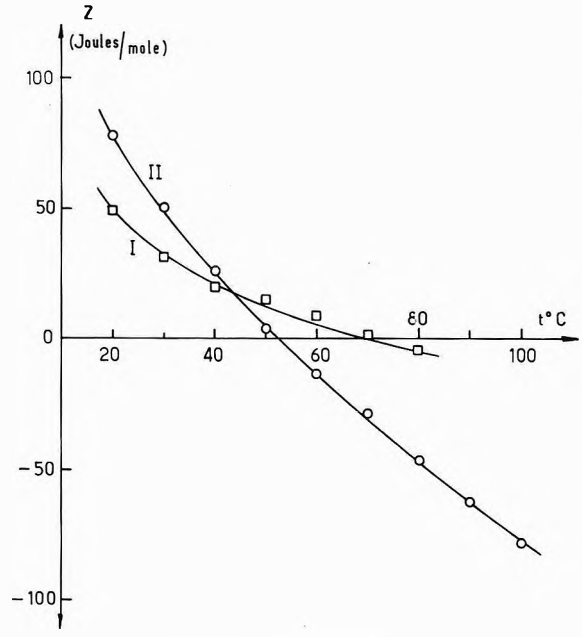

Figure 5. Sum $Z = H^E - S - I_4$ for C_8–C_{16} (curve I) and C_6–C_{16} (curve II) mixtures *vs.* temperature.

plotted. It is seen that the limits of integration vary almost linearly with the volume fraction of the first component and that the sum S increases regularly with temperature. In Figure 3 the excess enthalpy H^E and the excess volume V^E are plotted, using data reported in ref 6. The compression integral I_4 from 10 to 100° is plotted in Figure 4. The important point, using these data, is to determine whether or not the simplest assumption, expressed in the two eq 7, is a convenient approximation. If it is, the molar sum $Z = H^E - S - I_4$ should be nearly constant with temperature and equal to $\Delta Q_{\text{interch energy}}$. Otherwise equalities 7 should be replaced by inequalities 10 which will lead to smaller values for the limits of integration. The result is shown in Figure 5. It is seen that Z is small and positive at 20° and drops to negative values between 60 and 80°. Thus, the simplest assumption expressed in eq 7 is not really satisfactory even in the case of C_8–C_{16} mixtures. However the fact that small and positive values are obtained, as expected, for Z at room temperature is a result favoring eq 13a and 13b. As the temperature is increased, the "mixing" free volume fractions v_1^m and v_2^m become respectively greater and smaller than v_m given by eq 4. In other words, the ratio $\bar{a}_{22}/\bar{a}_{11}$, which, for small enough values of v_1 and v_2 (*i.e.* low enough temperatures), is approximately one, decreases gradually as the temperature is increased. A more quantitative analysis of this effect is not possible for this mixture, since excess enthalpy data above 50° are lacking.

C_6–C_{16} Mixtures. Experimental H^E and V^E data are plotted in Figure 3, the compression integral I_4 in Figure 4, and the final result Z in Figure 5. It is seen that Z presents the same behavior as for C_8–C_{16} measures, but the effect is even more pronounced. Thus Z drops from about +80 J/mol at 20° to −70 J/mol at 100°. To explain this behavior the same argument as for C_8–C_{16} mixtures can be developed. Abandoning hypothesis 7 we may seek the values v_1^m and v_2^m of the mixing free volume fractions, obeying inequalities 10b and 10c which will make Z constant by conveniently reducing the sum $S = xI_1 + (1 - x)I_2$. A detailed calculation along these lines is included in the microfilm edition of this paper (see footnote 22).[18] Let us only point out that it is always possible to choose v_1^m and v_2^m, linked by one relationship, so as to keep constant the value of Z when the temperature varies. The exact form of the relationship which links v_1^m and v_2^m is not known, however, the only condition imposed on it, *i.e.*, an excess volume of mixing equal to zero, being insufficient to define it unambiguously (see microfilm edition, footnote 23).[18]

C_6–C_{22} Mixtures. H^E and V^E data are not available for this mixture. Comparison with H^E and V^E data for C_6–C_{24} mixtures[6] suggests, at 50°, a positive and small value for Z.

C_6–C_{36} Mixtures. This mixture is nearly a polymer–solvent system. At 80° and for the equimolar volume fraction of C_{36} (*i.e.*, $\varphi_2 = 0.82$), the sum $S = xI_1 + (1 - x)I_2$ is equal to 710 J/mol. At the same temperature the compression integral I_4 is equal to −430 J/mol and $H^E \sim 111$ J/mol, so that $Z = -170$ J/mol. This substantially negative value for Z should be ascribed to rather severe departure from hypothesis 7. A more comprehensive study of this mixture is not possible at present since H^E and V^E data are lacking for temperatures other than 76°.

In Figure 6 are plotted the sums S for the four previous mixtures, reported to 1 g of mixture at 80°. The curves are almost symetrical about the $\varphi_2 = \frac{1}{2}$ axis.

B. Solutions of Polyisobutylene in n-Alkanes. The following mixtures have been considered: C_6–PIB, C_8–PIB, and C_{16}–PIB. In fact, as a result of the use of a computer, the only limitation in studying more systems was imposed by the availability of proper expansion polynomials for α, γ, and V_M. For example, use of mean values between C_6 and C_8 for the expansion polynomial γ of C_7 has lead to erroneous results, so that the study of the system C_7–PIB had to be discarded.

The expansion polynomials used for PIB were those determined by Eichinger and Flory.[8a] Excess enthalpies at 25° for the above systems were taken from the paper by

TABLE II

Mixture	Vol fraction of polymer	Vol of polymer/mole mixture at 25° cm^3	Wt of polymer/mole mixture, g	No. of mole equiv of C_4H_8	H^E/mole C_4H_8,[a] J	H^E/mole mixture, J
C_6–PIB	0.540	154.3	141.5	2.527	−142.1	−165.2
C_8–PIB	0.532	182.8	167.6	2.993	−66.9	−93.7
C_{16}–PIB	0.515	303.5	278.3	4.970	+2.5	+6.1

	S, J	V^E, cm^3/mole mixture	I_4, J/mole mixture	Z, J/mole mixture
C_6–PiB	572.5	−2.44	−808.5	+70.8
C_8–PIB	414.4	−1.65	−552.4	+45.1
C_{16}–PIB	103.5	−0.47	−162.3	+64.9

[a] Reference 9.

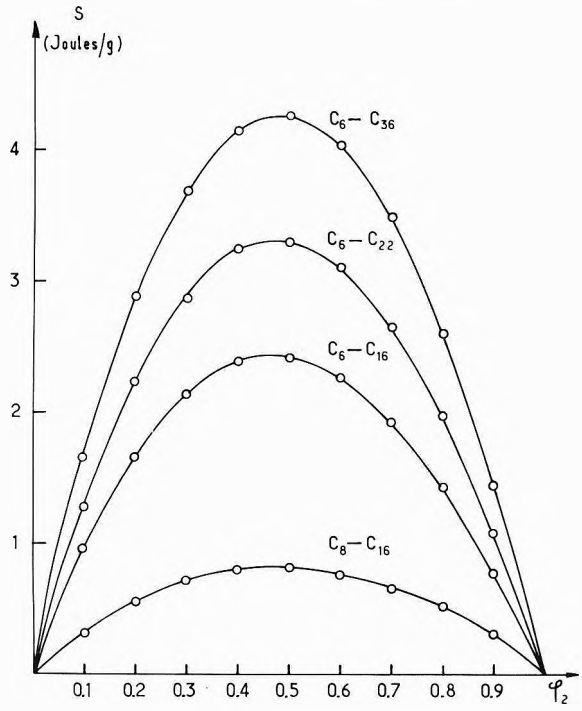

Figure 6. Sum S divided by the molecular weight of the mixture for C_8–C_{16}, C_6–C_{16}, C_6–C_{22}, and C_6–C_{36} mixtures at 80° as a function of the volume fraction of the component of higher molecular weight.

Delmas, *et al.*,[9] and excess volumes from that by Flory, *et al.*[7] The volume at 0°K of PIB, required to determine free volume fractions, was estimated from the expansion volume of PIB at the glass transition temperature given by Bondi[20] (*i.e.* 0.125 at −70°, see also ref 15). All calculations were performed considering a PIB of molecular weight of 10.000, with an estimated molar volume at 0°K of 9.059 cm^3. Molar fractions have been calculated as a function of volume fractions on this basis. Data for *n*-alkanes were the same as previously. Results for $S = xI_1 + (1 - x)I_2$ between 20 and 100°, assuming validity of hypothesis 7 are given in the microfilm edition of this work.[18] Excess enthalpies of mixing H^E, excess volumes V^E, compression integrals I_4, and final result $Z = H^E - S - I_4$ at 20° are summarized in Table II. In the sixth column of Table II are given the enthalpies of mixing per mol of C_4H_8 at infinite dilution, as reported by Delmas, *et al.*[9] To determine the excess enthalpy of a given weight of PIB, one has to multiply by the number of moles equivalent of C_4H_8 and the volume fraction of the solvent. This is done in the seventh column. The final result reported in the last column shows that Z is remarkably constant with the chain length of the *n*-alkane considered. It is very unfortunate that H^E and V^E data are not available at higher temperatures, to follow, as for *n*-alkane mixtures, the variation of Z with temperature.

VII. Conclusions

Phenomenological thermodynamics has been applied to the problem of the heat of mixing in solutions. No structure whatever has been assumed for the pure components in the liquid state and the solutions. Application of the theory to mixtures of *n*-alkanes and to mixtures of polyisobutylene with *n*-alkanes, after making the additional hypothesis that the mixing free volume fractions of the components are equal, leads at room temperature to small and positive values for the interchange energy. (The only heat effect considered in conventional theories of solutions.) This is a satisfactory result, the more so since the integrals I_1 and I_2 range from several thousands to several tens of thousands Joules per mole. However, for C_8–C_{16} and C_6–C_{16} mixtures, the sum $Z = H^E - (xI_1 + (1 - x)I_2) - I_4$ becomes negative as the temperature is increased from 20 to 100°, and is already negative for C_6–C_{36} mixtures at 80°. This behavior has been ascribed to the fact that the hypothesis of equal mixing free volume fractions in the components before mixing becomes less and less valid as the temperature is increased. Unfortunately, since H^E and V^E data as a function of temperature are not available at present, it is not possible to follow the variation of Z with temperature for PIB-*n*-alkane mixtures also.

What the value of the mixing free volume fractions, which need to be considered in the general case, is still unresolved. An attempt to treat this problem was made for C_6–C_{16} mixtures (see the microfilm edition). It seems however that a more rigorous procedure would require the use of three pair distribution functions, one for each kind of pair.

Acknowledgments. The author expresses his recognition to Professor H. Benoit, Director, Centre de Recherches sur les Macromolécules, Strasbourg, for his constant support during the course of this work. He also thanks Dr. C. Guez of the "Centre de Calcul de Strasbourg-Cronenbourg" for helpful advice in writing the computer program.

Supplementary Material Available. Footnotes 21-23 and Figures 7-16 will appear following these pages in the microfilm edition of this volume of the journal. Photocopies of the supplementary material from this paper only or microfiche (105 × 148 mm, 20× reduction, negatives) containing all of the supplementary material for the papers in this issue may be obtained from the Journals Department, American Chemical Society, 1155 16th St., N.W., Washington, D. C. 20036. Remit check or money order for $4.00 for photocopy or $2.00 for microfiche, referring to code number JPC-73-2977.

References and Notes

(1) J. Dayantis, *J. Phys. Chem.*, **76**, 400 (1972). See also *C. R. Acad. Sci., Ser. C*, **275**, 1254 (1972).
(2) I. Prigogine (with the collaboration of A. Bellemans and V. Mathot), "The Molecular Theorie of Solutions," North-Holland Publishing Co., Amsterdam, 1957.
(3) (a) P. J. Flory, R. A. Orwoll, and A. Vrij, *J. Amer. Chem. Soc.*, **86**, 3507 (1964); (b) **86**, 3515 (1964).
(4) P. J. Flory, *J. Amer. Chem. Soc.*, **87**, 1833 (1965).
(5) A. Abe and P. J. Flory, *J. Amer. Chem. Soc.*, **87**, 1838 (1965).
(6) (a) R. A. Orwoll and P. J. Flory, *J. Amer. Chem. Soc.*, **89**, 6814 (1967); (b) **89**, 6822 (1967).
(7) P. J. Flory, J. L. Ellenson, and B. E. Eichinger, *Macromolecules*, **1**, 279 (1968).
(8) (a) B. E. Eichinger and P. J. Flory, *Trans. Faraday Soc.*, **64**, 2035 (1968); (b) **64**, 2053 (1968); (c) **64**, 2061 (1968); (d) **64**, 2066 (1968); (e) *Macromolecules*, **1**, 285 (1968).
(9) G. Delmas, D. Patterson, and T. Somoynsky, *J. Polym. Sci.*, **57**, 79 (1962).
(10) D. Patterson, *J. Polym. Sci., Part C*, **16**, 3379 (1968).
(11) J. A. Barker, "Lattice Theories of the Liquid State," Pergamon Press, Elmsford, N.Y., 1963.
(12) J. M. H. Levelt and E. C. D. Cohen in "Stucies in Statistical Mechanics," J. de Boer and G. E. Uhlenbeck, Ed., North-Holland Publishing Co., Amsterdam, 1964.
(13) R. N. Haward, *J. Macromol. Sci., Rev. Macromol. Chem.*, **C(4)**, 191 (1970). The reader will find in this paper a detailed account of the different methods which permit the determination of the volume at 0°K.
(14) R. L. Scott, *J. Phys. Chem.*, **64**, 1241 (1960).
(15) M. L. McGlashan, K. W. Morcom, and A. G. Williamson, *Trans. Faraday Soc.*, **57**, 601 (1961).
(16) E. A. Guggenheim, "Mixtures," Clarendon Press, Oxford, 1952.
(17) Since dilute solutions ($\varphi_2 < 2$–3%)) are not considered in the present treatment, extrapolation of χ to zero concentration is somewhat arbitrary. We may, however, admit for present purposes that there is no sharp variation of the χ *vs.* φ_2 curve when φ_2 tends to zero, so that the values obtained by extrapolation of eq 38 and 40 remain meaningful.
(18) See paragraph at end of paper regarding supplementary material.
(19) A. Doolittle, *J. Appl. Phys.*, **22**, 1471 (1951).
(20) A. Bondi, *J. Polym. Sci., Part A-2*, **2**, 3159 (1964).

Monoisotopic Mass Spectra of Some Boranes and Borane Derivatives[1]

E. McLaughlin, L. H. Hall,[2] and R. W. Rozett*

Department of Chemistry, Fordham University, Bronx, New York 10458

(*Received July 5, 1973*)

Publication costs assisted by the Petroleum Research Fund

Least-squares-fitted monoisotopic mass spectra for B_5H_8Br, B_5H_8I, C_2H_5–$B_{10}H_{13}$, B_4H_{10}, B_5H_{11}, and $B_{10}H_{16}$ are given. Each represents the best monoisotopic mass spectrum presently available from measurements with a conventional mass spectrometer. Isotope cluster analysis is also used to show that the spectrum reported as $B_{20}H_{26}$ results from a mixture of $C_9B_{10}H_{28}$ and probably $C_9B_9H_{29}$.

Introduction

Analysis of the cluster of intensities due to the isotopic variants of the elemental formulas found in a mass spectrum allows one to simplify spectra, detect impurities, and establish the elemental composition of the ions if strongly polyisotopic elements are present.[3,4] The procedure has become convenient with the development of a computer program called MIMS which handles any number of overlapping isotope clusters, any combination of elements, and any fractional abundance of their isotopes.[5] MIMS uses all the polyisotopic information available to generate a least-squares-fit monoisotopic mass spectrum with intensities restricted to positive values. Two measures of success are available from the program. The first is the root-mean-square deviation, RMD, the usual measure of fit of a least-squares procedure. Past experience suggests that the present method provides a fit 25 times smaller on the average than hand-fitted spectra.[6] The second criterion is the absence of negative intensities in the monoisotopic spectrum. While the program allows one to restrict the intensities to nonnegative values simply by removing the formula of the peak in question, their presence is always a sign of badly fitting elemental formulas.[6] A well-fitting spectrum will have no negative intensities; a completely inappropriate set of formulas will produce on the average a sum of negative intensities equal to the sum of the positive intensities in the monoisotopic spectrum.

Monoisotopic Mass Spectra

Monoisotopic mass spectra prepared with the program MIMS are listed in Tables I–IV. Unpublished digital mass spectra of the halogenated pentaboranes were used to generate the monoisotopic spectra of Tables I and II.[7,8] The spectrum of ethyldecaborane (Table III) is a much improved calculation from published polyisotopic intensities.[9] The mass spectra of B_4H_{10} and B_5H_{11} have been studied by many workers.[4,10-18] The intensities of Tables IV and V represent the best-fitting results using data from a conventional mass spectrometer.[7] $B_{10}H_{16}$ was reinvestigated because of its poor fit (RMD 1.8).[6] The original dig-

TABLE I: Monoisotopic Mass Spectrum of B_5H_8Br

Formula	Intensity	Formula	Intensity	Formula	Intensity
B_2	4.07	B_5	20.8	B_3Br	1.06
B_2H	4.62	B_5H	14.2	B_3HBr	8.16
B_2H_2	9.55	B_5H_2	16.0	B_3H_2Br	9.52
B_2H_3	5.72	B_5H_3	6.90	B_3H_3Br	3.18
B_2H_4	0.02	B_5H_4	7.81	B_3H_4Br	0.0
B_2H_5	3.24	B_5H_5	4.05	B_3H_5Br	0.38
B_2H_6	0.0	B_5H_6	1.33	B_3H_6Br	0.13
B_2H_7	2.13[a]	B_5H_7	1.72		
		B_5H_8	0.16	B_4Br	5.84
B_3	3.08			B_4HBr	7.93
B_3H	5.86	Br	3.05	B_4H_2Br	12.5
B_3H_2	12.7	H Br	3.64	B_4H_3Br	16.3
B_3H_3	9.41	H_2Br	0.10	B_4H_4Br	2.73
B_3H_4	5.11	H_3Br	0.18[a]	B_4H_5Br	10.3
B_3H_5	1.59	H_4Br	0.59[a]	B_4H_6Br	0.24
B_3H_6	0.66				
B_3H_7	1.59	B Br	1.63	B_5Br	3.77
B_3H_8	3.26	BHBr	17.1	B_5HBr	13.2
		BH_2Br	0.13	B_5H_2Br	5.84
B_4	9.35				
B_4H	11.6	B_2Br	0.55	B_5H_3Br	7.23
B_4H_2	16.6	B_2HBr	2.75	B_5H_4Br	26.2
B_4H_3	25.2	B_2H_2Br	4.48	B_5H_5Br	4.53
B_4H_4	100.0			B_5H_6Br	39.3
B_4H_5	19.3			B_5H_7Br	0.0
B_4H_6	75.7			B_5H_8Br	74.6
B_4H_7	0.19			RMD	0.14

[a] Impurities suspected.

TABLE II: Monoisotopic Mass Spectrum of B_5H_8I

Formula	Intensity	Formula	Intensity
I	10.3	B_4H_2I	8.97
HI	5.34	B_4H_3I	2.11
BI	1.62	B_4H_4I	2.87
BHI	12.7	B_4H_5I	0.75
BH_2I	0.50	B_4H_6I	0.37
B_2HI	0.56	B_5I	1.34
B_2H_2I	2.11	B_5HI	6.85
B_2H_3I	4.34	B_5H_2I	1.18
B_3HI	4.64	B_5H_3I	3.25
B_3H_2I	5.52	B_5H_4I	0.0
B_3H_3I	2.44	B_5H_5I	1.60
B_3H_4I	0.32	B_5H_6I	0.0
B_3H_5I	0.25	B_5H_7I	2.15
B_4I	2.45	B_5H_8I	100.0
B_4HI	4.00	RMD	0.08

ital data were obtained, and a portion of the spectrum which contains doubly charged ions was removed. The improved fit (RMD 0.36) confirms the synthesis of $B_{10}H_{16}$ (Table VI).[7,8,19]

The spectra included here or published previously are the best-fitting monoisotopic borane spectra presently available from conventional mass spectrometers.[6,20] They represent the spectra with the smallest root-mean-square deviation for each compound from a complete survey of the literature up to the end of 1972. All polyisotopic mass spectra reported were resolved into monoisotopic spectra and their RMD determined. The RMD is, of course, a criterion of internal consistency rather than a measure of accuracy, but it is the single objective criterion easily avail-

TABLE III: Monoisotopic Mass Spectrum of $C_2H_5 \cdot B_{10}H_{13}$

Formula	Intensity	Formula	Intensity
B_6H_{10}	0.41	$B_{10}H_2$	2.02
B_7	0.91	$B_{10}H_3$	4.99
B_7H	0.15	$B_{10}H_4$	4.03
B_7H_2	2.33	$B_{10}H_5$	7.15
B_7H_3	1.07	$B_{10}H_6$	11.5
B_7H_4	2.66	$B_{10}H_7$	4.39
B_7H_5	0.0	$B_{10}H_8$	15.8
B_7H_6	1.66	$B_{10}H_9$	1.71
B_7H_7	0.00	$B_{10}H_{10}$	16.9
B_7H_8	0.10	$B_{10}H_{11}$	0.80
B_7H_9	0.54	$B_{10}H_{12}$	2.04
B_7H_{10}	0.00	$B_{10}H_{13}$	1.41
B_7H_{11}	1.09	$CB_{10}H_3$	3.33
B_8H	2.21	$CB_{10}H_4$	2.61
B_8H_2	1.40	$CB_{10}H_5$	3.31
B_8H_3	5.78	$CB_{10}H_6$	4.06
B_8H_4	3.60	$CB_{10}H_7$	4.32
B_8H_5	3.34	$CB_{10}H_8$	3.51
B_8H_6	0.14	$CB_{10}H_9$	1.63
B_8H_7	0.86	$CB_{10}H_{10}$	10.2
B_8H_8	0.0	$CB_{10}H_{11}$	1.04
B_8H_9	0.32	$CB_{10}H_{12}$	0.0
B_8H_{10}	1.00	$CB_{10}H_{13}$	2.32
B_8H_{11}	0.64	$CB_{10}H_{14}$	0.0
B_9H	2.82	$CB_{10}H_{15}$	2.64
B_9H_2	4.61	$CB_{10}H_{16}$	4.51
B_9H_3	6.43	$C_2B_{10}H_5$	2.23
B_9H_4	7.05	$C_2B_{10}H_6$	10.5
B_9H_5	5.76	$C_2B_{10}H_7$	5.17
B_9H_6	3.35	$C_2B_{10}H_8$	26.4
B_9H_7	4.12	$C_2B_{10}H_9$	5.83
B_9H_8	0.45	$C_2B_{10}H_{10}$	75.4
B_9H_9	0.54	$C_2B_{10}H_{11}$	5.12
B_9H_{10}	0.60	$C_2B_{10}H_{12}$	60.5
B_9H_{11}	1.63	$C_2B_{10}H_{13}$	4.91
B_9H_{12}	2.96	$C_2B_{10}H_{14}$	6.69
		$C_2B_{10}H_{15}$	7.28
		$C_2B_{10}H_{16}$	100.0
		$C_2B_{10}H_{17}$	1.01
		$C_2B_{10}H_{18}$	7.16
		RMD	0.014

TABLE IV: Monoisotopic Mass Spectrum of B_4H_{10}

Formula	Intensity	Formula	Intensity
B	9.14	B_3H_4	6.37
BH	1.72	B_3H_5	14.0
BH_2	7.04	B_3H_6	2.31
BH_3	0.60	B_4	5.26
B_2H	0.32	B_4H	10.5
B_2H_2	3.07	B_4H_2	15.4
B_2H_3	1.99	B_4H_3	18.6
B_2H_4	0.74	B_4H_4	58.5
B_2H_5	2.31	B_4H_5	13.4
B_2H_6	0.10	B_4H_6	100.0
B_3	1.30	B_4H_7	13.0
B_3H	2.49	B_4H_8	8.22
B_3H_2	10.5	B_4H_9	0.39
B_3H_3	11.7	B_4H_{10}	0.02
		RMD	0.03

able. Whenever possible spectra taken under conditions approaching those of a conventional analytical mass spectrometer were chosen. Spectra measured on molecular-

TABLE V: Monoisotopic Mass Spectrum of B_5H_{11}

Formula	Intensity	Formula	Intensity
B_4	4.63	B_5	14.9
B_4H	9.36	B_5H	11.8
B_4H_2	16.1	B_5H_2	16.7
B_4H_3	22.0	B_5H_3	13.8
B_4H_4	39.8	B_5H_4	14.0
B_4H_5	13.0	B_5H_5	69.6
B_4H_6	14.9	B_5H_6	8.23
B_4H_7	5.47	B_5H_7	100.0
B_4H_8	2.80	B_5H_8	7.41
B_4H_9	0.26	B_5H_9	28.5
B_4H_{10}	0.18	B_5H_{10}	0.55
		B_5H_{11}	0.20
		RMD	0.15

TABLE VI: Monoisotopic Mass Spectrum of $B_{10}H_{16}$

Formula	Intensity	Formula	Intensity
B_5H_6	8.77	B_8H_7	3.57
B_5H_7	23.6	B_8H_8	3.99
B_5H_8	2.80	B_8H_9	0.0
B_5H_9	18.7	B_8H_{10}	6.86
B_6H	15.8	B_8H_{11}	9.32
B_6H_2	1.39	B_9H	8.80
B_6H_3	16.9	B_9H_2	10.2
B_6H_4	19.0	B_9H_3	18.8
B_6H_5	12.3	B_9H_4	8.46
B_6H_6	9.55	B_9H_5	14.2
B_6H_7	1.68	B_9H_6	10.1
B_6H_8	2.69	B_9H_7	28.5
B_6H_9	1.54	B_9H_8	10.0
B_7	9.41	B_9H_9	4.42
B_7H	2.33	B_9H_{10}	0.0
B_7H_2	12.5	B_9H_{11}	26.0
B_7H_3	8.87	$B_{10}H_3$	14.5
B_7H_4	9.01	$B_{10}H_4$	6.77
B_7H_5	5.61	$B_{10}H_5$	0.0
B_7H_6	5.26	$B_{10}H_6$	36.1
B_7H_7	1.70	$B_{10}H_7$	0.0
B_7H_8	4.59	$B_{10}H_8$	100.0
B_7H_9	0.68	$B_{19}H_9$	7.19
B_7H_{10}	2.25	$B_{10}H_{10}$	36.8
B_8	8.30	$B_{10}H_{11}$	7.25
B_8H	11.4	$B_{10}H_{12}$	42.6
B_8H_2	6.02	$B_{10}H_{13}$	1.71
B_8H_3	17.4	$B_{10}H_{14}$	22.0
B_8H_4	12.2	$B_{10}H_{15}$	0.38
B_8H_5	11.5	$B_{10}H_{16}$	2.75
B_8H_6	6.52	RMD	0.36

beam mass spectrometers are simpler and free of reactive intermediates and pyrolysis products.[14-18] Chemiionization mass spectra are structurally revealing.[21] Neither are widely used for routine analysis and identification, however. On the other hand, they may be more significant for fundamental studies of mass spectra and structure. All published spectra have been resolved. If anyone prefers other monoisotopic spectra, they are available.

Mass Spectrum of Isocaborane(26)

The mass spectrum of $B_{20}H_{26}$ alone among the boranes has resisted every attempt to resolve it into a monoisotopic spectrum.[19] This failure has been attributed in the past to the presence of impurities,[6] and to the use of inaccurate data taken from the published histogram.[22] For this study we obtained the original measurements made on the isocaborane(26).[7] When the accurate polyisotopic intensities of $B_{20}H_{26}$, the usual isotopic abundances and a formula set derived from the $B_{20}H_{26}$ neutral, were run with the program MIMS, the sum of the negative intensities generated was equal to three-quarters of the positive intensities. The magnitude of the misfit makes it clear that one cannot fit the experimental spectrum with formulas derived from a $B_{20}H_{26}$ neutral using the usual isotopic abundances. We investigated the reason for this failure.

Isotope Abundances

The IUPAC table of chemical atomic weights for 1969 warns that commercial samples of boron, lithium, and uranium compounds may not have the usual isotopic abundances because of the "inadvertant or undisclosed separation of certain isotopes."[23] The large cross section for thermal neutrons of ^{10}B might provoke special interest in this isotope. Consequently we attempted to resolve the data for $B_{20}H_{26}$ with fractions of ^{10}B lower than the normal 20%. At an abundance of approximately 10%, the negative intensities in the monoisotopic spectrum disappeared, apparently confirming the hypothesis. However, when we performed a mass analysis on the original supply of decaborane used in the preparation of the $B_{20}H_{26}$, it showed no unusual isotopic distribution.[24] It is altogether improbable that a kinetic isotope effect could produce such an abnormal distribution if decaborane molecules with the usual isotopic distribution reacted in a few steps to form the product. The conclusion is forced on us that the boron of the $B_{20}H_{26}$ spectrum has approximately a normal isotopic distribution. The explanation for the unusual behavior of the spectrum must lie elsewhere.

Elemental Formulas

Apart from the fractional abundance of the isotopes, and the experimental data, only a set of formulas is used to generate the monoisotopic spectrum. The reliability of the experiments including the data of Table VI. Therefore the formula set must be inappropriate. The "$B_{20}H_{26}$" mass spectrum must contain elements other than boron and hydrogen. The general appearance of the spectrum (Figure 1) makes it equally clear that both boron and hydrogen are present.[19] Formula sets containing fewer than twenty boron atoms were tried. When a maximum of ten boron atoms are included, the negative intensities drop off drastically. At this point the monoisotopic spectrum fits well except for some intensities in the base peak region (231 amu). The spectrum consists mainly, therefore, of a compound containing ten boron atoms.[25] One can easily confirm the adequacy of the ten boron atom formulas by resolving the spectrum above and below the base peak region separately. In each case a ten boron formula set provides an adequate fit. It is not surprising that one can fit the data either with twenty boron atom formulas and a 10% ^{10}B abundance or with ten boron atom formulas and a 20% ^{10}B abundance. The isotope clusters for the two cases are remarkably similar.

The ten boron atom formulas nevertheless do not fit well three or four mass units on each side of the base peak. In fact it is clear from the experimental spectrum (Figure 1) that this region is quite unlike the remainder of the intensities which vary unusually smoothly and regu-

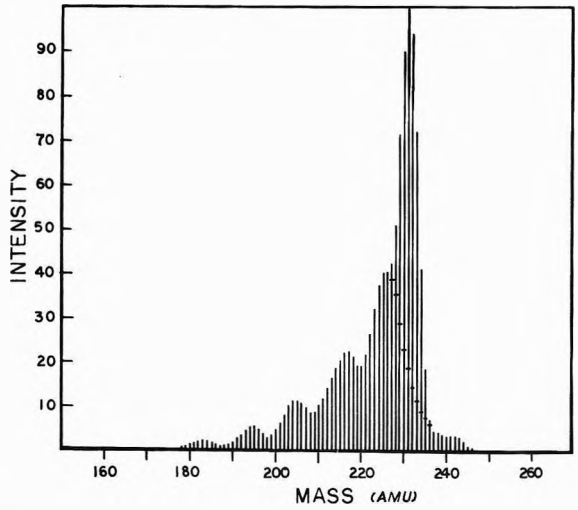

Figure 1. Experimental mass spectrum for $B_{20}H_{26}$.

larly. This local poor fit suggests that two sets of ions with different formulas are present in the base peak region. Overlapping sets of ions can be produced by the presence of a mixture of several different compounds, or by the different fragmentation pathways of a single complex parent molecule. The very regular character of the spectrum below the base peak region (Figure 1) suggests that one might be able to separate out intensities in the region of overlap which will be continuous with the intensities of the lower and higher mass regions. The shoulder on the large maximum in the base peak region (masses 225 and 226) indicates a local maximum similar to those at masses 183, 195, 205, and 217. The cross bars drawn across the experimental intensities in Figure 1 (227–236) indicate the suggested divisions. The divisions represent a linear interpolation between the two sections of the spectrum, modified slightly to make a smooth transition at each end. One may now deal with each component separately.

Major Component

The major component contains the region below and above the base peak region as well as the interpolated intensities within the 227 to 236 mass range. From our previous discussion it is clear that the component contains ten boron atoms. The regular character of the envelope of the intensities suggests that no other strongly polyisotopic element is present besides boron. The element most likely to be present besides boron and hydrogen is carbon. Hydrocarbon impurities are often found in borane samples. Vacuum pump oil and sealants (Apiezon T) are other possible sources. Reaction with the molten (100°) decaborane during the deuteron irradiation could generate alkyl boranes or carboranes. A set of formulas beginning with the parent formula $C_9B_{10}H_{28}$ fits the spectrum well (RMD 0.021). One could write this as $C_9H_{15}{\cdot}B_{10}H_{13}$ if this did not seem to imply that the compound was known to be an alkyl borane with a single side chain. In the formula set used we assume that only carbon and hydrogen atoms are lost during the fragmentation. This is suggested by the similarity of the envelope maxima as one moves toward lower masses. The fit of the B_{10} formulas is no less adequate in the low than in the high mass region. The ten largest peaks of the spectrum are easily rationalized in terms of the parent formula (Table VII). The neutrals listed are those thermodynamically most accessible, *i.e.*, the neutrals produced by the least endothermic reaction.

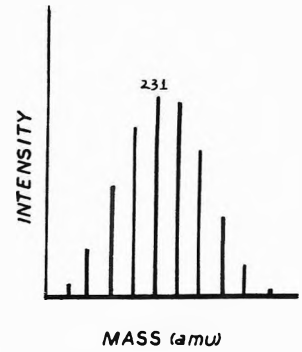

Figure 2. Residual intensities at masses 227 to 236 in the experimental mass spectrum of $B_{20}H_{26}$.

TABLE VII: Ten Largest Peaks of the Monoisotopic Mass Spectrum of $C_9B_{10}H_{28}$ ($B_{20}H_{26}$)

Mass	Neutrals lost	Intensity
227	$CH_3 + 2H_2$	100
225	$CH_3 + 3H_3$	89
229	$CH_3 + H_2$	72
230	CH_4	67
228	$CH_4 + H_2$	52
218	C_2H_4	46
223	$CH_3 + 4H_2$	42
216	C_2H_6	39
220	C_2H_2	39
219	C_2H_3	38

If the formula $C_9H_{15}{\cdot}B_{10}H_{13}$ represents the parent molecule, then there must be two double bonds or one triple bond in the side chain(s). One might also speculate that the major "component" is actually a mixture of decaborane derivatives with varying degrees of alkylation and/or unsaturation in the side chains.

Minor Component

Figure 2 shows the residual intensities at masses 227–236. The appearance of the spectrum is still that of a boron and hydrogen containing compound. Attempts to resolve the intensities with ions containing more than ten boron atoms were unsuccessful. The compound cannot contain ten boron atoms, or it would have been resolved with the major component. For the reasons mentioned previously, carbon was supposed to be the impurity element. A set of formulas beginning with $C_9B_9H_{29}$ adequately resolve the cluster of abundances (RMD 1.0). With the same reservations mentioned previously, this can be written as $C_9H_{15}{\cdot}B_9H_{14}$. One is left with the question whether these ions are fragmentation products of the major ingredient, or are from a different parent compound. If the mass of the parent peak is taken seriously, then this compound has one more hydrogen than the first component. A second indication that these ions are not fragmentation products of the ten boron compound is the absence of nine boron fragments outside of the region of the base peak. The second component seems much more stable than the first. The minor component may be a thermolytic product of the first compound but it is probably not a fragmentation product produced by the loss of a boron atom from the ions of the major component.

It is interesting to note that the highest mass of the spectrum of the major component corresponds to the formula $B_{20}H_{26}$, while the highest mass of the minor component corresponds to the formula $B_{20}H_{16}$, a known boron hydride.[26,27] In addition, the unique closed cage of icosa-

borane(16) would lead one to expect little fragmentation, except for the loss of hydrogen atoms. Nonetheless the unusual and unverified isotope abundance which this supposition requires, and the evidence that the minor and major components do not have the same number of boron atoms, preclude this interpretation.

Fitting Mass Spectra

There is a lesson to be learned from the possibility of fitting the experimental spectrum with formulas containing twenty boron atoms and an unusual isotopic distribution. Whenever a spectrum fits badly, usually because of the presence of several compounds, one can improve the apparent fit of the suggested formulas by several alternate methods. First, one can change the fractional abundances of the isotopes. The experimental data can always be fit exactly with monoisotopic elements and as many formulas as there are experimental intensities. One can move toward this "perfect" fit by supposing the elements present more monoisotopic. Lowering the fraction of the less abundant isotope is a step in this direction. A second, similar way to improve the fit is to substitute atoms of a (more) monoisotopic element for those of a polyisotopic element in the formula set. This is mathematically equivalent to making the same element more monoisotopic. Finally, one can increase the number of formulas used to resolve the spectrum. Increasing the number of variables used makes the fitting process less demanding.

Any one of these procedures may be the correct option in a given case. Experience suggests that, in general, it is safer to increase the number of formulas before changing the elemental composition of the formulas, and that both of these options should be attempted before changing isotope abundances. Independent chemical evidence about isotope ratios or formulas should be preferred to the simple mathematical criterion of the lowest RMD.

Conclusion

The evidence which leads one to question the identity of "$B_{20}H_{26}$" is negative. It in no way eliminates the possibility that $B_{20}H_{26}$ can be prepared. Nor does it strictly rule out the possibility of some unusual isotope fractionation process after the synthesis. But this is a highly improbable and unsupported hypothesis. Clearly there is need for a synthetic chemist to prepare a quantity of the compound sufficient for corroborative methods of analysis and for an elemental analysis.

References and Notes

(1) Acknowledgment is made to the donors of the Petroleum Research Fund, administered by the American Chemical Society, for partial support of this research. The instrumentation was supplied in part by the National Science Foundation (GP 8220) and by the New York State Science and Technology Foundation (NYSSF (6)-13).
(2) Department of Chemistry, Eastern Nazarene College, Wollaston, Mass. 02170.
(3) J. H. Beynon, "Mass Spectrometry and Its Application to Organic Chemistry," Elsevier, Amsterdam, 1960, p 305.
(4) J. F. Ditter, F. J. Gerhart, and R. E. Williams, *Advan. Chem. Ser.*, **No. 72**, 191 (1968).
(5) E. McLaughlin and R. W. Rozett, *J. Organometal. Chem.*, **52**, 261 (1973).
(6) E. McLaughlin, T. E. Ong, and R. W. Rozett, *J. Phys. Chem.*, **75**, 3106 (1971).
(7) Lowell H. Hall, II, Doctoral Dissertation, Johns Hopkins University, 1963.
(8) L. H. Hall, V. V. Subbanna, and W. S. Koski, *J. Amer. Chem. Soc.*, **86**, 3969 (1964).
(9) A. Quayle, *J. Appl. Chem.*, **9**, 399 (1959).
(10) Manufacturing Chemists Association Research Project, Serial No. 30, 31, 1960.
(11) I. Shapiro, C. O. Wilson, J. F. Ditter, and W. J. Lehmann, *Advan. Chem. Ser.*, **No. 32**, 127 (1961).
(12) T. P. Fehlner and W. S. Koski, *J. Amer. Chem. Soc.*, **85**, 1905 (1963).
(13) T. P. Fehlner and W. S. Koski, *J. Amer. Chem. Soc.*, **86**, 581 (1964).
(14) A. B. Baylis, G. A. Pressley, Jr., and F. E. Stafford, *J. Amer. Chem. Soc.*, **86**, 5358 (1964).
(15) A. B. Baylis, G. A. Pressley, Jr., and F. E. Stafford, *J. Amer. Chem. Soc.*, **88**, 929 (1966).
(16) A. D. Norman, R. Schaeffer, A. B. Baylis, G. A. Pressley, Jr., and F. E. Stafford, *J. Amer. Chem. Soc.*, **88**, 2151 (1966).
(17) A. B. Baylis, G. A. Pressley, Jr., and F. E. Stafford, *J. Amer. Chem. Soc.*, **88**, 2428 (1966).
(18) F. E. Stafford, G. A. Pressley, Jr., and A. B. Baylis, *Advan. Chem. Ser.*, **No. 72**, 137 (1968).
(19) L. H. Hall and W. S. Koski, *J. Amer. Chem. Soc.*, **84**, 4205 (1962).
(20) E. McLaughlin and R. W. Rozett, *Inorg. Chem.*, **11**, 2567 (1972).
(21) J. J. Solomon and R. F. Porter, *J. Amer. Chem. Soc.*, **94** 1443 (1972).
(22) E. McLaughlin and R. W. Rozett, *J. Phys. Chem.*, **76**, 1860 (1972).
(23) *Chem. Eng. News*, Jan 26, p 39 (1970).
(24) We would like to thank Professor W. S. Koski for a sample of the original decaborane.
(25) The paragraph entitled Fitting Mass Spectra which appears later in the article is pertinent here.
(26) L. B. Friedman, R. D. Dobrott, and W. N. Lipscomb, *J. Amer. Chem. Soc.*, **85**, 3505 (1963).
(27) N. E. Miller and E. L. Muetterties, *J. Amer. Chem. Soc.*, **85**, 3506 (1963).

Behavior of Diffuse Electrolyte Boundaries in an External Electric Field[1]

H. A. Levine,[2] D. K. Harriss, and J. C. Nichol*

The Department of Chemistry, University of Minnesota, Duluth, Duluth, Minnesota 55812 *(Received January 16, 1973; Revised Manuscript Received September 18, 1973)*

Publication costs assisted by the Department of Chemistry, University of Minnesota, Duluth

The behavior of a diffuse electrolyte boundary in an external electric field has been investigated for the case in which the boundary is formed in a cell of constant cross section between solutions of uni-univalent strong electrolytes FA and SA. The initial concentrations of the FA and SA solutions are those observed in a moving boundary experiment in which the FA solution is the leading electrolyte and the SA solution is the adjusted ("indicator") solution formed behind the moving boundary. Experimental results are presented for the system KCl–LiCl in acrylamide gel and in a sucrose density gradient at 1.00°. For the purpose of making theoretical calculations, differential equations are derived which relate the concentrations of the ions to the position in the diffusion cell and to the length of time elapsing after application of an external electric field. In these equations the electric field term is replaced by a term involving concentrations, mobilities, and the current density. The equations are solved numerically by finite differences. The qualitative behavior predicted by theory is in agreement with the experimental results for the KCl–LiCl system. The magnitude of the errors arising from assumptions made in the derivation of the equations is evaluated, and their practical usefulness is discussed.

Introduction

In an earlier report,[3] a study of intermittent current effects in free electrophoresis was presented. The observed time-dependent behavior was accounted for in part and in a very qualitative fashion by picturing the sequence of events as a succession of discrete steady-state steps. The moving boundary system assumed to exist at each step was considered to be governed by steady-state strong electrolyte moving boundary theory.[4] The acquisition of useful data for comparison with the theory was limited by the occurrence of convection behind the moving boundaries, arising from density gradient inversions. In this paper a treatment based on the differential equations of transport is presented and compared with experiments in which convection is avoided by the use of an acrylamide gel and of a sucrose density gradient. The general question of the effect of an external electric field upon a strong electrolyte diffusion boundary in terms of classical transport theory is considered, and a set of nonlinear partial differential equations is presented in which the ion concentrations are related to time and to the position in the cell. In these equations the electric field, which, for example, varies approximately twofold across the KCl–LiCl boundary discussed below, is replaced by a term involving concentrations, current density (constant in a cell of constant cross section), and ion mobilities (which show variations of a few per cent over the concentration range of interest (0.06–0.1 *M*)). It has not been found possible to obtain explicit closed-form solutions for the equations, and concentrations have therefore been calculated by the method of finite differences. Refractive index gradient *vs.* distance curves have been constructed from the concentrations by introducing the appropriate equivalent refractions. The curves so obtained for a hypothetical system, for which the physical constants are chosen to closely resemble KCl–LiCl, agree well in qualitative detail with the experimental schlieren photographs for times of application of the external electric field up to 2 hr. An experimental test of the quantitative validity of the equations could not be made because of the necessity of performing the experiments in gels or in sucrose gradients in order to avoid density convection. We have made an estimate from data in the literature (see Results and Discussion section) of the error in concentration calculations arising from assumptions made in the derivation, notably the neglect of interacting flows arising from specific ion effects and the assumptions that activity coefficients, diffusion coefficients, and electrical mobilities are independent of concentration. We conclude that the error is small (about 1–2% in concentration) for the KCl–LiCl system in water at ionic strengths up to about 0.5 when diffusion is proceeding in the absence of an external field, and somewhat larger if a field is present.

Experimental Section

Experiments were performed at 1.00°, using a Spinco Model H electrophoresis apparatus. A typical experiment would consist of layering 0.05 *M* LiCl over 0.1 *M* KCl in the desired medium, generating a moving boundary by application of an electric field so that KCl was the leading electrolyte and LiCl the adjusted (approximately 0.06 *M*) following or "indicator" electrolyte, allowing the boundary to undergo free diffusion by turning off the current after a steady state had been attained, and then turning on the current again and observing the subsequent boundary behavior. In experiments in aqueous solution this procedure could be modified by mechanically sharpening the steady-state moving boundary prior to free diffusion. Density inversions, and hence convective effects, were invariably produced in aqueous solutions shortly after application of an external electric field across the diffusion boundaries used in these experiments. In an attempt to reduce convection, some runs were carried out in concentrated (10–40%) sucrose solutions. The onset of convection was delayed sufficiently to permit observation of the first stage of the predicted effects, considerably beyond what was possible in water. The full sequence of events was first obtained in experiments using a 2.5% gelatin (USP powder)

gel. Successful results, presented below, were later obtained with a 7% acrylamide gel[5] and with a sucrose–water concentration gradient as supporting media (see discussion below, and Figures 4–6). The acrylamide gel was more satisfactory than the gelatin gel, generalized convection and blurring being observed fairly soon in the latter, presumably because of electrical forces causing disruption of the charged gel structure in gelatin. We were unable to form the acrylamide gel so as to avoid some initial blurring, but the gel did not deteriorate further upon passage of current. Completely clear pictures were obtained in the sucrose gradient. However, it suffers from the disadvantage of a superimposed refractive increment arising from the sucrose gradient. Nevertheless, the main features in its development are clearly the same as those observed in the acrylamide gel (Figures 4 and 5).

Theory

Our objective is to develop relationships which will enable us to predict the time-dependent behavior of electrolyte diffusion boundaries under the influence of an electric field, that is, relationships from which the concentration of each ion may be calculated for each position in the cell as a function of time. We will be concerned primarily with the following experimental situation. A boundary is formed (see below) between solutions of uni-univalent strong electrolytes FA and SA, in an infinitely long channel of constant cross-sectional area B cm^2. The positive x direction is taken to be along the channel, going from SA to FA (Figure 1). Cation F has a higher electrical mobility than cation S. Concentrations are assumed to vary only in the x direction. After the boundary has undergone diffusion for a time t_D, an electric field going from positive to negative in the positive x direction is applied for an additional period t_V. The equations to be developed here apply generally, regardless of the direction of the applied field or the relative magnitudes of the initial FA and SA concentrations. However, we are particularly interested in the case[3] for which the SA concentration is the same as the adjusted concentration which it would have if it were the "indicator" electrolyte in a moving boundary experiment in which FA is the leading electrolyte. In this case, for which the concentrations of the two electrolytes are related by the equality of their Kohlrausch regulating functions[6] (defined by $\omega = \Sigma C_i/u_i$ where C_i is the concentration and u_i the mobility of ion i), it turns out that a greater wealth of time-dependent detail is observed than for other concentration ratios. Consequently, a better comparison of theory with experiment is made possible.

The initial diffuse boundary may be produced in one of two ways.

(a) A moving boundary is formed in the usual manner with FA as the leading electrolyte and SA as the self-adjusted indicator electrolyte. The boundary is allowed to move far enough so that indicator solution of constant concentration C_{SA} extends for several cm behind it. The electric field is high enough so that a fairly sharp boundary is obtained but not so high that convection occurs. This corresponds to a current of a few mA (6–15 mA in our experiments) in the standard Tiselius cell of 0.75 cm^2 cross section. The current is then turned off, and ordinary diffusion without external electric field is allowed to proceed for time t_D.

(b) The same procedure as that in a is used, except that, after the current is turned off, the boundary is mechanically sharpened using the capillary sharpening technique of Kahn and Polson,[7] before ordinary diffusion is allowed to proceed. This latter procedure obviously cannot be followed for experiments with gels or density gradients.

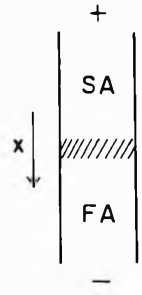

Figure 1. Diagram showing the experimental situation at the time of initial application of an external electric field to a uni-univalent electrolyte diffusion boundary FA–SA. Cross hatching represents the diffuse boundary.

We first derive relationships for the time period after t_D, during which the electric field is applied, since they include as a special case the relationships for the time period before t_D, during which the external electric field is zero.

A general equation relating concentration, C_j (in equiv l.$^{-1}$, for example) to time, t, and position, x, for an ion species, j, of charge z_j and mobility u_j moving in the x direction in a tube of uniform cross section under the influence of gradients of chemical and electrical potential, $\partial\mu_j/\partial x$ and $\partial V/\partial x$, may be written[8]

$$\frac{\partial C_j}{\partial t} = \frac{\partial}{\partial x}\left[\frac{C_j u_j}{|z_j|F}\left(\frac{\partial \mu_j}{\partial x} + z_j F\frac{\partial V}{\partial x}\right)\right] \quad (1)$$

where F is the Faraday. The concentration and mobility are given positive values in eq 1, regardless of the sign of the charge on the ion. The valence, including sign, is indicated by z_j, and the magnitude only by $|z_j|$. Electrolyte transport equations closely related to this type of equation were first thoroughly investigated by Nernst[9] and Planck,[10] and are frequently referred to as the Nernst–Planck equations. Interaction of flows arising from *specific* ion effects is neglected, although, as will be seen below (eq 6 and 7), the presence of V in eq 1 implies coupling terms arising from differences in ion mobilities. Mobilities (but not the electrical field) are assumed constant. Questions regarding the validity and weaknesses of this general type of transport equation, and its usefulness in a practical sense have been considered by Newman.[11] Our results support his conclusion that "the flux equation gives a fairly reasonable account of the physical processes involved without excessive complication," at least for the simple uni-univalent strong electrolyte case which we have studied.

The molar chemical potiential is related to the activity a_j by

$$\mu_j = \mu_j^0 + RT \ln a_j = \mu_j^0 + RT \ln C_j y_j/|z_j| \quad (2)$$

where y_j is the single ion activity coefficient. If the activity coefficient is assumed to be constant, differentiation of eq 2 gives

$$\frac{\partial \mu_j}{\partial x} = \frac{RT}{C_j}\frac{\partial C_j}{\partial x} \quad (3)$$

and eq 1 becomes

$$\frac{\partial C_j}{\partial t} = \frac{u_j}{|z_j|F}\left\{RT\frac{\partial^2 C_j}{\partial x^2} + z_j F\frac{\partial[C_j(\partial V/\partial x)]}{\partial x}\right\} \quad (4)$$

To eliminate V from eq 4 we make use of the following expression for the electric current[12] in a solution containing s ions

$$i = BI = \frac{FB}{10^3}\sum_{k=1}^{s}\frac{C_k u_k}{z_k}\left[\frac{1}{F}\frac{\partial \mu_k}{\partial x} + z_k\frac{\partial V}{\partial x}\right] = -\frac{FB}{10^3}\left[\frac{RT}{F}\sum_{k=1}^{s}\frac{u_k}{z_k}\frac{\partial C_k}{\partial x} + \sum_{k=1}^{s}C_k u_k\frac{\partial V}{\partial x}\right] \quad (5)$$

where C_k = concentration in equiv $l.^{-1}$, i = current (amp), I = current density (amp cm^{-2}), and B = cross-sectional area of uniform cell channel in cm^{-2}. At once

$$\frac{\partial V}{\partial x} = -\frac{RT}{F}\sum_{k=1}^{s}\frac{u_k}{z_k}\frac{\partial C_k}{\partial x}\frac{10^3 I}{F}\Big/\sum_{k=1}^{s}C_k u_k \quad (6)$$

If there is no external electric field, $I = 0$. However, inspection of eq 6 shows that $\partial V/\partial x$ is not then necessarily zero. The remaining terms in eq 6 comprise the self-electric field or gradient of diffusion potential.[9] They represent coupling of flows due predominately to the requirement that ions of different mobility move so as to maintain electroneutrality, time-of-relaxation and electrophoretic effects and concentration dependence of activity coefficients being disregarded.[13] Elimination of $\partial V/\partial x$ from eq 4 in using eq 6 yields

$$\frac{\partial C_j}{\partial t} = \frac{RTu_j}{|z_j|F}\left[\frac{\partial^2 C_j}{\partial x^2} - z_j\frac{\partial}{\partial x}\left\{\left\langle\frac{\sum_{k=1}^{s}\frac{u_k}{z_k}\frac{\partial C_k}{\partial x} + \frac{10^3 I}{RT}}{\sum_{k=1}^{s}C_k u_k}\right\rangle C_j\right\}\right] \quad (7)$$

The term $RTu_j/|z|F$ may be identified with the diffusion coefficient D_j (Nernst–Einstein relation[11]) if the solution is dilute.

In eq 7, assuming constancy of ion mobilities, the variables are the C's, x, and t, and the problem of taking account of V as an additional variable is eliminated.

We can now apply eq 7 to ions F, S, and A in the system described above. Here $z_F = z_S = -z_A = 1$. In calculating concentration profiles we need be concerned with relations for only two of these ions, since the concentrations are related by the condition of electroneutrality $C_F + C_S = C_A$. For ions F and S, eq 7 reduces to

$$\frac{\partial C_F}{\partial t} = \frac{RT}{F}u_F\left[\frac{\partial^2 C_F}{\partial x^2} - \frac{\partial}{\partial x}\times\left\{\left\langle\frac{(u_F - u_A)\frac{\partial C_F}{\partial x} + (u_S - u_A)\frac{\partial C_S}{\partial x} + \frac{10^3 I}{RT}}{(u_F + u_A)C_F + (u_S + u_A)C_S}\right\rangle C_F\right\}\right] \quad (8a)$$

$$\frac{\partial C_S}{\partial t} = \frac{RT}{F}u_S\left[\frac{\partial^2 C_S}{\partial x^2} - \frac{\partial}{\partial x}\times\left\{\left\langle\frac{(u_F - u_A)\frac{\partial C_F}{\partial x} + (u_S - u_A)\frac{\partial C_S}{\partial x} + \frac{10^3 I}{RT}}{(u_F + u_A)C_F + (u_S + u_A)C_S}\right\rangle C_S\right\}\right] \quad (8b)$$

The concentration profiles resulting from the initial period of diffusion for time t_D in the absence of an external electric field are calculated using eq 8 with $I = 0$. To perform this calculation, the concentration profiles at $t_D = 0$ must be known. The evaluation is simpler for case b above than for case a because the initial profiles will approximate the following step functions (*i.e.*, the boundary approximates an infinitely sharp boundary) where C_F^0 and C_S^0 are the concentrations in

$$C_{FA} = C_F = \begin{cases} C_F^0, x > 0 \\ 0, x < 0 \end{cases} \text{ and } C_{SA} = C_S = \begin{cases} C_S^0, x < 0 \\ 0, x > 0 \end{cases} \quad (9)$$

the body of the leading and indicator solutions.

For case a, Longsworth[12] has derived equations, based upon Weber's theory,[14] which give the concentration distribution across such boundaries. Longsworth has shown that predicted refractive index gradients calculated using these equations agree closely with the observed values across such boundaries. The initial concentrations, $C_j^0(x)$, are no longer step functions but are given by the expressions (see Longsworth's eq 17 and 18)

$$C_F^0(x) = C_F^0\left(1 - \frac{\sinh^{-1}\xi}{\xi\sqrt{1+\xi^2}}\right) \quad (10a)$$

$$C_S^0(x) = C_F^0\,\xi^2 \quad (10b)$$

where $\xi = \exp[vx/(2u_A RT/F)]$, $v = 10^3 Bu_F/(u_F - u_A)FC_F^0 = 10^3 B/2FC_F^0$ = boundary velocity, B = cross-sectional area of diffusion cell, u_F = mobility of ion F (mobilities assumed constant), u_A = mobility of ion A, F = Faraday, and C_F^0 = initial concentration of ion F in the body of the FA solution. In the derivation of eq 10 the relative mobility values are chosen to be $u_F = u_A = 2u_S$, a choice which makes possible a considerable simplification in the equations,[12] and which is a good approximation to the actual relative mobility values in our experimental KCl–LiCl system. It might be anticipated that the calculated concentration distribution across the initial boundary, and hence across the diffusion boundary arising from it, in general would be different in case a from that in case b. In our system the difference is extremely small (Figure 2).

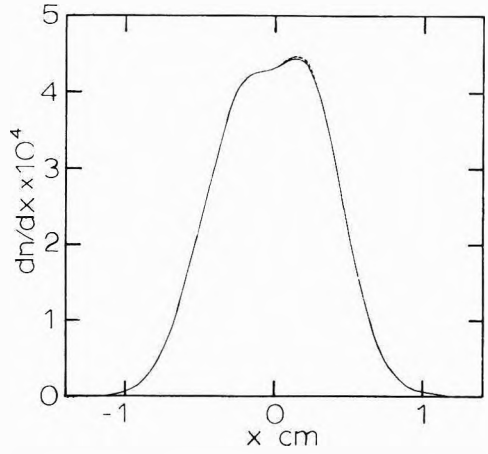

Figure 2. Refractive index gradient curves calculated for the FA–SA system after diffusion for 5400 sec at 1.00° in the absence of an external electric field. Boundaries are considered to be formed initially by an 8-mA current followed by mechanical sharpening to "infinite sharpness" (solid line) and by 8-mA current without mechanical sharpening (dashed line).

Once the concentration profiles at time t_D are known, relations 8a and 8b are used with appropriate values of I to calculate the profiles at the desired times t_V, during

which the electric field is applied after free diffusion for time t_D. The errors associated with calculations using these equations are discussed in the following section.

Results and Discussion

Relations 8 constitute a pair of nonlinear parabolic partial differential equations of the Fokker–Planck type, in two unknowns, C_F and C_S. Although we have not been able to obtain explicit solutions for these equations, we have solved them numerically, using the method of finite differences, to provide values of C_F, C_S, $\partial C_F/\partial x$, $\partial C_S/\partial x$, and dn/dx (where n = refractive index) at intervals of x and t_D or t_V. We have carried out the solution with the aid of the University of Minnesota's CDC 1604 and 6600 computers, and Cornell University's IBM 360 Model 44 computer for a model system in which $u_F = u_A = 2u_S = 3.688 \times 10^{-4}$ cm^2 V^{-1} sec^{-1}, where these and the values below are taken to eight significant figures in the computer calculations. These mobilities are good approximations to the experimental values for KCl–LiCl.[12] The concentrations for the starting solutions were taken as exactly 0.1 M FA and 0.06666667 M SA, the latter value being obtained from the mobilities and FA concentration using the requirement of the equality of the Kohlrausch regulating functions in the two solutions. (In an actual moving boundary experiment with 0.1 M KCl as the leading electrolyte, followed by LiCl, the adjusted concentration of the latter is nearer 0.06 M.[12]) By incorporating the equivalent refractions, $k_{KCl} = 0.01080$ and $k_{LiCl} = 0.00950$[12] into the computer program, we have also obtained the refractive index gradient dn/dx. The predicted results are shown in Figure 3 for the case in which the preliminary free diffusion is considered to proceed for 5400 sec at 1.00° from an initial boundary formed by mechanical sharpening of a moving boundary generated by an 8-mA current. The corresponding calculations for the case in which mechanical sharpening is omitted were not performed since the initial diffuse boundaries are practically identical (see Figure 2). Moving boundaries calculated for times up to 5400 sec from the start of application of the external electric field are shown in Figure 3. For all practical purposes a steady state is attained in this time. The positive x direction is the direction of cation migration, cation F leading. The current during the period of applied electric field is 8 mA. (The potential gradient, of course, changes across the boundary. In the initial FA solution (0.1 M), for example, it is about 1.5 V cm^{-1}, as calculated from the assumed mobilities, the current, and the cell dimensions. The complete potential gradient profile is readily calculable, since the concentrations are known across the boundary.) The $t_V = 0$ curve in Figure 3 and the solid curve in Figure 2 represent the same boundary. The negative dn/dx values predicted in the SA region (which extends up to the leading moving boundary) reflect a drop in SA concentration below that on either side of the minimum. In the usual situation for inorganic salts for which the density varies directly with concentration, the experimentally observed convection for the FA–SA system in water alone is to be expected. If convection can be avoided, the concentration fluctuations behind the boundary should persist for an extended period, eventually levelling out as a result of diffusion down the gentle concentration gradient.

In Figures 4–6 experimental results are presented for comparison with the calculated profiles of Figure 3. In Figure 4 are shown outlines of photographs of the schlieren boundary for an experiment with KCl–LiCl in acrylamide gel. These were not traced directly from the photographs, but were obtained by reading peak height *vs.* position in the cell with a Gaertner Model M 2001P comparator. The gel, containing KCl at 0.1 M concentration, was allowed to form in the center and bottom sections of an 11-cm^3 Tiselius cell. After the top sections were filled with aqueous 0.05 M LiCl and the electrodes placed in position, a 15 mA current was applied until a steady-state boundary had moved about one-third of the way down that center section in which the direction of positive current was downward (cross-hatched boundary, $t_D = 0$). Below the boundary is the original 0.1 M KCl, and above it LiCl at an adjusted concentration (about 0.06 M, if the relative mobilities of the ions are the same in the gel as in water[12]). Free diffusion was then allowed to proceed for 1800 sec followed by passage of a 10-mA current as described in the Figure 4 caption. In Figure 5 the tracings presented are for a similar experiment in a sucrose gradient. The sucrose concentration was 0 g l.$^{-1}$ at the top of the cell center section and 20 g l.$^{-1}$ at the bottom in the limb down which the steady-state boundary moved. It is evident that the sucrose gradient is not linear. However, the lack of linearity does not obscure the fact that there is essentially the same type of boundary development as in

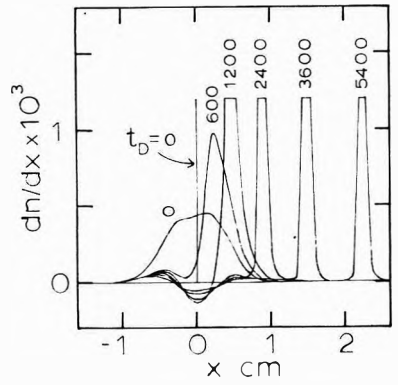

Figure 3. Predicted effect of external electric field on FA–SA electrolyte diffusion boundary. Refractive index gradient curves calculated for passage of an 8-mA current at 1.00° for times t_V in seconds (unlabeled numbers), after free diffusion for time t_D = 5400 sec (t_V = 0) from an initial boundary formed by passage of 8-mA current followed by mechanical sharpening (represented by the vertical line labeled t_D = 0).

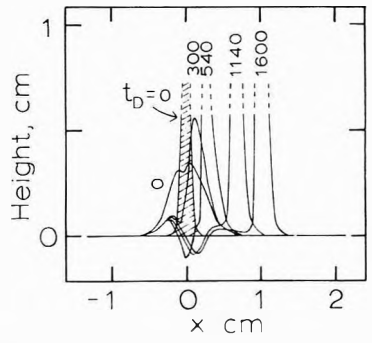

Figure 4. Outlines of schlieren photographs for the KCl–LiCl system in acrylamide gel at 1.00°. A 10-mA current was applied after free diffusion for 1800 sec from an initial steady-state boundary formed by a 15-mA current (cross-hatched boundary, t_D = 0). Unlabeled numbers are times as in Figure 3. Ordinate gives actual height on photographic plate (phase plate angle 82°). Solid lines show parts of boundaries actually in photographs. Dotted line extensions are intended to bring out peak positions more clearly.

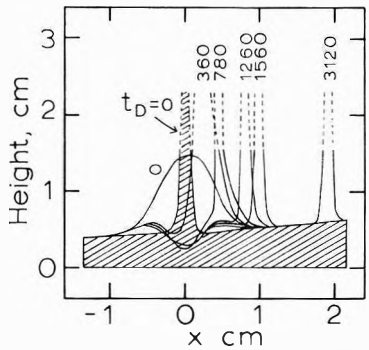

Figure 5. Outlines of schlieren photographs for the KCl–LiCl system in a sucrose density gradient at 1.00°. An 8-mA current was applied after free diffusion for 4056 sec from an initial steady-state boundary formed by a 15-mA current (cross-hatched boundary, $t_D = 0$). Axis labeling, peak extensions, and numbering are as in Figure 4. Phase plate angle 55°.

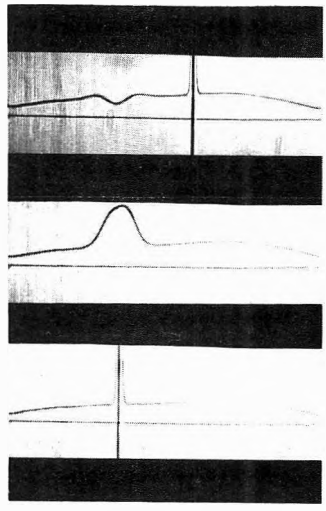

Figure 6. Schlieren photographs of the KCl–LiCl system in a sucrose density gradient at 1.00°. Bottom, middle, and top photographs correspond to outlines marked t_D = 0, 0, and 3120 in Figure 5.

the acrylamide gel. Figure 6 reproduces three of the actual photographs used to make the outlines of Figure 5.

It can be seen that the experimental gradients develop in a manner closely resembling that predicted by the transport equations. The asymmetry of the experimental schlieren patterns produced by free diffusion (peaks marked 0 in Figures 4 and 5) is matched by the corresponding curve of Figure 3. The specific shape of this boundary varies with the medium used. The predicted shape is intermediate between those observed in the acrylamide gel and sucrose media in which there is, respectively, an accentuation and smoothing out of a slight concavity at the top of the peak. The subsequent experimental patterns, showing the gradual restoration of the steady-state moving boundary, and the formation of a wave-like stationary boundary, for which dn/dx becomes negative in the middle, correspond closely to the theoretical patterns. This correspondence is significant because there is no attempt to take account of the effect of the gel or sucrose density gradient in the theoretical treatment. It provides some support, along with other studies of different but related time-dependent systems,[15] for the cautious use of the relatively simple relations of the Nernst–Planck type in interpreting, for example, sodium and potassium ion movements in cellular systems.[16]

An examination of experimental results in the literature will help to establish the magnitude of the errors in the concentrations calculated using such equations. Fujita and Gosting[17] have obtained a rigorous solution of the differential equations for one-dimensional free diffusion for ternary systems of the type FA–SA–H_2O in which the solute flows interact. Their only assumptions are that the volume change on mixing and the concentration dependence of the diffusion coefficients are negligibly small. Their solution yields the solute concentrations, $C(x,t)$, in terms of the two main and the two cross-term diffusion coefficients in the phenomenological flow equations. Furthermore, they have developed a general procedure, based on their solution, for computing the four required coefficients from the experimental data for a diffusion experiment. Gosting[18] and O'Donnell and Gosting[13] have also described a procedure for calculating these diffusion coefficients from ionic mobilities which they obtain from conductance and transference number data *via* the Nernst–Einstein relation. Concentrations may then be calculated using the rigorous solution of Fujita and Gosting. An estimate of the error in this method, in which specific ion effects are neglected and activity coefficients are assumed constant, may then be obtained by comparing concentrations calculated using it with those calculated using Fujita and Gosting's rigorous procedure for a system studied experimentally, such as KCl–LiCl–H_2O. This comparison will give a good indication of the error involved in using our eq 8 with $I = 0$ for calculating concentrations during free diffusion, since the assumptions made in the derivation of Gosting's equations[18] are the same as those we have made. (His eq 167, which gives an expression for the flow, J_j, is readily convertible to the corresponding expression for $\partial C_j/\partial t$. This expression becomes identical with eq 8 with $I = 0$ when written in terms of the mobilities and concentrations of F, S, and A.)

With these considerations in mind, we first calculated concentration profiles as a function of x by substituting diffusion coefficients computed by Dunlop and Gosting[19] from their experimental results for LiCl–KCl–H_2O into the concentration relationships derived by Fujita and Gosting.[17] The calculations were for t_D = 3600 sec for an experiment[19] performed at 25°, in which the top solution was 0.1000 *M* KCl + 0.2678 *M* LiCl and the bottom solution was 0.3000 *M* KCl + 0.2624 *M* LiCl. We then compared the concentrations so obtained with ones calculated for the same system using (1) a set of four D's obtained from the limiting ion conductances, λ_0, as described by O'Donnell and Gosting,[13] and (2) a second set of four D's calculated in the same way from conductance and transference number data[20,21] at the experimental average ionic strength of 0.45. This second calculation uses more realistic values for mobilities than the first but is subject to the criticism that the Nernst–Einstein equation holds strictly only at infinite dilution. We obtained the following results. For the calculation based on limiting mobility values, we found that the molar concentrations at 20 equal intervals across the diffusing boundary differed from those obtained by the exact procedure by values ranging from 0 to about −1.3%, and from 0 to about −0.2% of the average concentrations of KCl and LiCl, respectively. The corresponding differences for the calculation based on data at the average ionic strength were about 1.8 and 0.2%. As noted above the Fujita–Gosting theory assumes the constancy of the diffusion coefficients. Our calculations indicate that this is a good assumption

for the experiments discussed here. In the first place, our results show that the calculated concentrations are quite insensitive to the values chosen for the diffusion coefficients. The values for the latter which we determined for ionic strength 0.45 are about 20% lower than those for infinite dilution. The same is true for the mobility values from which they were obtained. Secondly, the concentration ranges in the actual experiments are much less than this, and examination of available tracer and binary diffusion data[22] reveals a correspondingly smaller variation in the diffusion coefficients. For Na^+ in KCl and in LiCl at 25°, a change from 0.06 to 0.1 M in supporting electrolyte concentration (the concentration range in our experiments) is associated with a drop in D_{Na^+} of about 0.2% in KCl and 0.9% in LiCl. For LiCl–H_2O and for KCl–H_2O the binary diffusion coefficients decrease by 0.6% over this range. Practically the same percentage drops are observed over the range for which Dunlop and Gosting obtained data.

Apart from approximations inherent in the equations, use of the finite difference method involves error inherent in the approximation of derivatives by finite differences as well as truncation errors. The identity of our equations with those derivable from Gosting's equations, mentioned earlier, makes possible a check on the error propagation. Using the mobility values for F, S, and A given above, we have calculated concentration profiles by Gosting's procedure for the 0.1 M FA–0.067 M SA system for a free diffusion period of 5400 sec. The concentrations of FA and SA so obtained differ by 0 to 1% from those obtained by our finite difference calculations.

The above error discussion deals only with the free diffusion case. If an external field is present, the concentration dependence of the mobilities is greater (2–3% on the basis of the change in equivalent conductance in the 0.06–0.1 M range[23]). It might then be expected that there would be a larger error in the calculated concentration values.

A final assumption is made in converting concentration profiles to refractive index gradient plots, *viz.*, that concentrations and refractive index increments are linearly related. This has been shown to be valid to within 1% for systems of the type under discussion in the concentration range with which we are concerned.[12]

By neglecting the terms in eq 8 which arise from the diffusion field,[14] we obtain the following system of equations

$$\frac{\partial C_F}{\partial t} = -\frac{RTu_F}{F}\frac{\partial}{\partial x}\left[\frac{(10^3 I C_F/RT)}{(u_F + u_A)C_F + (u_S + u_A)C_S}\right] \quad (11a)$$

$$\frac{\partial C_S}{\partial t} = -\frac{RTu_S}{F}\frac{\partial}{\partial x}\left[\frac{(10^3 I C_S/RT)}{(u_F + u_A)C_F + (u_S + u_A)C_S}\right] \quad (11b)$$

From eq 11 and the corresponding equation for C_A we can easily prove that for $t > t_D$, the Kohlrausch regulating function is a function of x and t_D only, *viz.*, $\omega(x,t) = \omega(x,t_D)$. Solving this equation for C_S and substituting in eq 11a, we obtain a first-order quasi-linear differential equation for C which can be solved exactly for t not too much larger than t_D (up to about t_D + 1200 sec) by the method of characteristics,[24] in the form $x = f(C_F,t)$. The first one or two profiles in Figure 3 are thus fairly well reproduced. The time restriction is necessary because at a sufficiently large time $\partial f/\partial C_F$ becomes zero, and it is no longer possible to solve $x = f(C_F,t)$ explicitly for C_F as a single-valued function of x and t (even in theory) *via* the implicit function theorem.[25] When the diffusion terms are dropped, then, C_F becomes a multiple-valued function of x and t. The electrical field corresponding to a given value of C_F turns out to be greater than that corresponding to a larger value of C_F, and this means, mathematically, that curves of constant concentration will cross, giving rise to more than one value of C_F at a point of intersection in the x,t plane. Physically, the above corresponds to a system in which there is no diffusion. In real systems, of course, diffusion does occur, the diffusion field becoming greater as the boundary sharpens until it is large enough to balance the external electric filed, as evidenced by attainment of a steady state. This is predicted by eq 8 for the FA–SA system (Figure 3).

Acknowledgment. We are indebted to Professor Lawrence E. Payne, who, in his capacity as Chairman of the Center of Applied Mathematics, Cornell University, provided time for calculations on the Cornell computer. We also wish to express our appreciation for use of the University of Minnesota's Computer Centers at Duluth and Minneapolis.

References and Notes

(1) This investigation was supported by Public Health Service Research Grant No. GM-10841 from the Division of General Medical Sciences, National Institutes of Health, and by Grants No. G-21720, GE-1043, and GE-4091 from the National Science Foundation.
(2) National Science Foundation Undergraduate Research Participant, 1962–1964.
(3) J. C. Nichol, *J. Phys. Chem.*, **66**, 830 (1962).
(4) V. P. Dole, *J. Amer. Chem. Soc.*, **67**, 1119 (1945).
(5) L. Ornstein, *N. Y. Acad. Sci.*, **121**, 321 (1964).
(6) F. Kohlrausch, *Ann. Phys.*, **62**, 209 (1897).
(7) D. S. Kahn and A. Polson, *J. Phys. Colloid Chem.*, **51**, 816 (1947).
(8) L. G. Longsworth, *J. Amer. Chem. Soc.*, **65**, 1755 (1943).
(9) W. Nernst, *Z. Phys. Chem.*, **4**, 129 (1889).
(10) M. Planck, *Ann. Phys. Chem., N. F.*, **40**, 561 (1890).
(11) J. Newman, *Advan. Electrochem. Electrochem. Eng.*, **5**, 87 (1967).
(12) L. G. Longsworth, *J. Amer. Chem. Soc.*, **66**, 449 (1944).
(13) I. J. O'Donnell and L. J. Gosting in "The Structure of Electrolyte Solutions," W. J. Hamer, Ed., Wiley, New York, N. Y., 1959, Chapter 11.
(14) H. Weber, "Die partiellen Differential-Gleichungen der mathematischen Physik," 5th ed, Braunschweig, 1910. Chapter 24.
(15) S. B. Malvadkar and M. D. Kostin, *J. Chem. Phys.*, **57**, 3263 (1972), and references cited therein.
(16) C. C. Ashley in "Membranes and Ion Transport," Vol. 2, E. E. Bittar, Ed., Wiley-Interscience, New York, N. Y., 1970, pp 2–10.
(17) H. Fujita and L. J. Gosting, *J. Amer. Chem. Soc.*, **78**, 1106 (1956).
(18) L. J. Gosting, *Advan. Protein Chem.*, **11**, 536 (1956).
(19) P. J. Dunlop and L. J. Gosting, *J. Amer. Chem. Soc.*, **77**, 5238 (1955).
(20) R. A. Robinson and R. H. Stokes, "Electrolyte Solutions," Butterworths Scientific Publications, London, 1965, Appendices 6.1 and 6.3.
(21) H. S. Harned and B. B. Owen, "The Physical Chemistry of Electrolytic Solutions," Reinhold, New York, N. Y., 1958, p 69.
(22) Reference 20, p 317 and appendices 11.1 and 11.2.
(23) Reference 21, appendix A, Table 6-2-2A.
(24) R. Courant and D. Hilbert, "Methods of Mathematical Physics," Vol. II, Interscience, New York, N. Y., 1962, Chapter 2.
(25) T. M. Apostol, "Mathematical Analysis," Addison-Wesley, Reading, Mass., 1957, p 147.

Effective Fixed Charge Density Governing Membrane Phenomena. VI. Activity Coefficients and Mobilities of Small Ions in Aqueous Solutions of Poly(styrenesulfonic acid)

Tetsuo Ueda and Yonosuke Kobatake*

Faculty of Pharmaceutical Sciences, Hokkaido University, Sapporo, Japan, 060 *(Received April 30, 1973)*

The mobilities of counter- and coions in polyelectrolyte solutions were determined by use of measurements of radioisotope fluxes in a diaphragm cell over a wide range of polyelectrolyte and of added salt concentrations. The mobility of the coions was almost identical with that in the free solution, while that of the counterions decreased greatly with decrease of the external salt concentration. The concentration dependences of mobilities of small ions in polyelectrolyte solution were the same as those of the activity coefficients. Thus the "additivity rule" found emperically for activity coefficients of counterions in the study of polyelectrolyte solutions was applicable for mobility in the same solutions. The additivity rule was applicable to both activity and mobility of small ions even in charged membranes. These findings permit a quantitative description of the membrane phenomena by using a parameter concerned with the degree of ion binding in the membrane, which may be determined easily by evaluating the activity coefficients of counterions in polyelectrolyte solutions.

Introduction

Knowledge of nonideal behavior of small ions in charged membranes is a prerequisite to the quantitative description of the transport processes observed in the membrane.[1-4] The nonideality of small ions in the membrane stems mainly from the strong ionic interaction between movable ions and the charges fixed on the membrane skeletons, and the situation is essentially the same as that in a polyelectrolyte solution. This general understanding of the problem prompted us to represent the nonideal behaviors of small ions in the membrane, more specifically, activity coefficient, γ_i, and mobility, u_i(i = +,−), by the following equations

$$\gamma_+ = \gamma_\pm^0 \frac{C_- + \phi X}{C_- + X} \qquad \gamma_- = \gamma_\pm^0 \tag{1}$$

$$u_+ = u_+^0 \frac{C_- + \phi' X}{C_- + X} \qquad u_- = u_-^0 \tag{2}$$

In eq 1 $\gamma_\pm^0$, C_-, X, and ϕ represent the mean activity coefficient of the electrolyte component in the bulk solution, the concentration of coions in the membrane, the stoichiometric fixed charge density, and a numerical positive constant smaller than unity, respectively. The system considered here contains a 1:1 type electrolyte. Equation 1 has the same functional form as the "additivity rule" found empirically in the field of polyelectrolyte solution studies.[5,6] ϕX is generally referred to as the thermodynamically effective charge density of the membrane or of the polyelectrolyte component, and ϕ represents the fraction of free counterions which is not bound in the vicinity of the polyions.[7] Equation 2 has been proposed to express the concentration dependences of mobilities of small ions in the membrane. u_i^0 represents the mobility of ion species i (i = +,−) in the bulk solution, and $\phi' X$ is the effective charge density of the membrane governing mobilities. In parts I and IV of this series[3,4] we reported the experimental results of γ_i and u_i observed for collodion-based poly(styrenesulfonic acid) membranes, and showed extensively the applicability of eq 1 and 2 to the quantitative representation of the membrane phenomena. Of special interest and importance is the experimental finding of the identity of the concentration dependences of mobility and activity coefficient of small ions in the membrane phase, that is ϕ and ϕ' appearing in eq 1 and 2 are identical with each other in the whole range of salt concentration studied for a given membrane. This fact has not been justified amply by experiments in polyelectrolyte solution, where little is known about mobilities of small ions. This mainly stems from experimental difficulty of mobility measurements of movable ions in the polyelectrolyte solution with added salt, in which the contribution of polyions on the specific conductivity of the solution under an electric field is hard to evaluate accurately.[7,8]

This paper intends to study the mobility and activity coefficient of small ions, and to examine whether eq 1 and 2 with $\phi = \phi'$ are valid in polyelectrolyte solution. Discussion is made in connection with the charged membrane and polyelectrolyte solution by using an identical polyion component, *i.e.* poly(styrenesulfonic acid) (PSSA) with a given degree of sulfonation.

Experimental Section

Materials. Poly(styrenesulfonic acid) was prepared from a fractionated polystyrene (degree of polymerization was 1700 ± 100) according to the method proposed by Carroll and Eisenberg.[9] Complete removal of excess small ions was performed by passing the solution of PSSA through column of both cation (H form) and anion (OH form) exchangers after extensive dialysis of reaction mixtures against nitric acid under complete darkness, and then against distilled water. PSSA was converted into the sodium form, PSS-Na, by passing through a column of ion-exchange resin (Amberlite IR-120). The degree of sulfonation was determined by titration of PSSA against NaOH, and was 0.89.

Sodium chloride of analytical grade was used as delivered. Radioactive isotopes used as tracers were sodium-22

and chlorine-36 in NaCl aqueous solution, and they were purchased from the Radiochemical Center.

The water used as solvent was obtained by passing distilled water through both cation and anion exchangers.

Determination of Activity Coefficient in Polyelectrolyte Solutions. Activity coefficients of small ions in polyelectrolyte solutions were determined by measuring the electromotive force (emf) of the following cells:

(a) determination of the mean activity coefficient, $(\gamma_+\gamma_-)^{1/2}$

Na-reversible glass electrode	PSS-Na (+ NaCl) solution	Ag-AgCl electrode

The emf of the above cell is given by

$$E = E_0 + \frac{RT}{F} \ln (\gamma_+\gamma_- C_+C_-)$$

(b) determination of counterion activity coefficient, γ_+

Na-reversible glass electrode	PSS-Na (+ NaCl) solution	salt bridge (agar, sat KCl)	calomel electrode

The emf of the cell is given by

$$E = E_0' + \frac{RT}{F} \ln (\gamma_+C_+)$$

provided that the liquid junction potential is neglected.

(c) determination of coion activity coefficient, γ_-

calomel electrode salt bridge (agar, sat KCl)	PSS-Na + NaCl solution	Ag-AgCl electrode

the emf of which is given by the following equation under the same assumption as in b

$$E = E_0'' + \frac{RT}{F} \ln (\gamma_-C_-)$$

Here, E_0's appearing in the above three equations are assumed to be constant and independent of concentrations both of added salt and of polyion. Note that single ion activity is an undefinable quantity in a thermodynamic sense.[10] Therefore, we use γ_i's measured by methods b and c as conventions as usual.[11] The glass electrode used was a Na-reversible electrode purchased from Toshiba-Beckmann. Silver–silver chloride electrode was prepared electrolytically by the method employed by Ives and Janz.[12] The emf of each cell was calibrated with simple NaCl solution before use. The potentiometer used for measuring the emf was a Radiometer Type PHM-4d.

Determination of Mobility u_i (i = +,−) in Polyelectrolyte Solutions. The mobility of small ions can be determined by measuring the isotope flux in a diaphragm cell.[8,13] A porous diaphragm (glass filter, Mesh No. 2, the mean pore size of which is 45 ± 5 μm) separates identical polyelectrolyte solutions with or without added salt, and two stirring rods are used to agitate the bulk solution vigorously. The rate of stirring was 150–200 rpm (*cf.* ref 8,13). No difference was observed when we used a glass filter of Mesh No. 3. Since the solution phase in the diaphragm is not agitated, the system under consideration is essentially the same as a membrane system discussed in part IV of this series.[4] Thus we describe the method and experimental procedures in minimum detail in this article. Radioisotope was introduced initially in the lower compartment. Isotope flux, J^*, directed from lower to upper compartment, is given by the following equation[4,14]

$$J^* = \frac{RT}{F} u_i \frac{\Delta C^*}{L} \tag{3}$$

where ΔC^* is the difference of tracer concentrations in the two compartments, L the effective thickness of the diaphragm, and R, T, and F have their usual thermodynamic meanings. Equation 3 can be rewritten as follows in terms of the measurable quantities

$$\frac{RT}{F} u_i = \frac{V}{K} \frac{(d/dt)(CPM)_1}{(CPM)_2} \tag{4}$$

where V is the volume of upper compartment, $(CPM)_k$ (k = 1,2) the radioactivity of lower and upper compartment, respectively, and K the ratio of the effective area and the thickness of the diaphragm. The value of K was determined by measuring the isotope flux in simple salt solution with no polyion. Equation 4 reads that measurements of the rate of increase of radioactivity in the upper compartment $(d/dt)(CPM)_1$ and the level of radioactivity in the lower compartment $(CPM)_2$ enable us to evaluate the mobility of species i in the polyelectrolyte solution.

The polyelectrolyte solution was degassed thoroughly *in vacuo* before filling the cell. Radioactivity was counted by a scintillation spectrometer (Beckmann, Type CMP-100).

All experiments were carried out in an air chamber thermostated at 25°.

Results and Discussion

System with No Added Salt. Figure 1 shows data of the activity coefficient, γ_{Na}, and the reduced mobility of counterions, u_{Na}/u_{Na}^0, in various concentrations of polyion, X (equiv/l. ≡ N), without added salt. The concentration of polyion examined ranged between 10^{-4} and 1.0 N. Open and closed circles in the figure indicate the data of γ_{Na^+} (○) and u_{Na}/u_{Na}^0 (●), respectively. Here the values of u_{Na}^0 in the bulk solution were taken from references[15] or an appropriate table.[16] For comparison, u_{Na}/u_{Na}^0 data reported by Prini and Lagos[17] in PSS–Na solution (90% sulfonated PSS) obtained by the tracer diffusion experiments in a capillary cell are also plotted in the figure (○). As seen in the figure, dependences of γ_{Na} and u_{Na}/u_{Na}^0 on the polyion concentration agreed quantitatively with each other within experimental accuracy in the whole range of concentrations studied. The degree of ion binding represented by $(1 - \gamma_+/\gamma_+^0)$ or $(1 - u_+/u_+^0)$ depends on the concentration of polyions. The activity coefficient of counterions in salt-free PSS–Na solution has been determined and reported by Nagasawa and Kagawa[18] in the range of polyion concentration, X, between 10^{-3} and 4×10^{-2} N. Their data agreed with ours in this limited concentration range.

Contrary to our present data and those of Prini and Lagos[17] for u_{Na}, Auer and Alexandrowicz summarized[19] various data appearing in the literature, which were evaluated from the electrical transference experiments combined with those of electrophoresis of polyions, and suggested that the degree of ion binding evaluated from γ_+ is about twice as large as that obtained from u_+. For the sake of comparison, the dotted line given in Figure 1 shows the value of $2\gamma_+$. It is evident that the experimen-

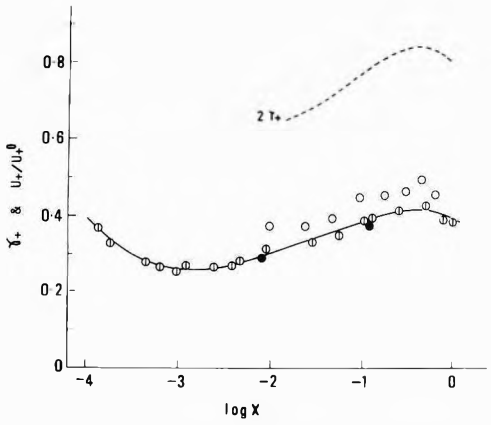

Figure 1. γ_{Na} and u_{Na}/u_{Na}^0 against log X relation in various concentrations of PSS-Na solution with no added salt. Polyion concentration, X, is expressed in equiv/l. (N): Φ; γ_{Na}; O; u_{Na}/u_{Na}^0; ●; u_{Na}/u_{Na}^0 after Prini and Lagos.[17]

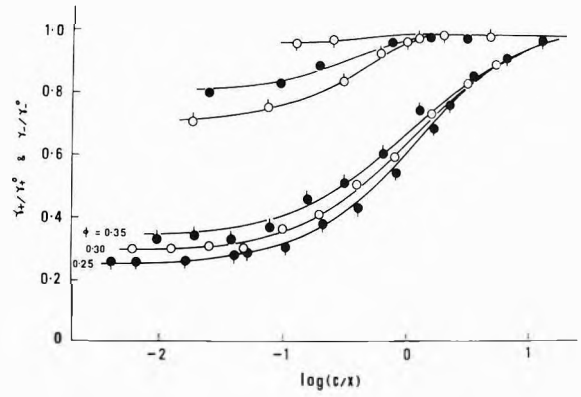

Figure 2. γ_+/γ_+^0 and γ_-/γ_-^0 against log C/X relation in various concentrations of PSS-Na with added salt: Q, γ_-/γ_-^0 with $X = 10^{-3}$ N; ●, γ_-/γ_-^0 with $X = 10^{-2}$ N; Ò, γ_-/γ_-^0 with $X = 5 \times 10^{-2}$ N, ●, γ_+/γ_+^0 with $X = 10^{-3}$ N; O, γ_+/γ_+^0 with $X = 10^{-2}$ N; ●, γ_+/γ_+^0 with $X = 5 \times 10^{-2}$ N.

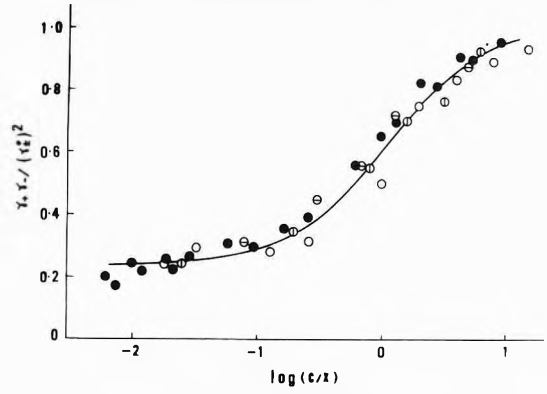

Figure 3. $\gamma_+\gamma_-/(\gamma_+^0)^2$ against log C/X relation in charged membrane and in polyelectrolyte solutions: ●, data for a collodion-based PSSA membrane with $X = 4.4 \times 10^{-2}$ N (see ref 3); O, Φ, and Θ, show the data of $\gamma_+\gamma_-/(\gamma_\pm^0)^2$ in PSS-Na with NaCl solutions of $X = 10^{-3}$, 10^{-2}, and 5×10^{-2} N, respectively.

tal values of u_+ obtained here and those of Prini and Lagos are much closer to γ_+ rather than $2\gamma_+$. This difference of the data of u_+ may be attributed to the difference in measuring condition, *i.e.*, the difference between tracer and electric transference methods. The latter method involves the translational motion of polyions caused by the external field applied. Whereas, in the tracer technique adopted here the situation is very close to the equilibrium condition so far as the polyion is concerned. As shown in our previous papers in this series,[3,4] no difference was observed for the degree of ion binding in charged membranes evaluated from data of mobilities and activities of small ions in the membrane. Since the polyelectrolyte components in the membrane are embedded in the membrane skeleton, the polymer in the membrane does not move translationally even in the presence of an external electric field applied across the membrane. This situation may be identical with that of tracer experiments adopted here. Therefore, it is feasible that the concentration dependence of u_i becomes identical with that of γ_i when the polyion component does not move translationally as is encountered in the present experiment and in the membrane systems, provided that the mass movement in the membrane is properly taken into account.[3,4,20]

Activity Coefficients of Small Ions in Polyelectrolyte Solutions with Added Salt. Figure 2 shows the activity coefficients of counter- and coions in polyelectrolyte solutions as functions of relative concentration of added salt, C/X. Activity coefficients of coions, γ_-/γ_-^0, show slight but systematic deviation from unity with increase of polyion concentration, X. Similarly, the activity coefficient of counterions, γ_+/γ_+^0, increases with increase of X when the concentration of added salt C is lower than X. This similar tendency was found also in the membrane system as shown in the previous papers.[4,20] Notwithstanding the complicated behavior of γ_+ as functions of X, the dependence of γ_+/γ_+^0 on the concentration of added salt at a fixed X seems to be rather simple, and follows eq 1 with a constant ϕ. Solid lines in Figure 2 indicate the theoretical curve of eq 1 by putting $\phi = 0.35$, 0.30, and 0.25 as indicated in the figure. Calculated values are in good accord with those observed, which implies that once the value of ϕ is determined for a given combination of polyelectrolyte and added salt component, one may predict the activity coefficient of small ions γ_+ at an arbitrary salt concentration. It must be noted that the determination of ϕ from the value of γ_+ obtained potentiometrically is not accurate in a high concentration range of the added salt. In the case of the membrane system, the value of ϕ can be determined accurately in the concentrated region as explored in our previous papers.[1-4,20,21]

Figure 3 shows the concentration dependence of the mean activity coefficient, $\gamma_+\gamma_-/(\gamma_\pm^0)^2$, of small ions both in polyelectrolyte solutions and in charged membranes. The degree of sulfonation of PSSA used in the membrane was 0.85. The data were taken for three membranes having different X.[4] Closed and open circles in the figure indicate the values of the mean activity coefficients in the membrane and in the polyelectrolyte solution, respectively. Contrary to rather complicated behavior of single ion activity coefficient given in Figures 1 and 2, the mean activity coefficient followed a single curve when plotted against C/X. Comparison of $\gamma_+\gamma_-/(\gamma_\pm^0)^2$ obtained in the membrane and polyelectrolyte solution shows that the concentration dependence of $\gamma_+\gamma_-/(\gamma_\pm^0)^2$ coincides with each other in the whole range of C/X examined. This fact suggests that the study of transport phenomena in charged membrane is essentially an extension of that of polyelectrolyte solution. In other words, the information obtained from the polyelectrolyte solution can be used successfully for the quantitative analysis of the membrane

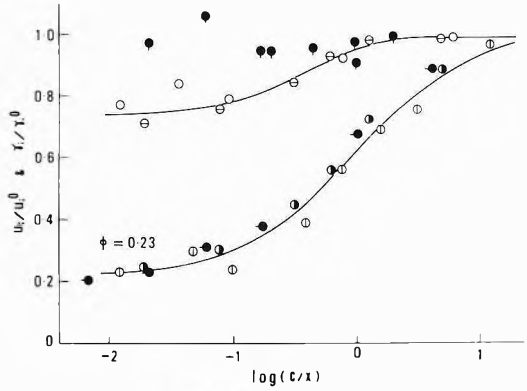

Figure 4. u_+/u_+^0, u_-/u_-^0, γ_-/γ_-^0, and $\gamma_+\gamma_-/(\gamma_\pm^0)^2$ as functions of log C/X in membranes and in polyelectrolyte solutions: ●, u_-/u_-^0 in membranes with $X = 0.224$ and 0.116 N;[4] ⊖, γ_-/γ_-^0 in solution with $X = 4 \times 10^{-2}$ N; ○, u_-/u_-^0 in solution with $X = 4 \times 10^{-2}$ N; ◒, u_+/u_+^0 in membrane with $X = 4.4 \times 10^{-4}$ N; ◑, $\gamma_+\gamma_-/(\gamma_\pm^0)^2$ in solution with $X = 4 \times 10^{-2}$ N; ⊕, u_+/u_+^0 in solution with $X = 4 \times 10^{-2}$ N.

phenomena. This will be confirmed further in the following section.

Mobilities of Small Ions in Polyelectrolyte Solutions. Figure 4 shows the concentration dependences of counter- and coion mobilities, u_+/u_+^0 and u_-/u_-^0, in PSS–Na solution where the concentration of PSS–Na was fixed at about 0.04 N. In Figure 4, ⊕ indicate mobility of counterions, and open circles describe that of coions, while the data of mean and coion activity coefficients are shown by symbols ● and ⊖, respectively. As in the case of γ_+ discussed above, mobility of the counterion was depressed greatly in the presence of polyion, while that of coion was little affected. Comparison of the data of mobility and activity coefficient reveals that the concentration dependences agreed with each other in polyelectrolyte solutions in the whole concentration range of added salt. Several theoretical attempts have been proposed on this point,[22-25] but no plausible explanation seems to be established. In Figure 4, the data of u_+/u_+^0 and u_-/u_-^0 obtained in the membrane study are also shown by symbols ◒ and ●, respectively. Again, it is noted that the concentration dependences of u_+ and u_- in polyelectrolyte solutions agree with those in charged membranes. The membranes used here were the same as those referred to in Figure 3.

Conclusion

All the results described in the present article and those in our previous papers indicate that the dependences of γ and u on salt concentration agree with each other both in polyelectrolyte solutions and in charged membrane, and that the nonideality of small ions can be represented by eq 1 and 2. These findings provide us with a simple way for quantitative representation of various membrane phenomena in terms of γ and u as illustrated in the preceding paper.[21] The value of ϕ may depend upon the nature of the charged group and its distribution or density on the polymer skeletons constituting the membrane. Once the nature and the density of charges fixed on the membrane matrix are known (*e.g.*, COO^-, SO_3^-, radicals, etc), one may find the value of ϕ from the data of γ_+ in polyelectrolyte solution, and can predict various membrane phenomena, *e.g.*, the Donnan equilibrium, membrane potential, electric resistance, ion fluxes, etc., in a quantitative manner by using the value of ϕ obtained from the study of polyelectrolyte solutions.

Acknowledgments. The authors are deeply indebted to Mr. M. Muratsugu and Mr. S. Suzuki for performing the experiments reported here. Thanks are also due to Dr. T. Norisue in Osaka University for giving us the diaphragm cells used in the present study.

References and Notes

(1) Y. Kobatake and N. Kamo, *Progr. Polym. Sci. Jap.*, **5**, 257 (1973).
(2) Y. Toyoshima, Y. Kobatake, and H. Fujita, *Trans. Faraday Soc.*, **63**, 2803, 2814, 2828 (1967).
(3) N. Kamo, Y. Toyoshima, H. Nozaki, and Y. Kobatake, *Kolloid-Z. Z. Polym.*, **284**, 914 (1971); 249, 1061, 1069 (1971).
(4) T. Ueda, N. Kamo, N. Ishida, and Y. Kobatake, *J. Phys. Chem.*, **76**, 2447 (1972).
(5) A. Katchalsky, Z. Alexandrowicz, and O. Kedem, "Chemical Physics of Ionic Solutions," Wiley, New York, N. Y., 1966, p 296.
(6) S. A. Rice and M. Nagasawa, "Polyelectrolyte Solutions," Academic Press, New York, N. Y., 1961, p 399.
(7) M. Nagasawa, I. Noda, T. Takahashi, and N. Shimamoto, *J. Phys. Chem.*, **76**, 2286 (1972).
(8) F. T. Wall, P. F. Grieger, J. R. Huizenga, and R. H. Doremus, *J. Phys. Chem.*, **20**, 1206 (1952); F. T. Wall and R. H. Doremus, *J. Amer. Chem. Soc.*, **76**, 1557 (1954); **79**, 1550, 1556 (1957).
(9) W. Carroll and H. Eisenberg, *J. Polym. Sci., Part A-2*, **4**, 599 (1966).
(10) E. A. Guggenheim, "Thermodynamics," North-Holland Publishing Co., Amsterdam, 1950.
(11) J. G. Kirkwood and I. Oppenheim, "Chemical Thermodynamics," McGraw-Hill, New York, N. Y., 1961.
(12) D. J. G. Ives and G. J. Janz, "Reference Electrodes," Academic Press, New York, N. Y., 1961.
(13) R. A. Robinson and R. H. Stokes "Electrolyte Solutions," Butterworths, London, 1959.
(14) N. Lakshminarayanaiah, "Transport Phenomena In Membranes," Academic Press, New York, N. Y., 1969.
(15) J. M. Nielsen, A. W. Adamson, and J. W. Cobble, *J. Amer. Chem. Soc.*, **74**, 446 (1952); J. W. Wang and S. Miller, *ibid.*, **74**, 1611 (1952).
(16) "Landolt-Börnstein Tabellen," Vol. II-7, 6th ed, Springer-Verlag, West Berlin, 1960.
(17) R. F. Prini and A. E. Lagos, *J. Polym. Sci., Part A*, **2**, 2917 (1964).
(18) M. Nagasawa and I. Kagawa, *J. Polym. Sci.*, **25**, 61 (1957).
(19) H. E. Auer and Z. Alexandrowicz, *Biopolymers*, **8**, 1 (1969).
(20) M. Yuasa, Y. Kobatake, and H. Fujita, *J. Phys. Chem.*, **72**, 2871 (1968).
(21) N. Kamo, M. Oikawa, and Y. Kobatake, *J. Phys. Chem.*, **77**, 92 (1973).
(22) G. S. Manning, *J. Chem. Phys.*, **51**, 924, 934 (1969).
(23) S. Lifson and J. L. Jackson, *J. Chem. Phys.*, **36**, 2410 (1962).
(24) J. L. Jackson and S. R. Corill, *J. Chem. Phys.*, **38**, 2410 (1963); **39**, 2418 (1963); **40**, 1460 (1964).
(25) E. Pefferkorn and R. Varoqui, *Eur. Polym. J.*, **6**, 663 (1970).

Investigation of Specific Acid Catalysis by Substituted Acetic Acids on the Proton Exchange of N,N'-Dimethylurea by Nuclear Magnetic Resonance

Jerry F. Whidby* and William R. Morgan

Philip Morris Research Center, Richmond, Virginia 23261 *(Received July 23, 1973)*

Publication costs assisted by the Philip Morris Research Center

Proton exchange rates of *N,N'*-dimethylurea catalyzed by hydronium and hydroxide ions have been found to be 2.5×10^6 and 1.0×10^6 M^{-1} sec^{-1}, respectively. The catalytic effect of added acetic acid, mono-, di-, and trichloroacetic acid, trifluoroacetic acid, and phosphoric acid has been attributed to the formation of a complex with the dimethylurea nitrogen protons. The catalytic rate constant k_b involving this complex is reported.

Introduction

The rates of exchange of protons in proteins have been postulated to reflect the structure and conformation of these molecules.[1,2] The proton exchange rate of model amides has been observed to be both acid and base catalyzed by H^+ and OH^- ions. Further observations have indicated that the acid-catalyzed exchange occurs through a mechanism involving protonation of the C=O groups with subsequent release of the N-H proton to the solvent.[3,4] Infrared studies on *N*-methylacetamide have shown that an additional catalytic effect exists when acetic acid is added to the exchanging system.[1]

This effect has been further separated into both an HA and A^- contribution but no explanation was offered as to the mechanism responsible for the catalytic increase. It is the purpose of this study to extend the available data on N-H exchange to urea systems and to further investigate the action of catalysts on these systems in order to obtain a better insight into the mechanism through which these effects occur.

Experimental Section

Nmr Data. All spectra in this study were obtained on a Varian A60-A analytical nmr spectrometer operating at 56.4 MHz and equipped with a variable-temperature probe. Except for data used in the evaluation of activation energies, all spectra were taken at 39° (ambient probe temperature). All temperatures are accurate to ±1° and were calibrated using either ethylene glycol or methyl alcohol. Spectra were recorded at a sweep rate of 0.2 Hz/sec and at a sweep width of 50 Hz. Instrument settings were made such that saturation did not occur.

Calculations. Values of τ were computed from individual spectra by fitting the observed spectra to the theoretical spectra predicted by Arnold.[5] Values of T_2 were obtained from the line widths of the CH_3 doublet under conditions of slow exchange and are limited by field inhomogeneity.

Corrections for T_2 were included in the computer program. The program was written in Fortran IV and run on a Xerox Sigma VIII computer.

pH. pH measurements were made with a Photovolt triple-purpose glass electrode and a saturated KCl silver|silver chloride reference electrode.

Buffer solutions, 0.05 *M* phthalate and 0.01 *M* borax, were prepared to give a pH of 4.035 and 9.068, respectively, at 40°. These solutions were then used to standardize the pH meter. All pH measurements were made in a water-jacketed vessel at 39.0 ± 0.1°. The pH of the urea solutions was varied by using concentrated sodium hydroxide or hydrochloric acid.

Solutions. A 1 *M* solution of *N,N'*-dimethylurea was prepared in distilled water.

Acetate solutions were prepared by neutralizing the appropriate acid with sodium hydroxide. Appropriate volumes of the above solutions were used to prepare the systems for analysis. By varying the amounts of Na acetate and urea solutions; the desired mole ratios of urea/acetate could be obtained. The pH of these solutions was then adjusted with HCl or NaOH.

N,N'-Dimethylurea. The urea was obtained commercially from Aldrich Chemical Co., determined to be pure by nmr, and used without purification.

Trichloroacetic Acid and Phosphoric Acid. Trichloroacetic acid and phosphoric acid were obtained from Fisher Scientific Co. and were used without purification.

Trifluoroacetic Acid. Trifluoroacetic acid was purchased from Eastman Chemical and was used without purification.

Acetic Acid. Acetic acid was obtained from Allied Chemical and was used without purification.

Dichloroacetic Acid and Monochloroacetic Acid. Dichloroacetic acid and monochloroacetic acid were obtained from Aldrich Chemical Co. and were used without purification.

General Acid–Base Catalysis

Several mechanisms of the general acid catalysis type may be proposed by which an N-H proton can be exchanged with a solvent proton. These are given in eq 1-3.

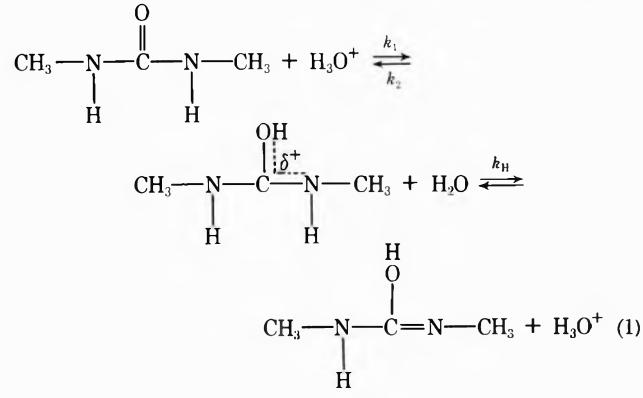

(1)

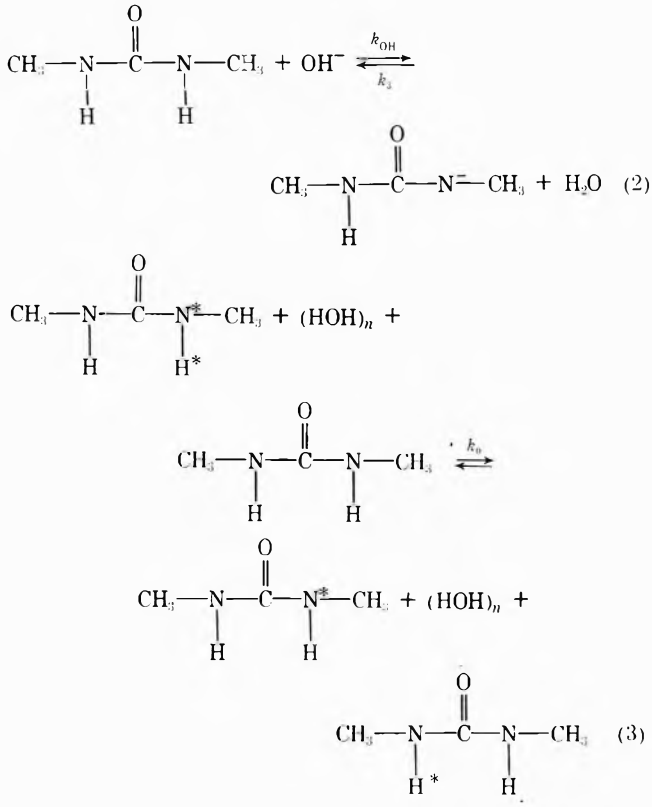

The mechanism depicted in eq 1 represents the acid-catalyzed exchange in which a hydronium ion protonates the oxygen atom causing the N–H proton to become more acidic. The NH proton is then abstracted by a solvent molecule (H_2O) effecting an observable exchange. The reprotonation of the N^- site is considered diffusion controlled and is not important in describing an effective nmr proton exchange.[1]

Equation 2 describes the direct abstraction of a proton by a base which in H_2O solution is the hydroxide ion. There also exists a self-catalyzed exchange through a water bridge as indicated in eq 3. For *N,N'*-dimethylurea, this contribution to the overall observed exchange rate is too small to be measured by high-resolution nmr line-broadening techniques.

In the presence of acetic acid, mono-, di-, and trichloroacetic acid, trifluoroacetic acid, and phosphoric acid, two additional mechanisms of exchange are introduced. These are shown in eq 4 and 5.

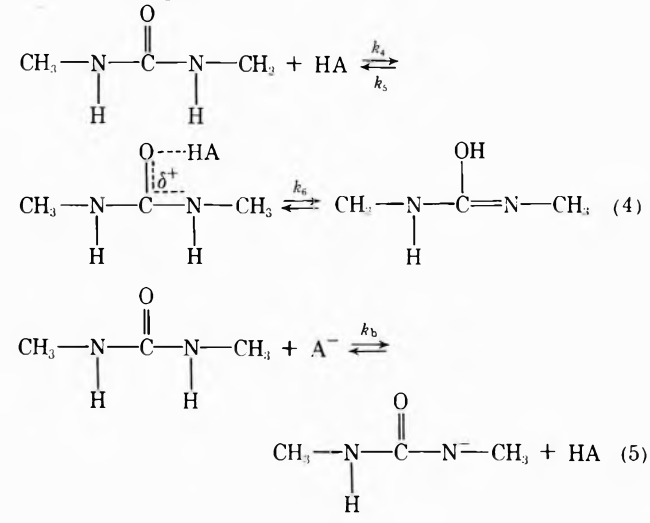

Equation 4 gives the contribution due to HA, the un-ionized acid in solution, and eq 5 the contribution from the conjugate base.

In the absence of added acetic acid, substituted acetic acids, or phosphoric acid, the net equations describing proton exchange in the acid- and base-catalyzed regions as obtained from mechanisms 1 and 2 are

$$1/\tau = k_1 k_H[H^+]/(k_2 + k_H) \quad \text{(acid catalyzed)} \quad (6)$$

and

$$1/\tau = k_{OH}[OH^-] \quad \text{(base catalyzed)} \quad (7)$$

In eq 6, k_2 may be assumed to be diffusion controlled[6] and the assignment $k_2 \gg k_H$ made, giving

$$1/\tau = k_1 k_H[H^+]/k_2 \quad (8)$$

The terms k_1, k_H, and k_2 may be combined to yield k_{ex}, producing the acid-catalyzed rate equation

$$1/\tau = k_{ex}[H^+] \quad (9)$$

The reverse reaction in the k_H step is not considered since a net observable nmr exchange has occurred with the completion of k_H.

Considering eq 4 and 5 for the effect of acetic acid, substituted acetic acids, or phosphoric acid one obtains

$$1/\tau = k_a[HA] + k_b[A^-] + k_{ex}[H^+] + k_{OH}[OH^-] \quad (10)$$

The effect of the addition of acetate ions is due to the second term of eq 10 since in all cases except acetic acid, the concentration of undissociated acid HA is negligible. For phosphoric acid the pH range of interest is 6–8 thus the important species are $H_2PO_4^-$ and HPO_4^{2-}. If this is taken into consideration, eq 10 in the acid-catalyzed region reduces to

$$1/\tau = k_b[A^-] + k_{ex}[H^+] \quad (11)$$

By plotting $1/\tau$ *vs.* $[A^-]$ at constant pH, one may obtain the value of k_b from the slope of the plot.

Results

Figure 1 shows the experimental data obtained for *N,N'*-dimethylurea in aqueous solution and in the presence of acetic acid and substituted acetic acids. Applying eq 9 and 7 to the acid- and base-catalyzed regions, respectively, for the aqueous solution one obtains a value of $k_{ex} = 2.5 \times 10^6\ M^{-1}\ sec^{-1}$ and $k_{OH} = 1.0 \times 10^6\ M^{-1}\ sec^{-1}$. These values agree quite well with other reported values for substituted ureas.[3,7] As indicated in Figure 1, the addition of acetic acid and substituted acetic acids to the urea solution produces an increase in k_{ex} by as much as 100-fold for acetic acid with no apparent effect on the value of k_{OH}. Table I gives the results of all the data obtained for the various exchange processes. This increase in k_{ex} with the addition of acetic acids or phosphoric acid indicates the presence of a specific acid-catalyzed exchange process. The addition of NaCl does not produce an increase in k_{ex}.

Figure 2 shows a plot of $1/\tau$ *vs.* the mole ratio of acetic acid and substituted acetic acids to dimethylurea at a pH of 6.0, and phosphoric acid at pH 7.0. The phosphoric acid catalyzed rate was too fast to be measured at a pH of 6.0. Considering the p*K*a of acetic acid and the substituted acetic acids and the pH of the solutions, one can assume the acetate ion, $[A^-]$, to predominate over the un-ionized acid [HA]. For phosphoric acid at pH 7, the primary

TABLE I: Kinetic Results for *N,N'*-Dimethylurea (DMU)

Compound (system)	k_{ex}, M^{-1} sec^{-1}	k_{OH}, M^{-1} sec^{-1}	ΔH_{ex}, kcal/mol	k_b, M^{-1} sec^{-1}
DMU	2.5×10^6	$(1.0 \pm 0.2) \times 10^6$	8.08 ± 0.12	NA
DMU + 1 *M* (HA)	1.48×10^8 [a]	$(1.1 \pm 0.3) \times 10^6$	3.33 ± 0.26	73.0
DMU + 1 *M* (MCA)	4.2×10^7 [a]	1.0×10^6	NA	15.0
DMU + 1 *M* (DCA)	2.09×10^7 [a]	1.0×10^6	NA	11.6
DMU + 1 *M* (TCA)	2.4×10^7 [a]	$(1.3 \pm 0.2) \times 10^6$	7.81 ± 0.11	6.5
DMU + 1 *M* (TFA)	2.5×10^7 [a]	$(0.8 \pm 0.2) \times 10^6$	7.76 ± 0.05	6.5
DMU + 1 *M* (NaCl)	1.1×10^6	$(1.6 \pm 0.2) \times 10^6$	NA	NA
DMU + H_3PO_4	NA	NA	NA	205 (pH 7.0)

[a] Value for the observed rate constant obtained from the intercepts in Figure 1.

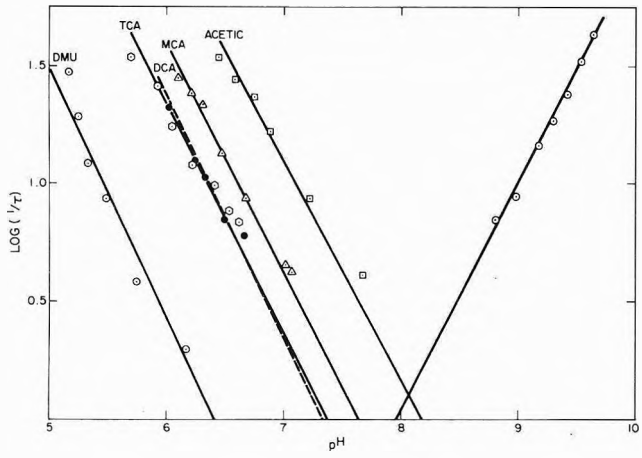

Figure 1. Log of the exchange rate $(1/\tau)$ of *N,N'*-dimethylurea *vs.* pH for various systems studied: O, 1 *M* dimethylurea (DMU); ⊙, 1 *M* DMU + 1 *M* trichloroacetic acid; ●, 1 *M* DMU + 1 *M* dichloroacetic acid; △, 1 *M* DMU + 1 *M* monochloroacetic acid; □, 1 *M* DMU + 1 *M* acetic acid.

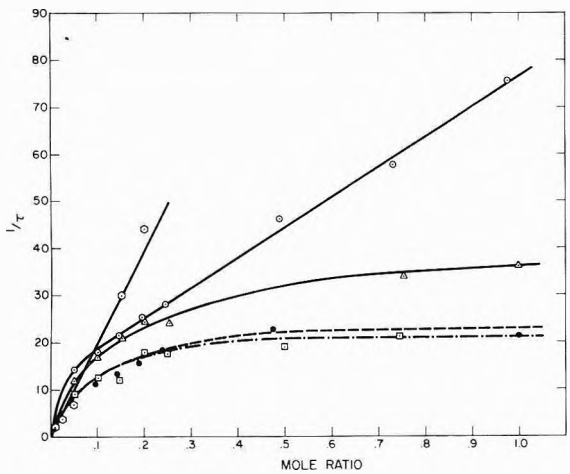

Figure 2. Plot of catalyzed rate $(1/\tau)$ *vs.* mole ratio of added acetate or phosphate: ⊙, phosphoric acid pH 7.0; O, acetic acid; △, monochloroacetic acid; ●, dichloroacetic acid; □, trichloroacetic acid.

species in solution are $H_2PO_4^-$ and HPO_4^{2-}. Using this along with the values of k_{ex} and k_{OH} obtained for aqueous dimethylurea and applying eq 11, one may calculate values of k_b for the added acetic acid or phosphoric acid species. These are given in Table I. The rapid increase in $1/\tau$ at low mole ratios may be attributed to the formation of a complex between the dimethylurea nitrogen proton and the acetate ion or the HPO_4^{2-} ion. These ions act as

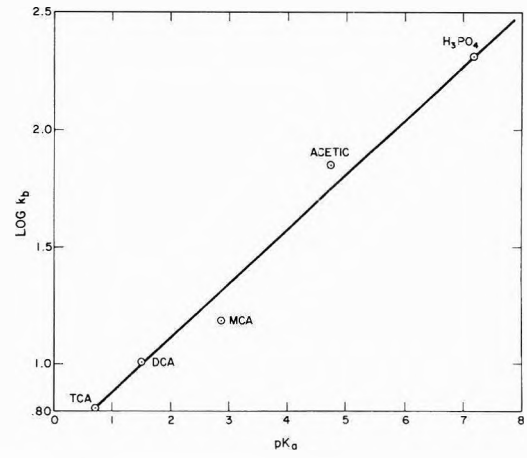

Figure 3. Brønsted plot of p*Ka* *vs.* log k_b.

TABLE II: Rate Constants for Various Methyl-Substituted Ureas

Compound	k_{ex}, M^{-1} sec^{-1}	k_{OH}, M^{-1} sec^{-1}
N,N'-Dimethylurea	2.5×10^6	1.0×10^6
Methylurea[a]	2.7×10^6	9.1×10^5
Benzylmethylurea[b]	2.4×10^6 (*N*-Me)	2.5×10^4 (*N*-Me)

[a] Reference 7. [b] Reference 3.

a stronger base than water to accept the more acidic nitrogen proton formed by the protonation of the carbonyl oxygen. Complexes of this type are well known, trifluoroacetic acid being used to precipitate proteins from blood for nitrogen analysis.[8]

Figure 3 shows a Brønsted plot for the various acids (at a mole ratio 1:1). The positive slope is a further indication of base catalysis by the $[A^-]$ or $[HPO_4^{2-}]$ ion and the linear relationship supports the general nature of the catalytic effect on dimethylurea proton exchange.

Conclusions

Several conclusions may be drawn from this study. First, comparing values of k_{ex} for several substituted methylureas, as given in Table II, one observes that k_{ex} remains constant for the three methyl-substituted ureas. A mechanism involving carbonyl protonation is expected to be insensitive to substituents since the decrease in basicity of the carbonyl oxygen is expected to be balanced by an increase in the acidity of the nitrogen proton in the O-protonated intermediate.[7,9] The variation in k_{OH} observed for the same series is an indication of the change in basicity for these compounds. This further substantiates

that O protonation predominates in the pH region studied.

Secondly, the nonlinear behavior at low concentrations of the acetic acids (as shown in Figure 2) is attributed to the formation of a weak complex between the acetate ion and the dimethylurea molecule of the type[8]

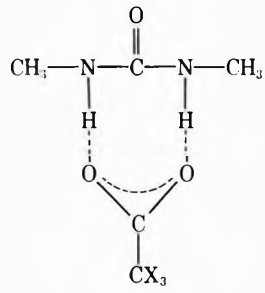

In the complex as shown, the acetate ion is in a position to remove a proton whenever the carbonyl oxygen is protonated. This has the effect of increasing the acidity of the nitrogen proton. At higher concentrations of acetate ions, the increased exchange rate is linear with added acetate ion and follows Brønsted behavior.

The catalytic behavior of the acids tested follows the order HPO_4^{2-} > acetic > monochloroacetic > dichloroacetic > trichloroacetic = trifluoroacetic > H_2O.

The presence of this complex in solution in the hydroxide ion catalyzed region is unimportant due to the much larger rate constant, k_{OH}, for hydroxide ion exchange.

References and Notes

(1) I. M. Klotz and B. H. Frank, *J. Amer. Chem. Soc.*, **87**, 2721 (1965).
(2) I. M. Klotz, *J. Colloid Interface Sci.*, **27** (4), 804 (1968).
(3) In a previous publication (L. C. Martinelli, C. D. Blanton, and J. F. Whidby, *J. Amer. Chem. Soc.*, **93**, 5111 (1970)), it was indicated that protonation by hydronium ion occurred on the N atom. The mechanism of hydronium ion protonation, whether on O or N, has been shown to be indistinguishable in dilute acid solution using high-resolution nmr techniques. Based on the results obtained in this work for the catalytic effect of acetic acid, it is now postulated that protonation prior to N–H exchange occurs predominantly *via* a mechanism involving a carbonyl protonated intermediate as in strongly acidic solutions.
(4) (a) W. I. Congdon and J. T. Edward, *J. Amer. Chem. Soc.*, **94**, 6096 (1972), and references therein especially ref 2; (b) W. I. Congdon and J. T. Edward, *ibid.*, **94**, 6099 (1972); (c) A. Azman, B. Lukman, and D. Hadzi, *J. Mol. Struct.*, **4**, 468 (1969).
(5) J. T. Arnold, *Phys. Rev.*, **102**, 136 (1956).
(6) M. Eigen, *Angew. Chem., Int. Ed. Engl.*, **3**, 1 (1964).
(7) R. S. Molday and R. G. Kallen, *J. Amer. Chem. Soc.*, **94**, 6739 (1972).
(8) H. Varley, "Practical Clinical Biochemistry," 3rd ed, William Heinemann Medical Books Ltd., London, 1963, p 591.
(9) A. Azman, B. Lukman, and D. Hadzi, *J. Mol. Struct.*, **4**, 469 (1969).

Stability and Solubility Constants for Silver Halides in Propionitrile–Sulfur Dioxide Mixtures

Mark Salomon* and Brian K. Stevenson

Power Sources Technical Area, U. S. Army Electronics Technology and Devices Laboratory, Fort Monmouth, New Jersey 07703

(Received June 18, 1973)

Publication costs assisted by the U.S. Army Electronics Technology and Devices Laboratory

Studies on the complex solubilities of AgCl, AgBr, and AgI are reported in propionitrile (PN) and in PN–SO_2 mixtures. Values of the complex ion formation constant K_{s2} and the stability constant β_2 were found to decrease rapidly upon addition of SO_2 to PN while the solubility product, K_{so}, was found to increase. The results are interpreted in terms of the medium effect and the theory of hard and soft acids and bases. The enhanced stability of the $Ag(SO_2)_2^+$ species is attributed to the formation of π bonds between low lying d orbitals on the sulfur atom and the 4d electrons of Ag^+.

Introduction

The behavior of solutes in a variety of solvents often shows such diverse behavior that it becomes difficult to explain them in quantitative terms. It is now generally accepted[1] that the dielectric constant and the Born charging model offer little, if anything, in the way of explanatory or predictive ability. The present paper again demonstrates the inapplicability of the Born model as studies are reported on the complex solubilities of silver halides in propionitrile (PN) and mixtures of PN with sulfur dioxide.

The most successful treatments of single ion solvation in nonaqueous solvents are usually concerned with the relative behavior of ions in some solvent, s, compared to a reference solvent such as water.[1-4] Treatments of this type have been referred to as the "medium effect"[1-4] or the "solvation theory."[5a] Because the solvation theory is based on at least one extrathermodynamic assumption, it can only explain experimental behavior. Predictive theories based on more discrete models of chemical bonding[5] are rarely applied to nonaqueous systems although there are instances where this approach, in combination with the solvation theory, can lead to a better under-

standing of the effect of solvent on chemical behavior. The present results on the stabilities of AgX_2^- complex ions (X = Cl, Br, I) in mixed PN–SO_2 solvents are interpreted in this manner.

Experimental Section

Materials. Propionitrile was distilled from vacuum dried No. 5A molecular sieves in air in a Nester-Faust spinning band still. The middle fraction (bp 96–97°, 765.8 mm) was collected in a dry flask containing No. 5A molecular sieves and transferred to an argon-filled drybox. About 500 ml of this solvent was used to prepare a stock solution of ~6–7 *M* SO_2. Compressed SO_2 was bubbled through concentrated H_2SO_4 and then through the distilled PN. This solution was stored over molecular sieves in a desiccator (P_2O_5 desiccant) for at least 1 week before use. The PN–SO_2 solutions used in this study were diluted in the drybox and allowed to stand for several days over molecular sieves before a sample was removed for analysis. The SO_2 content was determined by taking a 1–3-ml aliquot and adding standard (aqueous) KOH and back-titrating with standard HCl. Two study solutions where $[SO_2]$ = 0.95 and 3.30 *M* were prepared prior to their use.

The water content for the PN–SO_2 (0.95 *M*) mixture was determined to be ~27 ppm (upper limit) by vpc. A Hewlett-Packard Model 5750 gas chromatograph with a 6-ft stainless steel Poropack Q (10%) column was used for this analysis. Water analyses were not performed on the two other solvents as they were treated in an analogous manner to the PN–SO_2 (0.95 *M*) mixture.

The densities of the mixed PN–SO_2 solvents were determined pycnometrically at 25.0° and their dielectric constants were measured at 10 MHz by Payne.[6]

Tetraethylammonium perchlorate (TEAP) and tetraethylammonium chloride (TEACl) (Eastman Organics) were dried at 60° *in vacuo*. Reagent grade $AgClO_4$ (Alfa Inorganics) was dried at 60° *in vacuo*. Tetrapropylammonium iodide (TPAI) was recrystallized from an acetone–ether mixture and dried at 60° *in vacuo*. Tetrapropylammonium bromide (TPABr) was dried at 132° for 2 days and was not further treated. Tetrapropylammonium perchlorate (TPAP) was precipitated from an aqueous TPABr solution with $HClO_4$, washed with distilled water, recrystallized, and dried *in vacuo* at 60°. Tetrapropylammonium chloride (TPACl) was prepared by mixing an excess of aqueous HCl with tetrapropylammonium hydroxide. The TPACl was collected by evaporation of the water, recrystallized three times from acetone–ether, and washed several times with methanol. It was dried *in vacuo* at 120° for several days. All salts were stored in a desiccator over P_2O_5.

The salts were weighed out into volumetric flasks in the laboratory and then transferred to the drybox where the solutions were prepared. TPAP was used to maintain an ionic strength of 0.1000 *M*. All solutions referred to below are of constant ionic strength (0.1 *M*). The TPAI solutions in PN–SO_2 mixtures were yellow and the test for free iodine was negative. TPABr in PN–SO_2 were slightly yellow and all other solutions were colorless.

Potentiometric Measurements. Emf measurements were recorded as follows: the output of a Fisher Model 220 pH meter was accurately divided down and measured with a Systron-Donner Model 1033 DVM. A Weston cell was used to calibrate this system to within ±10 μV. The accuracy of the emf readings depended upon the region of the potentiometric curve under study (see Results below) and therefore varied from ±0.1 to ±2 mV. A high-purity Ag wire was coiled and etched and served as the indicator electrode. The reference electrode was a Pt wire sealed in the tip of a TS 7/15 inner joint and plated with Ag from a cyanide bath. A sealed TS 7/15 outer joint containing ~0.01 *M* $AgClO_4$ was placed over this Ag reference electrode.

A 125-ml TS three-neck flask was used as the cell. Machined Teflon stoppers with compression seals were used to prevent air leakage into the cell and loss of solvent and SO_2 out of the cell. Into the middle neck of the flask a Gilmont microburet (2 or 0.2 ml capacity) was inserted. The buret was filled with 0.1000 *M* $AgClO_4$.

General. All glassware was cleaned by immersion into chromic acid, thoroughly washed with distilled water, and air dried at 120° for 24 hr before being placed in the drybox. In the drybox 25 ml of standard halide solution (TPAX) was pipetted into the cells. A Teflon stirrer was placed at the bottom and the electrodes and buret inserted into the Teflon stoppers and the cell was removed from the drybox. The emf measurements were performed in a water bath maintained at 25.0 ± 0.1°. Magnetic stirring was maintained throughout and no particular care was taken to shield the set-up from stray light.

Results

The densities, dielectric constants, and Debye–Hückel "A" factors are given in Table I. The dielectric constant for pure PN is that value obtained by Dannhauser and Flueckinger.[7] Their value differs considerably from ϵ = 26.1 found by Coetzee, *et al*.[8] The difference between these two ϵ values does not seriously affect the calculated *A* values and ϵ = 28.8 was chosen arbitrarily.

Silver ion concentrations were calculated from

$$E = E^\circ + (RT/F)\ln[Ag^+] \quad (1)$$

having previously determined the formal potential E°. The Nernst equation (1) was obeyed to within 0.1 mV in the PN–SO_2 mixtures and to within 2 mV in pure PN.[9] The initial attempts to use the tetraethylammonium salts in PN–SO_2 (0.95 *M*) failed because of precipitation. Adding TEAP and $AgClO_4$ to water did not result in any precipitation and the source of this problem cannot therefore be due to bromide impurities (since TEABr is used to prepare TEAP) because the solubility products of AgBr in water and PN–SO_2 (0.95 *M*) are very similar (see below). Since the origin of this effect could not be determined, the tetrapropylammonium salts were chosen for all the studies in this paper.

Figure 1 shows some typical results for the titration of TPA–halide solutions by $AgClO_4$.[9] The curves in this figure represent the best, intermediate, and most difficult cases for the calculation of the stability constants. The curve for AgCl in PN–SO_2 (0.95 *M*) does not show a distinct break at the saturation point (indicated by the arrow). This behavior was typical of only the PN–SO_2 mixtures. The last three points marked x in Figure 1 for the AgI titration in pure PN resulted in such large errors in the calculated β values that they had to be rejected. Several other data points had to be rejected (see details below) as they gave rise to large errors in the calculated β_2 values. In general, those points at very low total Ag^+ concentrations and those close to the saturation point were

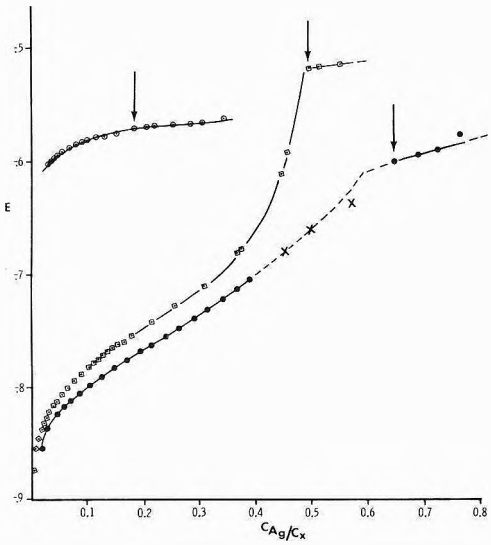

Figure 1. Titration curves at 25°: □, AgCl in PN; ●, AgCl in PN–SO_2(0.95 *M*); O, AgI in PN. The arrows indicate the start of precipitation. The three points marked x on the AgI curve were not included in the calculation of β_2.

TABLE I:[a] **Physical Properties of PN–SO_2 Solvents at 25°**

Solvent	χ_{SO_2}	$d°$	ϵ	A
PN	0.0	0.7768	28.8	2.293
PN–SO_2 (0.95 *M*)	0.066	0.8012	27.2	2.499
PN–SO_2 (3.30 *M*)	0.218	0.8645	26.1	2.658

[a] χ_{SO_2} is the SO_2 mole fraction; $d°$ is the density in g/ml; ϵ is the dielectric constant in Debye units; A is the Debye–Hückel constant in units of $M^{-1/2}$.

the least accurate. At the start of a titration where volumes of ~0.02 ml of titrant are being added, it is expected that any constant or systematic error in the buret reading would give rise to larger experimental errors. In many cases those points near the saturation region required long times (up to 1 hr) to equilibrate or approach equilibration. Data points were not taken for periods greater than 1 hr. Most points in the unsaturated and saturated regions of the titration curves equilibrated within 5–20 min.

Calculations

In all cases an attempt was made to fit the data to mononuclear species of the type AgX_n^{1-n} for $n = 1$ to 4. In unsaturated solutions, the mass balance conditions result in the following two equations for the total silver concentration, C_{Ag}, and total halide concentration, C_x,[10] and stability constants β[10]

$$C_{Ag} = [Ag^+]\left\{1 + \sum_1^n \beta_n[X^-]^n\right\} \quad (2)$$

$$C_x = [X^-] + [Ag^+]\sum_1^n n\beta n[X^-]^n \quad (3)$$

In these equations the β's correspond to the equilibria

$$Ag^+ + nX^- = AgX_n^{1-n} \quad (4)$$

In saturated solutions where solid AgX is present we have

$$\{C_x - C_{Ag} + [Ag^+]\}/[Ag^+] = \frac{K_{SO}}{[Ag^+]^2} + \sum_2^n (n-1)\beta_n\left\{\frac{K_{SO}}{[Ag^+]}\right\}^n \quad (5)$$

where K_{SO} is the solubility product. The stability constants were calculated by a non-linear least-squares method in which the relative error function U was minimized:[11] *i.e.* for i data points

$$U = \sum_1^i (1 - x_i/fx_i)^2 \quad (6)$$

where

$$x_i = (C_{x,i} - [X^-]_i)/[Ag^+]_i \quad (7)$$

and

$$fx_i = \beta_1[X^-]_i + 2\beta_2[X^-]_i^2 + \ldots + n\beta_n[X^-]^n \quad (8)$$

To obtain the concentration of halide ions, the average ligand number, $\bar{n}$, was used; $\bar{n}$ is defined[12] by

$$\bar{n} = (C_x - [X^-])/C_{Ag} \quad (9)$$

and from eq 2 and 3 we have

$$\bar{n} = \sum_1^n n\beta_n[X^-]/\sum_0^n \beta_n[X^-]^n \quad (10)$$

The calculations are started by assuming a value for $\bar{n}$ (we usually started with $\bar{n} = 2$), calculating $[X^-]_i$ from eq 9 and obtaining the β's by least squares. These β's are used to calculate new $\bar{n}$ values from eq 10 and the process repeated until the β's converged to within ±0.001%. The standard deviations of the β's were obtained by the pit-mapping method of Sillén.[13]

Only AgCl and AgBr in pure PN gave solutions for more than one β; the solutions were for β_2 and β_3. In all other cases the attempt to fit β_1, β_3, and β_4 values either failed to converge, oscillated between positive and negative values, or converged at a negative value (with a very large standard deviation) while values of β_2 and K_{SO} did not change appreciably. For these cases, β_2 was calculated from each point in the unsaturated region and the average values of log β_2 are reported below.

The solubility product was calculated from eq 5 for each point in the saturated region using the Newton–Raphson iterative method. The final value of log K_{SO} is therefore an average one.

Values of K_{s2} for the reaction

$$AgX + X^- = AgX_2^- \quad (11)$$

were obtained from

$$K_{s2} = \beta_2 K_{SO} \quad (12)$$

The variances of the log K_{s2} values are taken as the sum of the variances of log β_2 and log K_{SO}. The values of the stability and solubility constants obtained by the above methods are shown in Table II. In Figure 2 the deviation of x/fx (eq 7–8) from its theoretical value is shown for the three AgX species (Cl, Br, I) in pure PN. In the top curve for AgCl a large nonsystematic deviation is observed at low C_{Ag}/C_X values (corresponding to the beginning of the titration) and at high C_{Ag}/C_X values (corresponding to points near the saturation point). Removal of the questionable points results in the second curve for AgCl in Figure 2. Within experimental error, the three bottom curves do not show any systematic error which would indicate the presence of polynuclear or other mononuclear species in the concentration ranges studied in this work.

In adjusting the data in Table II to unit activity, the Güntelberg[14] equation was used

$$\log \gamma_\pm = -AM^{1/2}/(1 + M^{1/2}) \quad (13)$$

TABLE II: Equilibrium Constants in 0.1 *M* Solutions at 25°

System		Log β_2	Log β_3	Log K_{so}	Log K_{s2}
PN	AgCl	15.944 ± 0.005	16.707 ± 0.005	−14.287 ± 0.004	1.657 ± 0.006
	AgBr	16.242 ± 0.003	17.633 ± 0.007	−14.948 ± 0.006	1.294 ± 0.007
	AgI	17.254 ± 0.018		−16.079 ± 0.055	1.175 ± 0.057
PN–SO_2 (0.95 *M*)	AgCl	8.671 ± 0.028		−10.250 ± 0.021	−1.579 ± 0.035
	AgBr	9.926 ± 0.033		−11.400 ± 0.004	−1.474 ± 0.034
	AgI	12.58 ± 0.16		−13.405 ± 0.012	−0.83 ± 0.17
PN–SO_2 (3.30 *M*)	AgCl	6.58 ± 0.13		−9.082 ± 0.026	−2.50 ± 0.13
	AgBr	7.865 ± 0.049		−10.245 ± 0.029	−2.380 ± 0.057
	AgI	10.068 ± 0.089		−12.393 ± 0.047	−2.33 ± 0.10

TABLE III: Equilibrium Constants for Silver Halides in Various Solvents at 25° [a]

	Log β_2			Log K_{so}			Log K_{s2}			
Solvent (ϵ)	Cl	Br	I	Cl	Br	I	Cl	Br	I	Ref
H_2O (78.3,	5.4	7.6	11.2	−9.8	−12.3	−16.0	−4.4	−4.7	−4.8	15
MeOH (32.6)	8.4	11.1	15.3	−13.2	−15.5	−18.4	−4.8	−4.4	−3.1	16
PC (64.4)	21.2	20.9	22.1	−20.2	−20.6	−20.8	1.0	0.3	1.3	17
DMF (36.7)	17.0	16.9	18.1	−15.2	−15.3	−16.1	1.8	1.6	2.0	18, 19
DMSO (46.7)	12.2	11.7	12.8	−10.6	−10.6	−11.6	1.6	1.1	1.2	18, 20
HMPT (29.6)	16.1	16.5		−11.9	−12.3		4.2	4.2		18
TMS (30°) (43.3)	19.8	19.7		−18.1	−18.4	−19.0	1.7	1.3		21
DMAC (37.8)	17.2	16.9	17.3	−14.3	−14.5	−14.7	2.9	2.4	2.6	18
Me_2CO (20.7)	22.8	23.3	24.4	−21.2	−21.6	−23.0	1.6	1.7	1.4	22
AN (36.7)	13.7	13.8	14.0	−13.2	−13.7	−14.5	0.5	0.1	−0.5	16, 18, 20
PN	17.0	17.3	18.3	−15.3	−16.0	−17.1	1.7	1.3	1.2	
PN–SO_2 (0.95 *M*)	9.9	11.1	13.8	−11.5	−12.6	−14.6	−1.6	−1.5	−0.8	
PN–SO_2 (3.30 *M*)	7.9	9.1	11.4	−10.4	−11.5	−13.7	−2.5	−2.4	−2.3	

[a] All data based on unit activities in molar units. The entries for the last three solvents are the present results.

In eq 13, A is the Debye–Hückel constant and M is the molarity. Corrections for ion-pair formation were not made as there are no data available for the solvents studied here. Furthermore, Coetzee[8] reports that ion-pair formation is small in acetonitrile and isobutylnitrile and we assume PN to behave similarly. Table III[15-22] gives the logarithms of the equilibrium constants corrected by eq 13. Also included in Table III are data for other solvents of interest.

Discussion

As there is no apparent relation between K_{so} or β_2 and the dielectric constant (*cf.* Table III), the diverse behavior of the silver halides is best explained in terms of solvation. As a first step, use can be made of the solvation theory where water is used as the reverence solvent. For the reaction

$$(Ag^+ + X^-) \text{ in water} = (Ag^+ + X^-) \text{ in solvent (s)} \quad (14)$$

the free energy of transfer of the pair of ions Ag^+, X^- from water (w) to solvent s is given by

$$\Delta G_t^\circ(Ag^+, X^-) = 2.3RT\{\log K^0_{so,w} - \log K^0_{so,s}\} \quad (15)$$

Similarly for the transfer of the pair of ions Ag^+, AgX_2^-, we have

$$\Delta G_t^\circ(Ag^+, AgX_2^-) = 2.3RT\{\log(K^0_{s2,w} K^0_{so,w}) - \log (K_{s2,s}K_{so,s})\} \quad (16)$$

To obtain individual ionic values of ΔG_t°(ion), an extrathermodynamic assumption is required. Recently Parker, *et al.*,[22a] have suggested that chemists adopt a common assumption for all solvents: namely, that there is a negligible liquid junction potential between $Ag|AgClO_4$ (0.01 *M*) half-cells when connected by a bridge of 0.1 *M* TEA-picrate in that solvent of the pair which is the weaker solvator of Ag^+. On this basis a common assumption is available by which $\Delta G_t^\circ(Ag^+)$ can be evaluated. The data in Table IV were all obtained by this assumption with the exception of the last three entries (present systems) which were evaluated in the following manner. Neglecting the

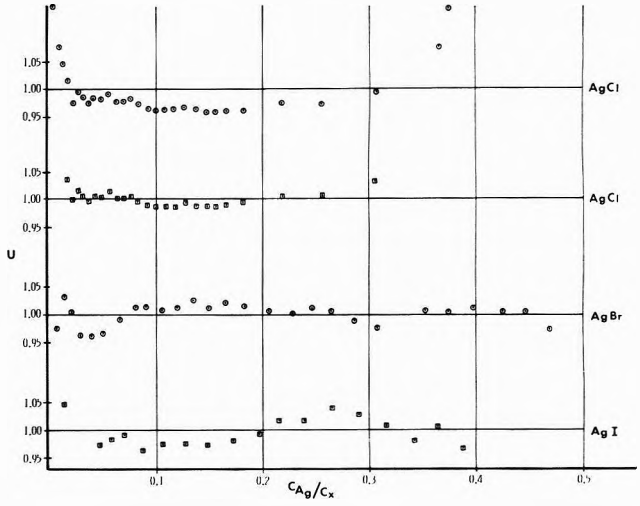

Figure 2. Deviation of experimental points from the theoretical value for AgCl, AgBr, and AgI in PN at 25°: U (the relative error function, eq 6) *vs.* C_{Ag}/C_{Cl}. The top curve for AgCl includes points containing nonsystematic errors. Removal of the first three and last two points results in the second curve for AgCl upon which the final values of β_2 and β_3 are based.

TABLE IV: Single Ion Free Energies of Transfer from Water at 25° [a]

Solvent	Ion						
	Ag^+	Cl^-	Br^-	I^-	$AgCl_2^-$	$AgBr_2^-$	AgI_2^-
MeOH	2.2	2.7	2.2	1.4	3.0	1.8	−1.2
PC	5.3	8.6	6.0	2.7	1.5	−0.8	−7.1
DMF	−3.1	10.0	7.2	3.3	2.1	−1.4	−6.0
DMSO	−7.6	8.7	5.6	1.6	0.6	−2.6	−6.6
HMPT	−9.4	12.8	10.0	6.3	0.5	−2.7	
TMS (30°)	2.9	8.9	5.7	1.2	0.1	−2.7	
DMAC	−4.6	11.2	8.0	3.3	0.8	−2.0	−7.2
Me_2CO	3.3	12.1	9.4	6.3	4.1	0.7	−2.2
AN	−4.1	8.7	5.3	2.0	2.0	−0.6	−3.8
PN	−2.0	9.5	7.0	3.5	1.2	−1.2	−4.7
PN–SO_2 (0.95 *M*)	−2.8	5.1	3.2	0.9	1.2	−1.2	−4.5
PN–SO_2 (3.30 *M*)	−3.0	3.8	1.9	−0.2	1.2	−1.2	−3.6

[a] $\Delta G_t°$ (ion) in kcal/mole (molar units).

last three entries in Table IV, it is seen that, for the transfer from water to every solvent (except acetone), $\Delta G_t°(AgX_2^-)$ changes sign between X = Cl and X = Br. Therefore, as a rough first approximation, it is assumed that

$$\Delta G_t^0(Ag^+, AgCl_2^-) + \Delta G_t^0(Ag^+, AgBr_2^-) \approx 2\Delta G_t^0(Ag^+) \quad (17)$$

The last three entries in Table IV were obtained *via* eq 17.

There are no unusual effects to be noted in the data of Table IV. $\Delta G_t°(Ag^+)$ values are, for the most part, negative (values in PC and MeOH may be negative as discussed elsewhere[1,23]) and $\Delta G_t°(X^-)$ is positive and is large for the smaller Cl^- ion. Thus the fact that K_{so} is much smaller in aprotic solvents is attributable mainly to the anion effect.[1-4,18-22a,23-26] For the large anion I^-, $\Delta G_t°(I^-)$ is generally small and the large differences in the equilibrium constants are strongly dependent upon the nature of the solvation of Ag^+. The equilibria

$$Ag(s)_2^+ + 2X^- = AgX_2^- + 2s \quad (\beta_2) \quad (18)$$

$$AgX + X^- = AgX_2^- \quad (K_{s2}) \quad (11)$$

also reflect the relative importance of the Ag^+ solvation to that of X^- and AgX_2^-. Equation 18 is written to show the competition between X^- and the solvent s. Equation 11 is of interest as it reflects on the stability of AgX_2^- with respect to X^-. The medium effect (Table IV) can explain why an equilibrium constant decreases or increases upon changing the solvent, but it still is too general to reveal accurate pictures of chemical bonding. While the magnitude and sign of $\Delta G_t°$(ion) does allow for some generalization on the nature of bonding, it is heavily dependent upon the extrathermodynamic assumption and agreement as to which assumption is most valid is not universal.[1-4,18-22a,23-26]

Additional insight into the nature of the bonding properties of these complex species can be obtained by reference to the theory of hard and soft acids and bases.[5,24] According to this theory, Ag^+ is a typical soft acid and will therefore form more stable complexes with ligands of high polarizability, *i.e.*, those which tend to enter into covalent bonding. Here the solvent is also considered to be a ligand competing with X^- as shown in eq 18. The ability to form covalent bonds will effect both the order of the stability of AgX_2^- as reflected in the value of β_2 and the magnitude of its solubility as reflected in the value of K_{s2}. Within experimental error, the data in Table III show that in every case β_2 does increase in the expected order

$$Cl < Br > I \quad (19)$$

Values of K_{s2} are more difficult to interpret; one expects that K_{s2} would increase in the order given in eq 19, but this is not always the case as the aqueous data reveal. This situation is due to the fact that Cl^- can enter into hydrogen bonding in aqueous solution resulting in an enhanced stability. Br^- and I^- are, on the other hand, strong structure breakers in water and therefore promote the formation of $Ag(H_2O)_2^+$.

For the AgCl + Cl^- system, Butler[25,26] has found that additions of H_2O to PC and DMSO result, as expected, in decreasing β_2 and K_{s2} values and increasing K_{so} values. Similar results are reported in this paper for the PN–SO_2 system and to compare Butler's results to the present ones in 0.95 *M* SO_2–PN solutions, we have calculated the water concentration in PC and DMSO required to give a value of −1.6 for log K_{s2}(AgCl). From Butler's data it is found that the required water concentrations are 16 *M* in DMSO and 2.5 *M* in PC. These results indicate that SO_2 is a much stronger ligand than is H_2O which is not entirely unexpected.[5,24] The decrease in K_{s2} upon addition of water to the organic solvent is due to the increased stability of Cl^- due to hydrogen bonding in addition to the fact that water acts as a strong ligand toward Ag^+ by virtue of its low-lying sp^3 lone pairs. It is obvious that H bonding cannot exist in PN–SO_2 mixtures and the reason for the great stability of $Ag(SO_2)_2^+$ is attributed to π-bond formation between Ag^+ and the sulfur atom (this is in addition to the σ-bond formed with the hybridized sp^2 lone pair on the sulfur atom). Since sulfur has low-lying d orbitals of the same principal quantum number as its bonding electrons, it can form π bonds with the 4d electrons of Ag^+.[5,24]

Acknowledgment. The authors are grateful to Dr. Richard Payne for measuring the dielectric constants of the PN–SO_2 mixtures and for providing them with tetrapropylammonium hydroxide.

Supplementary Material Available. Appendicies I–III will appear following these pages in the microfilm edition of this volume of the journal. Photocopies of the supplementary material from this paper only or microfiche (105 × 148 mm, 20× reduction, negatives) containing all of the supplementary material for the papers in this issue may be obtained from the Journals Department, American

Chemical Society, 1155 16th St., N.W., Washington, D. C. 20036. Remit check or money order for $4.00 for photocopy or $2.00 for microfiche, referring to code number JPC-73-3002.

References and Notes

(1) C. M. Criss and M. Salomon, "Physical Chemistry of Organic Solvents," A. K. Covington and T. Dickinson, Ed., Plenum Press, New York, N. Y., in press.
(2) A. J. Parker, *Chem. Rev.*, **69**, 1 (1969).
(3) O. Popovych, *CRC Crit. Rev. Anal. Chem.*, **1**, 73 (1970).
(4) J. F. Coetzee and C. D. Ritchie, Ed., "Solute–Solvent Interactions," Marcel Dekker, New York, N. Y., 1969.
(5) (a) R. G. Pearson, *J. Amer. Chem. Soc.*, **85**, 3533 (1963); (b) S. Ahrland, J. Chatt, and N. R. Davies, *Quart. Rev., Chem. Soc.*, **12**, 265 (1958).
(6) R. Payne, private communication.
(7) W. Dannhauser and A. F. Flueckinger, *J. Phys. Chem.*, **68**, 1814 (1964).
(8) J. F. Coetzee, D. K. McGuire, and J. L. Hedrick, *J. Phys. Chem.*, **67**, 1814 (1963).
(9) See paragraph of end of paper regarding supplementary material.
(10) J. N. Butler, "Ionic Equilibrium," Addison-Wesley, Reading, Mass., 1964.
(11) K. P. Anderson and R. L. Snow, *J. Chem. Educ.*, **44**, 756 (1967).
(12) J. Bjerrum, "Metal-Ammine Formation in Aqueous Solution," P. Haase and Son, Copenhagen, 1957.
(13) L. G. Sillén, *Acta Chem. Scand.*, **16**, 159 (1962).
(14) E. Güntelberg, *Z. Phys. Chem.*, **123**, 199 (1926).
(15) L. G. Sillén and A. E. Martell, "Stability Constants of Metal-Ion Complexes," The Chemical Society, London, 1964.
(16) D. C. Luehrs, R. T. Iwamoto, and J. Kleinberg, *Inorg. Chem.*, **5**, 201 (1966).
(17) J. N. Butler, *Anal. Chem.*, **39**, 1799 (1967); see also J. N. Butler, D. R. Cogley, J. C. Synnott, and G. Holleck, "Study of The Composition of Nonaqueous Solutions," Final Report, Air Force Contract No. AF-19(628)6131, Sept 1969; AD No. 699-589.
(18) R. Alexander, E. C. Ko, Y. C. Mac, and A. J. Parker, *J. Amer. Chem. Soc.*, 89, 3703 (1967).
(19) J. N. Butler, *J. Phys. Chem.*, **72**, 3285 (1968).
(20) M. K. Chantooni and I. M. Kolthoff, *J. Phys. Chem.*, **77**, 1 (1973).
(21) R. L. Benoit, A. L. Beauchamp and M. Deneux, *J. Phys. Chem.*, **73**, 3268 (1969).
(22) (a) R. Alexander, A. J. Parker, J. E. Sharp, and W. E. Waghorne, *J. Amer. Chem. Soc.*, **94**, 1148 (1972); (b) M. Salomon, in press.
(23) M. Salomon, *J. Phys. Chem.*, **74**, 2519 (1970); *J. Electrochem. Soc.*, **118**, 1610 (1971).
(24) S. Ahrland, *Struct. Bonding (Berlin)*, **1**, 207 (1966); **5**, 118 (1968).
(25) J. N. Butler, D. R. Cogley, and W. Zurosky, *J. Electrochem. Soc.*, **115**, 445 (1968).
(26) J. C. Synnott and J. N. Bulter, *J. Phys. Chem.*, **73**, 1470 (1969).

Hildebrand's Equations for Viscosity and Diffusivity

H. Ertl and F. A. L. Dullien*

Department of Chemical Engineering, University of Waterloo, Waterloo, Ontario, Canada

(Received July 31, 1973)

Publication costs assisted by the National Research Council of Canada

The liquid viscosities and self-diffusion coefficients of benzene, the monohalogenated benzene derivatives, and some normal paraffins have been determined as a function of temperature down to the proximity of the melting points. Based on these data it appears that Hildebrand's equation for viscosity is valid only down to $T/T_c \approx 0.46$, whereas in its original form the equation suggested by him for self-diffusion coefficient is not valid anywhere in the temperature range studied. A small modification of this equation, however, has been found to describe the experimental diffusivities well in every case.

Introduction

Hildebrand[1] has recently modified a viscosity equation originally suggested by Batschinski.[2] Batschinski's equation is

$$\frac{1}{\eta} = \frac{v - w}{C} \tag{1}$$

where v is the specific volume and w and c are constants. w is a nearly constant fraction of the critical volume but Batschinski failed to find a correlation for C. The investigation of eq 1 for organic liquids by Al-Mahdi and Ubbelohde[3] showed a wide variation of C with no trend recognizable.

It is assumed by eq 1 and also by Hildebrand's modified form, eq 2, that fluidity, ϕ, (ϕ = 1/viscosity) is governed by the volume increase. The form of the modified equation is

$$\phi = \frac{1}{\eta} = B\frac{V - V_0}{V_0} \tag{2}$$

where V_0 is a constant and is the molar volume at which viscous flow ceases.

For a large number of liquids values of the constant parameters B and V_0 have been given in ref 1 and 4. It has been shown there that V_0 is approximately a constant fraction of the critical volume, namely, $V_0/V_c \approx 0.3$. B, on the other hand, has been found to be linearly related to the chain length in the case of n-alkanes.

A clear statement about the applicable range of eq 2 has not been given in either ref 1 or 4. It has been demonstrated for CO_2 and C_3H_8 that eq 2 represents the experimental results up to the neighborhood of the critical point. However, for even larger volume an increased dependence on temperature develops which has been explained by Hildebrand and Lamoreaux[4] as due to the increase of translational momentum. The vast majority of the B and V_0 values have been obtained from viscosity measurements at variable temperature and atmospheric pressure. It is evident, however, that the effect of pressure

is not taken into account by eq 2, since at constant volume (and variable temperature and pressure) this equation would require the viscosity to remain constant. In actual fact, however, the constant volume viscosity decreases with increasing temperature.[5,6] For C_6H_6 and CCl_4 at constant volume $\eta \sim 1/T$.[7]

Eicher and Zwolenski[8] have recently applied eq 2 over large temperature intervals including the region close to the freezing point. Based on least squares fits they concluded that eq 2 is not satisfactory in describing the temperature dependence of liquid viscosities over wide temperature ranges. In the reply by Hildebrand and Lamoreaux[9] it was pointed out that a possible explanation for the failure of eq 2 at temperatures close to the freezing point is given by an effect which Ubbelohde and coworkers[10] have termed "pre-freezing." Molecules with a tendency of interlocking, resulting from branched and reentrant portions, give rise to the "pre-freezing" effect. However, as it is shown in this contribution, molecules with shapes which do not favor entanglement can also deviate from the predicted behavior of eq 2. On the other hand, a number of liquids do not exhibit a viscosity anomaly on approaching the freezing point.

Part of the present paper will deal with the basic question: what is the inapplicable temperature range for the different liquids? It will be shown that the occurrence of deviations from eq 2 depends on the value of the reduced freezing temperature, T/T_c.

Hildebrand[1] has suggested that an equation similar to eq 2 should also apply for the diffusion coefficient, D, if ϕ is replaced by D. This results in

$$D = B'\frac{V - V_0}{V_0} \qquad (3)$$

where B' is a constant. Only for benzene and carbon tetrachloride has Hildebrand provided plots of D *vs.* T which appear to be straight lines. These plots, however, cover only narrow temperature ranges. Over a wider temperature range they may not be straight lines as the more pertinent plots of D *vs.* V are not straight lines either (see Figure 3).

In the present work we show that the form of eq 3 is not suited to represent diffusivity data even over the limited temperature range for which eq 2 holds. A modification of eq 3 which gives D a stronger volume dependence has been found to represent the experimental data well.

Discussion

Viscosity. The authors have presented in a previous paper experimental results for the viscosities of the monohalogenated benzenes between 20° and their freezing points.[11] They also showed a relation between the occurrence of the "pre-freezing" effect and restricted rotation of the molecules.[12] It was also pointed out that the viscosity of liquids with a reduced freezing temperature $T_{fr} < 0.46$ deviates increasingly from the values extrapolated from the "high"-temperature behavior, as the freezing point is approached. This criterion was also found to hold in cases where other classifications according to the entropy of fusion or the molecular sphericity fail.[13] Since the transition from normal to anomalous behavior is a gradual one, the value of 0.46 has to be interpreted as a narrow temperature range around this value.

Viscosity is said to exhibit anomalous behavior if it deviates from the behavior at "high" temperature, *i.e.*, well above the freezing point. For this range it is well known

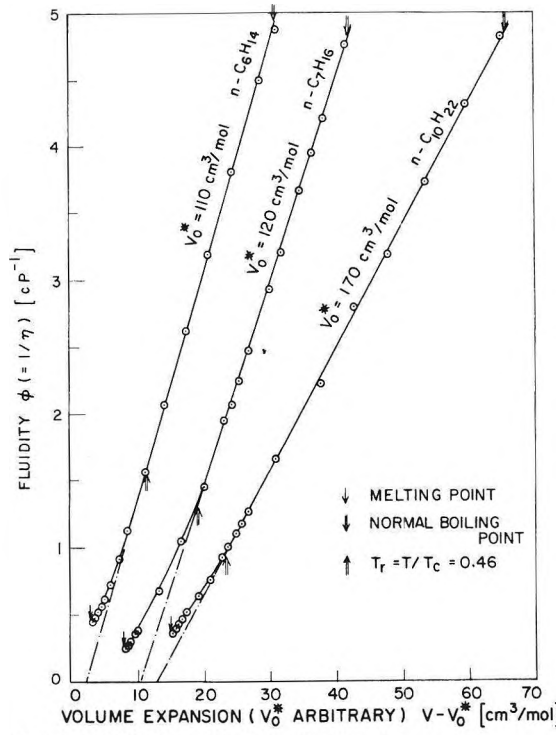

Figure 1. Hildebrand plots for fluidity of *n*-pentanes.

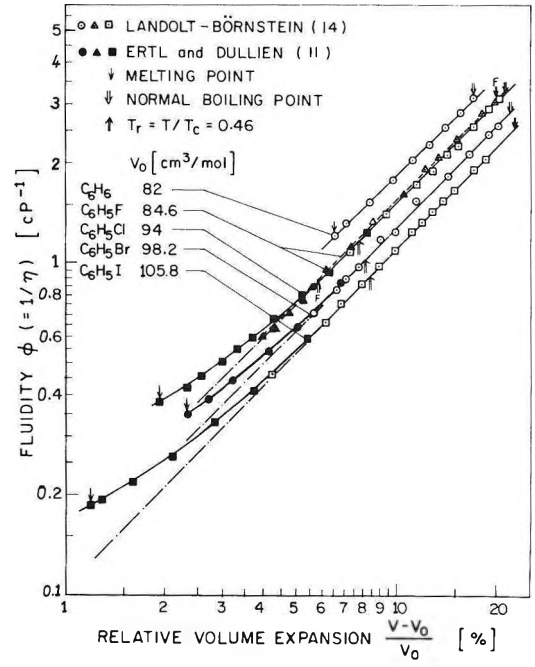

Figure 2. Log-log plots of fluidity *vs.* relative volume expansion of benzene and derivatives.

that an Arrhenius type equation is a suitable form to represent the viscosity-temperature dependence. Other forms of equations, *e.g.*, eq 2, are equally suitable. Since volume expansion is certainly the primary cause for the ease of viscous flow, eq 2 is superior to the Arrhenius type equation, due to its physical content.

Figure 1 depicts the fluidity (ϕ) behavior of three *n*-paraffins. The viscosity data were taken from Landolt-Bornstein.[14] In order to save space, the x axis has been drawn as the molal volume minus an arbitrary constant which is indicated for each liquid. A straight line in this plot indi-

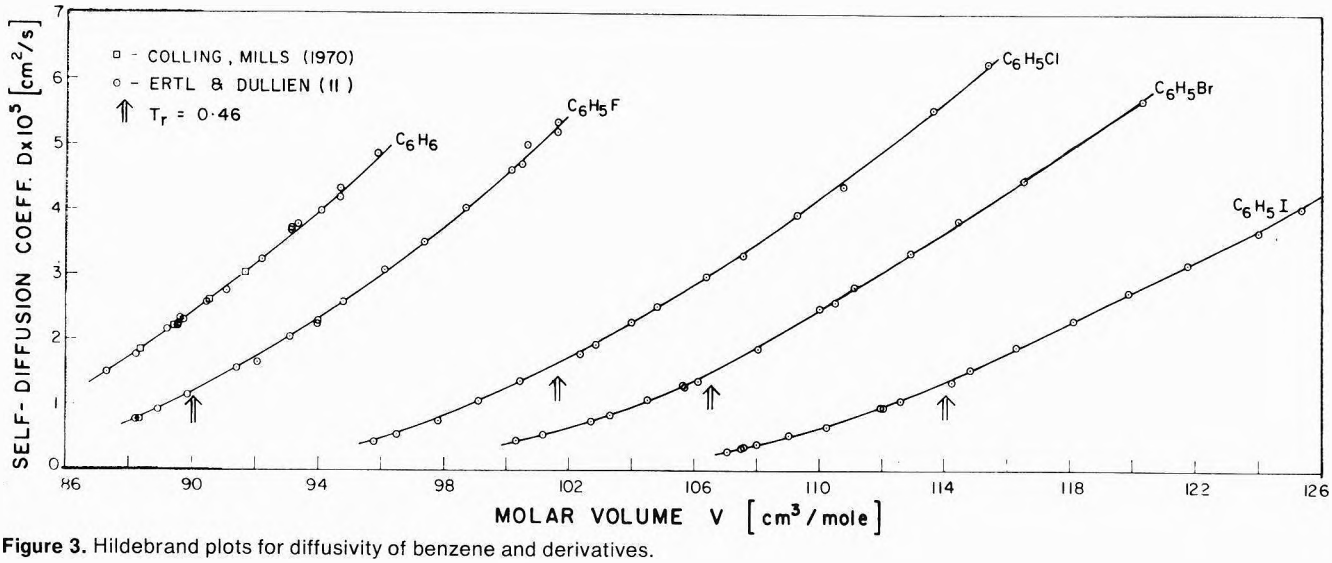

Figure 3. Hildebrand plots for diffusivity of benzene and derivatives.

TABLE I: Values of the Parameters in $1/\eta = B(V - V_0/V_0)$ for $T_r > 0.46$

Liquid	B, cP^{-1}	V_0, cm^3/mol	ϵ, %	n data
Benzene	18.2 (18.5)[a]	82.0 (82)	0.76	9
Fluorobenzene	15.5	84.6	0.80	14
Chlorobenzene	15.0	94.0	0.38	21
Bromobenzene	12.7	98.2	0.39	11
Iodobenzene	11.2	105.8	0.21	9
	(18.8)	(130)		
n-Heptane	20 [17.7][b]	130.6 [129.1]	0.43	15
	(15.2)	(183)		
n-Decane	16.9 [16.6]	183.0 [183]	1.20	12

[a] Round brackets: from Hildebrand.[1] [b] Square brackets: from Hildebrand and Lamoreaux.[3]

cates agreement with eq 2. For each liquid an anomaly is present. Similarly to the case of an Arrhenius plot,[12] the anomalies appear for reduced temperature values $T_r <$ 0.46.

The magnitude of the deviations as seen in Figures 1 and 2 is misleading with respect to η. Due to the form of eq 2 a given deviation of $1/\eta$ will result in increasing deviations for η as $1/\eta$ gets smaller. The failure of eq 2 is also clearly shown in Figure 2 which is a log–log plot of the fluidity, ϕ, of benzene and the halogenated benzenes *vs.* relative volume expansion, $(V - V_0)/V_0$. The V_0's used were obtained from a least-squares fit to the η data for T_r > 0.46. For these liquids also anomalous behavior is observed when $T_r < 0.46$.

It is interesting that no anomalous behavior is observed for benzene as this substance freezes at a high enough temperature (T_{fr} = 0.496 > 0.46) to preclude a noticeable reduction of rotational energy of the molecules in the liquid. As the example of the monohalogenated benzene derivatives clearly indicates, a relatively small loss in symmetry will lower the reduced freezing temperature sufficiently for the molecules to be closely crowded and the linear relation between fluidity and molal volume is violated. The values of the parameters B and V_0 are given in Table I. Also included in the table is the mean standard error, ϵ, and the number of data points, n, employed in the least-squares fit. $\epsilon = (100/n) \times [(y_i - \hat{y}_i/y_i]^{1/2}$, where y_i and $\hat{y}_i$ are the experimental and best fit values, respectively. As seen from the numbers in brackets, quite close agreements have been obtained with the values of B and V_0 quoted by Hildebrand[1] and Hildebrand and Lamoreaux.[3] Inspection of the magnitude of ϵ indicates excellent fit of eq 2 to the temperature range $T_r > 0.46$. The occurrence of viscosity anomalies of lower temperatures has been previously interpreted as due to a scarcity of free space which does not permit free rotation of molecules in the liquid.[12] This may lead to the formation of "clusters" which have to be considered as short-lived dynamic arrangements of adjacent molecules having coordinated movements.

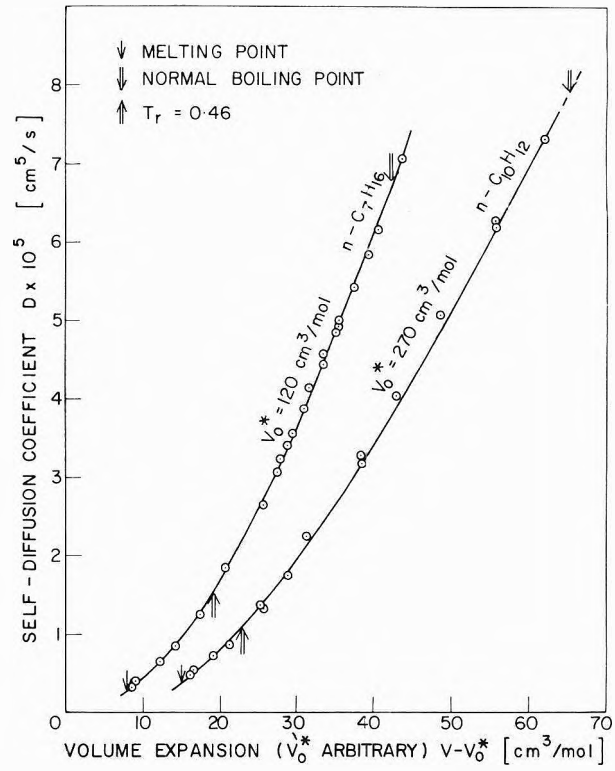

Figure 4. Hildebrand plots for diffusivity of *n*-paraffins.

It is obvious from Figures 1 and 2 that performing a least-squares fit over the whole normal liquid range, as done by Eicher and Zwolenski,[8] is inappropriate for liquids extending into $T_r < 0.46$.

TABLE II: Relevant Temperature Data for the Isomeric Hexanes and *p*- and *m*-Xylene

Liquid	T_f, °C	$T_f/T_c = T_{fr}$	T_b, °C	$T_b/T_c = T_{br}$	T_c, °C	T_{low}, °C	T_{low}/T_c	$T_{0.46}$, °C
2-Methylpentane	−153.7	0.24	60.3	0.669	224.9	−15.6	0.515	−44
3-Methylpentane	−162.9	0.219	63.3	0.667	231.2	−17.6	0.506	−42
2,2-Dimethylbutane	−99.9	0.354	49.7	0.66	216.2	−13.7	0.53	−49
n-Hexane	−95.3	0.35	68.7	0.673	234.7			−39
p-Xylene	13.2	0.463	138	0.665	345			
m-Xylene	−47.4	0.365	139	0.665	346			

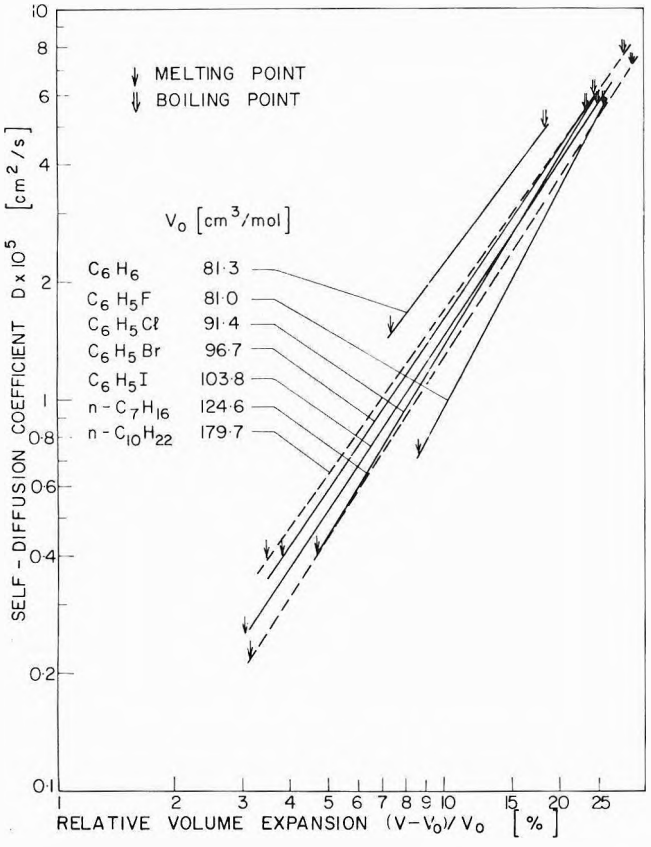

Figure 5. Log–log plots of diffusivity *vs.* relative volume expansion for *n*-paraffins, benzene, and derivatives.

The same authors have recently reported accurate experimental viscosity data for three isomers of *n*-hexane.[15] Hildebrand and Lamoreaux[4] have employed their viscosity data and found straight lines in the ϕ *vs.* V plots. This, however, is no indication for the validity of eq 2 for temperatures down to the freezing point since Table II clearly shows that the lowest experimental temperature, T_{low}, is still far above the temperature, $T_{0.46}$, corresponding to $T_r = 0.46$. As is known for the case of *n*-hexane, from the inspection of the T_{fr} values we also expect an anomalous viscosity behavior for the isomers, as T_{fr} is appreciably smaller than 0.46 for each liquid.

Hildebrand and coworkers[4] have found earlier that the molal volumes and viscosities of *p*- and *m*-xylene have almost identical values over their common liquid range with no evidence of "pre-freezing" of the para isomer above its melting point of 13.2°. The characteristic temperature data of the two liquids have also been included in Table II. Again, the nonanomalous viscosity behavior observed for *p*-xylene and the anomaly found for the meta isomer are plausible in the light of their T_{fr} values. $T_{fr} = 0.365$ for *m*-xylene and thus is appreciably smaller than 0.46, whereas T_{fr} for *p*-xylene is 0.463.

TABLE III: Values of the Parameters in $D = B[(V - V_0)/V_0]^m$

Liquid	$B \times 10^4$, cm²/sec	V_0, cm³/mol	m	ϵ, %	n data
Benzene	4.81	81.3	1.34	1.21	19
Fluorobenzene	6.18	81.0	1.80	1.9	18
Chlorobenzene	5.17	91.4	1.58	1.4	15
Bromobenzene	4.71	96.7	1.49	4.2	17
Iodobenzene	4.04	103.8	1.46	3.3	18
n-Heptane	4.05	124.6	1.51	2.9	27
n-Decane	4.09	179.7	1.38	4.4	19

Diffusion. Figure 3 is a D *vs.* V plot of experimental diffusivity data[11] of benzene and the monohalogenated benzenes. It is important that, unlike in the case of fluidity, a curvature is present at any temperature for all liquids and benzene is not an exception in this case. Therefore, the deviation from linear behavior cannot, in the case of diffusivity, be explained in terms of the rotational hindrance becoming important as the temperature is lowered. The curvature in the plots is a clear sign of the invalidity of the diffusivity equation, eq 3, suggested by Hildebrand.[1] The same conclusions are recognizable from the plot for two *n*-paraffins, Figure 3. For comparison with the viscosity plots the position at which $T_r = 0.46$ are also shown.

It has been found[11] that a modification of eq 3 in the form

$$D = B'\left(\frac{V - V_0}{V_0}\right)^m \tag{4}$$

represents the experimental data well. Important as this difference is between eq 3 and 4, both equations propose that log D *vs.* log $[(V - V_0)/V_0]$ is linear. The exponent m is found to be larger than 1. This implies a greater dependence of diffusivity on volume expansion as compared with viscous flow. In Table III are listed the parameters of eq 4 which were obtained by nonlinear regression technique.

Comparison of the V_0 values of Tables I and III shows that the values are very nearly identical but with V_0 of the diffusivity equation consistently larger. With respect to the B values the same trend is obtained for the halogenated benzenes. In agreement with the findings of Hildebrand and Lamoreaux,[3] the B values decrease with increasing molecular size and rotational inertia. No explanation is readily available for the values of B obtained for benzene and the two *n*-paraffins (Table III) which do not fit into a pattern.

Figure 5 is a plot similar to Figure 2 except that it shows the dependence of diffusion, rather than that of fluidity, on relative volume expansion. It is of interest to notice a basic difference between the plots in Figures 5 and

2, respectively. While the lines in the log ϕ *vs.* log $[(V - V_0)/V_0]$ plot are virtually parallel in the "high" temperature region, the lines in the diffusivity plot appear to converge. In spite of the different molecular shapes, the diffusion coefficients of the halogenated benzenes and normal paraffins are within a narrow band at the boiling points. No trend of D for the halogenated benzenes at fixed volume expansion is observable. The same is true with respect to the volume expansion at the freezing point. On the other hand, the volume expansion at the boiling points has about the same value for molecules of similar shape.

Conclusions

We can summarize the foregoing by the following points. (1) Equation 2 is not universally applicable for liquids. (2) Equation 2 is restricted to temperatures corresponding to T_r greater than about 0.46 at which unhindered molecular rotation is possible. (3) Equation 3, suggested by Hildebrand for self-diffusion, does not conform to experimental results. (4) The modified form of eq 3 (eq 4) represents the diffusivity well.

References and Notes

(1) J. H. Hildebrand, *Science*, **174**, 490 (1971).
(2) A. J. Batschinski, *Z. Phys. Chem.*, **84**, 643 (1913).
(3) A. A. K. Al-Mahdi and A. R. Ubbelohde, *Trans. Faraday Soc.*, **51**, 361 (1955).
(4) J. H. Hildebrand and R. H. Lamoreaux, *Proc. Nat. Acad. Sci. U. S.*, **69**, 3428 (1972).
(5) E. A. Moelwyn-Hughes, "Physical Chemistry," Pergamon Press, New York, N. Y., 1961, pp 717–719.
(6) A. A. Miller, *Macromolecules*, **4**, 757 (1971).
(7) A. A. Miller, *J. Phys. Chem.*, **67**, 2809 (1963).
(8) L. D. Eicher and B. J. Zwolenski, *Science*, **177**, 369 (1972).
(9) J. H. Hildebrand and R. H. Lamoreaux, *J. Phys. Chem.*, **77**, 1471 (1973).
(10) A. R. Ubbelohde, "Melting and Crystal Structure," in "Phase Transitions," Solvay Institute, 14th Chemistry Conference, Interscience, London, 1971.
(11) H. Ertl and F. A. L. Dullien, *A.I.Ch.E. J.*, in press.
(12) H. Ertl, and F. A. L. Dullien, *Proc. Roy. Soc., Ser. A*, in press.
(13) D. B. Davies and A. J. Matheson, *Trans. Faraday Soc.*, **63**, 596 (1967).
(14) H. H. Landolt and R. Bornstein, "Zahlenwerte und Funktionen," 6th ed, Vol. II, Part 5a, Springer-Verlag, Berlin, 1969.
(15) L. D. Eicher and B. J. Zwolenski, *J. Phys. Chem.*, **76**, 3295 (1972).

Appendix. Nomenclature

B = constant, mol^{-1} cm sec
B' = constant, $cm^2\ sec^{-1}$
C = constant, $cm^2\ sec^{-1}$
D = self-diffusion coefficient, $cm^2\ sec^{-1}$
m = exponent (eq 4)
n = number of data points
v = specific volume, $cm^3\ mol^{-1}$
V = molar volume, $cm^3\ mol^{-1}$
V_0 = constant (eq 2, 3, and 4), $cm^3\ mol^{-1}$
T = temperature

Greek Letters

η = absolute viscosity, mol $cm^{-1}\ sec^{-1}$
ϵ = mean standard error
ϕ = fluidity $(=1/\eta)$, mol^{-1} cm sec
ω = constant (eq 1), $cm^3\ mol^{-1}$

Subscripts

c = critical
r = reduced

Reactions of Beams of Lithium Chloride and Lithium Bromide with Potassium Chloride Surfaces

Robert B. Bjorklund and Joseph E. Lester*[1]

Department of Chemistry and Materials Research Center, Northwestern University, Evanston, Illinois 60201

(Received July 5, 1973)

Publication costs assisted by the Materials Research Center, Northwestern University

As a test of an equilibrium treatment of gas–solid reactions, we have used a mass spectrometer to measure the reaction products of LiCl and LiBr molecular beams with KCl single crystals as a function of beam flux and crystal temperature. The data exhibit an increase in the dimerization of beam molecules and certain reaction products with decreasing crystal surface temperature. Using the calculated equilibrium partial pressures of the reaction products, one can correctly predict the trends of the experimental data with varying crystal temperature and beam flux, but not the relative measured concentrations of products. The agreement is better at higher temperatures.

Introduction

Interpretation of the evaporation rates of the products of the vaporization of solids and of the products of gas–solid reactions by the use of equilibrium thermodynamic properties was first attempted by Langmuir. His analysis of vaporization rates using the kinetic theory of gases was quite successful in correlating the vaporization rates of several metals with their equilibrium thermodynamic properties. Recently, Batty and Stickney have applied a quasiequilibrium approach to analyze the data from the

reaction of gaseous O_2 and solid tungsten and molybdenum at high temperature (>1200°K) and low pressure.[2a] They introduced an experimentally determined equilibration parameter for the impinging O_2, and were able to improve the agreement between the measured evaporation rates of the volatile products and the calculated equilibrium partial pressures. Since more accurate thermodynamic data are available for the alkali halides, a similar comparison for the reaction of one alkali halide beam with another alkali halide crystal at a lower temperature (<750°K) might be a better test of the model. The possibility of forming dimers and mixed dimers on the surface would yield information as to whether thermal and chemical equilibration of the beam with the surface is occurring. Blander has done a statistical mechanical analysis of association of alkali halide molecules in the vapor,[2b] and Schoonmaker and Porter determined the association constants of alkali fluoride dimers and mixed dimers in the gas phase.[3] Recently, Schoonmaker and Lo have measured the condensation coefficient of NaCl beams on the 100 face of single crystals of NaCl and found appreciable condensation at crystal temperatures as high as 675°K.[4] In this paper we report the measurement of the reaction products of lithium halide beams with KCl crystals, and compare the experimental results with the corresponding gas-phase equilibrium partial pressures.

Experimental Section

Optical quality single crystals of KCl, 2 cm × 2 cm × 0.5 cm, cleaved along the 100 plane were obtained from Optovac Corp. Reagent grade LiCl and LiBr were used as the beam materials. The temperature of the crystal was maintained to ±0.5° by a Leeds and Northrup temperature controller in response to the potential of a chromel–alumel thermocouple in the crystal center. Temperatures reported are for the bulk crystal. A chromel–alumel thermocouple was spot welded to the rear of the effusion cell and its potential was used as a signal input for a Leeds and Northrup temperature controller. The beam source was maintained to ±1.0°.

Intensities of products leaving the KCl surface were measured with an EAI model QUAD 250A quadrupole mass spectrometer using an off-axis channeltron electron multiplier as a detector.[5] The experiments were done in a Ultek stainless steel vacuum system at a pressure of 10^{-7} to 10^{-6} Torr. The KCl crystal and heater were positioned in the center of the chamber about 9 cm from the aperature of the mass spectrometer. A nickel effusion cell beam source was mounted on a platform adjacent to the spectrometer aperature so that the angle between the beam axis and the spectrometer axis was approximately 45°. (Details of similar experimental apparatus may be found in ref 6.)

Both the effusion cell and spectrometer aperature were equipped with a shuttering device. The beam shutter permitted a measurement of KCl^+ before and after beam impingement. The spectrometer shutter was used to measure the background gas contribution to the intensity of products leaving the crystal surface.

Six potentiometers were used to select the m/e ratio of detected products. These were set to yield the desired potentials at the beginning of the series of measurements and checked from time to time to ensure that the peaks being monitored were at their maxima. The ion source was operated at an emission current of 400 μA and an electron energy of 30 V.

Experimental Results

Five species were detected from the reaction of the LiCl beam with the KCl crystal. The ions assigned to the monomers and dimers of both reactants ($LiCl^+$, KCl^+, Li_2Cl^+, and K_2Cl^+) and the mixed dimer ion ($LiKCl^+$) were measured at steady-state conditions as a function of crystal temperature at a fixed beam flux. The results are shown in Figure 1. We assume that K_2Cl_2, Li_2Cl_2, and $LiKCl_2$ are ionized to K_2Cl^+, Li_2Cl^+, and $LiKCl^+$[7] and that the dimer contributions to the monomer peaks are small.[8] The plotted intensities have been corrected for isotopic abundance ratios and the mass transmission probability of our mass spectrometer. No attempt was made to correct for the relative ionization cross sections of the molecules because of the lack of cross section data for these mixed alkali halide systems. The corrections to the spectral intensity data in no way influence the conclusions reached.

The LiBr beam–KCl crystal reaction has a greater number of reaction products. In addition to the monomer exchange reaction products (LiCl and KBr), four dimers are possible from the monomers, plus an additional five mixed dimers. Thus, a total of 13 possible molecules could evaporate from the crystal surface. Figure 2 is a plot of the seven species we measured, again corrected for isotopic abundance and transmission probability. $LiKCl^+$ at mass 81 has not been corrected since $^{81}Br^+$ is part of the measured intensity. Since the Br input into the system is constant, although its distribution is not, the data at this m/e were included to show the $LiKCl^+$ trend.

A difficulty that was not encountered in the previous system arises in assigning a parent molecule to the dimeric ions measured. Li_2Cl^+ could be formed from Li_2Cl_2 or Li_2ClBr upon ionization. Based on electron affinities, Br is more likely to be lost in the ionization of a mixed anion dimer than Cl. Therefore, the majority of the Li_2Br^+ intensity is believed to come from Li_2Br_2, while Li_2Cl^+ has contributions from both Li_2Cl_2 and Li_2ClBr.

Data were obtained for three LiCl fluxes in the LiCl–KCl system and for four LiBr fluxes in the LiBr–KCl system. The crystal temperatures at which certain ion intensities have slope changes in the log I *vs.* $1/T$ plots are listed in Table I.

Calculation of Equilibrium Partial Pressure. A comparison was made between the intensities measured in our gas–solid reactions and the calculated gas-phase equilibrium partial pressures for the same system. The latter were divided by T to yield quantities of the same dimensions as I^+ but which are arbitrarily scaled with respect to the experimental numbers because of the unknown mass spectrometric parameters. For the LiCl/KCl system, five equations were needed to solve for the partial pressures of the species present at equilibrium. Three equations for dimerization reactions were used

$$K_p = P_{K_2Cl_2}/P_{KCl}^2 \quad (1)$$

$$K_p' = P_{Li_2Cl_2}/P_{LiCl}^2 \quad (2)$$

$$K_p'' = P_{LiKCl_2}/P_{LiCl}P_{KCl} \quad (3)$$

The conservation of mass (expressed as pressures of reactants) provided the last two equations

$$P_{LiCl}^{\text{initial}} = P_{LiCl} + 2P_{Li_2Cl_2} + P_{LiKCl_2} \quad (4)$$

$$P_{KCl}^{\text{initial}} = P_{KCl} + 2P_{K_2Cl_2} + P_{LiKCl_2} \quad (5)$$

Ideal gas thermochemical data[9] for the $(MX)_n$ monomers

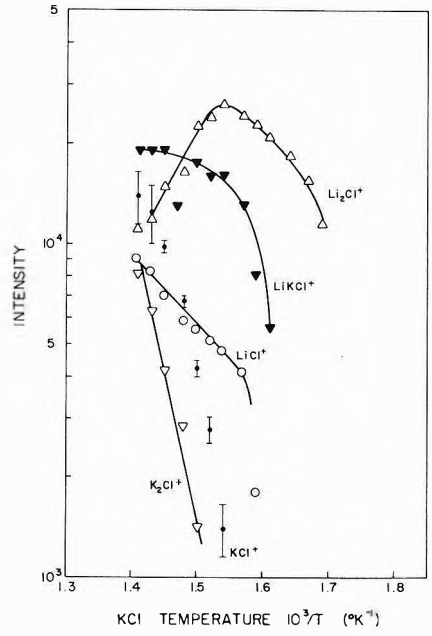

Figure 1. Measured mass spectrometric intensities (corrected for isotopic ratios and mass transmission probability) *vs.* reciprocal bulk crystal temperature for reaction products of LiCl beam with KCl crystal. The effusion cell temperature was held constant at 784°K.

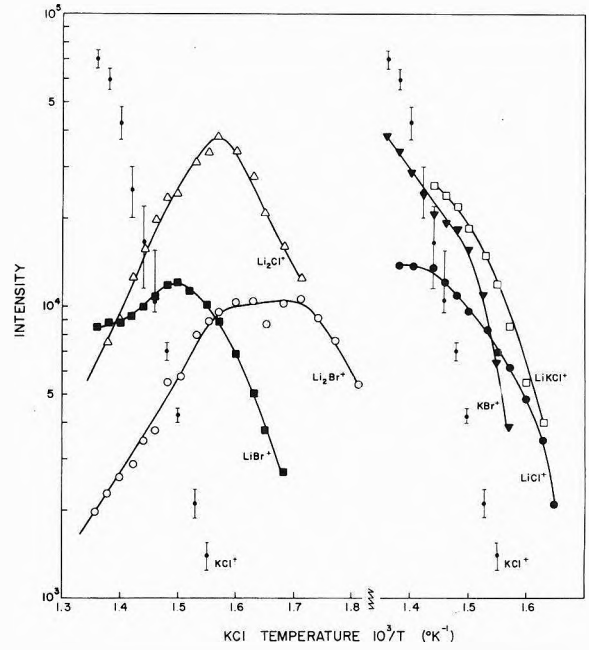

Figure 2. Measured mass spectrometric intensities (corrected for isotopic abundance and mass transmission probability) *vs.* reciprocal bulk crystal temperature for reaction products of LiBr beam with KCl crystal. The effusion cell temperature was held constant at 743°K.

TABLE I: Temperatures (°K) at which Certain Species Show a Change in Slope in P/T and I *vs* $1/T$ Plots[a]

	Effusion cell temperature			
	763	773		784
	Effective beam pressure			
	1.4×10^{-10}	2.1×10^{-10}		3.4×10^{-10}
	LiCl/KCl			
Li_2Cl^+	639	658		650
	Effusion cell temperature			
	729	737	743	753
	Effective beam pressure			
	1.0×10^{-10}	1.5×10^{-10}	2.0×10^{-10}	2.9×10^{-10}
	LiBr/KCl			
$LiBr^+$	655	654	665	673
LiBr(calcd)	630	630	640	640
Li_2Cl^+	635	633	636	643
Li_2Cl_2(calcd)	660	670	670	680
Li_2ClBr(calcd)	630	640	640	650
Li_2Br^+	624	633	626	633

[a] For measured ion intensities this is the KCl bulk crystal temperature. Effective beam pressure (atm) = $4.0 \times 10^{-4}[P_{eq}(LiX) + 2P_{eq}(Li_2X_2)]$.

and dimers were used to calculate the K_p's using the formula

$$K_p(T) = \exp\left[\frac{\Delta FEF}{R} - \frac{\Delta H^\circ_{298}}{RT}\right] \quad (6)$$

For the mixed dimer no thermochemical data were available so an average free energy function (FEF), corrected for rotational entropy differences[10] and an average ΔH°_{298}, were calculated from the $(MX)_2$ dimer data.

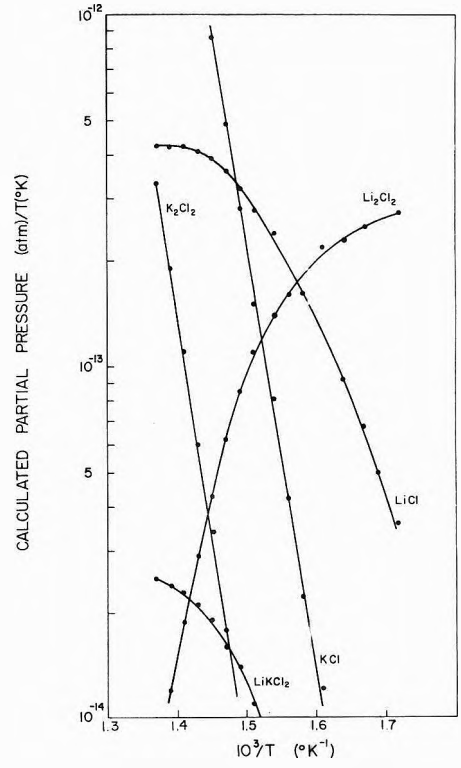

Figure 3. Calculated equilibria partial pressures of a mixture of LiCl and KCl divided by its temperature *vs.* reciprocal temperature. The initial P_{LiCl} corresponds to the effective (monomer) beam pressure of our effusion cell at 784°K.

To simulate our reaction conditions the "effective beam pressure" of the LiCl at the crystal surface was calculated from the equilibrium pressure of the LiCl in the cell at the temperature of operation. It should be noted that approximately 50% of the beam at our effusion cell operating temperatures is Li_2Cl_2, but for our calculation we as-

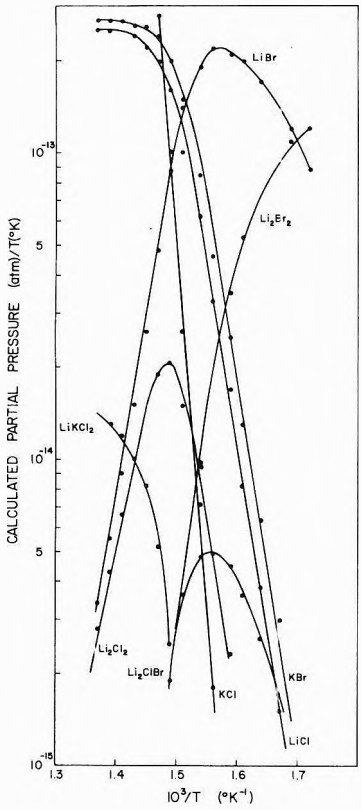

Figure 4. Calculated equilibria partial pressures of a mixture of LiBr and KCl divided by its temperature *vs.* reciprocal temperature. The initial P_{LiBr} corresponds to the effective (monomer) beam pressure of our effusion cell at 743°K.

sumed all the incident molecules to be monomers. Thus, our particular source 4.0×10^{-4}).[10] The initial P_{KCl} is a sum of $P_{eq}(LiCl)$ and $2P_{eq}(Li_2Cl_2)$, multiplied by the geometric probability of a molecule reaching the surface (for our particular source 4.0×10^{-4}).[10] The initial P_{KCl} is a function of the crystal temperature (we assume the reactions take place between the beam and KCl molecules adsorbed on the surface). In the temperature range studied, the KCl crystal is vaporizing, that is $KCl_{crys} \rightarrow KCl_{ads} \rightarrow KCl_{gas}$,[11] and we have assumed that the initial "effective pressure" of KCl at any temperature is the crystal's equilibrium vapor pressure multiplied by a vaporization coefficient of 0.5.[12] "Calculations were made of the equilibrium partial pressures of the five possible species present for the temperature range 580–730°K based on a constant LiCl pressure and a KCl pressure that is proportional to the KCl vapor pressure." A plot of P/T for these species is shown in Figure 3.

A similar treatment of the LiBr–KCl system was done. To solve for the 13 partial pressures, three "pressure conservation" equations and ten equilibrium expressions were used. In addition to the dimerization reactions, the exothermic exchange reaction of the LiBr and KCl to form LiCl and KBr was used. Figure 4 is a plot of P/T for the species in this system which correspond to products measured for the gas–solid reaction. Table I lists the system temperatures at which certain calculated partial pressures exhibit changes of slope in the log P/T *vs.* $1/T$ plots.

Discussion

First, we wish to point out that we have adopted an equilibrium calculation for comparison with our data not because we feel that an equilibrium model adequately represents the system behavior, but to test the model with this type of system. A comparison of the experimental results of the beam–crystal reactions with the calculated gas-phase equilibrium partial pressures assumes that in the reaction taking place between the adsorbed beam molecules and the crystal surface molecules, the reactants can be represented by a gas with two degrees of translational freedom and full rotational and vibrational freedom. It also presumes that the desorption energies of all the molecules are identical, that only one degree of translational freedom is added during the desorption, and that all molecules desorb. Thus, if the beam thermally and chemically equilibrates with the crystal, then the product intensities should follow the calculated intensities (with arbitrary scaling to account for mass spectrometer constants). As can be seen from the figures, this is not the case, but there are several interesting similarities.

A rough calculation was made in order to determine if the data satisfied the condition of conservation of beam elements for the LiBr–KCl case. The calculated spectrometer sensitivity based on the vapor pressure of the KCl crystal and estimates of the ionization cross sections of the dimers relative to the monomers were used to convert the experimental ion intensities of Figure 2 to fluxes of molecules leaving the surface. The Br^+ contribution to the $LiKCl^+$ intensity was estimated to be the measured intensity of mass 81 at the lowest crystal temperature. This was subtracted out before each LiKClX flux was calculated. Again Li_2Br^+ was considered to be formed mostly from Li_2Br_2, while for this calculation Li_2Cl^+ and $LiKCl^+$ were assumed to have equal contributions from M_2ClBr and M_2Cl_2. In the high- (crystal) temperature region where the Li_2Br^+, Li_2Cl^+, and $LiBr^+$ intensities are increasing and the $LiCl^+$, KBr^+, and $LiKCl^+$ intensities are decreasing as the temperature is lowered, the two summations of fluxes of the Li and Br containing species at each temperature are constant within a factor of 1.5. Thus there is a conservation of beam elements at the high temperatures. In the low-temperature region these two sums decrease with temperature as the beam elements remain on the surface.

For the LiBr–KCl system, it is apparent in Figures 2 and 4 that the slopes and relative positions of corresponding species are in poor agreement between the experiment and calculation. Only the slopes of the KCl curves are similar. The calculated pressures of two products, K_2Br_2 and $LiKBr_2$, were of equal or greater magnitude than some of the measured products, but these two could not be detected. However, Table I shows that the trends with increasing beam flux where certain species reach a maximum are similar between the calculation and experiment, although the temperatures themselves are not. One can predict from the calculation a decrease in KCl pressure upon beam impingement which is in agreement with experiment. And there is a qualitative agreement about which species reach a maximum (with the exception of Li_2Br_2 since no sticking coefficient is included in the calculation).

For the LiCl–KCl case, the conclusions are similar although the slopes in Figures 1 and 3 are more nearly the same. Again, $P_{Li_2Cl_2}/T$ continues to increase as the temperature is lowered since no sticking coefficient is included. The beam actually increased the KCl leaving the surface, probably because of the additional Cl on the surface.[13] Auger measurements of the (100) surfaces of several alkali halides have indicated that the surfaces are non-

stoichiometric.[14] Since the Cl from the beam and crystal could not be distinguished, either experimentally or in the calculation, the LiCl beam is not expected to exhibit the same trend as the LiBr beam material did, and it does not (Figure 1).

Lowering the crystal temperature while maintaining a constant beam flux increases the association of monomers on the surface as evidenced by the Li_2Cl^+ and Li_2Br^+ curves in Figures 1 and 2. At the low crystal temperatures where no KCl^+ was detected, these two ions, whose progenitors are presumed to be Li_2Cl_2, Li_2ClBr, and Li_2Br_2, were the dominant species measured. Their measured intensities eventually decrease, presumably because the desorption activation energy cannot be overcome or because they associate into higher polymers as the temperature is decreased further. The formation of the mixed dimers, LiKClBr and $LiKCl_2$, is also thermodynamically favored as the crystal temperature is decreased, but the accompanying decrease in surface KCl causes a net drop in the measured $LiKCl^+$. The $LiBr^+$ trend is the result of there being a high surface KCl concentration at high temperatures which can react with the beam LiBr to form LiCl and KBr. At lower temperatures there are fewer KCl molecules on the surface and the quantity of LiBr reevaporated from the crystal increases. At still lower temperatures the dimerization reaction to Li_2Br_2 is more favorable and consequently the $LiBr^+$ intensity decreases.

There are several obvious flaws in the model that could be corrected without too much effort if one is willing to adopt a steady-state kinetic model rather than an equilibrium model. First, not all of the beam material adsorbs on the surface. Schoonmaker and Lo reported a condensation coefficient of 0.99 for a NaCl beam on a NaCl crystal at 675°K.[4] We feel that α is lower for our particular systems. Second, the activation energies of desorption for the products certainly differ. By including individual activation energies in the calculations, one would increase the complexity of the minimization problem drastically. Since the numbers are essentially unknown, the energies would have to be treated as parameters and the experimental curves fit. We are presently measuring decay curves (upon shuttering the beam) for several of the species present in the hopes that adequate experimental data can be obtained to determine the activation energies of desorption. Finally, a reaction path leading to the incorporation of beam molecules into the lattice would have to be included if beam condensation, not accompanied by reevaporation, were appreciable.

Acknowledgment. The authors thank the National Science Foundation for support of this research. R. B. thanks Nancy Sell for development of the apparatus and William Marx for help with computer programming.

References and Notes

(1) Address correspondence to GTE Laboratories, Waltham, Mass. 02154.
(2) (a) J. C. Batty and R. E. Stickney, *J. Chem. Phys.*, **51**, 4475 (1969); (b) M. Blander, *ibid.*, **41**, 170 (1964).
(3) R. C. Schoonmaker and R. F. Porter, *J. Chem. Phys.*, **30**, 282 (1959).
(4) R. C. Schoonmaker and V. Lo, *J. Chem. Phys.*, **58**, 727 (1973).
(5) J. E. Lester, *Rev. Sci. Instrum.*, **41**, 1513 (1970).
(6) N. J. Sell, Ph.D. Dissertation, Northwestern University, 1971.
(7) L. Friedman, *J. Chem. Phys.*, **23**, 477 (1955).
(8) J. Berkowitz and W. A. Chupka, *J. Chem. Phys.*, **29**, 653 (1958).
(9) "JANAF Thermochemical Data," Dow Chemical Co., Midland, Mich., 1965.
(10) W. Marx, unpublished data.
(11) J. P. Hirth and G. M. Pound, *J. Chem. Phys.*, **26**, 1216 (1957).
(12) R. S. Bradley and P. Volans, *Proc. Roy Soc.*, **217**, 508 (1953).
(13) N. J. Sell, W. F. Marx, and J. E. Lester, *High Temp. Sci.*, **4**, 222 (1972).
(14) T. E. Gallon, I. C. Higginbotham, M. Frutton, and H. Tokutaka, *Surface Sci.*, **21**, 224, 241 (1970).

Thermotropic Mesomorphism in Chiral Carbonylbis(amino acid esters)

C. H. Lochmüller* and R. W. Souter

P. M. Gross Chemical Laboratory, Duke University, Durham, North Carolina 27706 *(Received July 2, 1973)*

A number of optically active carbonylbis(amino acid esters) have been found to show at least one phase transition prior to forming the isotropic liquid. Wide-line proton nuclear magnetic resonance, polarizing microscopy, and differential scanning calorimetric methods were used to study the mesophase behavior of the chiral compounds, which are useful as stationary phases for the direct gas chromatographic resolution of enantiomers. Results of polarizing microscopy and of differential scanning calorimetry experiments (including determination of enthalpies and entropies of phase transitions) indicate that the mesophases are smectic, and wide-line nuclear magnetic resonance results show that a significant amount of molecular motion exists in the preisotropic liquid temperature regions.

Introduction

Numerous organic compounds exhibit mesophase behavior, the major structural requirements being that the molecules have a high length-to-width ratio and that they contain dipolar or readily polarizable groups.[1] A significant amount of research has been devoted to studies of properties and uses of liquid crystalline materials[2-4] but with the exception of cholesteryl esters, very little work exists for characterization of mesophases exhibited by optically active compounds.[5,6]

In some polymeric ester species the great freedom of mobility has been attributed to the ability of the ester OCO groups to act as hinges,[7] and in a large number of cholesteryl alkanoates it has been postulated that ester carbonyls contribute major cohesive forces between molecules in the cholesteric mesophase.[8] Nuclear magnetic resonance (nmr) has proven quite useful as a tool for the examination of liquid crystalline phase transitions and for study of oriented solutes[2] and it is well established that nmr is an excellent method to study molecular motion in polymeric species.[7] Resonance lines for solids often sharpen considerably with increasing temperature as motions of groups and segments of polymeric chains are freed. In particular, wide-line nmr has also been used to observe phase transitions in various plastic crystals[9] and to study orientation effects for an ordered smetic phase.[10]

Thermal and optical methods have been used extensively in studies of phase transitions in liquid crystalline compounds. Differential thermal analysis (dta) and differential scanning calorimetry (dsc) have proven to be well suited to determination of transition temperatures and of heats and entropies of transitions.[11-15] Polarizing microscopic observations and combinations of those with thermal measurements[16-18] have aided identification and characterization of mesophases, and thermodynamics of solution with liquid crystalline solvents has been studied by dsc and by gas–liquid chromatography (glc).[19,20]

For this work, nuclear magnetic resonance, polarizing microscopy, and differential scanning calorimetric methods were combined to elucidate the mesomorphic behavior discovered in a series of chiral carbonylbis(amino acid esters), and the results are presented below.

Experimental Section

Preparation of Materials. The carbonylbis(amino acid esters) were prepared by the condensation of the appropriate amino acid esters with phosgene, and the structures were verified as previously described.[21,22] Each compound was recrystallized from cyclohexane (except the valine isopropyl ester compound, which was recrystallized from dioxane–water) and was found to be pure by thin-layer chromatography on silica gel in at least two solvents. All physical properties of the valine isopropyl ester compound were identical with those of a previously examined commercial sample (from Miles-Yeda, Rehovoth, Israel).

Differential Scanning Calorimetry. A Perkin-Elmer DSC-1 differential scanning calorimeter was used for all experiments. Aluminum planchets with crimp-sealed covers were used to contain the samples. Heating and cooling rates of 5°/min were used throughout, and the calorimeter was continuously purged with dry N_2 gas.

In each dsc measurement the peak maximum of the recorded trace was taken as the transition temperature (peak maxima actually indicate the temperatures at which the transitions are proceeding at the maximum rate). A pure indium metal standard was used to check the temperature scale and to calibrate the caloric response of the system,[23] and heats of transition (q) were calculated knowing the sensitivity, the weights of samples and standard, the heat of fusion of the standard, and the appropriate peak areas. Entropies were calculated by dividing transition heats by absolute temperature (q/T). Relative areas of sample peaks were obtained by first electrostatically copying the charts onto heavy, uniform paper and then cutting out the peaks and weighing them on an analytical balance (with precautions to avoid buoyancy effects). Typically the sample weights were 4–8 mg.

Polarizing Microscopy. A Bausch and Lomb Optical Co. polarizing microscope CK 7656 with 10× magnification, strain-free optics, a heated stage, and provision for photomicroscopy was used for all studies reported.

All samples were prepared by melting a small amount of the compound between two microscope slides. Adequate time was allowed after preparation of samples and also between experiments for the compounds to cool to normal crystalline solids at room temperature.

Nuclear Magnetic Resonance. Proton spectra for a carbonylbis(L-valine isopropyl ester) sample in a 5-mm tube were recorded using a Bruker HFX-90 spectrometer operating in either the wide-line or the high-resolution mode. In the wide-line experiments the signal modulation amplitude was adjusted to the maximum level which did not

TABLE I: Thermal Transition Properties of Carbonylbis(amino acid esters)

Compound	Transition temp, °K[a]	Transition heat, q, kcal/mol[b]	Transition entropy, ΔS, cal/mol °K	% total ΔS for smectic → isotropic
Carbonylbis(L-valine methyl ester)	382 C → S	0.73	1.91	69
	415 S → I	1.73	4.17	
Carbonylbis(L-valine ethyl ester)	361 C → S	0.44	1.21	81
	388 S → I	2.00	5.15	
Carbonylbis(L-valine isopropyl ester)	364 C → S	2.25	6.18	38
	372 S → S′	0.10	0.27	
	382 S′ → I	1.55	4.06	
Carbonylbis(L-valine *tert*-butyl ester)[c]	398 S → C	1.54	3.87	68
	402 I → S	3.27	8.13	
Carbonylbis(D-leucine isopropyl ester)	328 C → S	5.38	16.4	7.9
	383 S → I	0.54	1.40	

[a] C = crystal, S = smectic, I = isotropic. [b] Heats of transition calculated based on ΔH_f of indium, 780 cal/mol. [c] Results based on cooling curves: heating produced only one broad transition at 427°K. The reported temperature are *transformation* temperatures.

artifically broaden the resonance line. The reported temperatures were maintained at ±0.2° in the sample area of the insert using a Bruker B-ST 100/700 temperature control unit. The spectrometer was adjusted to minimize any field drift and was run unlocked. Resolution of the magnet measured in a 5-mm insert using o-dichlorobenzene was better than 0.08 Hz (at 90 MHz) in the normal high-resolution mode.

Results

The general structure of the carbonylbis(amino acid esters) is shown in I. Each compound has two asymmetric centers of the same optical configuration. In the leucine compound R′ is isobutyl and R is isopropyl, while in the valine series R′ is isopropyl and R is methyl, ethyl, isopropyl, or *tert*-butyl.

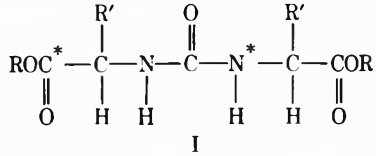

I

Results of the calorimetric measurements are shown in Table I. The *tert*-butyl ester compound exhibits monotropic behavior. Only one peak appears upon heating (427°K), but when the sample is cooled at the same rate two peaks appear (4° apart) which are displaced in temperature from the peak position in the heating cycle. A sample of the *tert*-butyl compound was zone refined for 24 hr and again examined by differential scanning calorimetry. Even at a very low heating rate of 1.25°/min, still only one peak was observed. Because the two peaks from cooling were displaced in temperature from the position of the heating cycle peak, the phase change temperatures reported are really transformation temperatures (rather than transition temperatures), or the temperatures at which rates of transformation become appreciable.

Three phase transitions were detected for carbonylbis(L-valine isopropyl ester) whereas only two were found for the methyl and ethyl analogs. A sample of the valine isopropyl ester compound was subjected to 24 hr of zone refining and the resulting material showed essentially no change in the calorimeter trace (compared to an unrefined sample) or in any other measured properties.

Wide-line nmr experiments were conducted with carbonylbis(L-valine isopropyl ester). The sample was melted into a 5-mm tube, cooled, and then examined as a function of temperature until it melted to an isotropic liquid. The three phase transitions detected by dsc and by polarizing microscopy were again observed. The onset of a large degree of molecular motion at the first phase transition was seen as a dramatic line narrowing. A similar effect was observed at the second transition, and finally again at the point where the sample turned to isotropic liquid, after which the line width remained essentially constant.

Resonance lines sharpened so significantly in the wide-line experiments at the phase transition temperatures of carbonylbis(L-valine isopropyl ester) that examination by high-resolution proton nmr was warranted. In the spectra as a function of temperature, phase changes were clearly observable as narrowed lines and large signal amplitude increases (Figure 1).

Viewed under crossed polarizers, the carbonylbis(L-valine isopropyl ester) preparation used for the photomicrographs in Figure 2 displayed a brilliant blue as the predominant birefringent color. This blue background of the solid phase up to the first phase transition was interrupted by irregular fissures and brightly colored areas (2A). At 91° a dramatic change of the blue background to red violet occurred and the interrupting areas became mostly gray shades. In addition, the whole sample appeared as a field of irregularly shaped plates (2B). The second change occurred at 100° when the purple background and the gray areas broke into smaller sections bounded by fine white or yellow lines and the sample acquired a grainy texture (2C). Finally at about 109° as the isotropic liquid quickly formed, a dark background displaced the smooth-edged very bright plates of the sample (2D).

The room temperature solid phase of carbonylbis(L-valine ethyl ester) appeared as a very highly ordered pattern under crossed polarizers, and the major colors were gray-violet and gray. The line patterns or striations became much rougher at 93° and darkened. At 108° dark areas between the light striations began to expand, and finally

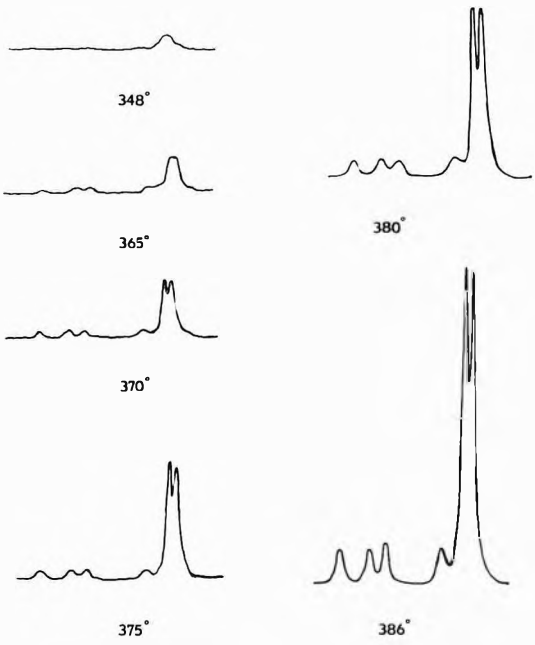

Figure 1. High-resolution nmr spectra of carbonylbis(L-valine isopropyl ester) as a function of temperature: solid at 348°; first smectic mesophase 365°, 370°; second smectic mesophase 375°, 380°; isotropic liquid 386°.

darkened the whole field as the isotropic liquid formed. Upon cooling, white cloudy areas appeared on the dark background, and suddenly the ordered white patterns formed. Thereafter the patterns returned to the shaded, highly lined type initially described.

Upon heating to 107°, carbonylbis(L-valine methyl ester) under crossed polarizers lost its crystalline appearance and all colors in the field sharpened and changed to completely different shades. Small droplets also appeared, each composed of a series of concentric rings. These gradually disappeared until at 141° and above the isotropic liquid darkened the background completely.

Viewed under crossed polars, the carbonylbis(L-valine *tert*-butyl ester) sample acquired a granular texture as clear droplets began forming at 150°. The red-brown and blue-violet colors became quite diffuse at that point and at 155° the sample had melted to isotropic fluid. Upon cooling, white lined patterns moved across the field in one direction, and within another 5° a gray front swept across the field from the opposite direction.

At slightly above 60°, the carbonylbis(D-leucine isopropyl ester) sample as viewed under crossed polarizers lost its brown crystalline appearance as the field brightened. At this point a number of irregularly shaped, multicolored smooth platlets were formed which were randomly spotted with small vacuoles. These smooth areas expanded rapidly at 100–112° to leave a field of isotropic fluid.

Discussion

Quite good correlation was found to exist between the transition temperatures determined by nmr, dsc, and optical observation of the morphological forms, and the same number of mesophase transitions was noted for each compound by each method used in its study. The temperature range over which mesomorphic behavior was observed decreased as the size of the ester group increased in the valine series (Table I).

Results of a detailed wide-line nmr study of the thermal behavior of carbonylbis(L-valine isopropyl ester) indicate onset of a significant amount of molecular motion at the first phase transition and rapid increase in that motion with rising temperature. The increasing molecular mobility is quite likely to be associated with loosening of ester carbonyl groups as the order of the crystal lattice is lost.[7] High-resolution nmr experiments with this compound show the ester methyls and valine isopropyl methyls to have the largest gain by far in signal amplitude as temperature increases through the mesophase range.

Per cent of the total transition entropy due to the transition to isotropic liquid has been calculated as this offers a criterion for deciding whether that transition is cholesteric → isotropic, nematic → isotropic, or smetic → isotropic.[12] Table I shows the mesophase → isotropic entropy gain to be a large percentage of the total ΔS for each compound.

Entropy changes at cholesteric → isotropic and at nematic → isotropic transitions are a very small percentage (<5%) of the total, while for smectic → isotropic transitions, the ΔS percentage may be greater by an order of magnitude or more.[12] Based on these thermodynamic criteria, the mesophase → isotropic transitions for the compounds in Table I are very probably smetic → isotropic in each case.

Smectic states are closely allied with the true crystalline state[24] and this high order is evidenced by the fact that they always occur over lower temperature ranges than nematic or cholesteric phases which may occur in the same compound. This observation would require that the small 372°K phase transition of carbonylbis(L-valine isopropyl ester) is a transition between two different smectic states.

Hydrogen bonding of disubstituted ureas in solution has been proposed to be *via* formation of very stable six-member rings[25] as II and from X-ray analysis, the same type of bonding is known to exist for crystalline urea.[26]

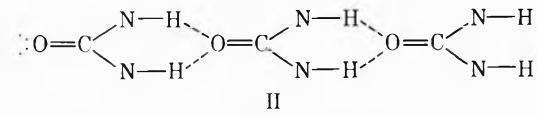

II

Carbonylbis(amino acid esters) in the crystalline state may be similarly bonded, with weak van der Waals attractions at the terminal OCO moieties. Crystal → smectic transitions may involve breakdown of these weak terminal attractions with consequent free rotation of the OCO groups. The nmr results presented showed large signal amplitude increases for valine isopropyl methyls and for isopropyl ester methyls in smectic temperature regions of carbonylbis(L-valine isopropyl ester). Loss of weak terminal attractions with retention of strong hydrogen bonding of urea portions of the compounds would yield arrangements of parallel molecular layers with molecular axes normal to the layers, which is the normal smectic orientation.[24] Weakening or breaking of the strong amide bonds at the transition to nonordered, isotropic fluid might be expected to yield large entropy changes.

The temperature range over which smectic behavior was observed decreased as the size of the ester group increased in the valine series (see Table I). This may perhaps indicate that terminal attractions decreased as the size of the ester alkyl group increased from methyl up to *tert*-butyl (where a very small smectic range was observed).

The conclusion from the dsc results that the mesophases preceding the isotropic liquid may in each case be smectic is supported by some polarizing microscopy obser-

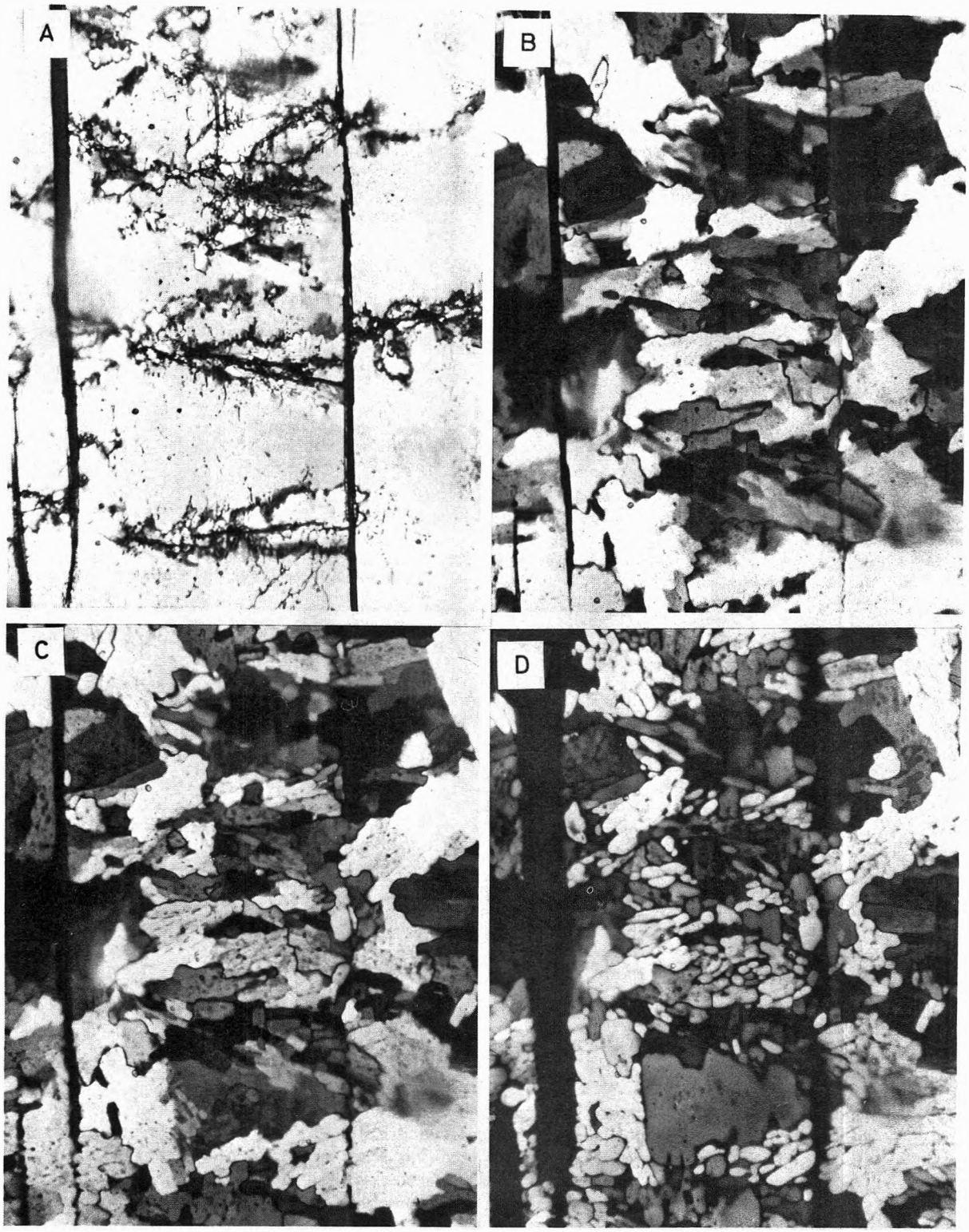

Figure 2. Polarized photomicrographs of carbonylbis(L-valine isopropyl ester): (A) crystalline solid, (B) first smectic phase, (C) second smectic phase, and (D) changing to isotropic liquid.

vations. The methyl ester compound formed ringed droplets, possibly a form of the stepped drops characteristic of some smectic mesophases.[1] Furthermore, in the second mesophase region for carbonylbis(L-valine isopropyl ester), formation of small rods or needles was observed. These elongated, irregularly shaped birefringent bodies may be another focal-conic arrangment, the "batonnets" described by Gray.[1] No threaded textures or spherical droplets bearing crosses of arms were observed for any mesophase upon heating or cooling. These would be indicative of the existence of a nematic phase. In addition, no rapid or violent motion of particles, often characteristic of nematic phases, was observed. This evidence, taken with the dsc results, would seem to indicate that the mesophases which form prior to the isctropic liquid in each compound are smectic.

Conclusions

Mesomorphic behavior which has been discovered in a series of optically active carbonylbis(amino acid esters) has been characterized by several methods. The phase transition temperature ranges in the L-valine ester series are affected by changes of ester substituent. On the basis of entropy calculations from dsc measurements and of microscopy observations, it is apparent that the mesophases are most likely smectic. Comparison of carbonylbis(L-valine isopropyl ester) and carbonylbis(D-leucine isopropyl ester) shows that replacement of the valine isopropyl chiral center substituent by isobutyl in the leucine compound radically changes the observed thermal behavior, but the mesophase is still smectic.

Acknowledgment. The authors are indebted to the Research Corporation of New York for a Cottrell Research Grant, and to the National Science Foundation for supplying part of the funds for the purchase of the Bruker HFX-90 nmr spectrometer. The loan of the microscopy equipment for the authors' use by Dr. Jacques Poirier of this Department is also gratefully acknowledged.

References and Notes

(1) G. Gray, "Molecular Structure and the Properties of Liquid Crystals," Academic Press, London, England, 1962.
(2) G. Brown, J. Doane, and V. Neff, "A Review of the Structure and Physical Properties of Liquid Crystals," CRC Press, Cleveland, Ohio, 1971.
(3) G. Brown, G. Dienes, and M. M. Labes, "Liquid Crystals," Gordon and Breach Science Publishers, London, England, 1966.
(4) T. Kallard, Ed., "Liquid Crystals and Their Applications," Optosonic Press, New York, N. Y., 1970.
(5) W. Helfrich and Chan Oh, *Mol. Cryst. Liquid Cryst.*, **14**, 289 (1971).
(6) M. Leclercq, J. Billard, and J. Jacques, *Mol. Cryst. Liquid Cryst.*, **8**, 367 (1969).
(7) I. Slonim and A. Lyubimov, "The NMR of Polymers," Plenum Press, New York, N. Y., 1970.
(8) H. Gibson and J. Ponchan, *J. Phys. Chem.*, **77**, 837 (1973).
(9) I. Darmon and C. Brot, *Mol. Cryst.*, **1**, 417 (1966).
(10) J. DeVries and H. Berendsen, *Nature (London)*, **221**, 1139 (1969).
(11) E. Barrall, II, R. Porter, and J. Johnson, *Mol. Cryst.*, **3**, 299 (1968).
(12) R. Porter, E. Barrall, II, and J. Johnson, *Accounts Chem. Res.*, **2**, 53 (1969).
(13) E. Barrall, II, R. Porter, and J. Johnson, *J. Phys. Chem.*, **71**, 895 (1967).
(14) E. Barrall, II, R. Porter, and J. Johnson, *J. Phys. Chem.*, **71**, 1224 (1967).
(15) E. Barrall, II, R. Porter, and J. Johnson, *J. Phys. Chem.*, **70**, 385 (1966).
(16) S. Jabarin and R. Stein, *J. Phys. Chem.*, **77**, 399 (1973).
(17) E. Barrall, II, R. Porter, and J. Johnson, *Mol. Cryst.*, **3**, 103 (1967).
(18) N. Hartshorne and A. Stuart, "Crystals and the Polarizing Microscope," 4th ed, Edward Arnold, Ltd., London, England, 1970, pp 503–555.
(19) D. Martire, P. Blasco, P. Carone, L. Chow, and H. Vicini, *J. Phys. Chem.*, **72**, 3489 (1968).
(20) L. Chow and D. Martire, *J. Phys. Chem.*, **73**, 1127 (1969).
(21) C. Lochmuller and R. Souter, *Org. Magn. Resonance*, in press.
(22) C. Lochmüller, J. Harris, and R. Souter, *J. Chromatogr.*, **71**, 405 (1972).
(23) "Selected Values of Chemical Thermodynamic Properties," National Bureau of Standards Circular 50V, U. S. Government Printing Office, Washington, D. C. 1952.
(24) S. Petrie, H. Bücher, R. Klingbiel, and P. Rose, Eastman Organic Chemical Bulletin No. 45 (1973), Eastman Kodak Co., Rochester, N. Y.
(25) T. Kozlova, N. Kozlov, and V. Zharkov, *Russ. J. Phys. Chem.*, **45**, 1197 (1971).
(26) I. Millar and H. Springall, "A Shorter Sidgwick's Organic Chemistry of Nitrogen," Clarendon Press, Oxford, 1969, p 169.

Physical Properties of Thin Soap Films Measured by Electron Spin Resonance Exchange Broadening

M. J. Povich*[1] and J. Adin Mann

Department of Biochemistry and Biophysics, University of Hawaii, Honolulu, Hawaii 96822 *(Received February 25, 1972)*

The dependence of esr exchange broadening on viscosity is employed to study the physical state of thin soap films. This is accomplished by forming a cylindrical soap film inside of a rectangular esr sample cavity, and subsequently recording the esr spectrum of a nitroxide free radical dissolved in the soap film. The exchange broadening phenomenon is dependent upon the translational mobility of the free radical and is markedly more sensitive to changes in shear viscosity than rotational effects (high-field broadening). No abnormal viscosity effects were observed in the thin soap films studied.

Introduction

The purpose of this paper is to report a study of the physical state of thin soap films. The primary justification of this work is the relevance of soap films to the study of molecular forces.

In the study of van der Waals and electric double layer forces, the soap film offers several natural advantages and has been investigated in some detail in this connection.[2-4] However, the usefulness of the soap film in the study of molecular forces explicitly depends upon a thorough understanding of its physical properties and structure. The most widely accepted structure for a soap film is the sandwich model, which has been developed primarily from thickness and composition studies.[5] The sandwich model consists of an aqueous core sandwiched between two monolayers of surfactant. De Vries[4] applied the

LVDO theory of colloid stability to the sandwich model and separated the soap film forces into van der Waals attraction, π_{vdw}, electrical double layer repulsion, π_{el}, and hydrostatic pressure (for vertical films), π_h. At the equilibrium thickness

$$\pi_{el} + \pi_{vdw} + \pi_h = 0 \quad (1)$$

With this model, experiment and theory are in moderate agreement. At high ionic strength, however, the double layer repulsion is of shorter range so that the thinning forces should lead to film collapse. The stability of soap films at high ionic strength has resulted in uncertainty concerning the physical state of the soap film aqueous core. Deryagin[2a] suggested that a rigidfied water structure opposed the thinning forces. Similarly, Gibbs proposed a "hydrous-gel" exists. Henniker[6] stated that the stability of thin soap films is itself evidence of rigidity in water near surfaces.

In this paper we report a study of the physical state of thin soap films using free radical probes and electron spin resonance.

The technique consists of dissolving a water-soluble nitroxide free radical in a surfactant solution, and then forming a soap film inside an esr cavity. The esr spectrum of the free radical, which is sensitive to viscosity, is obtained after the film reaches its equilibrium thickness. In general, we have found the viscosity of the soap film to be similar to the bulk surfactant solution.

Exchange Broadening

Many free radicals and transition metal complexes can be used to study colloidal systems by esr. However, due to their stability, versatility, and relatively simple esr spectrum, nitroxide free radicals (NFR) have been widely used. An example of a NFR, which is often called the spin-labeled alcohol (SLOH), is illustrated in Figure 1. The effect of orientation and rotational motion on the esr spectrum of NFR's has been intensively studied.[7-12]

In this work we are concerned with the *translational mobility* of SLOH.

As the concentration of SLOH increases each of the three hyperfine lines begin to broaden. According to Pake and Tuttle,[13] the important line-broadening mechanism is electron spin exchange which occurs upon collisions between NFR's. Assuming that exchange takes place during each encounter, the exchange contribution to the esr line width is proportional to T/η

$$\Delta\omega(\text{Gauss}) = (1/\pi\sqrt{3})(hZ/g\beta)(N_R/N_S)(k/\pi b\lambda^2)(T/\eta) \quad (2)$$

where η is the viscosity, Z is the number of new neighbors encountered in a random jump of length λ, N_R and N_S are the numbers of free radical and solvent molecules per unit volume, and b is the radius of the free radical. A number of workers[14-16] have investigated the exchange phenomenon in various solvents and have found regions of concentration, temperature, and viscosity where the exchange contribution to the line width is directly proportional to T/η as the collision theory predicts.

The T/η dependence of the line width for SLOH in aqueous glycerol mixtures is presented in Figure 2. The deviations from linearity at low values of T/η are due to rotational effects. At high values of T/η the broadened hyperfine lines begin to coalesce into one line, and eventually exchange narrowing occurs. As $T/\eta \to 0$, the value of the intercept increases with concentration. This has been attributed to a static dipole–dipole broadening by Edelstein, *et al.*[15] A good fit between experimental and theoretical slopes is obtained for $Z = 3$ new neighbors and $b = \lambda = 4$ Å.

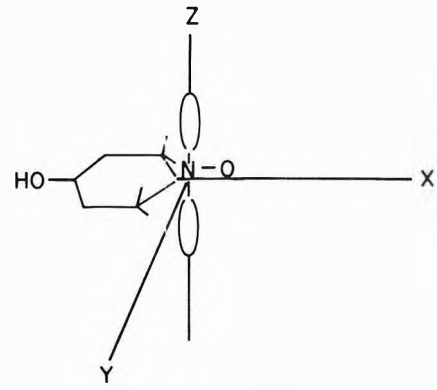

Figure 1. A nitroxide free radical, spin-labeled alcohol (SLOH). The unpaired electron density is characterized by the p-orbital distribution on nitrogen.

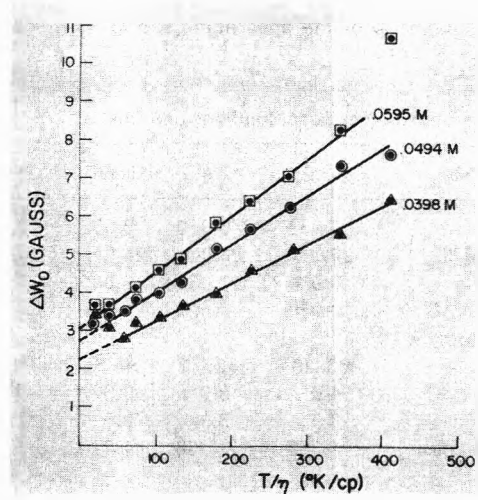

Figure 2. Center line width ($M = 0$) of SLOH as a function of T/η, illustrating the exchange contribution to the line width. Measurements were performed on SLOH dissolved in 51 wt % glycerol. T/η was changed by varying the temperature.

Methods and Materials

In our earlier work,[17] we formed a rectangular soap film inside of an esr TE_{012} cavity using a wire frame. Due to evaporation and the possibility of wire frame effects, the earlier results were difficult to interpret.

In the present study, the wire frame has been eliminated by forming cylindrical soap films, using the system illustrated in Figure 3. Only the cylindrical soap film was allowed inside the sensitive region of the cavity. As an additional precaution, a brass side plate with a narrow horizontal slot was adapted to each side of the cavity to reduce the amplitude of the modulating (100 kHz) magnetic field near the top and bottom of the cavity.

Before a soap cylinder was formed, the spectrum of the cavity (clean) and frame (wet with solution) was taken. No signal could be obtained from the cavity and frame at the gain and modulation amplitude used to observe the subsequent films.

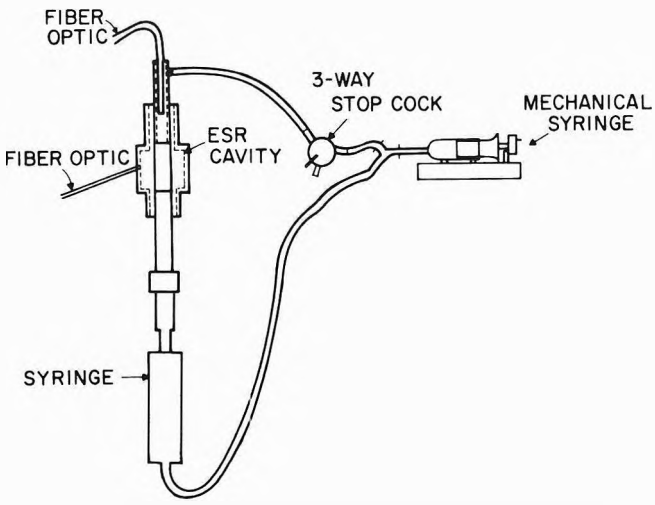

Figure 3. Schematic of the apparatus used to form soap cylinders in a TE_{012} esr cavity.

TABLE I: Composition of Soap Solutions and Results

Composition	Film I	Film II	Film III	Film IV
SLOH, *M*	0.052	0.052	0.052	0.052
Glycerol, wt %	24.0	24.0	24.0	3.0
HDTAB, *M*	0.030	0.030	0.030	0.027
NaCl + HDTAB, *M*	0.030	0.590	1.57	0.027
Film thickness, Å (exptl)	263–294	52–71	50–63	278–331
W_0 (flat cell), G	4.0	3.9	3.6	5.4
W_0 (film), G	3.9	3.9	3.6	7.5
Refractive index	1.363	1.368	1.376	1.338

Once the film thins to about 2000 Å spectra may be taken; however, the microwave power must be kept low to reduce heating of the film. As the soap film approaches its equilibrium thickness (black soap film) spectra may be obtained at higher microwave power and without instrumental drift.

All chemicals used were reagent grade unless otherwise specified. The hexadecyltrimethylammonium bromide (HDTAB) was purchased from Eastman Organic Chemicals and recrystallized from isopropyl alcohol. The CMC of both recrystallized and nonrecrystallized HDTAB was 9.4×10^{-4} *M* in doubly distilled water. The spin-labeled alcohol, 4-hydroxy-2,2,6,6-tetramethylpiperidine 1-oxyl, was prepared by the method of Rozantsev,[18] and recrystallized twice from hexane. All solutions were prepared with doubly distilled water. The composition of the solutions are presented in Table I.

The cylindrical soap films thin much slower than rectangular soap films, therefore long-lived soap films are required. Drainage times of 3–4 hr, or longer, are not unusual. Thus far, glycerol has been necessary to obtain the needed film stability. Also, we have found the film composition less likely to change (due to evaporation) when glycerol is present.

Equilibrium film thicknesses were measured by the optical reflectance of a laser pencil using the apparatus described by Mann, Caufield, and Gulden.[19] The experimental film thicknesses were calculated using the well-known isotropic refractive index model. Equations for this calculation may be found in ref 3.

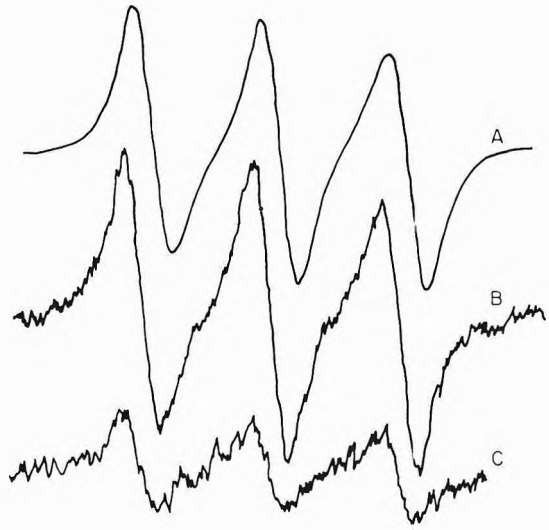

Figure 4. Esr spectra obtained from solution I, (A) flat cell spectrum, (B) cylindrical soap film spectrum, and (C) spectrum of esr cavity after film broke. When the film breaks, it necessarily contaminates the cavity, which accounts for the signal in (C).

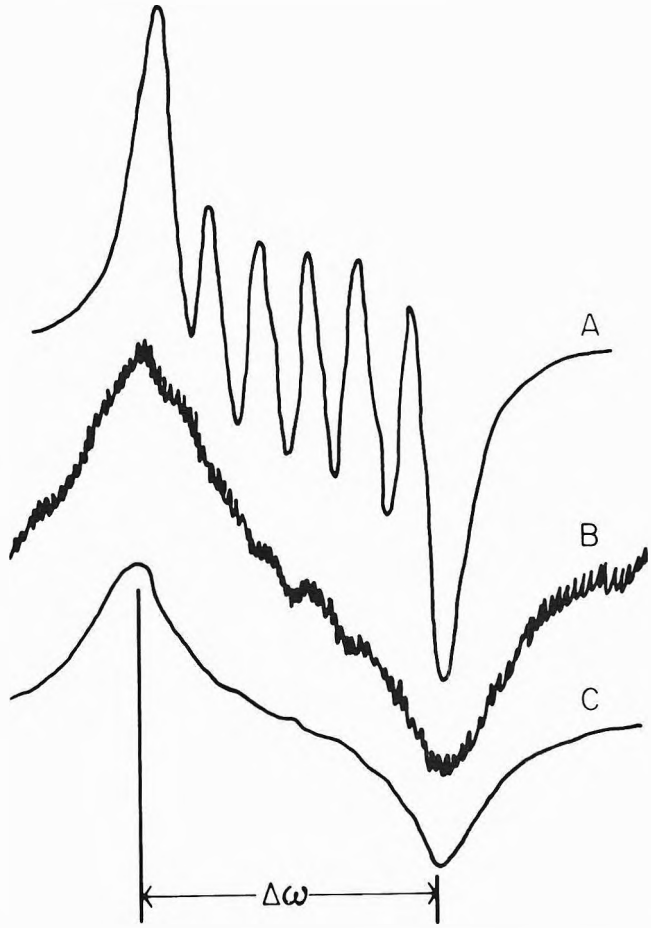

Figure 5. Manganese probed soap film: (A) bulk soap solution, 0.7 *M* $MnSO_4$ in 3% sodium dodecyl sulfate (SDS); (B) thick soap film; (C) 1.5 *M* $MnSO_4$ in 3% SDS. Almost identical results were obtained using 0.03 *M* HDTAB as the surfactant. $\Delta\omega$ = 539 G).

For the variable T/η experiments, a 51 wt % aqueous glycerol solution was studied at various temperatures using a Varian V-4540 variable temperature controller cal-

ibrated with a copper–constantan thermocouple. The viscosity data were taken from the Handbook of Chemistry and Physics.[20]

All esr measurements were obtained using a Varian V-4502 esr spectrometer with field dial control.

The TE_{012} cavity was equipped with optical slits which were covered by a thin glass slide to prevent evaporation. The iris opening was covered from the waveguide side of the cavity with transparent tape. The syringe, which was used to adjust the internal pressures of the soap cylinder (as needed), contained 10.0 ml of distilled water to saturate the internal atmosphere of the soap cylinder. Water was also placed between the glass slide and the optical slits (but not inside the cavity) to offset evaporation from the external side of the soap cylinder. The ends of the fiber optics were also sealed to prevent gas diffusion out of the cylinder.

Results

Table I presents the center line width, W_0, of the bulk solutions and thin films. In most cases, W_0(film) is similar to W_0(bulk), indicating that no anomalous viscosity effects have developed in the thin soap films. Film IV exhibits a greater W_0 than bulk, which is most likely due to evaporation. Sample spectra are illustrated in Figure 4. Experimental equilibrium film thicknesses are presented in Table I.

Figure 5 presents spectra of Mn^{2+} solutions in sodium dodecyl sulfate (SDS), and the spectrum of a thick cylindrical Mn^{2+} soap film. Due to the broad esr line width of the Mn^{2+} ion and the extreme thinness of soap films with high concentrations of Mn^{2+}, no spectrum of an equilibrium Mn^{2+} film could be obtained. Films with Mn^{2+} were also formed using HDTAB as the surfactant.

Discussion

The results of films I, II, and III indicate that there are no abnormal viscosity effects in these soap films. We conclude that the shear viscosity coefficient is independent of film thickness in the range above 50 Å.

Film IV, drawn from a solution containing a lower concentration of glycerol, shows a greater W_0 than bulk. Since film IV contained less glycerol than I, II, and III, evaporation of water from the film would be more likely to occur. Evaporation of water from the film would increase the concentration of the nonvolatile components. Increasing the concentration of SLOH increases W_0, while increasing the concentration of glycerol decreases W_0.

The net effect of evaporation on solution IV was found to increase W_0. This was determined by placing a sample of solution IV in the laboratory, open to the atmosphere. The amount of evaporation was measured by weight loss, and the esr spectrum was recorded periodically. After a weight loss of approximately 33%, the esr line width, W_0, was equal to 7.5 G. Since the line width of film IV was 7.5 G, it is reasonable to conclude that approximately 33% of the water evaporated from film IV.

The effect of evaporation on solutions I, II, and III was also investigated, and was found to increase W_0. However, the rate of increase of W_0 with respect to the amount of water evaporated was less than for solution IV.

The results of the Mn^{2+} soap films indicate an increase in Mn^{2+} concentration from 0.7 $\sim$1.5 *M*. These films were similar to film IV in that they did not contain glycerol, again suggesting the possibility of evaporation. Since the esr results of the Mn^{2+} films were the same for soap films formed from cationic and anionic surfactants, electrical adsorption is not a likely mechanism for the increase in concentration.

The esr experiments show that there is no change in the physical state of soap films formed from surfactant solutions containing high amounts (24%) of glycerol. These findings are in agreement with the work of Clunie, *et al.*,[21] and Lyklema, *et al.*,[22] that there are no abnormal viscosity effects or rigid layers in thin soap films. For films containing lesser amounts of glycerol, the esr experiments indicate that evaporation occurred in spite of the precautions taken to prevent evaporation. Whether this evaporation was due to an unsaturated atmosphere in the esr cavity or an intrinsic higher vapor pressure of the thin films is not known. More stringent control of the esr cavity humidity is required before further conclusions can be drawn concerning the vapor pressure of soap films formed from surfactant solutions of low glycerol content.

References and Notes

(1) Partial support received from NSF Chemistry Department Development Grant No. 3855.
(2) (a) J. Th. G. Overbeek, *J. Phys. Chem.*, **64**, 1178 (1960); (b) J. A. Mann, *J. Colloid Interface Sci.*, **25**, 437 (1967).
(3) H. G. Bruil, "Specific Ionic Effects in Free Liquid Films," Communications, Agricultural University of Wageningen, The Netherlands, 1970.
(4) A. J. de Vries, *Recl. Trav. Chim. Pays-Bas*, **77**, 383 (1958).
(5) J. S. Clunie, J. M. Corkill, and J. F. Goodman, *Disc. Faraday Soc.*, **42**, 34 (1966).
(6) J. C. Henniker, *Rev. Mod. Phys.*, **21**, 322 (1949).
(7) O. H. Griffith and A. S. Waggoner, *Accounts Chem. Res.*, **2**, 17 (1969).
(8) H. M. McConnell and B. G. McFarland, *Quart. Rev. Biophys.*, **3**, 91 (1970).
(9) W. Snipes and A. Keith, *Res./Develop.*, Feb, 22 (1970).
(10) T. J. Stone, T. Buckman, P. L. Nordia, and H. M. McConnell, *Proc. Nat. Acad. Sci. U. S.*, **54**, 1010 (1965).
(11) M. S. Itzkowitz, *J. Chem. Phys.*, **46**, 3048 (1967).
(12) G. Poggi and C. S. Johnson, Jr., *J. Magn. Resonance*, **3**, 436 (1970).
(13) C. E. Pake and T. R. Tuttle, *Phys. Chem. Rev. Lett.*, **3**, 423 (1959).
(14) W. Plachy and D. Kivelson, *J. Chem. Phys.*, **47**, 3312 (1967).
(15) N. Edelstein, A. Kwok, and A. H. Maki, *J. Chem. Phys.*, **41**, 3473 (1964).
(16) M. T. Jones, *J. Chem. Phys.*, **38**, 2892 (1963).
(17) M. Povich, J. A. Mann, and D. E. Holmes, *J. Colloid Interface Sci.*, **35**, 176 (1971).
(18) E. Rozantsev, "Free Nitroxide Radicals," Plenum Press, New York, N. Y., 1970, p 215.
(19) J. Mann, K. Caufield, and G. Gulder, *J. Opt. Soc. Amer.*, **61**, 76 (1971).
(20) "Handbook of Chemistry and Physics," 42nd ed, Chemical Rubber Publishing Co., Cleveland, Ohio, 19xx, p 2212.
(21) J. S. Clunie, J. F. Goodman, and J. R. Tate, *Trans. Faraday Soc.*, **64**, 1965 (1968).
(22) J. Lyklema, P. C. Scholten, and K. J. Mysels, *J. Phys. Chem.*, **69**, 116 (1965).

A Kinetic Theory Model for Insoluble Monolayer Transport Properties. The Dilute Gas Case[1]

E. R. Cooper and J. Adin Mann*

Departments of Chemistry and Biochemistry and Biophysics, University of Hawaii, Honolulu, Hawaii 96822
(Received December 4, 1972)

Publication costs assisted by The Petroleum Research Fund

A microscopic description of momentum transport in gaseous insoluble monolayers is developed. The substrate is taken into account by means of a Fokker–Planck or friction term in the kinetic equations. Numerical estimates are obtained for the shear and dilational viscosity coefficients by employing rigid ellipsoids to model the molecular interaction potential.

Introduction

The object of this paper is the systematic presentation of a microscopic model for calculating surface transport coefficients for the special case of an insoluble gaseous monolayer spread at the air-water interface. Calculations are reported only for the dilute gaseous monolayer case. As an obvious consequence of the limitations on obtaining numerical estimations from accurate microscopic theories, calculations of surface transport coefficients are limited by the necessity of adopting simplifying approximations. Therefore it is pertinent to comment on the reasons for attempting what must be by necessity an imperfect computation.

It is well documented that transport properties can be associated with a phase interface.[2a] More specifically, the "surface viscosity" of monomolecular films spread at the air–water interface has been studied experimentally by numerous authors.[2b] That a viscosity coefficient can be associated with monomolecular films is convincingly demonstrated by observing two-dimensional flow patterns in terms of experimental arrangements adapted from the standard methods of determining three-dimensional viscosity coefficients.[2] Unfortunately there is always the question of including accurately the effect of the substrate on the two-dimensional measurement. For example, one experimental arrangement involves observing the time damping of an oscillating disk carefully placed in the surface region. Indeed, the oscillations of the disk do damp out more quickly in the presence of a monomolecular film. However, there is a major difficulty in subtracting out the substrate effect on the disk in order to calculate a surface viscosity rigorously and accurately. The hydrodynamic problem is discussed by Goodrich and Chatterjee.[3] As a consequence of such difficulties, the comparison of experimental and theoretical results involving surface viscosities can be misleading since there must be doubts that the experimentally determined numbers represent the "abstract" surface viscosity.

A simple calculation of the surface viscosity coefficient by dimensional arguments illustrates a difficulty in comparing even orders of magnitude of the theoretical and observed surface viscosity coefficients. Suppose that the interfacial region is between 1 and 10 nm thick and involves a fluid monolayer. Then one would expect the surface viscosity to be roughly 5×10^{-9} g/sec, corresponding to a fluid viscosity of 0.05 P. The surface viscosity coefficients of a gaseous monolayer should be even smaller. In contrast the surface viscosity of such monomolecular films is reported to be of the order of 10^{-4} g/sec or greater.[2b] A more careful calculation was reported by Blank and Britten[4] who used a fluctuation theory approach for the calculation of surface transport coefficients. Their calculation of the surface viscosity coefficient was still many orders of magnitude too small. The viscosity coefficient estimated by the simple dimensional argument and that calculated by Blank and Britten[4] are in reasonable agreement but such numbers do not agree at all with surface viscosity coefficients reported by the experimentalists.[2b] As Blank and Britten[4] point out, a possible resolution of this interesting dilemma is that the experimental techniques are not reporting the surface viscosity coefficients as defined in the theoretical models. However, the Blank and Britten approach probably underestimates the substrate contribution to surface transport.[2]

An important question, then, is whether a more detailed microscopic model of two-dimensional transport could result in a satisfactory comparison with experimental results. Since kinetic theory has been successfully developed for dilute gases,[5,6] we feel that we can obtain reliable estimates of both the shear and dilational viscosity coefficients in the dilute region corresponding to a surface area/molecule greater than about 1000 Å^2/molecule. Further, we hope that our approach will shed some light on the difficulties encountered in understanding the experimental results in the dense regions and hopefully provide a framework for future considerations of such regions in terms of kinetic theory.

Although we realize that the surface film is a three-dimensional, binary fluid mixture, we model it as a two-dimensional single-component fluid, where the interaction between the substrate and monolayer is treated as a friction or Fokker–Planck term in the equation for the singlet distribution function. Therefore, we ignore mass transport into and out of the two-dimensional layer and lump the complex monolayer–substrate interaction into a friction term. Practical advantages are gained by such a description. For the dilute monolayer gas, we can solve the singlet equation and obtain numerical estimates of the transport coefficients based on a rigid ellipsoid interaction model. Further, the extension to denser gases (at least for a spherical interaction) can be expressed quite naturally in terms of the Rice–Allnatt[7,8] kinetic theory for liquids. Since their model also employs friction constants (molecular friction constants), we can add the substrate friction constant to the soft-potential friction constant in the Rice–Allnatt theory.

We show that the substrate-monolayer interaction term in the singlet equation can be cast into a Fokker-Planck term for rigid-sphere interaction potentials. We assume that this is also the case if the monolayer molecules are treated as rigid ellipsoids, and that a term exists for both translational and rotational motion. We thus obtain a singlet equation for a gas of rigid ellipsoids which are constrained to move in two dimensions with the linear and angular momentum vectors perpendicular at all times. We first discuss the singlet equation and its solution and then present numerical estimates of the surface shear and surface dilational viscosity coefficients for the ellipsoid model.

Theoretical

I. Singlet Equation. In the absence of external fields, the equation[9] determining the singlet distribution function $f_1(\mathbf{r}_1,\mathbf{v}_1,\mathbf{M}_1,t)$ for a dilute gas of rigid ellipsoidal bodies confined to a plane is

$$\left(\frac{\partial}{\partial t} + \mathbf{u}\cdot\frac{\partial}{\partial \mathbf{r}_1}\right) f_1 = \partial_c(f_1,f_2) \tag{1}$$

where $\mathbf{v}_1$ and $\mathbf{r}_1$ are the velocity and location of the mass center of molecule one in the surface, $\mathbf{M}_1$ is the angular momentum (always perpendicular to v_1 and therefore in the direction of the surface normal), and for rigid ellipsoids

$$\partial_c(f_1,f_2) = (2\pi)^{-2}\int d\hat{e}_1\int d\hat{e}_2\int d\mathbf{v}_2\int d\mathbf{M}_2\int d\hat{k}\, S_x^{(1)}\hat{k}\cdot\mathbf{g}\{f_1'f_2' + f_1f_2\} \qquad \hat{k}\cdot\mathbf{g} > 0 \quad \hat{k}\cdot\mathbf{g} < 0 \tag{2}$$

Here $\hat{e}_i$ is a unit vector along the symmetry axis of body i (the projection of molecule i onto a mathematical surface appropriately located in the monolayer-thick interfacial region), $\hat{k}$ is a unit vector normal to molecule one at the point of contact, $\mathbf{g}$ is the relative velocity of the two molecules at the point of contact, and a prime denotes a function of precollisional variables. A general expression for the operator $\partial_c(f_1,f_2)$ has been given by Hoffman and Dahler,[9] but eq 2 is the specific form used for our calculations. The quantity $S_x^{(1)}$ is the element of arc length per unit angle on the excluded area (the area excluded to the mass center of molecule two by molecule one). It is the two-dimensional analog of the excluded volume surface element given in ref 10 and is given by

$$S_x^{(1)} = h_1 + h_2 - x_1h_1' + x_2h_2' + (1 - x_1)h_1'' + (1 - x_2)h_2'' \tag{3}$$

Here $x_i = \hat{k}\cdot\hat{e}_i$, the derivatives are with respect to x_i, and the supporting functions, h_i, are

$$h_1 = (a^2 + (b^2 - a^2)x_1^2)^{1/2} + Cx_1 \tag{4}$$

and

$$h_2 = (a^2 + (b^2 - a^2)x_2^2)^{1/2} - Cx_2 \tag{5}$$

Here a is the length of the minor axis of the ellipsoid, b is the major axis length, and C is the distance of the mass center from the geometric center. A more detailed discussion of the rigid ellipsoid geometry can be found in ref 10.

The key statement of our model is that the singlet equation for the monolayer film is of the form

$$\left(\frac{\partial}{\partial t} + \mathbf{v}\frac{\partial}{\partial \mathbf{r}_1}\right) f_1 = \partial_c(f_1,f_2) + \frac{\zeta}{m}\frac{\partial}{\partial \mathbf{v}_1}\cdot\left\{(\mathbf{v}_1 - \mathbf{u}_s)f_1 + \frac{kT}{m}\frac{\partial}{\partial \mathbf{v}_1}f_1\right\} + \frac{\zeta'}{m}\frac{\partial}{\partial \mathbf{M}_1}\cdot\left\{\mathbf{M}_1f_1 + IkT\frac{\partial}{\partial \mathbf{M}_1}f_1\right\} \tag{6}$$

where ζ is the substrate friction coefficient for the translational motion and ζ' is the friction coefficient for the rotational motion. (Note: we have assumed velocity independent friction coefficients.) Here $\mathbf{u}_s$ is the substrate stream velocity, m is the molecular mass of the monolayer, I is the moment of inertia of the monolayer, k is Boltzmann's contant, and T is the temperature. The well-documented coupling of the substrate to monolayer is taken into account explicitly and simply by the inclusion of friction coefficients in eq 6. The basis for our assertion of the friction terms in eq 6 is that we can show that such is the case for a binary mixture of rigid spheres with the mass of one component much larger than the mass of the other (see Appendix A). We note that the mass ratio of molecules that form insoluble monolayers and water is at least 10:1.

II. Linearization of the Singlet Equation. To generate the "normal" solutions to the singlet equation, we introduce an ordering parameter ϵ and write $f_1 = f_1^{(0)} + \epsilon f_1^{(2)} + \ldots$. This parameter enters the singlet equation as

$$\epsilon\left\{\frac{\partial_0}{\partial t} + \epsilon\frac{\partial_1}{\partial t} + \cdots + \mathbf{v}_1\cdot\frac{\partial}{\partial \mathbf{r}_1} - \frac{\zeta}{m}(\mathbf{u}_1 - \mathbf{u}_s)\frac{\partial}{\partial \mathbf{v}_1}\right\} f_1 = \partial_c(f_1,f_2) + \frac{\zeta}{m}\frac{\partial}{\partial \mathbf{v}_1}\cdot\left\{(\mathbf{v}_1 - \mathbf{u}_1)f_1 + \frac{kT}{m}\frac{\partial}{\partial \mathbf{v}_1}f_1\right\} + \frac{\zeta'}{m}\frac{\partial}{\partial \mathbf{M}_1}\cdot\left\{\mathbf{M}_1f_1 + IkT\frac{\partial}{\partial \mathbf{M}_1}f_1\right\} \tag{7}$$

where $\mathbf{u}_1$ is the monolayer stream velocity. A more detailed discussion of the ordering procedure has been given by Chapman and Cowling[5] and Hoffman and Dahler.[9] The first two equations of this sequence are

$$0 = \partial_c(f_1^{(0)},f_2^{(0)}) + \frac{\zeta}{m}\frac{\partial}{\partial \mathbf{v}_1}\cdot\left\{(\mathbf{v}_1 - \mathbf{u}_1)f_1^{(0)} + \frac{kT}{m}\frac{\partial}{\partial \mathbf{v}_1}f_1^{(0)}\right\} + \frac{\zeta'}{m}\frac{\partial}{\partial \mathbf{M}_1}\cdot\left\{\mathbf{M}_1f_1^{(0)} + IkT\frac{\partial}{\partial \mathbf{M}_1}f_1^{(0)}\right\} \tag{8}$$

and

$$\mathfrak{D}f_1^{(0)} = -\mathcal{J}(\phi) \tag{9}$$

where

$$\mathfrak{D} = \left(\frac{\partial}{\partial t} + \mathbf{v}_1\cdot\frac{\partial}{\partial \mathbf{r}_1} - \frac{\zeta}{m}(\mathbf{v}_1 - \mathbf{u}_s)\cdot\frac{\partial}{\partial \mathbf{v}_1}\right) \tag{10}$$

$$\mathcal{J}(\phi) = J(\phi) + F(\phi) \tag{11}$$

$$J(\phi) = -\partial_c(\phi_1f_1^{(0)},f_2^{(0)}) - \partial_c(f_1^{(0)},\phi_2f_2^{(0)}) \tag{12}$$

$$F(\phi) = -\frac{\zeta}{m}\frac{\partial}{\partial \mathbf{v}_1}\cdot\left\{(\mathbf{v}_1 - \mathbf{u}_1)\phi_1f_1^{(0)} + \frac{kT}{m}\frac{\partial}{\partial \mathbf{v}_1}(\phi_1f_1^{(0)})\right\} - \frac{\zeta'}{m}\frac{\partial}{\partial \mathbf{M}_1}\cdot\left\{\mathbf{M}_1\phi_1f_1^{(0)} + IkT\frac{\partial}{\partial \mathbf{M}_1}(\phi_1f_1^{(0)})\right\} \tag{13}$$

and where we have written $f_1^{(1)} = \phi_1f_1^{(0)}$ (ϕ being the distortion to the local equilibrium distribution function $f^{(0)}$].[11] Solution of eq 8 and 9 is sufficient for a linear phenomenal theory.

The solution of (8) is the local equilibrium distribution function

$$f^{(0)} = n(m/2\pi kT)(2\pi IkT)^{-1/2}e^{-W^2-\Omega^2} \tag{14}$$

where $\mathbf{W} = (m/2kT)^{1/2}(\mathbf{v} - \mathbf{u})$, $\Omega = (2IkT)^{-1/2}\mathbf{M}$, and n is the number density. (Note: n, $\mathbf{u}$, and T are all functions of r and t, *i.e.*, they are defined locally.) Since we require

$$\begin{bmatrix} n \\ n\mathbf{u} \\ nkT \end{bmatrix} = \int d\mathbf{v} \int d\mathbf{M} f^{(0)} \begin{bmatrix} \psi^1 \\ \psi^2 \\ \psi^3 \end{bmatrix} = \int dv \int dM f \begin{bmatrix} \psi^1 \\ \psi^2 \\ \psi^3 \end{bmatrix} \quad (15)$$

where $\psi^1 = 1$, $\psi^2 = \mathbf{v}$, $\psi^3 = \frac{1}{2} m(\mathbf{v} - \mathbf{u})^2 + (M^2/2I)$, we have that

$$n^{-1} \int d\mathbf{v} \int d\mathbf{M} \psi^i \phi f^{(0)} \equiv \langle \psi^i, \phi f^{(0)} \rangle = 0 \quad (16)$$

The hydrodynamic equations, which give the time derivatives of n, u, and T (*i.e.*, of $f^{(0)}$), can be constructed by multiplying eq 9 by the summational invariants ψ^i and integrating. Thus from

$$\langle \psi_1^i, \mathfrak{D} f_1^{(0)} \rangle = -\langle \psi_1^i, \mathcal{J}(\phi_1) \rangle = 0 \quad (17)$$

we obtain the zeroth order (in ϵ) hydrodynamic equations

$$\frac{\partial_0 n_1}{\partial t} + \frac{\partial}{\partial \mathbf{r}_1} \cdot (\mathbf{u}_1 n_1) = 0 \quad (18)$$

$$n_1 m \left(\frac{\partial_0 \mathbf{u}_1}{\partial t} + \mathbf{u}_1 \cdot \frac{\partial}{\partial \mathbf{r}_1} \mathbf{u}_1 \right) = -\frac{\partial p_1}{\partial \mathbf{r}_1} - n_1 \zeta (\mathbf{u}_1 - \mathbf{u}_s) \quad (19)$$

and

$$\tfrac{3}{2} \left(\frac{\partial_0 T_1}{\partial t} + \mathbf{u}_1 \cdot \frac{\partial T_1}{\partial \mathbf{r}_1} \right) = -T_1 \frac{\partial}{\partial \mathbf{r}_1} \cdot \mathbf{u}_1 \quad (20)$$

where $p_1 = n_1 k T_1$. We now can rewrite (9) as

$$f^{(0)} \left\{ \left[2[\mathbf{W}]^{(2)} + \frac{2}{3} \left(\frac{1}{2} W^2 - \Omega^2 \right) \mathbf{U}^{(2)} \right] \odot^2 \frac{\partial \mathbf{u}}{\partial \mathbf{r}} + \left(\frac{2kT}{m} \right)^{1/2} \times \mathbf{W} [(W^2 - 2) + (\Omega^2 - \tfrac{1}{2})] \cdot \frac{\partial \ln T}{\partial \mathbf{r}} \right\} = -\mathcal{J}(\phi) \quad (21)$$

where $[\mathbf{W}]^{(n)}$ is a rank n irreducible Cartesian tensor,[12] $\odot^n$ denotes a contraction on n indices and $(\mathbf{U}^{(2)})_{ij} = \delta_{ij}$ for $i,j = 1,2$. (For convenience we have now dropped the subscript one.) We now approximate ϕ by

$$\phi = -n^{-1} \left[\left(\frac{2kT}{m} \right)^{1/2} \mathbf{A} \frac{\partial}{\partial \mathbf{r}} \ln T + \mathbf{B} \odot^2 \frac{\partial \mathbf{u}}{\partial \mathbf{r}} \right] \quad (22)$$

Since there can be no visco-thermal coupling in the absence of external fields, eq 21 separates into the two equations

$$f^{(0)} \left\{ 2[\mathbf{W}]^{(2)} + \frac{2}{3} \left(\frac{1}{2} W^2 - \Omega^2 \right) \mathbf{U}^{(2)} \right\} = n^{-1} \mathcal{J}(\mathbf{B}) \quad (23)$$

and

$$f^{(0)} \{ (W^2 - 2) + (\Omega^2 - \tfrac{1}{2}) \} \mathbf{W} = n^{-1} \mathcal{J}(\mathbf{A}) \quad (24)$$

To solve for ϕ then, we must determine $\mathbf{A}$ and $\mathbf{B}$, from which we obtain the thermal conductivity and viscosity, respectively. Even though we are concerned only with a solution of the viscosity equation (23), we note that the solution technique for the thermal conductivity equation (24) is quite similar.

III. Solution of the Viscosity Equation. The contribution (to first order in the gradients) to the pressure tensor from the monolayer is given by

$$\mathbf{P} = 2nkT \langle \mathbf{WW}, f \rangle = p\mathbf{U}^{(2)} - 2kT \langle \mathbf{WW}, \mathbf{B} f^{(0)} \rangle \odot^2 \frac{\partial \mathbf{u}}{\partial \mathbf{r}} \quad (25)$$

For a three-dimensional gas $\mathbf{B}$ is usually expanded in products of irreducible tensors in $\mathbf{W}$ and Ω, but since $\mathbf{W} \cdot \Omega = 0$, we only need to expand $\mathbf{B}$ as

$$\mathbf{B} = \sum_{q\,s\,l} S_q^{(s)}(W^2) S_{-1/2}^{(l)}(\Omega^2) [\mathbf{W}]^{(q)} \odot^q \mathbf{B}^{qsl} \quad (26)$$

where $S_m^{(n)}(\mathbf{x})$ is a Sonine polynomial.[6]

The subsidiary conditions, eq 16, imply that

$$\mathbf{B}^{000} = 0 \quad (27)$$

and

$$\mathbf{B}^{010} + \frac{1}{2} \mathbf{B}^{001} = 0 \quad (28)$$

Also, since there can be no coupling through J of tensors of different rank, we have that $q = 0,2$.

For our expansion of $\mathbf{B}$, the pressure tensor becomes

$$\mathbf{P} = p\mathbf{U}^{(2)} - kT[\mathbf{B}^{200} - \mathbf{U}^{(2)}\mathbf{B}^{010}] \odot^2 \frac{\partial \mathbf{u}}{\partial \mathbf{r}} \quad (29)$$

where $\mathbf{B}^{200}$ is traceless and symmetric on its first two indices. Since the two-dimensional space is assumed isotropic, there exist coefficients b^{200} and b^{010} such that

$$\mathbf{B}^{200} = b^{200} \mathbf{B}_2^{(a)}(2) \quad (30)$$

and

$$\mathbf{B}^{010} = b^{010} \mathbf{U}^{(2)} \quad (31)$$

where $(\mathbf{B}_2^{(a)}(2))_{ijkl} = \frac{1}{2}(\delta_{il}\delta_{jk} + \delta_{ik}\delta_{jl} - \delta_{ij}\delta_{kl})$. Thus $\mathbf{P}$ becomes

$$\mathbf{P} = p\mathbf{U}^{(2)} - 2\bar{\eta}\mathbf{S} - \bar{K} \left(\frac{\partial}{\partial \mathbf{r}} \cdot \mathbf{u} \right) \mathbf{U}^{(2)} \quad (32)$$

where the surface shear viscosity is $\bar{\eta} = \frac{1}{2} k T b^{200}$, the surface dilational viscosity is $\bar{K} = -kTb^{010}$, and $\mathbf{S} = \frac{1}{2}[(\partial \mathbf{u}/\partial \mathbf{r}) + (\partial \mathbf{u}/\partial \mathbf{r})^t] - \frac{1}{2}\mathbf{U}^{(2)}(\partial/\partial \mathbf{r}) \cdot \mathbf{u}$. Here $(\partial \mathbf{u}/\partial \mathbf{r})^t$ is the transpose of $\partial \mathbf{u}/\partial \mathbf{r}$.

We now truncate the expansion for $\mathbf{B}$ after the inclusion of a few lead terms. We thus approximate $\mathbf{B}$ by

$$\mathbf{B} = \phi^1 \mathbf{B}^1 + \phi^2 \odot^2 \mathbf{B}^2 + \phi^3 \odot^2 \mathbf{B}^3 + \phi^4 \odot^2 \mathbf{B}^4 \quad (33)$$

where $\phi^1 = S_0^{(1)}(W^2) - 2S_{-1/2}^{(1)}(\Omega^2)$, $\Phi^2 = [\mathbf{W}]^{(2)}$, $\Phi^3 = S_{-1/2}^{(1)}(\Omega^2)[\mathbf{W}]^{(2)}$, $\Phi^4 = S_2^{(1)}(W^2)[\mathbf{W}]^{(2)}$, $\mathbf{B}^1 = \mathbf{B}^{010}$, $\mathbf{B}^2 = \mathbf{B}^{200}$, $\mathbf{B}^3 = \mathbf{B}^{201}$, and $\mathbf{B}^4 = \mathbf{B}^{210}$. Multiplying eq 23 by each of the ϕ^i and integrating[6] we obtain equations for the $\mathbf{B}^i$ and hence $\bar{\eta}$ and $\bar{K}$. We find that

$$\bar{K} = kT/\tilde{J}_{11} \quad (34)$$

and

$$\bar{\eta} = \frac{kT}{2} \{ \tilde{J}_{22} - J_{24}^2/\tilde{J}_{44} - (J_{23} - J_{24}J_{34}/\tilde{J}_{44})^2/(\tilde{J}_{33} - J_{34}^2/\tilde{J}_{44}) \}^{-1} \quad (35)$$

where

$$\begin{aligned} \tilde{J}_{11} &= J_{11} + \zeta/mn + 2\zeta'/mn \\ \tilde{J}_{33} &= J_{33} + \zeta/mn + \zeta'/mn \\ \tilde{J}_{ii} &= J_{ii} + \zeta/mn \quad (i = 2,4) \end{aligned} \quad (36)$$

$$J_{11} = \frac{1}{2} \langle \phi^1, J(\phi') \rangle \quad (37)$$

and

$$J_{ij} = J_{ji} = \frac{1}{2} \langle \phi^1, J(\phi^j) \rangle \odot^4 \mathbf{B}_2^{(a)}(2) \quad (\text{for } i,j = 2,3,4) \quad (38)$$

Equations 34 and 35 are model dependent only in the sense that the molecular model has a C_∞ symmetry axis.

Numerical Results

The collision integrals, J_{ij}, must be computed in order to determine the surface viscosity coefficients, $\bar{\eta}$ and $\bar{K}$.

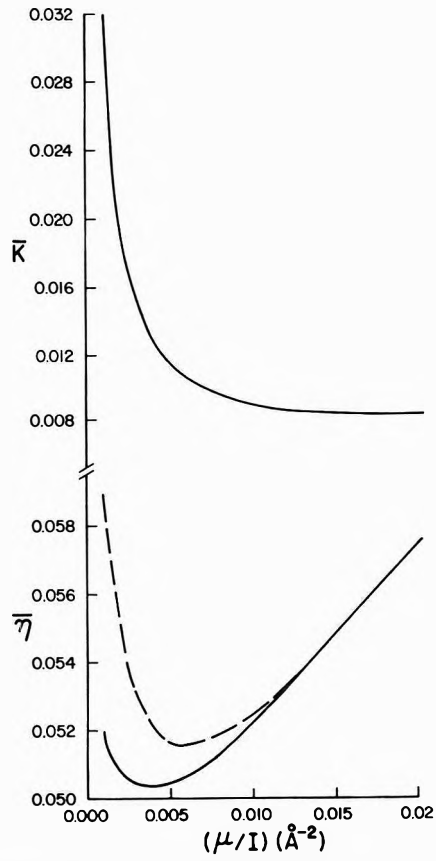

Figure 1. The viscosity coefficients are given in terms of the group $(mkT/\pi)^{1/2}L^{-1}$ (L was set to 10^{-8} cm for convenient plotting) and as functions of μ/I (in Å^{-2}). Here R = 5, Σ = 120 Å^2, C = 0, and the dashed line is the calculation with ϕ^3 and ϕ^4 omitted.

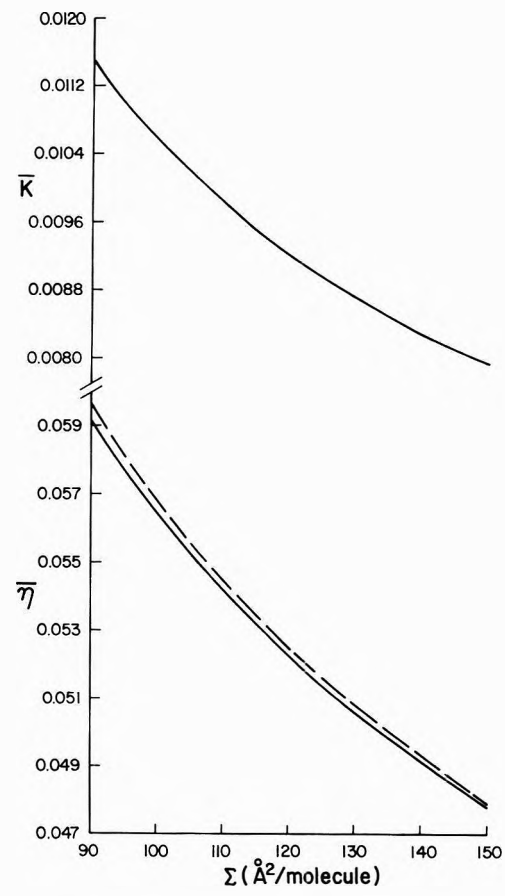

Figure 2. The viscosity coefficients are given in terms of the group $(mkT/\pi)^{1/2}L^{-1}$ (L was set to 10^{-8} cm for convenient plotting) and as functions of Σ (in Å^2). Here R = 5, μ/I = 0.01 Å^{-2}, C = 0, and the dashed line is the calculation with ϕ^3 and ϕ^4 omitted.

TABLE I: Model Parameters for Long-Chain Fatty Acids

	R	Σ, Å^2	I, Å	$\mu/I = 6/l^2$, Å^{-2}
C_{12}	3.8	96.4	19.4	0.0159
C_{14}	4.38	111.3	22.3	0.0120
C_{16}	4.85	125.9	25.2	0.00945
C_{18}	5.5	140.0	28.0	0.00765

The collision integrals were parameterized in terms of the projection of the surfactant molecule onto the appropriate interfacial surface. A further simplification was obtained by assuming that such projections were ellipsoidal regions each having a minor axis of length a and a major axis of length b. The geometrical area for each molecule is $\Sigma = \pi ab$. The load distance parameter was defined in eq 4 and 5. Other parameters used are the ratios $R = b/a$ and $\mu/I = 6/l^2$, where l is the length of the molecule, and μ the reduced mass of a pair of colliding molecules. The formula for μ/I obtains for a uniform mass distribution along the symmetry axis of the ellipsoidal "molecule."

Four of the sixfold integrations of the J_{ij} were evaluated by a method outlined by Hoffman[13] for rigid convex bodies. The remaining twofold integrations were done numerically using the trapezoidal algorithm, which is known to converge rapidly for periodic functions such as ours. We found that the difference between a 90 × 90 and a 100 × 100 point grid was one part per billion for each of the integral types. The programming was done in double precision using FORTRAN IV and run on the University of Hawaii IBM 360/65 system. We estimated that the accuracy of our numerical results was between six and eight significant figures. In Appendix B we list the necessary tensor integrals used in computing the J_{ij}.

Table I lists examples of the values of the parameters that model the often-studied long-chain fatty acid series. Since the formalism applies to the dilute monolayer situation, we assumed that the long axis of the molecule was flat in the surface.[2a] Estimates of the cross-sectional areas of the molecules were made from film balance data and crystalographic data from which the minor axis length was estimated. The volume per molecule was estimated from density numbers so that molecular lengths could be directly calculated. Our numbers are consistent with those published in the surface chemistry literature. Other molecules, such as cholesterol, have similar values of these parameters which are required in the calculation of $\bar{\eta}$ and $\bar{K}$. The calculations were carried out and reported here for those ranges of the parameters that should cover many interesting special cases.

In Figure 1 we give $\bar{\eta}$ and $\bar{K}$ as functions as μ/I with the other parameters held fixed. Here, as in all the figures, the substrate friction constant was set equal to zero in order to study the isolated interface as a limiting case. We note that $\bar{\eta}$ has a minimum around $\mu/I \sim 0.0005$ Å^{-2}, whereas $\bar{K}$ decreases sharply and appears to approach a limiting value. In Figure 2 we give $\bar{\eta}$ and $\bar{K}$ as functions of Σ and in Figure 3 as a function of R. In both cases $\bar{\eta}$ and $\bar{K}$ decrease with increasing R. Molecules with μ/I much smaller than the 0.01 Å^{-2} show an increase in $\bar{\eta}$ with R.

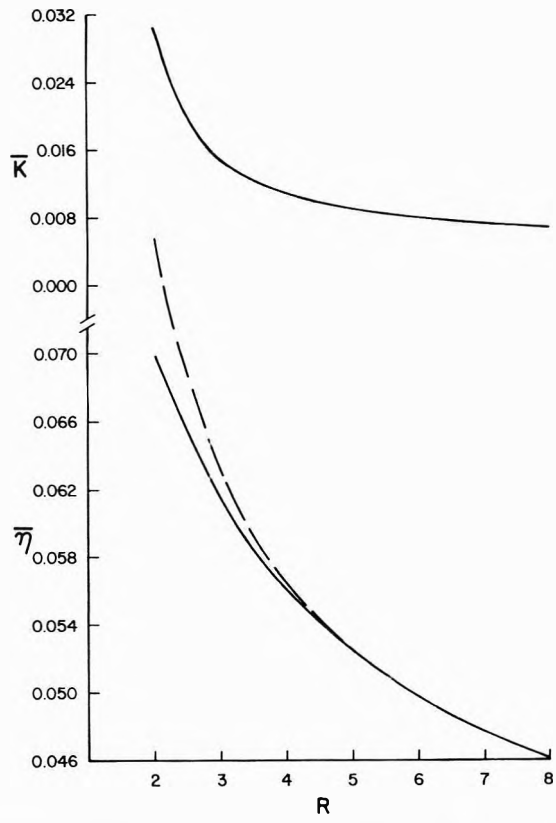

Figure 3. The viscosity coefficients are given in terms of the group $(mkT/\pi)^{1/2}L^{-1}$ (L was set to 10^{-8} cm for convenient plotting) and as functions of R. Here $\Sigma = 120$ Å^2, $\mu/I = 0.01$ Å^{-2}, $C = 0$, and the dashed line is the calculation with ϕ^3 and ϕ^4 omitted.

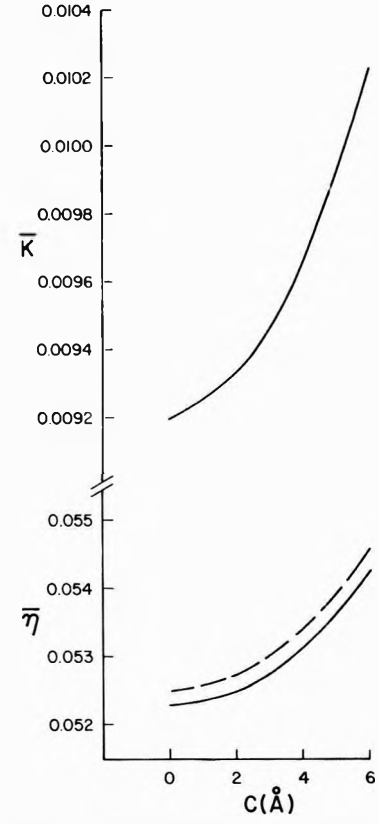

Figure 4. The viscosity coefficients are given in terms of the group $(mkT/\pi)^{1/2}L^{-1}$ (L was set to 10^{-8} cm for convenient plotting) and as functions of C (in Å). Here $R = 5$, $\Sigma = 120$ Å^2, $\mu/I = 0.01$ Å^{-2}, and the dashed line is the calculation with ϕ^3 and ϕ^4 omitted.

TABLE II: Surface Shear and Surface Dilational Viscosities for $R = 5$, $\Sigma = 120$ Å^2, $C = 0$, and $\mu/I = 0.01$ Å^{-2} as Functions of ζ_R

$\bar{\eta}(mkT/\pi)^{1/2}2L^{-1a}$	$\bar{K}(mkT/\pi)^{1/2}2L^{-1}$	ζ_R
0.05247	0.009228	0
0.05247	0.009228	10^{-3}
0.05244	0.009227	10^{-2}
0.05219	0.009156	10^{-1}
0.04985	0.009102	10^{0}
0.03439	0.008106	10^{1}
0.00840	0.003871	10^{2}
0.00098	0.000622	10^{3}

[a] L was taken to be 10^{-8} cm for convenient scaling.

Figure 4 shows how $\bar{K}$ and $\bar{\eta}$ vary with the load, and as C increases both $\bar{K}$ and $\bar{\eta}$ increase. Also, in all of the graphs we see that the value of $\bar{\eta}$ is hardly changed if we omit ϕ^3 and ϕ^4 from the expansion set. Therefore, it is sufficient to include only ϕ^1 and ϕ^2 in our expansion.

Table II shows the variation of $\bar{\eta}$ and $\bar{K}$ as a function of the dimensionless friction coefficient defined as

$$\zeta_R = \frac{\zeta}{n}(\pi mkT)^{-1/2}/L$$

where L was set to 10^{-8} cm for convenient scaling. For convenience we have ignored the difference between ζ and ζ', since little insight is to be gained by showing an independent variation of the two friction coefficients. We note that the values of $\bar{\eta}$ and $\bar{K}$ are strongly dependent upon the viscous drag of the substrate for ζ_R greater than ten. As discussed in the next section, we can estimate $\zeta \sim (m\mu^{(-)}/\Gamma h)$, where $\mu^{(-)}$ is the viscosity of the substrate, h is taken to be the depth of the interfacial region, and Γ is the total surface density. Estimates based upon $h \sim 10^2$ Å, a molecular weight of 200, and $n \sim 10^{-3}$ Å^{-2} give $\zeta_R \sim 10^2$, and hence a significant dependence of $\bar{\eta}$ and $\bar{K}$ on ζ. This estimate is one of three constructed in the next section and in Appendix A, eq 47, 54, and A13. Each formula produces very similar numerical estimates of the friction coefficient for the given monolayer state.

Discussion

As mentioned before, there seem to be no reliable numbers in the literature for the absolute surface shear and dilational viscosity for dilute gaseous monolayers.[2] The work of Boyd and Harkins[14] contains numbers that may be comparable to those that we have calculated. Their Figure 4[14] shows viscosity points for the C_{14} normal alcohol down to perhaps a few tenths of a dyne/cm. Unfortunately, to quote Boyd and Harkins,[14] "the bottom of the plot represents −0.002 surface poise, to show that 'negative viscosities' are not significant." However, their data suggest that the surface viscosity of such a gaseous film is less than about 10^{-4} surface poise. Joly[2b] reported surface shear viscosity numbers for dense gaseous films of triglycerides that ranged to 10^{-6} surface poise. Our calculation for dilute gaseous monolayers predicts shear viscosity coefficients in a range close to 10^{-12} surface poise for such surfactant molecules. Accurate comparisons are difficult since our calculations involved the assumption that the monolayer was a dilute gas.

Additional experimental evidence has been presented that suggest a difficulty with the traditional view of the experimental techniques for determining surface viscosity coefficients. Povich[15] has reported esr spin label experiments in which long-chain, fatty acid molecules containing a nitroxide free-radical moiety are incorporated into ultrathin soap films. The composition of the systems is controlled so that the soap film surfaces contain a significant fraction of these molecules. When the concentration of the spin-labeled surfactant is sufficiently high, a major contribution to the esr line shape is the spin relaxation caused by collisions between nitroxide moieties. In the proper spin label concentration range, the esr line shape provides a measure of the viscosity coefficient associated with the momentum transport of the labeled molecules. The results of Povich's[15] work suggest that the surface viscosity as defined by a collision model involving momentum transport is much smaller than the coefficients reported from use of the conventional experimental techniques.

A detailed comparison with the results of the calculation by Blank and Britten[4] is not useful since the surface density for which the models were constructed is very different. We do note that their viscosity is larger than ours, which is consistent with usual gas–liquid viscosity comparisons.

After having worked both with the theoretical and experimental aspects of the problem, we wish to suggest, as did Blank and Britten, that the discrepancy of 2 to 8 orders of magnitude between the theoretical and experimental surface viscosity numbers is probably due to the difficulty in these experiments of relating observables back to monolayer viscosity numbers. Several brief remarks concerning the experimental aspects of the problem are appropriate. The difficulties presented by the traditional methods are well discussed by Gains and Joly.[2] However, new approaches to the measurement of shear viscosities are documented in recent papers by Mannheimer and Schechter,[16] by Goodrich and collaborators,[17] and by Lifschutz, *et al.*[18] Attempts are made to handle accurately the substrate correction theoretically. The capillary ripple method for determining surface transport properties as developed by Mann and Hansen[19-21] handles the hydrodynamic problem accurately. However, Hegde and Slattery[22] criticize their interferometer method as ignoring certain solid–fluid boundary effects. In fact all of these methods involve lines of contact between solid surfaces and the fluid interface of interest, and modeling of the interaction must be a part of converting to monolayer viscosity coefficients. Huh and Scriven[23] have written an interesting paper on the failure of a simple hydrodynamic model for the study of movement of a solid–liquid–fluid contact line. As they put it, "the way the hydrodynamic model breaks down suggests that in reality there may be steep gradients, rheological anomalies, and discontinuous processes around the contact line." It appears likely that all of these experimental methods will depend on a systems analysis approach similar to that taken by Mann and Ahmad[24] in the capillary ripple problem in order to handle lines of contact effectively.

Obviously we are strongly suggesting continued experimental and theoretical work directed toward clarifying the physical nature of the apparent discrepancy between the monolayer viscosity as calculated and the surface viscosity as measured.

We conclude with a number of comments concerning the physical interpretation of our formalism. The key equation of the kinetic theory formalism is eq 6 in which the substrate interaction with the monolayer is introduced. The monolayer is the collection of all surfactant molecules modelled as ellipses distributed on a mathematical surface. The substrate is the set of all solvent molecules including those located in the surface and surrounding the surfactant molecules residing there. The two friction coefficients, ζ and ζ', are introduced as parameters, in order to account for the monolayer–substrate coupling, but can be calculated in principle. An important point is that the kinetic theory is not just a parametric theory. (This should be contrasted to the Eyring theory of surface viscosity as discussed by Joly.[2b]) A well-documented perturbation scheme was used to produce zero- and first-order solutions of kinetic eq 6. The related zero-order hydrodynamic equations are given as eq 18, 19, and 20. Comparison of these equations to the macroscopic surface transport equations is relevant.

Since all of the surfactant molecules are assumed to be in the surface, the three-dimensional singlet distribution function for the surfactant molecules must be nonzero only at the surface. The problem is reduced to the determination of a two-dimensional distribution function, f_1, eq 1, *et seq.* From a somewhat more general viewpoint, there is a distribution function $\bar{f}_1(\bar{\mathbf{r}},\bar{\mathbf{v}},\bar{\mathbf{M}},t)$, where the bars indicate surface quantities, such that

$$\bar{f}_1(\bar{\mathbf{r}},\bar{\mathbf{v}},\bar{\mathbf{M}},t) = \int dz \int dv_z \int dM_x dM_y (F_1 - F_1^{(\pm)}) \quad (39)$$

F_1 is the three-dimensional singlet distribution function and $F_1^{(\pm)}$ is the singlet distribution function that would obtain for the solute in the absence of adsorption. For the special case of solute molecules constrained to move in the surface let $F_1^{(\pm)} \equiv 0$ and

$$F_1 = f_1 \delta(z)\delta(v_z)\delta(M_x)\delta(M_y) \quad (40)$$

so that $\bar{f}_1 = f_1$. As a result, each of the eq 18, 19, and 20 can be interpreted as a monolayer hydrodynamic equation directly. Therefore, $\Gamma^{(1)} = m\bar{n}^{(1)} = mn_1$, $\mathbf{u}^{(1)} = \mathbf{u}_1$, and $\pi = \bar{n}^{(1)} kT = n_1 kT = p_1$ are the appropriate identifications for the comparison of our results with the two-dimensional hydrodynamic equations constructed from continuum arguments. Hence eq 18 is

$$\frac{\partial \Gamma^{(1)}}{\partial t} + \frac{\partial}{\partial \bar{\mathbf{r}}} \cdot \Gamma^{(1)} \mathbf{u}^{(1)} = 0 \quad (41)$$

and expresses the mass conservation of the solute component on the surface.

Equation 19 is

$$\Gamma^{(1)} \frac{\partial \bar{\mathbf{u}}^{(1)}}{\partial t} + \Gamma^{(1)} \left(\bar{\mathbf{u}}^{(1)} \cdot \frac{\partial}{\partial \bar{\mathbf{r}}} \right) \bar{\mathbf{u}}^{(1)} = -\frac{\partial \pi}{\partial \bar{\mathbf{r}}} - \bar{n}^{(1)} \zeta (\bar{\mathbf{u}}^{(1)} - \mathbf{u}_s) \quad (42)$$

where $\mathbf{u}_s$ is $\mathbf{u}^{(-)}(-\delta)$ and is the substrate velocity field at a depth δ below the surface. The superscript is used to refer to the relevant variables of component 1, the surfactant. Notice that the monolayer viscosity coefficients are not determined by the zero-order equation from which eq 42 was constructed. However, the friction coefficient, ζ, does enter in the zero-order equation in the term that explicitly couples the motion of the molecules of the monolayer to the substrate. A method for calculating ζ accurately can be constructed, in principle, from the kinetic theory of dense gas mixtures. A practical method for estimating the order of magnitude of the friction coefficient is

required and can be constructed from the appropriate continuum equation of surface motion.

The form of the continuum equation for momentum transport that parallels eq 42 is

$$\Gamma\frac{\partial\bar{\mathbf{u}}}{\partial t} + \Gamma\left(\bar{\mathbf{u}}\frac{\partial}{\partial\bar{\mathbf{r}}}\right)\bar{\mathbf{u}} = \frac{\partial\gamma}{\partial\bar{\mathbf{r}}} - \hat{e}_z\cdot[\mathbf{P}^b]_0\cdot\mathbf{U}_{e_z} \tag{43}$$

where γ is the surface tension. $\mathbf{P}^b$ the bulk pressure tensor, $[\,]_0$ indicates that the jump at the surface is to be computed, and $\mathbf{U}_{ez}$ ($= \hat{e}_x\hat{e}_x + \hat{e}_y\hat{e}_y$) is the dyadic operator that extracts the surface components of the three-dimensional vector $\hat{e}\cdot[\mathbf{P}^b]_0$. It follows that

$$-\hat{e}_z\cdot[\mathbf{P}^b]_0\cdot\mathbf{U}_{e_z} = -([P_{zx}{}^b]_0\hat{e}_x + [P_{zy}{}^b]_0\hat{e}_y)$$

In case the upper phase is a gas, a good approximation is

$$\begin{aligned} -[P_{zx}{}^b]_0 &= -\mu^{(-)}\left(\frac{\partial u_x{}^{(-)}}{\partial z}\right)_0 \\ -[P_{zy}{}^b]_0 &= -\mu^{(-)}\left(\frac{\partial u_y{}^{(-)}}{\partial z}\right)_0 \end{aligned} \tag{44}$$

where it is assumed that $u_z{}^{(-)} = 0$ identically, and $\mu^{(-)}$ is the substrate viscosity. Hence

$$-\hat{e}_z\cdot[\mathbf{P}^b]_0\cdot\mathbf{U}_{e_z} = -\mu^{(-)}\left(\frac{\partial u_x{}^{(-)}}{\partial z}\Big|_0\hat{e}_x + \frac{\partial u_y{}^{(-)}}{\partial z}\Big|_0\hat{e}_y\right)$$

so that

$$\Gamma\frac{\partial\bar{\mathbf{u}}}{\partial t} + \Gamma\left(\bar{\mathbf{u}}\cdot\frac{\partial}{\partial\bar{\mathbf{r}}}\right)\bar{\mathbf{u}} = \frac{\partial\gamma}{\partial\bar{\mathbf{r}}} - \mu^{(-)}\frac{\partial u}{\partial z}\Big|_0 \tag{45}$$

obtains as an expression for the momentum transport balance at the surface.

We will construct estimates of the friction coefficient from two viewpoints. First, suppose that the surface is a one-component region contacting the solvent substrate without slip. The last term of eq 42 is written as an approximation of the last term of eq 45 by introducing a distance δ into the substrate and a correction for the sparse ulation of the monolayer

$$\bar{n}^{(1)}\zeta\delta(\bar{\mathbf{u}}^{(1)} - \mathbf{u}^{(-)}(-\delta))/\delta \sim (\bar{n}^{(1)}\Sigma)\,\mu^{(-)}\frac{\partial u^{(-)}}{\partial z}\Big|_0 \tag{46}$$

where Σ is the area per molecule so that $(\bar{n}^{(1)}\Sigma)$ is the fraction of 1 cm of surface covered by the solute. The estimate of ζ is therefore

$$\zeta = \Sigma\mu^{(-)}/\delta \tag{47}$$

One expects δ to be of the magnitude of a few molecular dimensions.

The surface tension, γ, appears in eq 45 as contrasted to the surface pressure, π, term in eq 42. Asserting that eq 45 goes into

$$0 = \partial\gamma_0/\partial\bar{\mathbf{r}} \tag{48}$$

when the surfactant excess goes to zero allows γ to be replaced by $-\pi(= \gamma - \gamma_0)$ in eq 45. This estimate follows the spirit of eq 1, *et seq.*, faithfully except for the insertion of $-\pi$ for γ.

Second, assume that the surface is a two-component mixture so that solvent molecules are allowed to move in the plane of the surfactant. An attempt to reach eq 42 gives some insight into the character of the approximation made when the solvent–monolayer coupling was included through the friction coefficient alone.

Ahmad and Hansen[25] have shown that an extraordinarily simple form of eq 44 is satisfactory for describing spreading in certain surfactant–substrate systems. For example, for spreading in the x direction

$$-[P_{zx}{}^b]_0 = -\frac{\mu^{(-)}}{h'}\bar{\mathbf{u}}_x \tag{49}$$

where h' is the depth below which $u_x{}^{(-)}$ is zero, was shown to have a surprisingly wide range of validity. With this approximation, eq 45 goes into

$$\Gamma\frac{\partial\bar{\mathbf{u}}}{\partial t} + \Gamma\left(\bar{\mathbf{u}}\cdot\frac{\partial}{\partial\bar{\mathbf{r}}}\right)\bar{\mathbf{u}} = \frac{\partial\gamma}{\partial\bar{\mathbf{r}}} - \frac{\mu^{(-)}}{h}(\bar{\mathbf{u}} - \mathbf{u}^{(-)}(-h)) \tag{50}$$

The surface can be thought of as a mixture so that

$$\Gamma = \Gamma^{(1)} + \Gamma^{(s)} \tag{51}$$

and

$$\bar{\mathbf{u}} = \frac{\Gamma^{(1)}}{\Gamma}\bar{\mathbf{u}}^{(1)} + \frac{\Gamma^{(s)}}{\Gamma}\bar{\mathbf{u}}^{(s)} \tag{52}$$

Substitution of these relations into eq 50 sets up a partitioning of the surface equation of motion into terms that involve the substrate component at the surface, the surfactant molecules at the surface, and the surface tension term that depends on both components. Following Kirkwood and Bearman,[26] who worked out the 3D case, the surface tension, γ, can be written as the sum of partial tensions with $\gamma^{(1)} \to \bar{n}^{(1)}kT = \pi$ in the dilute gas limit. An additional force term, analogous to Kirkwood and Bearman's $\mathbf{F}_2{}^*$, must be introduced in the partitioning. However such terms can be ignored in the dilute gas limit. The form of the last term in eq 50 suggests an obvious partitioning of the substrate coupling term. Therefore

$$\begin{aligned} &\Gamma^{(1)}\frac{\partial\bar{\mathbf{u}}^{(1)}}{\partial t} + \Gamma^{(1)}\left(\bar{\mathbf{u}}^{(1)}\cdot\frac{\partial}{\partial\bar{\mathbf{r}}}\right)\bar{\mathbf{u}}^{(1)} + \\ &\qquad\frac{1}{2}\frac{\partial}{\partial\bar{\mathbf{r}}}\cdot\frac{\Gamma^{(1)}\Gamma^{(2)}}{\Gamma}(\bar{\mathbf{u}}^{(1)} - \bar{\mathbf{u}}^{(s)})(\bar{\mathbf{u}} - \bar{\mathbf{u}}^{(s)}) = \\ &\qquad\qquad -\frac{\partial\pi}{\partial\bar{\mathbf{r}}} - \frac{\mu^{(-)}}{h}\frac{\Gamma^{(1)}}{\Gamma}(\bar{\mathbf{u}}^{(1)} - \mathbf{u}^{(-)}(-h)) \end{aligned} \tag{53}$$

Comparison to eq 46 suggests the identification that

$$\zeta = \mu^{(-)}m/\Gamma h \tag{54}$$

If the additional "momentum" flux term of eq 53 can be ignored. The offending flux can be rewritten in terms of the diffusion velocities ($\bar{\mathbf{u}}^{(i)} - \bar{\mathbf{u}} = \bar{\mathbf{J}}^{(i)}/\Gamma^{(i)}$) for the two species

$$\begin{aligned} &\frac{\Gamma^{(1)}\Gamma^{(s)}}{\Gamma}(\bar{\mathbf{u}}^{(1)} - \bar{\mathbf{u}}^{(s)})(\bar{\mathbf{u}} - \bar{\mathbf{u}}^{(s)}) = \\ &\qquad\frac{\Gamma^{(1)}\Gamma^{(s)}}{\Gamma}\left(\frac{\bar{\mathbf{J}}^{(1)}}{\Gamma^{(1)}} - \frac{\bar{\mathbf{J}}^{(s)}}{\Gamma^{(s)}}\right)\left(\frac{\bar{\mathbf{J}}^{(1)}}{\Gamma^{(1)}} - \frac{\bar{\mathbf{J}}^{(s)}}{\Gamma^{(s)}}\right) \end{aligned}$$

We must assume that the relative diffusion velocities are sufficiently small that they can be ignored to first order at least. This assumption, while physically plausible, cannot be supported rigorously at this time.

Note that the velocity fields for the solvent, $\mathbf{u}^{(-)}(-\delta)$, in eq 46 and $\mathbf{u}^{(-)}(-h)$ in eq 53 could be different. The fact that both δ and h must be taken as adjustable parameters is a defect in both estimation procedures. However, physically reasonable values of δ and h give similar values of the friction coefficient. Therefore, while the mixture model is closer to reality than the single component model, the latter model, as we have shown, leads to a

tractable statistical mechanical calculation that in the end does include a considerable part of the solvent contribution to monolayer transport. Finally, a third estimate is constructed in Appendix A as a result of showing that a friction coefficient formalism is appropriate for a binary mixture of rigid spheres in the absence of external forces. The estimate calculated from eq A13 is consistent with the estimates calculated from the hydrodynamic models, eq 47 and 54.

We draw two conclusions from the experimental work of Ahmad and Hansen[25] and Povich[15] that are appropriate to mention in connection with the discussion of the possible range of values of the friction coefficient. Estimates of numbers such as h appear to be possible from the type of experiments reported by Ahmad and Hansen.[25] Further the spin label work of Povich[15] shows that the translational motion of labeled moieties in ultrathin soap films is not widely dissimilar from that of bulk fluids. Therefore, we conclude, first, that a linear substrate coupling term as used in eq 6, 46, and 53 is an appropriate parameterization. Second, we do not expect the unusually large friction coefficients for water substrates that might obtain if the surfactant were to induce structure into the substrate region. For water, $\zeta_R \sim 10^4/h$ where h is in Å. Hence $\zeta_R < 10^4$. Table II shows the range of surface viscosity values obtained when the friction coefficient is varied over a domain consistent with eq 54 and the various estimates of h.

Finally, we estimate the self-diffusion coefficient, $\bar{D}^{(1)}$, for the surfactant molecules. It is possible to do this calculation within the framework of the kinetic theory that we have developed; however, the calculation has not been completed. The mean free path model of Hirschfelder, Curtis, and Bird[6] while crude is easily adapted to the interface case so that

$$\bar{D}^{(1)} \sim \bar{\eta}/\Gamma^{(1)} \tag{55}$$

For our particular choice of parameters, $\bar{D}^{(1)} \sim 10^{-2}$ cm²/sec. Only the much more dense monolayer situation has been examined experimentally.[25] Sakata and Berg[27] report the "self-diffusion" coefficient of a myristic acid monolayer compressed to 39 Å²/molecule to be 3×10^{-4} cm²/sec. Therefore our result is probably reasonable but it is hazardous to compare the two numbers since the surface densities involved are so different and eq 55 is of unknown reliability.

We are working on the problem of extending these calculations to the dense gas region. Unfortunately, a more accurate molecular description of interfacial transport requires a theory of polyatomic solutions beyond that available today. Nevertheless it appears possible to calculate upper bounds for the relevant transport coefficients for comparison with experimentally determined numbers. We may be able to answer the question as to whether the simple theoretical models are wrong or whether, indeed, the interpretation of the experiments involving surface viscosity is deficient.

Acknowledgments. We wish to express our thanks to Professors D. K. Hoffman, Robert S. Hansen, and John S. Dahler for helpful suggestions and discussions regarding this paper. E. R. Cooper wishes to express his gratitude to the National Science Foundation Postdoctoral Program for financial support of this work.

Appendix A

We can show that the singlet equation for the monolayer can be written in terms of a friction coefficient that couples the substrate to the monolayer. The construction is done in three-dimensions following Montgomery[28] and then specialized to the two-dimensional case.

The singlet equation for a binary mixture of rigid spheres in the absence of external forces is

$$\left(\frac{\partial}{\partial t} + \mathbf{v}_1 \cdot \frac{\partial}{\partial \mathbf{r}_1}\right) f_1^{(1)} = \Omega_{12} + \Omega_{1s} \tag{A1}$$

where

$$\Omega_{12} = \sigma_1^2 \int d\mathbf{v}_2 \int d\hat{k}\, \hat{k}\cdot\mathbf{v}_{21} \{f_{12}^{(2)}(\mathbf{r}_1, \mathbf{v}_1', \mathbf{r}_1 + \sigma_1\hat{k}, \mathbf{v}_2', t) - f_{12}^{(2)}(\mathbf{r}_1, \mathbf{v}_1, \mathbf{r}_1 - \sigma_1\hat{k}, \mathbf{v}_2, t)\} \quad \hat{k}\cdot\mathbf{v}_{21} > 0 \tag{A2}$$

and

$$\Omega_{1s} = \sigma^2 \int d\mathbf{v}_s \int d\hat{k}\, \hat{k}\cdot\mathbf{v}_{s1} \{f_{1s}^{(2)}(\mathbf{r}_1, \mathbf{v}_1', \mathbf{r}_1 + \sigma\hat{k}, \mathbf{v}_s', t) - f_{1s}^{(2)}(\mathbf{r}, \mathbf{v}_1, \mathbf{r}_1 - \sigma\hat{k}, \mathbf{v}_s, t)\} \quad \hat{k}\cdot\mathbf{v}_{s1} > 0 \tag{A3}$$

Here 1 and 2 refer to one species, s refers to the other species, $\hat{k}$ is a unit vector normal to the surface of molecule 1 at the point of contact, $\mathbf{v}_{\alpha 1} = \mathbf{v}_\alpha - \mathbf{v}_1$ (α = 2,s), σ_1 and σ_s are the sphere diameters, and $\sigma = \frac{1}{2}(\sigma_1 + \sigma_s)$. The singlet distribution function is $f^{(1)}$, the pair distribution function is $f^{(2)}$, and the prime denotes a function of precollision variables.

We now focus on Ω_{1s} and show that it can be reduced to a Fokker-Planck term if we assume that $m_1 \gg m_s$, an assumption that should certainly be valid for the surface film if 1 is the monolayer and s the substrate. We write

$$f_{1s}^{(2)}(\mathbf{r}_1, \mathbf{v}_1, \mathbf{r}_1 \pm \sigma\hat{k}, \mathbf{v}_s, t) = f_s^{(0)} f_1^{(1)} \tag{A4}$$

where $f_s^{(0)} = (m_s/2\pi kT)^{3/2} \exp(-m_s C_s^2/2kT)$ and $\mathbf{C}_s = \mathbf{v}_s - u_s$. Since energy and momentum are conserved during a collision, we have

$$\frac{1}{2}m_s C_s'^2 = \frac{1}{2}m_s C_s^2 + \frac{1}{2}m_1 C_1^2 - \frac{1}{2}m_1(C_1^2 + 2\mathbf{C}_1\Delta\mathbf{v}_1 + (\Delta\mathbf{v}_1)^2) \tag{A5}$$

where $\mathbf{C}_1 = \mathbf{v}_1 - \mathbf{u}_s$ and $\mathbf{C}_1' = \mathbf{C}_1 + \Delta\mathbf{v}_1$. Here $\Delta\mathbf{v}_1$ is given by

$$\Delta\mathbf{v}_1 = (2\tau/(1+\tau))\hat{k}(\hat{k}\cdot\mathbf{v}_{s1}) \tag{A6}$$

where $\tau = (m_s/m_1) \ll 1$.

We can now expand $f_s^{(0)\prime}$, $\mathbf{v}_{s1}$, and $f_1^{(1)\prime}$ in powers of τ as done by Montgomery[28] to obtain

$$f_1^{(1)\prime} = f_1^{(1)} + \Delta\mathbf{v}_1 \cdot \frac{\partial}{\partial \mathbf{v}_1} f_1^{(1)} + \frac{1}{2}\Delta\mathbf{v}_1\Delta\mathbf{v}_1 \odot^2 \frac{\partial^2}{\partial v_1 \partial v_1} f_1^{(1)} + O(\tau^{3/2}) \tag{A7}$$

$$f_s^{(0)\prime} = f_s^{(0)}(1 + m_s\mathbf{C}_1\cdot\Delta\mathbf{v}_1/\tau kT + m_s(\Delta v_1^2)/2\tau kT + m_s^2(\mathbf{C}_1\cdot\Delta\mathbf{v}_1)^2/2(\tau kT)^2 + O(\tau^{3/2})) \tag{A8}$$

and

$$\mathbf{v}_{s1} = \mathbf{C}_s(1 - \mathbf{C}_s\cdot\mathbf{v}_1/C_s^2 + C_1^2/2C_s^2 - (\mathbf{C}_s\cdot\mathbf{C}_1)^2/2C_s^4 + O(\tau^{3/2})) \tag{A9}$$

Inserting these expansions into (A3) we find that to order τ

$$\Omega_{1s} = \frac{\zeta_H}{m_1}\frac{\partial}{\partial \mathbf{v}_1}\left\{(\mathbf{v}_1 - \mathbf{u}_s) f_1^{(1)} + \frac{kT}{m_1}\frac{\partial}{\partial \mathbf{v}_1} f_1^{(1)}\right\} \tag{A10}$$

where

$$\frac{\zeta_H}{m_1} = \frac{8}{3}\sigma^2 n_s \tau (2\pi kT/m_s)^{1/2} \quad \text{(A11)}$$

or

$$\zeta_H = \frac{8}{3} n_s \sigma^2 (2\pi m_s kT)^{1/2} \quad \text{(A12)}$$

Repeating this construction in two dimensions leads to

$$\zeta_H^{(2)} = 2\sigma n_s^{(2)} (2\pi m_s kT)^{1/2} \quad \text{(A13)}$$

where $n_s^{(2)}$ is the number of solvent molecules per unit area.

Appendix B

The quantities, J_{ij}, are various linear combinations of contraction of tensor integral (13) of the form

$$[\xi,\psi] = -(2\pi n)^{-2} \int d\hat{e}_1 \int d\hat{e}_2 \int d\hat{k}\, \$_x^{(1)} \int d\mathbf{v}_1 d\mathbf{v}_2 \int d\mathbf{M}_1 d\mathbf{M}_2 f_1^{(0)} f_2^{(0)} \hat{k}\cdot\mathbf{g}\, \xi_1[\psi_1' + \psi_2' + \psi_1 + \psi_2'] \quad \text{(B1)}$$

$$\hat{k}\cdot\mathbf{g} > 0 \qquad \hat{k}\cdot\mathbf{g} < 0$$

Contractions of these tensor integrals involve basic integrals of the form

$$(N)^{(\nu)} = (2\pi)^{-2} \int_0^{2\pi} d\theta_1 \int_0^{2\pi} d\theta_2 \$_x^{(1)} \frac{N}{D^\nu} \quad \text{(B2)}$$

where θ_i is defined by $\cos\theta_i = \hat{k}\cdot\hat{e}_i$, $D = (1 + a_1^2 + a_2^2)^{1/2}$, $a_i = (-1)^{i+1}(\mu/I)^{1/2}(\zeta^{(i)} \times \hat{k})$, $\zeta^{(i)}$ is a vector from the center of mass of body i to the point of contact, and N is some product of the following quantities

$$1,\ A_i = a_i^2$$

In units of $(\pi kT/m)^{1/2}L$ (L is set equal to 10^{-8} cm for convenience), the pertinent scalar contractions for evaluating the J_{ij} are the following

$$[W^2; W^2] = 4(1)^{(1)} - 4(1)^{(3)}$$

$$[\mathbf{W}^0\mathbf{W}; \mathbf{W}^0\mathbf{W}] = 4(1)^{(1)} - 2(1)^{(3)}$$

$$[\mathbf{W}^0\mathbf{W}; \mathbf{W}^0\mathbf{W}W^2] = 12(1)^{(1)} - 5.5(1)^{(3)} - (1)^{(5)}$$

$$[\mathbf{W}^0\mathbf{W}; \mathbf{W}^0\mathbf{W}\Omega^2] = 2(1)^{(1)} - 2(1)^{(3)} + 2(A_1)^{(3)} - 2(A_1)^{(5)}$$

$$[W^2\mathbf{W}^0\mathbf{W}; \mathbf{W}^0\mathbf{W}W^2] = 60(1)^{(1)} - 34(1)^{(3)} + 10.875(1)^{(5)} - 7.5(1)^{(7)}$$

$$[W^2\mathbf{W}^0\mathbf{W}; \mathbf{W}^0\mathbf{W}\Omega^2] = 6(1)^{(1)} - 2.75(1)^{(3)} - 0.5(1)^{(5)} - 6(A_1)^{(3)} + 13.25(A_1)^{(5)} - 15(A_1)^{(7)}$$

and

$$[\Omega^2\,\mathbf{W}^0\mathbf{W}; \mathbf{W}^0\mathbf{W}\Omega^2] = 3(1)^{(1)} - (1)^{(3)} + 8(A_1)^{(1)} + 2(A_1)^{(3)} + 4.75(A_1)^{(5)} - 8(A_1^2)^{(3)} + 27(A_1^2)^{(3)} + 27(A_1^2)^{(5)} - 15(A_1^2)^{(7)} - 15(A_1A_2)^{(7)}$$

Here $(A_1)^{(\nu)} = (A_2)^{(\nu)}$, $\mathbf{W}^0\mathbf{W} = [\mathbf{W}]^{(2)} = \mathbf{WW} - {}^1/_2 W^2\mathbf{U}^{(2)}$, and the semicolon means that we have corrected all tensors, beginning on each side of the semicolon and contracting nearest indices.

Appendix C

$f_1(\mathbf{r}, \mathbf{v}, \mathbf{M}, t)$ = singlet distribution function for ellipsoids
$\mathbf{r}$ = location of molecular mass center
$\mathbf{v}$ = velocity of molecular mass center
$\mathbf{M}$ = angular momentum of a molecule
$\mathbf{u}$ = average monolayer velocity
$\mathbf{u}_s$ = average substrate velocity
m = molecular mass of the monolayer
I = moment of inertia of a monolayer molecule
$\mathbf{g}$ = postcollisional relative velocity of two ellipsois molecules at point of contact
$\hat{k}$ = unit vector normal to ellipsoid molecule one at the point of contact
$\$_x^{(1)}$ = element of arc length per unit angle on the excluded area
e_i = unit vector along the symmetry axis of molecule i
h_i = supporting function for ellipsoid i
a = length of the ellipsoid minor axis
b = length of the ellipsoid major axis
R = ratio of major to minor axis length
C = distance of the mass center from the geometrical center
ζ = translational friction constant
ζ' = rotational friction constant
$f^{(0)}$ = local equilibrium distribution function
ϕ = distortion to the local equilibrium distribution function
n = number density
k = Boltzmann's constant
T = temperature
$\mathbf{W}$ = $(m/2kT)^{1/2}(\mathbf{v} - \mathbf{u})$
$\mathbf{\Omega}$ = $(2Ikt)^{-1/2}\mathbf{M}$
$\mathbf{P}$ = 2D pressure tensor
$\bar{\eta}$ = surface shear viscosity coefficient
$\bar{K}$ = surface dilational viscosity coefficient
Σ = projected molecular area
μ = reduced mass
ζ_R = dimensionless friction coefficient
$\mu^{(-)}$ = shear viscosity of the substrate
Γ = total surface density
$\Gamma(i)$ = surface density of species i
$\bar{\mathbf{u}}$ = the mass average surface velocity
$\bar{\mathbf{u}}^1$ = surface velocity of component 1
$\bar{r}$ = surface point
$n^{(1)}$ = surface number density
$\hat{e}_x, \hat{e}_y, \hat{e}_z$ = orthogonal unit vectors in the indicated directions
$[f]_0$ = $\lim \epsilon \to 0\,(f(\epsilon) - f(-\epsilon))$, $\epsilon > 0$
h, δ = depths of the interfacial region
γ = surface tension
$\mathbf{P}^b$ = pressure tensor of the substrate in the bulk
$\bar{D}^{(1)}$ = self-diffusion coefficient

References and Notes

(1) Acknowledgment is made to the Donors of The Petroleum Research Fund, administered by the American Chemical Society, for the partial support of this research.
(2) (a) G. L. Gaines, "Insoluble Monolayers at Liquid-Gas Interfaces," Wiley-Interscience, New York, N. Y., 1966; (b) M. Joly in "Surface and Colloid Science," Vol. 5, E. Matijevic, Ed., Wiley, New York, N. Y., 1972.
(3) F. C. Goodrich and A. K. Chatterjee, *J. Colloid Interface Sci.*, **34**, 36 (1970).
(4) M. Blank and J. Britten, *J. Colloid Sci.*, **20**, 789 (1965).
(5) S. Chapman and T. G. Cowling, "The Mathematical Theory of Non-Uniform Gases," Cambridge University Press, Cambridge, 1952.
(6) J. O. Hirschfelder, C. F. Curtiss, and R. B. Bird, "Molecular Theory of Gases and Liquid," Wiley, New York, N. Y., 1964.
(7) S. A. Rice and A. R. Allnatt, *J. Chem. Phys.*, **34**, 2144 (1961).
(8) S. A. Rice and A. R. Allnatt, *J. Chem. Phys.*, **34**, 2156 (1961).
(9) D. K. Hoffman and J. S. Dahler, *J. Stat. Phys.*, **1**, 521 (1969).
(10) E. R. Cooper and D. K. Hoffman, *J. Chem. Phys.*, **53**, 1100 (1970).
(11) Equation 9 is not a Fredholm integral equation of the second kind

with a symmetric kernel.
(12) J. A. R. Coope, R. F. Snider, and F. R. McCourt, *J. Chem. Phys.*, **43**, 2269 (1965).
(13) D. K. Hoffman, *J. Chem. Phys.*, **50**, 4823 (1969).
(14) E. Boyd and W. D. Harkins, *J. Amer. Chem. Soc.*, **61**, 1188 (1939).
(15) M. J. Povich, Thesis, University of Hawaii, 1972.
(16) R. J. Mannheimer and R. S. Schechter, *J. Colloid Interface Sci.*, **27**, 342 (1968); **32**, 195 (1970); **32**, 212 (1970).
(17) F. C. Goodrich and L. H. Allen, *J. Colloid Interface Sci.*, **37**, 68 (1971).
(18) N. Lifschutz, M. G. Hegde, and J. C. Slattery, *J. Colloid Interface Sci.*, **37**, 73 (1971).
(19) J. A. Mann in "Techniques of Surface Chemistry and Physics," R. J. Good, *et al.*, Ed., Marcel Dekker, New York, N. Y., 1972.
(20) R. S. Hansen and J. Ahmad, *Progr. Surface Membrane Sci.*, 4, 1 (1971).
(21) E. H. Lucassen-Reynders and J. Lucassen, *Advan. Colloid Interface Sci.*, **2**, 347 (1969).
(22) M. G. Hegde and J. C. Slattery, *J. Colloid Interface Sci.*, **35**, 183 (1971).
(23) C. Huh and L. E. Scriven, *J. Colloid Interface Sci.*, **35**, 85 (1971).
(24) J. A. Mann and J. Ahmad, *J. Colloid Interface Sci.*, **29**, 158 (1969).
(25) J. Ahmad and R. S. Hansen, *J. Colloid Interface Sci.*, in press.
(26) R. J. Bearman and J. G. Kirkwood, *J. Chem. Phys.*, **28**, 136 (1958).
(27) E. K. Sakata and J. C. Berg, *Ind. Eng. Chem., Fundam.*, **8**, 570 (1969).
(28) D. Montgomery, *Phys. Fluids*, **14**, 2088 (1971).

A CNDO/2 Calculation on the Helical Conformations of a Tetrapeptide of Poly-L-alanine. V. The ϕ–ψ Energy Surface[1]

Hans Stymne, Gunnar Wettermark,

Division of Physical Chemistry, The Royal Institute of Technology, Stockholm 70, Sweden

Robert Schor,*

Department of Physics and Institute of Materials Science, The University of Connecticut, Storrs, Connecticut 06268

and Carl W. David

Department of Chemistry, The University of Connecticut, Storrs, Connecticut 06268 *(Received July 18, 1973)*

Publication costs assisted by The University of Connecticut Research Foundation

The ground-state potential energy surface for the helical conformations of a tetrapeptide of poly-L-alanine has been calculated using the CNDO/2 method. The potential energy surface contains four nonequivalent minima. The absolute minimum is found in a region close to both the right-handed α helix and the right-handed 3_{10} helix. A second local minimum of about 2 kcal/mol of residue higher is found near the corresponding left-handed helices. The 2_7 helix may be represented by the third minimum of about 3 kcal/mol of residue. The last local minimum of about 5 kcal/mol of residue is near the fully extended chain conformation. The results are compared to our previous calculations on the same system as well as to our calculations on the tetrapeptide of polyglycine.

Introduction

Theoretical studies of the conformations of isolated helices (under vacuum) of polypeptide chains with intramolecular interactions have been carried out by many workers[2,3] using semiempirical potential functions for rotation around single bonds, nonbonded interactions, dipole–dipole interactions between amide groups, and hydrogen bonding potential energy functions. More recently semiempirical quantum mechanical techniques have been used to study glycyl and alanyl residues,[4] polypeptide chains,[5] and model peptide molecules.[6] A detailed study by extended Hückel theory of a polypeptide chain of poly-L-alanine long enough to incorporate an intramolecular hydrogen bond (see Figure 1) has been presented.[7] In the present work, we present the corresponding results using the CNDO/2 method. It should now be possible to make a preliminary but more detailed comparison of the two methods on these systems and of the differences between the tetrapeptide of glycine and poly-L-alanine.

Method

Santry's modification[8] of the CNDO/2 method[8-12] was applied. The CNDO/2 method provides an approximate SCF solution to the LCAO molecular Hartree–Fock equations, in which all valence electrons are included and in which electronic repulsion is explicitly introduced.

The methods of determining the coordinates of the atoms in the helical conformations of the polypeptide chain as shown in Figure 1 is due to Némethy and Scheraga.[13] The peptide unit is considered to have a rigid planar structure with fixed bond angles and bond lengths. The coordinates of the atoms in a peptide unit for the bond angles and distances taken from Leach, Némethy, and Scheraga[14] are given in Table I. Figure 2 shows a representation of a dipeptide segment of poly-L-alanine. The new conventions[15] for the rotation angles ϕ and ψ are used in the present work. (The rotation angles ϕ and ψ as given by the former convention[16] are related to the new rotation angles ϕ and ψ by $\phi_{new} = \phi_{old} - \pi$, $\psi_{new} = \psi_{old} - \pi$.)

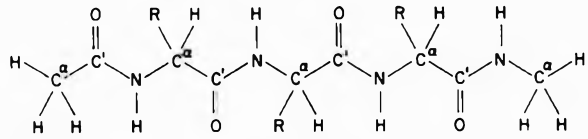

Figure 1. Diagrammatic representation of a tetrapeptide of poly-L-alanine with R = CH_3 including the rotation angles $\phi(N-C^\alpha)$ and $\psi(C^\alpha-C')$ around the single bonds.

TABLE I: Coordinates for the Atoms in a Planar Peptide Unit

Atom	j	x_j, Å	y_j, Å	z_j, Å
C^α	1	0.00	0.00	0.00
C′	2	1.42	0.58	0.00
O	3	1.61	1.80	0.00
N	4	2.37	−0.34	0.00
H (amide)	5	2.18	−1.32	0.00
C^α	6	3.80	0.00	0.00

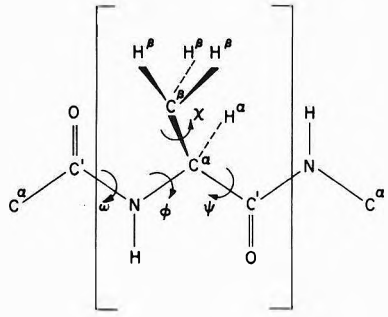

Figure 2. Diagrammatic representation of a dipeptide segment of poly-L-alanine. A residue is enclosed within brackets. χ = 60°, *i.e.*, all methyl groups are staggered with respect to the polypeptide backbone; ω = 180°, *i.e.*, all peptide units are in the planar trans conformation.

The calculations were performed on an IBM 360/75 computer. (The execution time for a tetrapeptide of poly-L-alanine was approximately 3 min for each point on the potential energy surface.) The largest grid size was taken to be 30°, but a width as small as 5° was used for studying certain energy contours which varied more rapidly with ϕ and ψ. Since R = CH_3, the potential energy surface is no longer centrosymmetric, and the whole range of ϕ and ψ was used.

Results

The ground-state potential energy surface for four peptide units (three residues) is shown in Figure 3. Since R = CH_3, the map is not centrosymmetric about the point ϕ = 0°, ψ = 0°.

There are four nonequivalent minima in the contour map; (1) the absolute minimum $\phi \simeq -40°$, $\psi \simeq -35°$ whose energy has been set equal to zero. It should be noted that the minimum is quite shallow in this region and the interpolation is uncertain. Hence the estimated

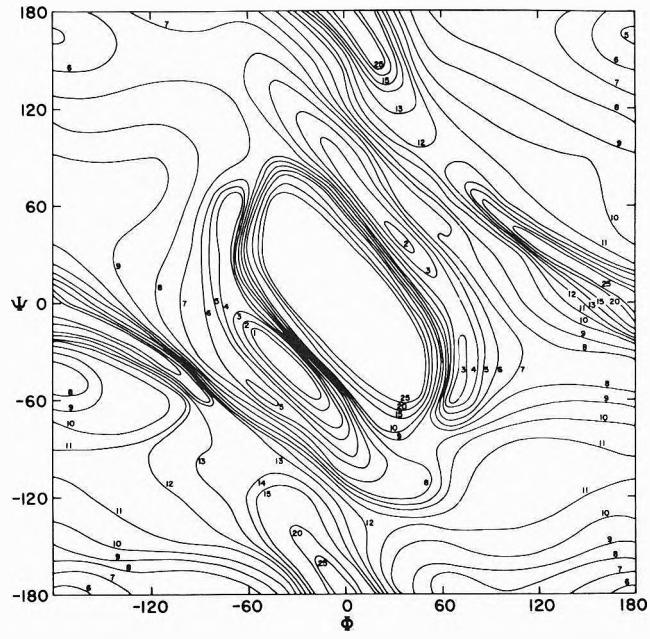

Figure 3. Ground-state potential energy surface for a tetrapeptide of L-alanine calculated by CNDO/2 method. The contours of constant energy are chosen relative to the most stable conformation which is chosen as zero energy and are in units of kcal/mole of residue.

error bars in the position of the minimum is about ±15° in both ϕ and ψ; (2) a local minimum at $\phi \simeq 35°$, $\psi \simeq 40°$ whose energy is approximately 2 kcal/mol of residue; (3) a local minimum $\phi \simeq 75°$, $\psi \simeq -40°$ of about 4 kcal/mol of residue; and (4) a local minimum $\phi \simeq -180°$, $\psi \simeq 165°$ of approximately 5 kcal/mol of residue near the fully extended chain conformation.

The absolute minimum at $\phi \simeq -40°$, $\psi \simeq -35°$ has shifted substantially from the calculated absolute minimum for the tetrapeptide of glycine at $\phi \simeq -20°$, $\psi \simeq -60°$.[17] The present absolute minimum is closer to the right-handed α helix $\phi \simeq -48°$, $\psi \simeq -57°$ and significantly closer to the right-handed 3_{10} helix at $\phi \simeq -49°$, $\psi \simeq -26°$. It is interesting to note, however, the suggestion of a faint minimum near the right-handed α-helix conformation.

A local minimum of about 2 kcal/mol of residue at $\phi \simeq 35°$, $\psi \simeq 40°$ is very close to the left-handed 3_{10} helix at $\phi \simeq 49°$, $\psi \simeq 26°$. Additionally, one notes the suggestion of a valley which runs straight through the left-handed α-helix conformation. The difference in stability between the right-handed α helix and the left-handed α helix (and between the right-handed 3_{10} helix and the left-handed 3_{10} helix) is approximately 2 kcal/mol of residue with the right-handed conformations being the most stable. This result agrees with our extended Hückel calculations on the tetrapeptide of poly-L-alanine.[18]

The local minimum at $\phi \simeq 75°$, $\psi \simeq -40°$ of approximately 3 kcal/mol of residue is broad and it is particular-

TABLE II: Gross Charges on the Atoms in a Planar Peptide Unit for Various Helical Conformations of the Tetrapeptide of Poly-L-alanine

Conformation	N^a	H^a	O^b	C'^b	C^b	$H^{\alpha\,a}$	$H^{\alpha\,b}$
Fully extended chain	−0.19	+0.12	−0.38	0.36	−0.09	+0.01	+0.03
Antiparallel-chain pleated sheet	−0.18	+0.11	−0.37	0.36	−0.09	+0.01	+0.03
Right-handed α helix	−0.20	0.15	−0.38	0.37	−0.10	+0.02	+0.03

[a] Atomic charge taken from the fourth peptide unit. [b] Atomic charge taken from the first peptide unit.

ly difficult to determine the angle ψ with precision. This minimum may therefore "correspond" to the 2_7 and the 2.2_7 helices at $\phi \simeq 75°$, $\psi \simeq -70°$ for polyglycine.[19] Maigret, *et al.*,[20] found the conformation $\phi \simeq -80°$, $\psi \simeq -40°$ to be the most stable conformation in their calculation on *N*-acetyl-*N'*-methylalanylamide. The local minimum $\phi \simeq -60°$, $\psi \simeq 60°$ of approximately 4 kcal/mol of residue obtained for the tetrapeptide of glycine[17] has disappeared in the present calculation and this ϕ, ψ pair is now on a 6 kcal/mol of residue contour. There is a suggestion, however, of the formation of a new local minimum at about $\phi \simeq -70°$, $\psi \simeq 50°$, of slightly less than 4 kcal/mol of residue.

The local minimum near the fully extended chain conformation of about 5 kcal/mol of residue has shifted from $\phi \simeq -180°$, $\psi \simeq -180°$ for the tetrapeptide of glycine[17] to $\phi \simeq -180°$, $\psi \simeq -165°$ in the present case. Hence, there is a faint suggestion of pleating[21] on substituting the bulkier CH_3 group for H in the side chains.

The partial charges which are sensibly independent of the rotation angles ϕ and ψ are substantially the same as for the tetrapeptide of glycine[17] and are given in Table II for some selected conformations.

Conclusions

The CNDO/2 calculations on the helical conformations of the tetrapeptide of poly-L-alanine, in agreement with all our previous calculations, show that the difference in the computed energy between the absolute minimum (near a contracted form of the polypeptide chain) and the extended forms of the polypeptide chain is about 5 kcal/mol of residue. In addition, there is essentially only one easy direction on the ϕ–ψ map for the chain to unwind in going from the contracted to the extended form.

The right-handed α-helical conformation for poly-L-alanine is predicted to be about 2 kcal/mol of residue lower in energy than the left-handed α-helical conformation. This difference appears to be a real one and not an artifact of the calculations.

The present calculations indicate, however, a new feature which is perhaps somewhat unexpected. The absolute minimum is now significantly closer to the 3_{10} helix than to the α helix. Further theoretical work is in progress which may help to make a more definite assignment.

Acknowledgments. The authors wish to thank Professors Roald Hoffmann and Angelo Rossi for fruitful discussions. Valuable computational assistance was provided by Miss Brigitta Byström.

References and Notes

(1) This work was supported by Grant No. 2741 from the Swedish Natural Science Research Council.
(2) (a) D. A. Brant and P. J. Flory, *J. Amer. Chem. Soc.*, **87**, 633, 2791 (1965); (b) G. N. Ramachandran, C. M. Venkatachalm, and S. Krimm, *Biophys. J.*, **6**, 849 (1966).
(3) R. A. Scott and H. A. Scheraga, *J. Chem. Phys.*, **45**, 2091 (1966).
(4) R. Hoffmann and A. Imamura, *Biopolymers*, **7**, 207 (1969).
(5) A. Rossi, C. W. David, and R. Schor, *Theor. Chim. Acta*, **14**, 429 (1969).
(6) J. F. Yan, F. A. Momany, R. Hoffmann, and H. A. Scheraga, *J. Phys. Chem.*, **74**, 420 (1970).
(7) A. Rossi, C. W. David, and R. Schor, *J. Phys. Chem.*, **74**, 4551 (1970).
(8) D. P. Santry, *J. Amer. Chem. Soc.*, **90**, 3309 (1968).
(9) J. A. Pople, D. P. Santry, and G. A. Segal, *J. Chem. Phys.*, **43**, 129 (1965).
(10) J. A. Pople and G. A. Segal, *J. Chem. Phys.*, **43**, 136 (1965).
(11) J. A. Pople and G. A. Segal, *J. Chem. Phys.*, **44**, 3289 (1966).
(12) D. P. Santry and G. A. Segal, *J. Chem. Phys.*, **47**, 158 (1967).
(13) G. N. Némethy and H. A. Scheraga, *Biopolymers*, **4**, 369 (1966).
(14) S. J. Leach, G. Némethy, and H. A. Scheraga, *Biopolymers*, **3**, 155 (1965).
(15) IUPAC–IUB Commission on Biochemical Nomenclature, *Biochemistry*, **9**, 3471 (1970).
(16) J. T. Edsall, P. J. Flory, J. C. Kendrew, A. M. Liquori, G. Némethy, G. N. Ramachandran, and H. A. Scheraga, *Biopolymers*, **4**, 121 (1966); *J. Biol. Chem.*, **241**, 1004 (1966); *J. Mol. Biol.*, **15**, 399 (1966).
(17) R. Schor, H. Stymne, G. Wettermark and C. W. David, *J. Phys. Chem.*, **76**, 670 (1972).
(18) A. R. Rossi, C. W. David, and R. Schor, *J. Phys. Chem.*, **76**, 2793 (1972).
(19) G. N. Ramachandran and V. Sasisekharan, *Advan. Protein Chem.*, **23**, 323 (1968).
(20) B. Maigret, B. Pullman, and M. Dreyfus, *J. Theor. Biol.*, **26**, 321 (1970).
(21) L. Pauling and R. B. Corey, *Proc. Nat. Acad. Sci. U. S.*, **37**, 251 (1951).

COMMUNICATIONS TO THE EDITOR

Effect of Photoionization Energy on the Distance Distribution between Trapped Electrons and *N,N,N',N'*-Tetramethyl-*p*-phenylenediamine Cations in Organic Glasses

Publication costs assisted by the U. S. Atomic Energy Commission

Sir: Trapped electrons are produced in a variety of organic glasses by radiolysis or by photoionization of a suitable solute.[1] In both cases an ion pair is initially formed from which the charged species must separate. The electron can move in a conduction state, as indicated by photoconductivity studies,[2,3] before it is trapped. However, the distance distribution of trapped electrons, e_t^-, from a positive hole is not definitely known in organic glasses.[1] Here we demonstrate an effect of photoionization energy on the distance distribution between trapped electrons and *N,N,N',N'*-tetramethyl-*p*-phenylenediamine cations ($TMPD^+$) in 2-methyltetrahydrofuran and 3-methylpentane glasses at 77 K. We demonstrate that the electrons travel further before trapping when photoionized by higher energy light.

TMPD was obtained by dissolving the dihydrochloride from Eastman Kodak Co. in water and precipitating the free base with KOH under argon. The TMPD was finally sublimed under high vacuum. 2-Methyltetrahydrofuran and 3-methylpentane were rigorously purified over sodium metal such that the purified solvents showed only slight or no luminescence under ultraviolet excitation. These samples were prepared in 3-mm o.d. Pyrex tubes with a TMPD conentration of typically 1.5×10^{-3} *M*.

The samples were photoionized at 77 K with an air-cooled Philips SP-900 high-pressure mercury lamp. Suitable filters were used to obtain bands peaking at 313 or at 365 nm with full width at half-height equal to 40 nm. The emitted luminescence is detected at right angles to the ultraviolet excitation light. TMPD fluorescence at 386 nm is selected for detection by Corning filters 5-61 plus 7-60 and is detected by a 1P28 photomultiplier tube.

Photoionizations of TMPD were carried out for 1–20 sec. A shutter in front of the ionizing lamp closed as a shutter in front of the detection system opened in order to study the isothermal fluorescence following ultraviolet excitation. The fluorescence lifetime of TMPD in 3-methylpentane glass at 77 K is 7.4 ± 1.1 nsec,[4] and it is expected to be similar in 2-methyltetrahydrofuran glass. Thus it seems safe to conclude that the isothermal fluorescence arises entirely from e_t^- and $TMPD^+$ recombination. Our shutter time is 40–50 msec.

The isothermal fluorescence decays in a nonexponential fashion. Because of its low intensity, the fluorescence can only be followed over about 10 sec before it falls below our sensitivity level. On an expanded time scale three exponentials are needed to fit the first 10 sec of decay. However, an initial isothermal fluorescence decay rate can be defined from the slope of an exponential that fits the first 2 to 3 sec of the decay curve. This initial rate represents the initial rate of isothermal e_t^- and $TMPD^+$ recombination and must be related to some distance distribution function between them. This initial rate is independent of ultraviolet excitation time but it does depend on the ultraviolet excitation wavelength. For 313-nm excitation the initial decay rate is 2.4 ± 0.2 sec, while for 365-nm excitation the initial decay rate is 1.7 ± 0.1 sec in 2-methyltetrahydrofuran glasses. The same trend is found in 3-methylpentane matrices; for 313-nm excitation the initial decay rate is 4.3 ± 0.4 sec, while for 365-nm excitation the initial decay rate is 2.6 ± 0.2 sec. These results imply different e_t^-, $TMPD^+$ distance distributions as a function of ultraviolet excitation wavelength in both organic glasses.

The photoionization process of TMPD is well understood in terms of a two-photon transition *via* a triplet state intermediate.[2] Recent work has indicated that the isothermal luminescence from photoionized TMPD in organic glasses is most probably due to an electron tunneling mechanism.[5] The tunneling rate will clearly depend on the initial distance distribution. The faster initial decay rate for lower energy photoionization is consistent with a shorter average distance between e_t^- and $TMPD^+$. It is also interesting to note that the initial decay rates are longer in 3-methylpentane glass compared to 2-methyltetrahydrofuran glass. Thus, we also conclude that the initial distance distribution between trapped electrons and cations is greater in the 3-methylpentane glass. This is consistent with the lower polarity of 3-methylpentane, and is also consistent with the difference in average spatial distributions of trapped electrons produced by radiolysis in organic glasses of differing polarity.[6]

When TMPD is photoionized, the first photon, regardless of its energy, is used to populate the triplet state. The second photon promotes an electron to the conduction state of the glassy matrix. If direct excitation to the conduction state of the matrix occurs, one expects the mobile electron to have a kinetic energy related to the energy of the second ionizing photon. This would lead to a greater distance distribution for higher energy photoionizing light since the mobile electrons would be produced with greater kinetic energy. Thus, we appear to have found the first straightforward example in which the kinetic energy and hence the total travel distance of a photoexcited electron reflect the photon energy of the photoionization process in organic glasses. The low mobility of mobile electrons in these organic glasses[7,8] indicates that the mobile electron is rapidly thermalized. Thus, it is expected that only the electrons trapped very close to the cation will reflect a distance distribution characteristic of their initial kinetic energy. These are the very electrons which are involved in the isothermal recombination luminescence process. Scavenging studies would probe the outer reaches of the electron–cation distance distribution. So scavenging studies are not expected to be sensitive to the initial kinetic energy of the mobile electron and hence not sensitive to the photon energy of the photoionization process. A previous scavenging study in aqueous glasses, in which electrons were produced by both photoionization and γ radiolysis, did not appear to show a difference in the average electron range, even though the average initial kinetic energy of the mobile electrons is expected to be quite different for the two modes of mobile electron production.[9]

The experimental data might also be formally explained in terms of different electron trapping sites having different energy barriers for their population and depopulation. However, one would also have to postulate a nonstatistical distribution of the different energy traps around $TMPD^+$. Furthermore, this model would imply that preformed trapping sites exist, whereas recent pulse radiolysis results show that electron-induced dipole orientation makes the dominant contribution to the trapping potential.[10,11]

Acknowledgment. This work was supported initially by the U. S. Air Force Office of Scientific Research under Grant No. 70-1852 and is currently supported by the U. S. Atomic Energy Commission under Contract No. AT(11-1)-2086. We thank K. K. Ho for his assistance.

References and Notes

(1) L. Kevan in "Advances in Radiation Chemistry," M. Burton and J. L. Magee, Ed., Vol. 4, Wiley-Interscience, New York, N. Y., 1973.
(2) A. C. Albrecht, *Accounts Chem. Res.*, **3**, 328 (1970).
(3) T. Huang, I. Eisele, D. P. Lin, and L. Kvan, *J. Chem. Phys.*, **56**, 4702 (1972).
(4) D. S. Kliger, J. D. Laposa, and A. C. Albrecht, *J. Chem. Phys.*, **48**, 4326 (1968).
(5) F. Kieffer, C. Meyer, and J. Rigaut, *Chem. Phys. Lett.*, **11**, 359 (1971).
(6) D. P. Lin and L. Kevan, *J. Chem. Phys.*, **55**, 2629 (1971).
(7) L. Kevan, *J. Phys. Chem.*, **76**, 3830 (1972).
(8) Y. Maruyama and K. Funabashi, *J. Chem. Phys.*, **56**, 2342 (1972).
(9) H. Hase and L. Kevan, *J. Phys. Chem.*, **74**, 3358 (1970).
(10) L. Kevan, *J. Chem. Phys.*, **56**, 838 (1972); *Chem. Phys. Lett.*, **11**, 140 (1971).
(11) N. V. Klassen, H. A. Gillis, and G. G. Teather, *J. Phys. Chem.*, **76**, 3847 (1972).

Department of Chemistry
Wayne State University
Detroit, Michigan 48202

Hermann Moeckel
Josephine Yuen
Larry Kevan*

Received August 17, 1973

SOLVENT EFFECTS ON CHEMICAL PHENOMENA, Volume 1

by EDWARD S. AMIS and JAMES F. HINTON

For decades, scientists have been fascinated by the solvation of ions and molecules. This book is the first of two volumes that will offer a unique and long needed compilation of solvation phenomena and their chemical and physical effects. The first volume features a wealth of different kinds of valuable information: in-depth discussion of each type of solvation, e.g., positive, negative, selective, mixed, and inner- and outer-sphere; detailed, step-by-step explanation of methods for measuring ion solvation and evaluating the reliability of these measurements; a concise, but thorough review of unusual mixed solvent effects, i.e., phenomena that show maxima and minima—always at about the same mole action—with the addition of a second solvent; and an extensive summary of solvent effects—including electrolytes, internal cohesion, protic vs. aprotic solvents, polarization, and viscosity—on the rates and mechanisms of chemical reactions.

1973, 496 pp., $32.50

ADVANCES IN PHYSICAL ORGANIC CHEMISTRY, Volume 10

edited by V. GOLD

CONTENTS: H. HOGEVEEN: The Reactivity of Carbonium Ions Towards Carbon Monoxide. R. E. CARTER and L. MELANDER: Experiments on the Nature of Steric Isotope Effects. M. FLEISCHMANN and D. PLETCHER: Physical Parameters for the Control of Organic Electrode Processes. D. BETHELL and M. R. BRINKMAN: Chemically Induced Dynamic Nuclear Spin Polarization and Its Applications. P. W. CABELL-WHITING and H. HOGEVEEN: The Photochemistry of Carbonium Ions.

1973, 252 pp., $16.50

In Two Volumes

DIATOMIC INTERACTION POTENTIAL THEORY

A Volume in the PHYSICAL CHEMISTRY Series

by JERRY GOODISMAN

This two-volume work covers the theoretical material involved in the calculation of potential energy curves and their relation to experimental results. The discussions are devoted to diatomic systems in their ground state, with attention given to the variety of approaches one may use. The author provides numerous examples of actual calculations and includes an extensive bibliography. He also provides an up-to-date account of recent research in this field, showing which problems have already been solved and which will require further study. Volume 1 discusses the basic quantum mechanical methods involved in the calculation of $U(R)$, with emphasis on variation and perturbation techniques. Volume 2 demonstrates the applications of these techniques to the actual calculation of interaction potentials.

Volume 1/FUNDAMENTALS
1973, 314 pp., $24.00

Volume 2/APPLICATIONS
1973, 432 pp., $34.00

ADVANCES IN MAGNETIC RESONANCE, Volume 6

edited by JOHN WAUGH

CONTENTS: D. H. LEVY: Gas Phase Magnetic Resonance of Electronically Excited Molecules. J. JONAS: NMR Studies in Lipids at High Pressure. R. W. KREILICK: Nuclear Magnetic Resonance Investigations of Organic Free Radicals. J. A. WEIL, T. BUCH, and J. E. CLAPP: Crystal Point Group Symmetry and Microscopic Tensor Properties in Magnetic Resonance Spectroscopy. S. VEGA: Second and Fourth Moments in NQR Spectroscopy for Spins with $I = 1$.

1973, about 300 pp., in preparation

BAND STRUCTURE SPECTROSCOPY OF METALS AND ALLOYS

edited by D. J. FABIAN and L. M. WATSON

This book is based on the proceedings of a University of Strathclyde international conference on the electronic structure of metals and alloys as studied by the techniques of band structure spectroscopy. These include all those solid state spectroscopies which probe the electron states in the valence or conduction bands of a metal, such as soft X-ray emission and absorption, X-ray photoelectron spectroscopy, ultra-violet photoemission and isochromat spectroscopy. The book carefully interrelates both theoretical and experimental aspects and devotes sections to the liquid and amorphous states, and to a discussion of chemical bonding in metallic compounds. The contributing authors are all experts in their individual fields, which enables the book to provide an up-to-date account of current research in the electronic structure of solids. Particular emphasis is paid to alloys, where the use of band structure spectroscopy has played an important part in the development of a theory.

1973, 772 pp., $33.00

MOLECULAR CRYSTALS AND MOLECULES

by A. I. KITAIGORODSKY

A Volume in the PHYSICAL CHEMISTRY Series

This book deals with organic crystal physics, i.e., with the most important problems of molecular crystallography and certain aspects of molecular structure. Primarily, it reports the author's own results in applying the atom-atom potential model—which treats the energy of molecular interactions as the sum of the interactions of the component atoms—to the lattice structure, lattice dynamics, and thermodynamics of crystals, and to the conformation of molecules. Topics discussed include: the structure of crystals; lattice energy and lattice dynamics; methodology in investigating structure and molecular movement; thermodynamic theory and experiments; and conformations of organic molecules, macromolecules, and biopolymers.

1973, 572 pp., $44.00

INTRODUCTION TO CHEMICAL ULTRASONICS

by M. J. BLANDAMER

The technique of ultrasonic relaxation has provided chemists with a great deal of valuable information, particularly in the fields of rotational isomerism and salt solutions. This work is written for the chemist who is interested in finding out how this technique can be applied to a wide range of systems and how the relevant information can be obtained from measurements of ultrasonic absorption. The basic theory is developed from a chemical standpoint with special emphasis on the thermodynamic and kinetic parameters which describe how a system at equilibrium responds to perturbation by a sound wave. These theoretical aspects are covered in the first few chapters and the application examined in the remaining few chapters of the book.

1973, 138 pp., $8.00

EXCITED STATES, Volume 1

edited by E. C. LIM

This new serial publication provides an authoritative guide to advances in fundamental research on the formation, properties, and relaxation of electronically excited states of polyatomic molecules. The study of molecular excited states has made rapid growth in recent years due to the development of various experimental and theoretical techniques, growing interest in and understanding of radiationless transitions, and increasing use of knowledge in photochemistry, radiation chemistry, photobiology, and molecular photophysics. The series will cover such topics as molecular luminescence, radiationless transitions, elementary photochemical processes, geometries and dipole moments of excited states, excitons and phonons in molecular crystals, energy transfer, and many others.

1973, in preparation

prices subject to change without notice

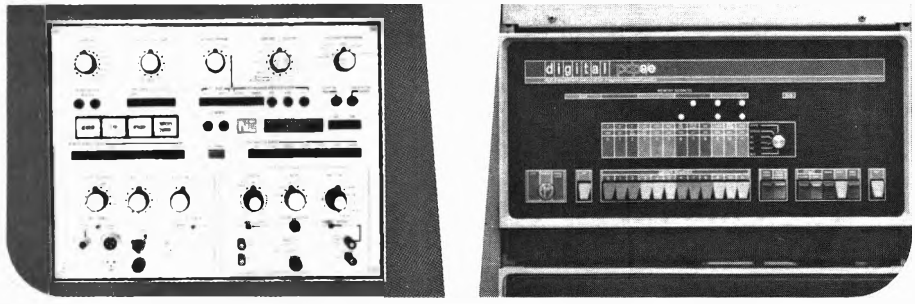

Do you need a signal averager...or a general purpose computer?

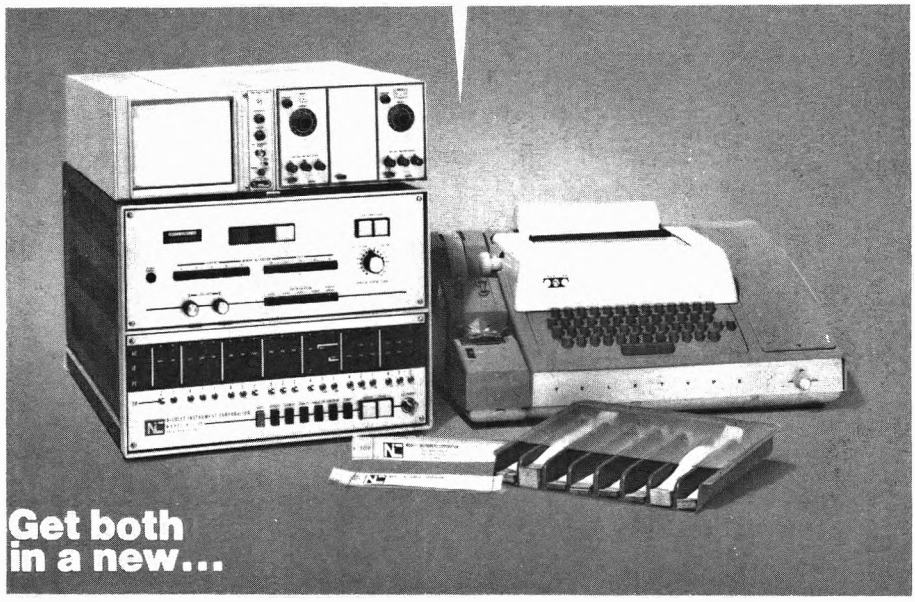

NICOLET NIC-80 DATA SYSTEMS

The new NIC-80 Series data acquisition and processing system combines the benefits of a hard-wired signal averager with the advantages of a general purpose computer. The result is an easy-to-use data system that permits the scientist to concentrate on his research rather than on electronic data processing.

The NIC-80 Series offers digitizing speeds of up to 10 microseconds with 12-bit resolution, high resolution timing of up to 1 microsecond, high timing accuracy (100 nanoseconds), 20-bit word length to eliminate double precision programming, easy interface with a wide range of experiments through specialized hardware and software, extensive processing capability through available software, flexible control of experimental variables through keyboard entries, continuous display even at high data rates, a broad selection of peripheral equipment, and the most thorough applications assistance offered anywhere. For ultra-high-speed applications, digitizing speeds of up to 10 nanoseconds can be achieved with an optional transient recorder.

The NIC-80 Series is presently offered in three different configurations which differ only slightly in hardware design but have a unique software package for each system. For example, the NMR-80 System contains complete programs for Ft nmr work. The MED-80 System is oriented to biomedical applications where the statistical analysis of bioelectric potentials is the task. A third system, called the LAB-80 System is a general purpose laboratory data system designed for use with various spectrometers or other laboratory instruments.

Included in all of the above systems is the hardware for on-line CRT display of incoming data or processed data as well as software for the control of x-y or y-t recorders.

Options and accessories include a high-speed paper tape reader, a disk memory unit, a silent keyboard/printer, x-y or y-t recorders, a transient recorder, paper tape punch, and magnetic tape interface.

LAB-80 capabilities include: averaging and processing of fast scan infra-red spectrophotometer data for sensitivity improvement, background compensation, and color correction; ultra-high-speed data acquisition (10 nanoseconds sampling interval, via Biomation transient recorder), averaging, and processing of data from laser-excited fluorescence decay studies; averaging and processing of electron paramagnetic resonance spectrometer data; and high-speed acquisition (via transient recorder), averaging and processing of pulsed nmr data.

Call or write to discuss your averaging and processing requirements.

NICOLET INSTRUMENT CORPORATION

5225 Verona Road, Madison, Wisconsin 53711
Phone 608/271-3333 TWX: 910-286-2713

12 NOV 2517